Development of Photoresponsive Metal Based Single-Chain Nanoparticles

Zur Erlangung des akademischen Grades eines

DOKTORS DER NATURWISSENSCHAFTEN

(Dr. rer. nat.)

von der KIT-Fakultät für Chemie und Biowissenschaften

des Karlsruher Instituts für Technologie (KIT)

genehmigte

DISSERTATION

von

BSc(Hons 1st). Aidan Essie Izuagbe

1. Referent: Prof. Dr. Peter W. Roesky
2. Referent: Prof. Dr. Andreas-Neil Unterreiner
3. Cotutelle-Referent: Prof. Dr. Christopher Barner-Kowollik

Tag der mündlichen Prüfung: 12th of Dezember 2023

The presented thesis was developed between January 2020 and November 2023 in a binational PhD agreement (‘cotutelle de these’) between the Queensland University of Technology (QUT, Australia) and the Karlsruhe Institute of Technology (KIT, Germany) under the supervision of Prof. Dr. Christopher Barner-Kowollik (QUT) and Prof. Dr. Peter Roesky (KIT).

Keywords

Azobenzene, Catalysis, *cis/trans* isomerization, Compaction, DOSY, Dynamic, Gold, Intramolecular cross-linking, Light-induced polarity change, Merocyanine, Metal, Nitroxide-mediated radical polymerization, Orthogonal, Particle core morphology, Photoresponsive, Photoswitch, Polymer chemistry, Reversible addition−fragmentation chain-transfer polymerization, Reversible change, SEC, Single-chain nanoparticle (SCNP), Spiropyran, Tetra-chlorination, Unfolding, Visible light

Zusammenfassung

Enzyme sind das Vorzeigebeispiel eines Katalysators, da ihr feines Zusammenspiel von präzise gefalteten tertiären Strukturen um katalytische Taschen biologische Substrate hoch selektiv und effizient katalytisch umsetzt. Die strukturellen Eigenschaften, die Enzyme zu solch erfolgreichen Katalysatoren machen, dienen als Inspiration für eine Klasse weicher Nanomaterialien, die als Single Chain Nanoparticles (SCNP) bekannt sind. Mit solchen intramolekular gefalteten linearen Polymeren eifern Chemiker dem Design natürlicher Katalysatoren nach. SCNPs haben in den letzten zehn Jahren großes Interesse geweckt, da SCNP-Technologien zunehmend in praktischen Anwendungen eingesetzt werden. Die bedeutendste und beliebteste Anwendung für die Katalyse ist die Funktion, für die ihre natürlichen Gegenstücke bestimmt sind. Katalytischen SCNPs beinhalten häufig katalytische Metallzentren, die in das SCNP-Polymergerüst eingebettet sind. Obwohl sich gezeigt hat, dass die Katalyse erfolgreich und effizient ist, ist eine deutliche Weiterentwicklung der SCNP-Technologie erforderlich, um die Effizienz von natürlichen Enzymen zu erreichen. Das SCNP-Design ermöglicht jedoch zusätzlich zur Katalyse die Implementierung anspruchsvoller Funktionalitäten wie Photoresponsivität, die mit Enzymen nicht möglich sind. Die hierin präsentierte Arbeit konzentriert sich auf organometallische SCNPs, die die einzigartigen Eigenschaften von Metallzentren für SCNP-Funktionalität und -Struktur heranziehen. Photochemische Prozesse werden untersucht, um zusätzliche Kontrolle über die Funktionalität der Metallzentren und die dreidimensionale SCNP-Struktur zu erreichen.

Im ersten Kapitel dieser Arbeit stand die photokontrollierte SCNP-Katalyse im Mittelpunkt. Lineare Polymere mit goldkomplexierten Phosphinliganden, die in der Lage sind, die Hydroaminierung von Alkinen zu katalysieren, wurden mit mit sichtbarem Licht schaltbaren Azobenzol-Vernetzern intramolekular verbunden, wodurch photoresponsive SCNPs erzeugt wurden. Ihre Responsivität für sichtbares Licht wurde charakterisiert und während der gesamten SCNP-Bildung konserviert. Die Photoisomerisierung zwischen cis- und trans-Isomer der Vernetzer führt zu leichten morphologischen Veränderungen des SCNP, die als Indiz für eine größere

Änderung der SCNP-Eigenschaften insgesamt angenommen werden kann. Vorläufige katalytische Experimente zeigen einen Unterschied der SCNP-Katalyse durch Photoisomerisierung zwischen cis- und trans-Form.

Metalle werden neben der Bereitstellung katalytischer Funktionalität auch als Strukturelemente im SCNP verwendet, die häufig den intramolekularen Kollaps eines linearen Polymers bei der Bindung von Liganden, die an das Polymerrückgrat gebunden sind, versursachen. Die Photoisomerisierung von Spiropyran in eine offene, zur Metallkomplexierung fähige Merocyaninform wurde im zweiten Kapitel ausgenutzt, um lineare Polymere durch lichtinduzierte Metallkomplexierung zu SCNPs zu falten. Organometallische SCNPs wurden durch Belichtung eines mit Spiropyran dekorierten linearen Polymers mit einer Reihe von späten Übergangsmetallen synthetisiert. Die intramolekulare Verdichtung entsteht durch die Bildung von mehrkernigen Metallkomplexen zwischen Spiropyran und Metallen. Der reversible Charakter des Spiropyran-Photoswitches wurde in dem Versuch untersucht, die Metallspezies über photo- und chemische Reize zu vertreiben und das lineare Polymer zu regenerieren. Vorläufige Ergebnisse zeigten eine teilweise Entfaltung des SCNP durch die externen Stimuli, die eine weitere Verfolgung der reversiblen SCNP-Faltung aussichtsreich machen.

Abstract

Enzymes are considered as the ultimate catalysis owing to a fine interplay between precisely folded tertiary structures around catalytic pockets able to catalyse biological substrates selectively and efficiently. The structural properties that make enzymes such successful catalysts serve as inspiration for a class of soft nano materials known as Single Chain Nanoparticles (SCNP). Consisting of linear polymers intramolecularly folded, SCNPs constitute one such attempt by chemists to emulate the design of nature's catalysts. SCNPs have received significant attention in the last decade, as scientists begin to adopt SCNP technologies for a range of applications. The most significant and popular applications being for catalysis, the function that their natural counterparts are intended for. Taking further inspiration from enzymes, catalytic SCNPs are often the result of catalytic metal centres embedded in the SCNP polymeric scaffold. While shown to be successful and efficient catalysis, significant advancement in SCNP technology will be needed to begin even approaching the efficiency of enzymes. SCNP design does however allow for the implementation of sophisticated functionality such as photoresponsivity, not possible with enzymes. The work presented in this thesis focuses on organometallic SCNPs capitalising on the unique properties metal centres imbue on SCNP functionality and structure. Photochemical processes are investigated to add additional control over the metal-facilitated functionality and structure.

Photo-controlled SCNP catalysis was the focus in the first chapter of this thesis. Linear polymers bearing gold complexed phosphine ligands, capable of catalysing the hydroamination of alkynes, were intramolecularly collapsed using visible light switchable azobenzene crosslinkers, culminating in a photoresponsive SCNP. Visible light switching of the azobenzene crosslinks was characterized and seen to be conserved throughout SCNP formation. Photoisomerization between the *cis* and *trans* isomer of the crosslinks lead to slight morphological changes in the SCNP, assumed to be indicative of a greater change to the overall SCNP properties. Preliminary catalytic results were collected, revealing a difference between SCNP catalysis upon crosslink photoisomerization.

Metals in addition to providing catalytic functionality, are also used as structural elements within SCNPs, often constituting the intramolecular collapse of a linear polymer upon formation with ligands attached to the polymer backbone. The photo-isomerization of spiropyran into an open merocyanine form capable of metal complexation was exploited in the second chapter to fold linear polymers into SCNPs via light induced metal complexation. Organometallic SCNPs were synthesized upon exposure of a linear polymer decorated with spiropyran pendant groups to light and a range of late transition metals. Intramolecular compaction arises from the formation of coordination complexes between the spiropyran and metals. The reversible nature of the spiropyran photoswitch was investigated in an attempt to expel the metal species via photo and chemical stimuli and regenerate the linear polymer. Preliminary results showed partial unfolding of the SCNP encouraging further pursuit of reversible SCNP folding.

Contents

List of Figures

List of Tables

List of Schemes

List of Equations

List of Abbreviations

ABCN	Azobis(cyclohexanecarbonitrile)
ABO	Antibonding Orbitals
ACN	Acetonitrile
ADMET	Acyclic Diene Metathesis
AFM	Atomic Force Microscopy
AIBN	Azo(bisisobutyronitrile
ATRP	Atom Transfer Radical Polymerization
BHT	Butylated Hydroxytoluene
BTA	1,3,5-Tricarboxamide
CDI	Carbonyldiimidazole
CH	Cyclohexane
COSY	Correlation Spectroscopy
CPS	Constant-Temperature Measurement
CTA	Chain Transfer Agent
DAD	Diode Array Detector
DCC	N,N'-Dicyclohexylcarbodiimide
DCM	Dichloromethane
DLS	Dynamic Light Scattering
DMAP	Dimethyl Amino Pyridine
DMEM	Dulbecco's Modified Eagle Medium
DMSO	Dimethyl Sulfoxide
DNA	Deoxyribonucleic Acid
DOSY	Diffusion Ordered Spectroscopy
DP	Degree Polymerization
EDTA	Ethylenediaminetetraacetic Acid
EDX	Energy Dispersive X-ray
ESI-MS	Electro Spray Ionisation Mass Spectrometry
Et_2O	Diethyl Ether
EtOAc	Ethyl Acetate
FRET	Förster Resonance Energy Transfer
FRP	Free radical polymerizations
GPC	Gel Permeation Chromatography
HPLC	High-performance Liquid Chromatography
HRMS	High Resolution Mass Spectrometry
HSQC	Heteronuclear Single Quantum Coherence
IP	Ionic Polymerization
IR	Infrared
ISC	Inter-system Crossing
IVR	Intramolecular Vibrational Energy Redistribution
LAM	Less Activated Monomer
LC	Liquid Chromatography
LCST	Lower Critical Solution Temperature

LED	Light Emitting Diode
MA	Methacrylate
MAM	More Activated Monomer
MCR	Multi Component Reaction
MD	Molecular Dynamic
MMA	Methyl Methacrylate
MO	Molecular Orbital
MS	Mass spectrometry
NaBARF	Sodium Tetrakis[3,5-bis(trifluoromethyl)phenyl]borate
NCS	n-Chlorosuccinimide
NMP	Nitroxide Mediated Polymerization
NMR	Nuclear Magnetic Resonance
PBS	Phosphate Buffered Solution
PEG	Poly Ethylene Glycol
PEGMEMA	Poly Ethylene Glycol Methyl Ether Methacrylate
PFP	Pentafluorophenyl
PMEDTA	N,N,N′,N″,N″-Pentamethyldiethylenetriamine
PSS	Photo Stationary State
PTFE	Polytetrafluoroethylene
RAFT	Reversible Addition−Fragmentation Chain-Transfer
RDRP	Reversible Deactivation Radical Polymerization
RF	Retention factor
RI	Refractive Index
ROMP	Ring Opening Metathesis Polymerization
SAM	Self-assembled Monolayer
SAS	Small Angle Scattering
SAXS	Small-angle X-ray Scattering
SCNP	Single Chain Nanoparticle
SEC	Size Exclusion Chromatography
TAD	Triazolinedione
TAM	Thioacetamide
TCCA	Trichloro Cyanuric Acid
TEM	Tunnelling Electron Microscopy
TEMPO	2,2,6,6-Tetramethylpiperidine 1-oxyl
THF	Tetrahydrofuran
TLC	Thin Layer Chromatography
TMS	Tetramethylsilane
TPPO	Triphenyl Phosphine Oxide
UCST	Upper Critical Solution Temperature
UV	Ultra Violet

Statement of Original Authorship

The work contained in this joint thesis undertaken between Queensland University of Technology (QUT) and Karlsruhe Institute of Technology (KIT) has not been previously submitted to meet requirements for an award at these or any other higher education institution. To the best of my knowledge and belief, the thesis contains no material previously published or written by another person except where due reference is made.

Signature: _____

Aidan Izuagbe

Date: _____

Acknowledgments

I would like to thank my principal supervisors Christopher Barner-Kowollik and Peter Roesky for their invaluable advice and guidance throughout the last 4 years of research. Additionally, I want to thank Professor Roesky for allowing me the experience to travel to Germany and conduct my research in a new country. I also want to thank my associate supervisor Bryan Tuten, not only for the extensive chemical knowledge he imparted, but also for his words of motivation in all things non chemistry related.

I would like to thank all the people who contributed to my research throughout the course of my PhD. David Marshall for his constant assistance in running the weekly mass spec runs and rectifying all problems I had (or more often caused). Vinh Truong for surprising me with new chemicals that I complained about needing. My honours supervisor Philipp Kamm for introducing me to the world of postgraduate research and afternoon beers at the bot bar, as well as Sandra Weidbrauk who guided me through my first thesis. I would also like to extend my thanks to Kai Mundsinger for his scientific advice, collaboration and for always making time to help. Katharina Ehrmann for her late-night inspirational talks about chemistry and perseverance and for always offering a hand when I needed it.

I would like to express my deepest appreciation for the Macroarc groups at both nodes. The best times during my PhD were with all the people I have had the pleasure of knowing from all different corners of the globe. I must also thank my fellow bay 1 chemists, who hands down made our bay the greatest bay to ever grace the Macroarc labs. I would also like to thank the Roesky research group who have helped me get settled in Germany.

I would also like to thank all my family back home in Australia, who have made this all possible from day one, inspiring an interest in science within me from an early age. Finally, I would like to thank my wonderful partner Rebecca who has supported me and stuck by me no matter what. Now we can finally go on holiday.

Academic Output

Publications in peer-reviewed journals:

- Visible Light Switchable Single-Chain Nanoparticles

  Aidan E. Izuagbe, Vinh X. Truong, Bryan T. Tuten, Peter W. Roesky, and Christopher Barner-Kowollik

  Macromolecules **2022**, 55, 20, 9242–9248

- Single Chain Nanoparticles in Catalysis

  Kai Mundsinger,* **Aidan Izuagbe**,* Bryan Tuten, Peter Roesky and Christopher Barner-Kowollik

  Angew. Chem. Int. Ed. **2023**, e202311734

  Contributed Equally *

Conference Contributions:

- Orthogonal Two Colour Switching of Single-Chain Nanoparticles

  Aidan E. Izuagbe, Vinh X. Truong, Bryan T. Tuten*, Peter W. Roesky*, and Christopher Barner-Kowollik*

  Advanced Polymers via Macromolecular Engineering (APME), **2023**

Covid Impact Statement

A portion of this thesis was completed during the COVID pandemic. Thus access to the laboratories was occasionally limited and international travel was severely impacted. In the case of the former, synthesis of polymers/small molecules and catalytic tests were impacted due to the occupancy limits placed on the laboratories, leading to the pursuit of less synthetically demanding approaches to afford the final SCNP designs to compensate for the reduced availability of laboratory access. The most significant effect of the COVID pandemic on the current research was the limitation of travel. The PhD program was to be completed as part of a joint program between the Queensland University of Technology (QUT) and the Karlsruhe Institute of Technology (KIT). The specialties of the supervisory teams at each university were to be applied to the different aspects of the PhD project. The synthesis of polymers/small molecules and their characterization along with photochemical analysis was to be completed at the QUT under the supervision of Prof. Dr. Christopher Barner-Kowollik. Characterization of their catalytic properties was to be completed at the KIT under the supervision of Prof. Dr. Peter Roesky. Due to the strict travel restrictions imposed by the Australian government, travel from QUT to the KIT in Germany was not possible until the final year of the PhD program. Consequently, catalytic experiments were critically delayed until this time. As a result, focus was placed on other project aspects that were not the primary focus of initial PhD and could be completed while in Australia.

1 Introduction

Catalytic systems play an important role in our lives, from their fundamental use in chemical industry and research, to their critical role in biological systems. Enzymes serve as the gold standard for catalytic performance and bear sequence-defined macromolecular architectures that fold into highly precise secondary and tertiary structures.[1] This precise folding culminates in shielded catalytic pockets, facilitating a highly selective binding of specific substrates in complex biological media.[2] Additionally, enzymes display both properties of homogenous and heterogenous catalysts. They remain in the same phase as substrates to enable high selectivity, while also being relatively easy to recover due to their polymeric nature.[3,4] On the other hand, synthetic catalysts are conventionally either homogeneous or heterogenous, where homogenous catalysts display preferable catalytic properties over heterogenous equivalents. Isolating and reusing homogeneous catalysts from a reaction mixture is a common issue, often requiring extensive workup procedures.[5] Furthermore, many homogeneous catalysts are comprised of metal complexes, posing additional problems in terms of environmental effects. Chemists looking to overcome the recyclability of homogeneous catalysts have focused their attention on the specific structural properties of enzymes. Polymeric catalysts known as Single Chain Nanoparticles (SCNPs) are one such 'bio-inspired' catalyst. SCNPs consist of a single linear polymer chain, folded intramolecularly to generate a discrete nanoparticle. SCNPs have been shown to achieve catalytic properties akin to that of enzymes and are therefore imbued with catalytic functionalities, often via transition metal complexes. Such favourable catalytic properties, much like enzymes, are owed to the folded macromolecular scaffold, which has the potential for increased substrate selectivity.[6,7] The polymeric nature of catalytic SCNPs means they are able to be easily recovered via techniques such as precipitation, and reused for multiple catalytic cycles. A goal for SCNP design is achieving dynamic control over the morphology of the polymeric scaffold, in order to control catalysis.[7] Although dynamic morphological control through a variety of methods is possible, light remains highly appealing for its temporal control and milder conditions. Light can also be adapted to either an existing SCNPs morphology or to

the folding of a linear polymer into an SCNP.[8,9] Both of these concepts are explored in the present thesis to generate metal-functionalised photoresponsive SCNPs.

Chapter 2 provides an overview of polymer chemistry with an emphasis on controlled free-radical polymerizations. Fundamental photochemistry principles are also discussed, followed by an introduction into the photo-active groups, azobenzenes and spiropyran used in the present thesis. Finally, SCNPs are discussed in-depth, first introducing their synthesis and characterization and then focusing on metal-functionalised SCNPs and dynamically controllable SCNP morphologies.

Chapter 3 outlines the research gaps in the current literature and lists the research aims and objectives of the thesis.

Chapter 4 details the design of a linear, gold-decorated polymer that is intramolecularly crosslinked via visible light-addressable azobenzene photoswitches into a photoresponsive catalytic **Azo-SCNP**. The photoswitching properties of the SCNP are described and it is investigated as a photoresponsive catalyst for the hydroamination of alkynes.

Chapter 5 proposes a new method of light-induced folding of a linear polymer decorated with spiropyran photoswitches into an SCNP through the photo-induced generation of spiropyran metal complexes. The variability of the metal complexes, as well as the reversible nature of the formed spiropyran complexes are investigated and preliminary results are presented.

Chapter 6 summarises the critical findings of the present thesis.

Chapter 7 provides an outlook on the direction of future research relating to the SCNP systems introduced in the present thesis.

2 Literature Review

2.1 Polymer Chemistry

2.1.1 Polymer Fundamentals

The process of polymerization derives from the Greek words *polys* (many) and *meros* (part).[10] Combining low molecular weight subunits known as monomers in a repetitive fashion generates macromolecular structures known as polymers. The earliest description of a polymer like molecule came from the Swedish chemist Jöns Jacob Berzelius, who in 1833 described molecules with the same empirical formula differing only in their overall molecular weight.[10] His description was limited in the fact that it only considered the number of atoms in a molecule meaning that glucose ($C_6H_{12}O_6$) could be considered a polymer of formaldehyde (CH_2O). Nonetheless, Berzelius' description served as the nucleation point for the field of polymer science. Advancements in polymer synthesis came with early examples of rubber vulcanization by American and British chemists in 1843.[11] The first synthetic polymer was developed by Belgian chemist Leo Bakeland in 1907, who by heating phenol and formaldehyde in an early form of a condensation polymerization generated a hard thermoset polymer finding wide spread use in a plethora of products.[12] Despite these discoveries a suitable description and understanding of a polymer was still lacking. It was not until almost a century after Jöns Jacob Berzelius description that Hermann Staudinger in 1919, a German chemist, described polymers as monomers being linked via covalent bonds. This deviated from earlier definitions that described polymers as colloids or aggregates held together by secondary forces.[13] It took some time for Staudinger's work to be recognised, after which polymer science truly became its own field of study. Comparatively modern synthetic polymers such as Nylon and Teflon owe existence to Staudinger's description.

Polymers consisting of linked monomers can be described in terms of their degree of polymerization (*DP*), which is a measure of the average number of monomers in a single polymer chain.[14,15] For polymers consisting of a singular monomer type this is given by equation 1, where M_n is the overall molecular weight of the polymer sample and M_o is the molecular weight of the monomer.

Unless stated otherwise chapter 2.1.1 is based off books by Odian.[14] and Stevens[15]

$$DP = \frac{M_n}{M_o}$$ **equation 1**

M_n can be derived by equation 2, where N_i is the number of molecules of certain mass and M_i is the mass of a polymer chain *i*.

$$M_n = \frac{\sum N_i M_i}{N}$$ **equation 2**

At the end of a polymerization, a statistical distribution of polymers with different chain lengths arises. In addition to the average number molecular weight, M_n, the weight average molecular weight M_w is used, describing the weight average of the sample equation 3.

$$M_w = \frac{\sum N_i M_i^2}{\sum N_i M_i}$$ **equation 3**

A sample where all chains are the same length, is termed a monodisperse polymer, where dispersity is represented as *Đ* (equation 4). In statistical polymerizations, monodispersity cannot be achieved and polymers are typical described as polydisperse.

$$Đ = \frac{M_w}{M_n}$$ **equation 4**

Due to synthetic polymer's inherent structural ambiguity, specific characterization techniques are required to determine the size as well as morphologies of polymers. The most common technique for the determination of polymer size is Size Exclusion Chromatography (SEC). SEC involves passing an ensemble of polymer chains in solution through a gel column consisting of beads with varying pore sizes. Elution through the column is controlled by the exclusion or inclusion of the polymer into these pores. Large polymers will enter fewer pores, while smaller polymers will be able to enter a greater number of pores, resulting in a shorter retention or longer retention time, respectively. In SEC, the elution time of a polymer is proportional to

the intrinsic viscosity of the polymer, allowing for the determination of relatively accurate molecular weights utilising the Mark-Houwink equation, where η is the intrinsic viscosity K and α are solvent polymer specific parameters – also known as the Mark-Houwink parameters (equation 5).

$$\eta = KM^{\alpha} \qquad \textbf{equation 5}$$

2.1.2 Free Radical Polymerization

Polymerization techniques are typically divided into two classes, step-growth, and chain-growth polymerizations. Step-growth polymerizations are defined by a constant and rapid consumption of bifunctional monomer units into dimers, trimers and eventually polymers with relatively high dispersity, Đ > 2.[16,17] Chain growth polymerizations are generally defined by the continuous addition of monomers to an initiating centre, growing linearly, one monomer at a time resulting in the growth of a polymer chain.[18] Chain growth polymerizations differ from each other based on how they initiate and subsequently propagate. Common chain growth techniques include Ring Opening Metathesis Polymerization (ROMP)[19], Ionic Polymerization (IP)[20] and Free Radical Polymerizations (FRP)[21], the latter of which constitutes the focus of the current section. Chain growth polymerizations consist of three steps, the generation of the active centre, propagation of a polymer chain from the active centre, and termination of the propagating polymer.[22] FRP initiation begins with the introduction of free radicals via the homolysis of radical initiators, mostly commonly thermally labile azo initiators such as azobisisobutyronitrile (AIBN) or peroxides.[23,24] Initiators able to absorb light and generate a radical via an excited state allow for photo-initiated free radical polymerizations.[25] In addition, to photo and thermal initiated polymerizations external stimuli such ionising radiation or sonication have also been used for FRP initiation.[26,27]

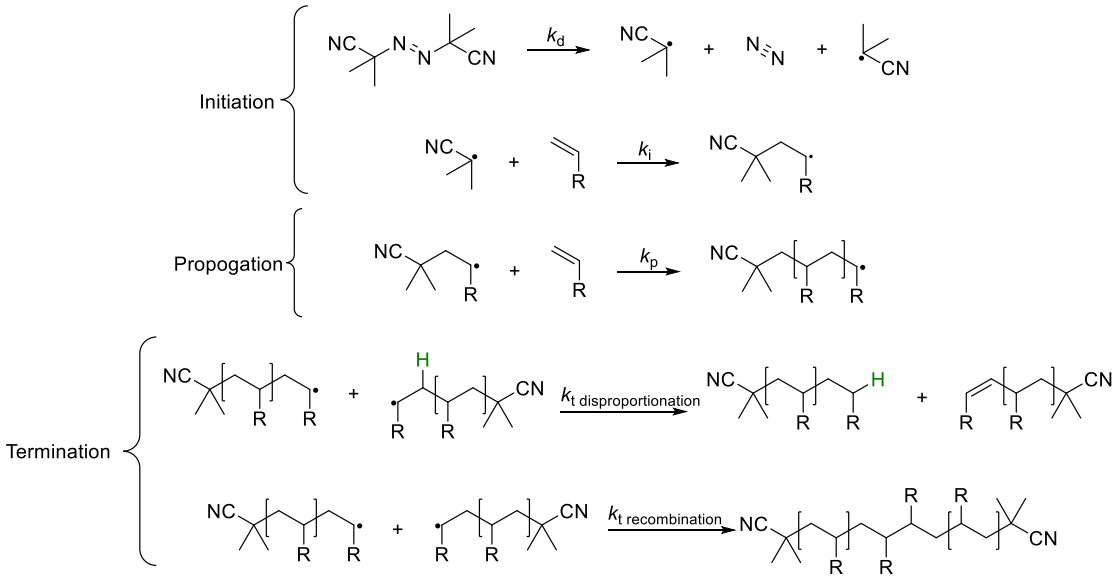

Figure 1. Fundamental steps of free radical polymerizations

Thermal decompositions of AIBN as an example, results in the formation of free radicals able to initiate macromolecular growth with suitable monomers. The active centre is known as a propagating radical, formed through the attack of a free radical to the π bond of a monomer bearing an unsaturated carbon. The attack results in the formation of a new σ bond between the radical and the monomer, while generating a new free radical on the more stable carbon of the monomer, able to attack a second monomer.[28] Consequently, an unsaturated carbon is fundamental to free radical polymerization, and all FRP monomer classes bear these, e.g acrylates, styrenics, methacrylates and acrylamides.

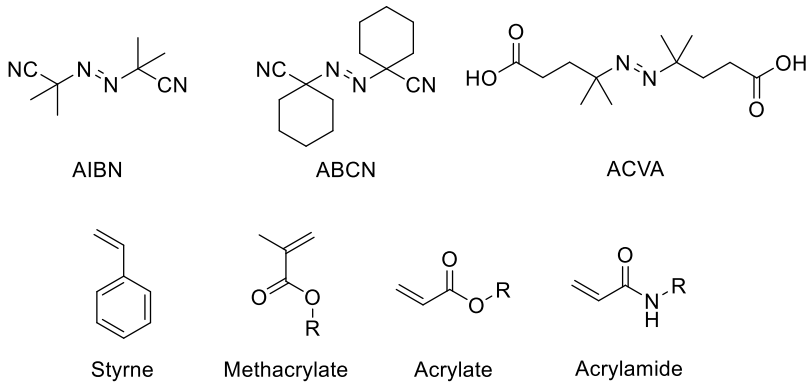

Figure 2. Commonly used initiators and monomers in FRP

Once a propagating radical is formed, an additional monomer adds via radical attack and subsequent radical formation. The process continues and extends the polymeric chains. An initiator species (I) that decomposes into two radicals (R) with a rate coefficient k_d can be described by Figure 3. Here only a fraction (f) of the generated radicals will become polymerizing radicals. Two radicals (R) terminate either via recombination or disproportionation with a rate co-efficient k_t.[29,30]

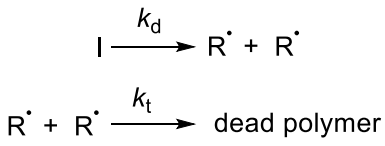

Figure 3. (top) Disassociation of an initiator species into two radicals (bottom) radical-radical termination leading to dead chains.

This leads to equation 6 which describes the concentration of radicals, (R) over time.

$$\frac{d[R]}{dt} = 2fk_d[I] - 2k_t[R]^2 = 0 \qquad \textbf{equation 6}$$

Following initiation, polymerization proceeds into the propagation phase, where the quantity of initiated radicals matches the quantity of terminated radicals. Active radicals attack monomers leading to the formation of a new bond and new radical centre on the growing chain. The relatively stable radical concentration allows for the simplification of equation 6 with a steady state assumption resulting in equation 7.

$$[R] = \left(\frac{fk_d[I]}{k_t}\right)^{\frac{1}{2}} \qquad \textbf{equation 7}$$

Addition of monomers to a radical is explained by equation 8, with a rate coefficient of k_p.

$$\frac{-d[M]}{dt} = k_p[M][R] \qquad \textbf{equation 8}$$

Substitution of equation 7 into equation 8 results in a simple solution for the rate of polymerization (equation 9).

The derivation of free radical polymerization rate is sourced from the book "Handbook of Radical Polymerization"[30]

$$R_p = k_p[M]\sqrt{\frac{f k_d[I]}{k_t}}$$ **equation 9**

R_p = Rate of propagation

k_p = Propagation rate coefficient

k_d = Dissociation rate coefficient of the radical initiator

k_t = Average (termination) rate coefficient

[I] = Initiator concentration

[M] = Monomer concentration

f = Initiator efficiency

The termination during FRP occurs via two main processes, either by chain recombination or disproportionation, both occurring due to radical-radical coupling reactions. Recombination describes the process by which the radicals on two propagating chains combine to form a new σ bond, observed as a new polymer with a doubled molecular weight.[31] Disproportionation occurs when a hydrogen atom from the end of one polymer is abstracted to a second polymer. A terminal saturated end group is formed on the chain that abstracts a hydrogen, and an unsaturated terminal group forms on the other polymer.[32] Propagating radicals are also able to undergo a process known as chain transfer, where an end group radical is transferred to a new position on a polymer chain either intra or intermolecularly. This leads to a propagating side chain impurity[33] (Figure 4).

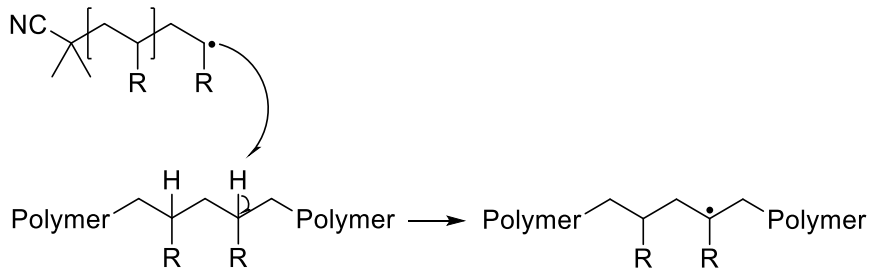

Figure 4. Chain transfer of an end-group, propagating radical to a new position on a polymer.

The rate of termination R_t can be described in terms of the rate coefficient k_t and the concentration of radicals, R in the polymerization (equation 10).[29]

$$R_t = -2k_t[R]^2 \qquad \textbf{equation 10}$$

Chain termination is a diffusion-controlled process in contrast to propagation which is chemically controlled and to a lesser extent, diffusion controlled.[34] When the monomer concentration is low due to a high degree of polymerization and large polymers, the viscosity of the solution increases and the translational diffusion of growing polymers through the reaction medium decreases.[35] Consequently this leads to k_t being chain length dependent, as larger polymers diffuse slower than smaller polymers.[36] As a result, termination reactions between growing polymers also decrease as they no longer are able to collide with each other and terminate. Critically, the rate of propagation is not dramatically affected by the increase in viscosity as the small molecule monomers are still able to diffuse through the reaction medium. Under isothermal conditions this results in an auto acceleration process known as the *Trommsdorf effect* or *gel effect*.[37] For FRP it is important that the polymerization is conducted in a solvent with a high enough dilution, that this critical point is not reached, quenching the polymerization before this effect takes place is also important. Termination during FRP also occurs via the radical interactions between impurities, most notable the combination with dissolved oxygen which results in a chain end bearing a less reactive oxygen centred radical.[38] Chain termination throughout the polymerization consequently leads to high dispersity polymers during the FRP process. When very narrow distributions and targeted molecular weights are required, conventional FRP cannot be employed. In FRP the highest molecular weight polymers are achieved at that beginning of the polymerization, with molecular weight gradually decreasing throughout the course of polymerization.[39] FRP constitutes a cost-effective chain growth technique that finds extensive usage in industrial applications.[40]

Furthermore, the uncontrolled termination products leave little possibility for further chain extension into more complex macromolecular architectures such as block co-polymers. To achieve highly precise molecular weights, low dispersities and access to

complex architectures, radical polymerizations that minimize termination reactions and retain end group functionality are needed.

2.1.3 Reversible-Deactivation Radical Polymerizations (RDRP)

Being able to precisely target molecular weights with low dispersities is an appealing aim for polymer chemists. Polymers displaying such precision are afforded characteristics that make them highly useful in a variety of applications.[41–45] Critical to generating polymers with low dispersities and precise molecular weights is the preclusion or minimization of chain termination events.[46] In the 1950's, styrene was polymerised via the addition of an electron from an anionic radical to the unsaturated carbon of styrene, forming a carbanion ion able to add to another styrene, coined anionic polymerization. Using a carbanion as the propagating species meant that bi-molecular termination reactions between two polymers were not possible. Polymers grown using anionic polymerization grow until complete consumption of the monomer occurred.[47] The rate of initiation in anionic polymerization is drastically faster than the rate of propagation, meaning that all polymer chains begin growing at the same time and same rate. This absence of termination events and the rapid initiation lead to polymers with very narrow dispersity. The term 'living' is used to characterise such polymers.[48] The molecular weight throughout a living polymerization will be linear with respect to monomer conversion. In contrast, FRP rapidly consumes monomer at the start of the polymerization resulting in the highest molecular weights, decreasing as the reaction continues.[39] Furthermore, due to the absence of chain termination, end-group manipulation is accessible. The ability to chain-extend from the anionic chain termini affords an efficient route to the formation of block copolymers[49,50] with even more complicated architectures such as graft copolymers possible.[47] In the case of anionic polymerization, a low tolerance to impurities and diverse functional groups hampered its use in a large number of applications.[51] Consequently, polymerizations displaying living characteristics that show tolerance to impurities and functional groups was necessary.

Reversible Deactivation Radical Polymerizations (RDRP) is one such technique, using radicals as the propagating species in place of an anion, they display a higher tolerance to impurities and monomer functionalities.[52] Techniques covered under the umbrella term of RDRP typically display some sort of reversible deactivation of the propagating

chain facilitated by a control agent.[53] This reversible process leads to a reduction in the number of termination events that occur – while not entirely removed – resulting in polymers with narrow dispersitys.[54] Consequently, the increasing molecular weight during the polymerization is linearly correlated with the consumption of monomers owed to the end group fidelity.[55] The retention of the end group readily allows chain extension and the generation of complex macromolecular architectures using RDRP techniques is common. Due to the inevitable yet minimised radical-radical couplings that occur, RDRP techniques are not truly living, instead they are described as "pseudo living" or less deprecative, controlled polymerizations.[54] RDRP techniques are generally classed into one of three techniques, the first known as Nitroxide Mediated Polymerization (NMP) discovered by the Commonwealth Scientific and Industrial Research Organization (CSIRO) in Australia.[56] Atom Transfer Radical Polymerization (ATRP), implemented first by the groups of Matyjaszewski[57] and Sawamoto[58] and Reversible Addition Fragmentation Transfer Polymerization (RAFT) again by the CSIRO.[59] NMP and RAFT polymerization are the primary RDRP techniques used within this thesis so they will be discussed in the subsequent sections.

2.1.4 Nitroxide Mediated Polymerization

NMP utilises alkoxyamine initiators, formed utilising a sterically hindered nitroxide precursor, to polymerise typically, styrenes, acrylates and acrylamides. The alkoxyamine NO-C bond is thermally labile, yielding two different radical fragments at temperatures typically higher than 100 °C.[60] The first is a stable radical centred on the oxygen of the nitroxide and the other is a more reactive carbon centred radical responsible for chain propagation. After a short amount of time propagating, the radical centred on the polymer chain recombines with the nitroxide radical, temporarily capping the growing chain. This new alkoxyamine bond formed between the chain and the nitroxide is able to be cleaved thermally, regenerating the propagating radical in a reversible process.[61] The process is defined by the equilibrium $k_a \leftrightharpoons k_d$ where k_a is the rate coefficient of activation of the propagating radical and k_d is the deactivation upon combination with a nitroxide.[46]

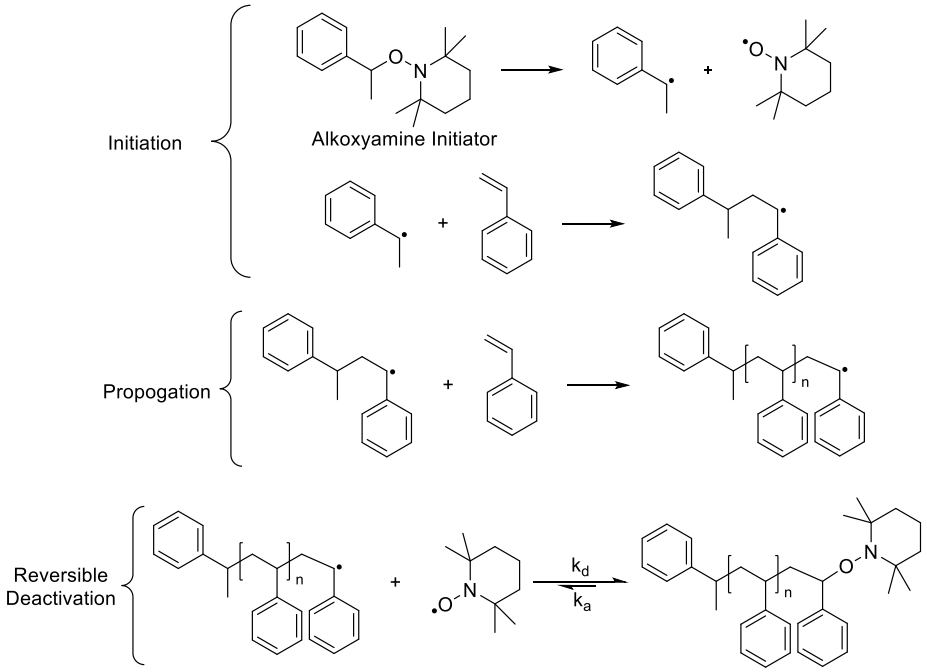

Scheme 1. Generalized overview of nitroxide mediated polymerization using the example of styrene polymerization.

Integral to NMP is the persistent radical effect. Due to the transient nature of the propagating radical, it will rapidly react with a new monomer or couple either irreversibly with another radical or reversibly with the stable nitroxide radical.[62,63] During NMP, the nitroxide is the persistent radical and as the transient radical combines irreversibly with itself, nitroxide concentration increases respectively. This increase in concentration means that chain termination events occurring via recombination or disproportionation are reduced as the propagating chain tends to recombine with the persistent nitroxide radical shifting the equilibrium so that $k_a << k_d$. Nitroxides utilized in NMP are themselves unable to initiate polymerization or undergo self-dimerization making them a suitable persistent radical. Their stability is primarily owed to the mesomeric structures formed between the high energy delocalization of the unpaired electron between the nitrogen and oxygen atoms.[61] Variation of the groups that are attached to the nitroxide functionality strongly affect the observed stability. As an example, a nitroxide attached to a phenyl group will display increased stability owing to an increase in delocalization. However, due to delocalization, electron density increases at the aromatic carbon *para* to the nitrogen and results in a cross combination between two nitroxides.[64] Thus, simply increasing the delocalization energy is not necessarily the best way to further increase nitroxide

stability. Judicial selection of inert, bulky substituents α to the nitrogen prevents two nitroxides from combining in a radical-radical coupling. TEMPO based initiators are commonly used for these reasons, as well they are relatively easy to synthesize and cheap.[61,65]

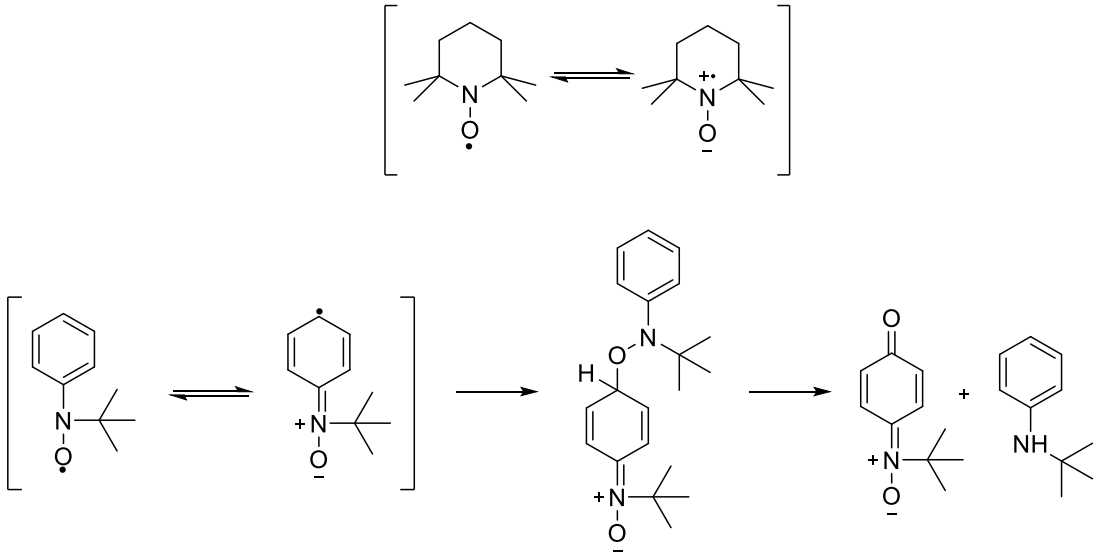

Scheme 2. (Top) Mesomeric resonance structures of a TEMPO radical. (bottom) Radical cross-coupling of a phenyl substituted nitroxide.

NMP is considered to contain the simplest initiator system of the RDRP techniques, requiring only a single reagent in the nitroxide initiator, acting as both radical source and the controlling agent. There are no additional reagents left in the polymerization that need to be removed.[66] In the case of ATRP, metal impurities pollute the polymer and require additional purification. NMP also circumvents the use of the unpleasant sulphur chemistry required for RAFT polymerizations. The simplistic nature of NMP implies that there is less room to fine tune the reaction kinetics compared to other RDRP techniques that utilise multiple reagents for initiation and control.[67] Another disadvantage is the requirement of high temperatures, especially when using TEMPO initiators to cleave the alkoxyamine bond and generate radicals. As mentioned at the start of this section, typical temperatures often exceed 100 °C and limit the diversity of monomers able to participate in NMP.[68] Replacement of TEMPO based initiators with nitroxides that display higher disassociation rates can be used to conduct NMP at lower temperatures. Commonly employed are N-*tert*-butyl-2-methy-l1-phenylpropyl nitroxide (TIPNO) and the commercially available N-*tert*-butyl-N-(1-diethylphosphono-2,2-dimethylpropyl) nitroxides (SG-1).[69] Using SG-1 based

initiators, polymerizations of vinyl chloride have been completed at temperatures as low as 40 °C.[70]

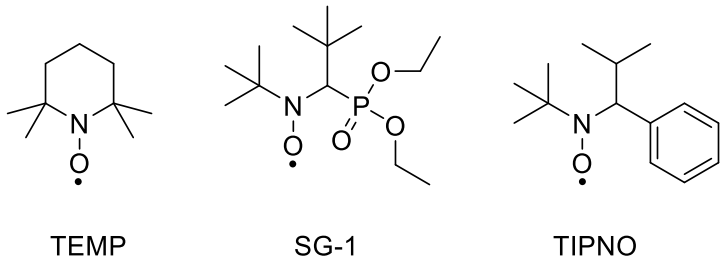

Figure 5. Commonly used nitroxide initiators

Methacrylates also find limited use in NMP, with low conversions and high dispersity reported.[71] The poor polymerization performance of methacrylates during NMP is due to the preference of disproportionation between the methacrylate radical and the nitroxide radical as opposed to the reversible deactivation.[71] Disproportionation is particularly prevalent with TEMPO initiators, but is also evident with SG-1 and TIPNO based initiators arising from a β-hydrogen transfer from the propagating methacrylate unit and the initiator.[72] NMP with methacrylate monomers has been achieved via the use of additives that stabilize the nitroxide, [73,74] as well as via copolymerization with suitable NMP monomers such as styrene derivatives.[75,76] Despite limitations that NMP bears over other RDRP techniques, its ease of use and minimal need for purification means it is still readily used for the generation of complex architectures. Applications, were purification is necessary and difficult such as in electronic device manufacture, in sensitive biological systems or green technologies can benefit from the aforementioned properties of NMP over other RDRP techniques.[66,77–80]

2.1.5 Reversible Addition Fragmentation Transfer (RAFT) Polymerization

The other RDRP Polymerization technique utilized in the current thesis is Reversible Addition Fragmentation Transfer (RAFT) polymerization. RAFT polymerization utilizes a sulfur-based thiocarbonylthio – or related – agent that facilitates the transfer of propagating radicals from one chain to another, effectively distributing a set number of radicals over the entire population of polymer chains.[59,81] True deactivation like the capping of propagating radicals with nitroxides as achieved in NMP is not present

in the RAFT process. Instead, the propagating radicals react with the RAFT agent forming a stable RAFT radical adduct intermediate. The generalized mechanism is presented in Scheme 3. Initiation of RAFT polymerizations differs from NMP in that a radical source is needed in addition to the RAFT control agent also known as the chain transfer agent (CTA). As in conventional FRP, the primary radicals are often provided by thermally activated azo initiators like AIBN, which generate two radicals that attack the unsaturated carbon of a monomer and initiate macromolecular growth.[82] The initial polymeric radical subsequently attacks the thiocarbonyl sulfur of the RAFT agent and generates a tertiary carbon centered radical. The first radical intermediate adduct either fragments back into the starting species or into a new radical able to initiate polymerization and a polymeric RAFT agent. Monomers continue to add propagating radicals before recombining with the polymeric RAFT agent and transferring the radical to the polymer previously attached to the RAFT agent. This transfer is considered as the most significant part of RAFT polymerization and in ideal circumstances is equally completed over all dormant polymer chains that have not undergone termination. The rate of polymer propagation should be significantly lower than the rate of addition/fragmentation of the polymeric RAFT agent.[83] In this case, less than one monomer will be added per one addition/fragmentation event, ensuring that propagating polymers will be approximately the same size as each other throughout the course of the polymerization.

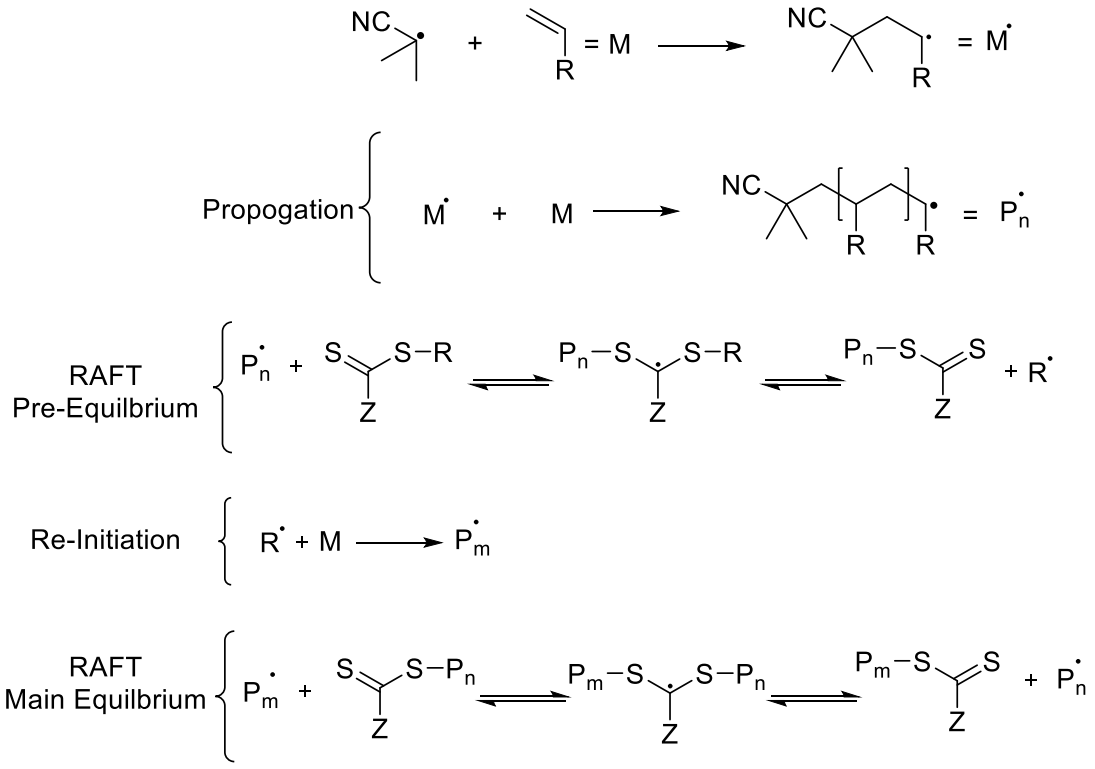

Scheme 3. Generalised RAFT polymerization mechanism.

Termination in RAFT polymerizations occurs much like in other RDRP techniques. It is important to note that the exact number of dead chains generated from RAFT can be directly predicted by the number of initiator molecules introduced into the system.[84] If two primary radicals are introduced, then only two dead polymers will be present at the end of the polymerization constituting a high living character. RDRP techniques such as NMP and ATRP will continue to generate radical species even at 100% monomer conversions, resulting in many termination events and dead polymers.[85] A consequence of the high livingness of RAFT is the ease of chain extension when compared to other RDRP techniques. Unlike ATRP and NMP, RAFT does not possess any inherent rate retardation due to the transferal of radicals to the RAFT agent generating dormant radicals as opposed to actual deactivation of radicals as in ATRP and NMP.[36] The design of the RAFT agent plays a significant role in the polymerization process, controlling the main equilibrium between dormant and active chains throughout the course of polymerization. As mentioned previously, a higher rate of CTA-radical coupling is critical to an efficient process. Preferential CTA coupling is achieved by ensuring that the C=S bond is more reactive towards addition of a radical than the C=C bond of a monomer.[86] Adjusting, the R and Z groups is used

to modulate the reactivity of RAFT agents primarily as a consequence of the monomer intended for polymerizations.[87] Judicious selection of Z and R groups affords a diverse range of monomers compatible with RAFT. Monomers employed for RAFT are generally categorized as either a more activated monomer (MAM) or as a less activated monomer (LAM). MAMs are those monomers where the double bound is conjugated with aromatic substituents, a nitrile, or carbonyl groups, LAMs posses' double bonds adjacent to an oxygen, nitrogen, or halogen or to an unsaturated carbon.[86]

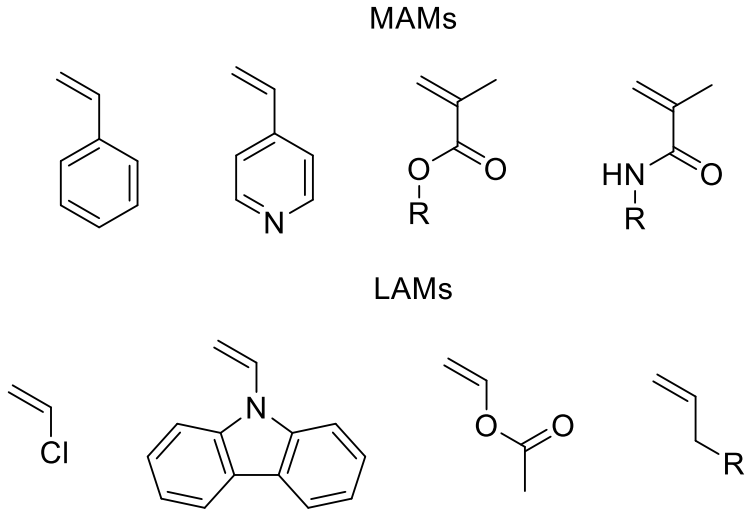

Figure 6. (Top) More activated monomers (MAMs): styrenics, heteroaromatics, methacrylates and methacrylamides. (Bottom) least activated monomers (LAMs): vinyl halides, N-carbazole, vinyl acetate, alkenes.

The Z group primarily stabilizes the generated tertiary radical of the RAFT radical intermediate species. For MAMs, displaying a relatively stable monomer radical, increasing the stabilizing effect of the Z group is critical to ensure that the radical, centered between the sulfur atoms and generated upon monomer addition, is preferably formed. The inverse is true for radicals centered on LAMs, a less stabilizing Z group is required for an effective polymerization.

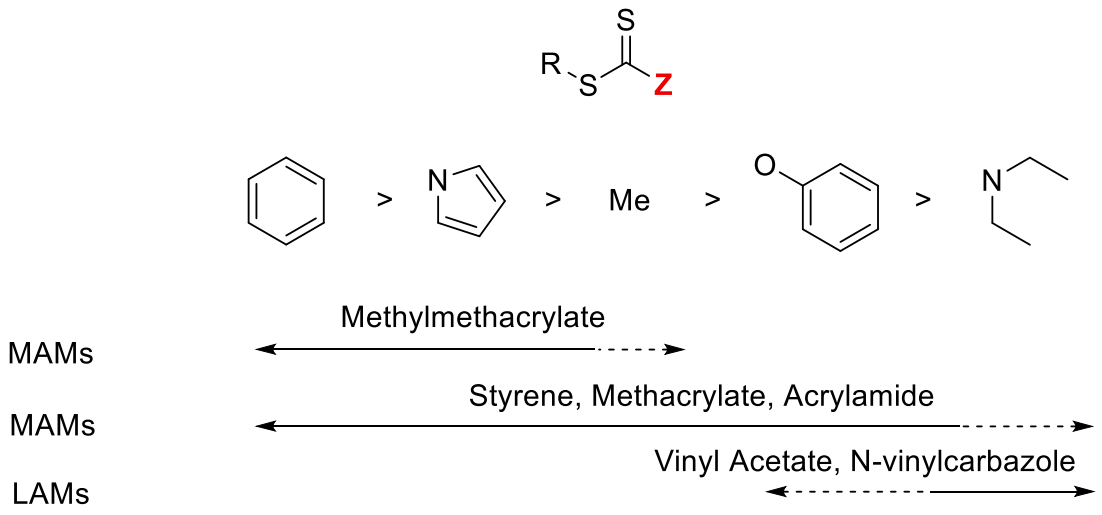

Figure 7. Compatibility of stabilising Z groups with various monomers/monomer classes.

The R group is primarily chosen to ensure a high rate of fragmentation from the RAFT group and subsequently also displays a high potency for reinitiating the polymerization process. Thus, the R group has to balance being a sufficiently good leaving group to ensure fragmentation, but also possess a highly reactive radical to enable its swift reaction with the monomer unit, resulting in an opposite reactivity trend compared to the Z group, i.e. more reactive R groups are required to propagate LAMs while less reactive are required for MAMs.

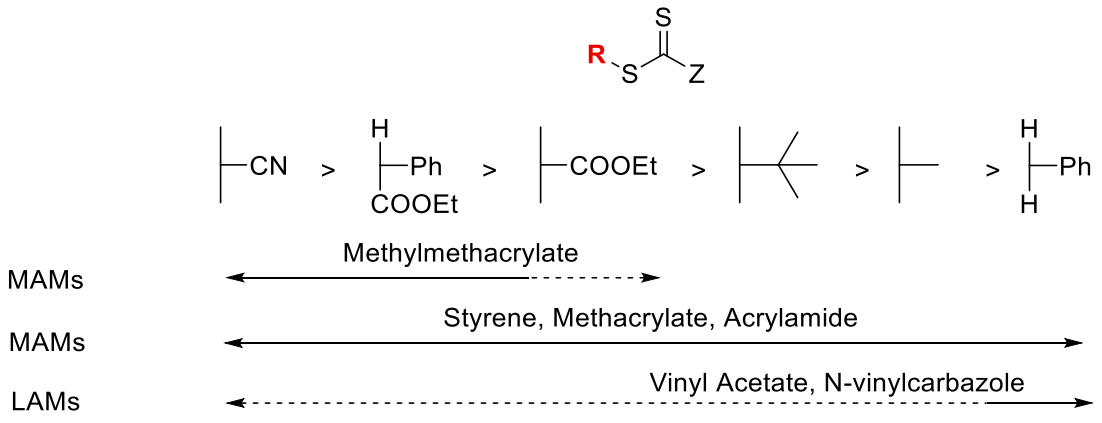

Figure 8. Compatibility of stabilising R groups with various monomers/monomer classes.

2.2 Photochemistry

2.2.1 Photochemistry Fundamentals

Photochemistry is the field of chemistry that describes the interactions of light with molecular compounds. Driving chemical reactions with light – while not always well understood throughout history – has long been observed and used to generate distinct properties in materials. Ranging from light induced bleaching of fabrics in 1000 BC by the ancient Egyptians to spoiling of gun cotton when exposed to ultraviolet light (UV), photochemistry has consistently been part of human civilization.[88,89] Modern synthetic chemists strive to employ light into chemical processes, where chemical reactions can be activated by light, affording milder reaction conditions and spatiotemporal control.[90,91] The prerequisites for chemical changes induced by light were first described by Grotthus in 1817[92] and Draper in 1842,[93] stating that for a photochemical reaction to take place light must first be absorbed. A fundamental understanding of the concepts underpinning the transformation of matter by light was developed in 1837 by Trommsdorff.[94] He described the yellowing and subsequent 'explosion' of santonin crystals upon exposure to sunlight, the product of which was later identified as a photorearrangement reaction. More photochemical processes such as photodimerization[95] and photoisomerization[96] followed and helped to place photochemistry into the mainstream of scientific rhetoric. Since these early experiments, photochemistry has seen several theoretical and technological advancements. Better descriptions of photochemical events via quantum mechanical processes and improved methods of irradiation with lasers and LEDs has meant that the field of photochemistry now has a wide variety of applications.[97–100]

The *Grotthus-Draper* law states that for a photochemical process to occur, light must first be absorbed. In a more modern context, this law describes how a photon of a certain wavelength is absorbed by a molecule, causing an electron to transfer into an excited state. It is from this state that photochemical processes occur.[93] The electron relaxes to a pre-absorption ground state through several electronic pathways. A molecule's absorptivity is defined as the ratio between incident light that hits a solution and the transmitted light containing a molecule. Beer-Lambert's law correlates this experimentally observed absorptivity to the molecule's intrinsic molar extinction coefficient as well as its concentration and the path length which the light travels

through. The molar extinction coefficient is an intrinsic property of the molecule and is used to correlate the absorptivity to concentration.[101]

$$A = \varepsilon l c \qquad \textbf{equation 11}$$

A = Absorbance
ε = Molar Extinction Coefficient
l = Optical path length
c = Concentration

When considering the excitation of electrons within a molecule, understanding the three-dimensional configurations of molecular orbitals is critical. The wavelike properties of electrons means that the probability of finding an electron around a nucleus is determined by its wave function. When two nuclei are chemically bonded via their electrons, a molecular orbital (MO) forms. However, as the electrons behave like waves, the corresponding wave functions interfere constructively and destructively. This generates bonding (σ, π) and antibonding orbitals (σ^*, π^*). Antibonding orbitals are regions of destructive wave interference typically denoted by '*' in energy diagrams. A third type of orbital contains electrons that do not take part in the chemical bond, known as a non-bonding orbital (n). Non-bonding orbitals typically contain lone pair electrons such as those on nitrogen and oxygen. Upon absorption of a photon, an electron in a bonding or non-bonding molecular orbital is excited into a higher energy anti-bonding molecular orbital (Figure 9). Once excited, the electron can relax via several mechanisms back to its original bonding orbital.

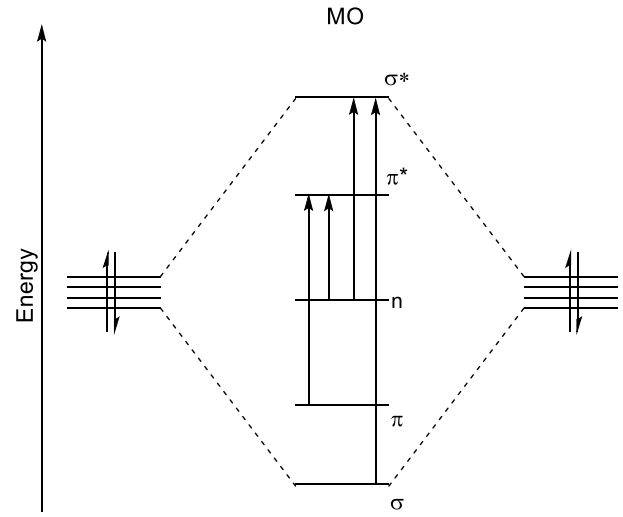

Figure 9. Molecular orbital diagram, common electronic transitions are represented by vertical arrows.

Electronic transitions are described by the Frank-Condon principle, [102] which states that the probability of an electronic transition between two electronic states is a direct result of the overlap between the vibrational wave functions of the two states. This transition occurs vertically without an immediate change to the nuclear geometry of the molecule. This can be further explained by the *Born-Oppenheimer* approximation which assumes that the nuclear geometry of a molecule is considered static. This assumption is rooted in the fact that electronic transitions occur orders of magnitude faster than any corresponding nuclear re-configurations due to the massive size of nuclei compared to electrons.[103]

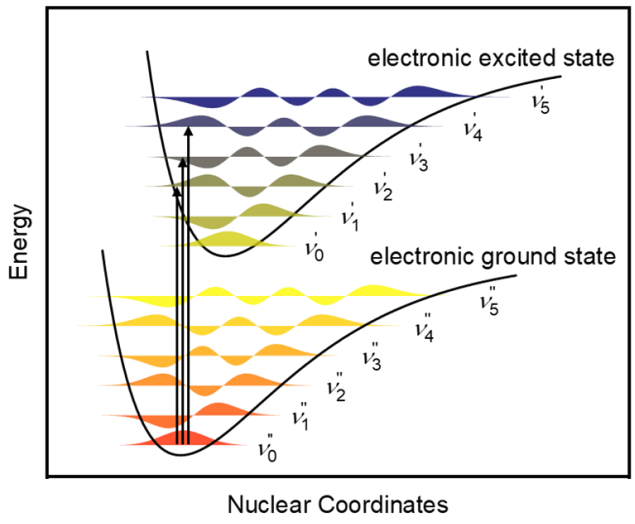

Figure 10. Frank-Condon principle energy diagram depicting the vertical excitation between vibrational levels of a ground state and of an excited state. Adapted from Ref[104]

The two vibrational wave functions between a ground and excited state need to significantly overlap to better facilitate this transition.[105] Once the transition has occurred, the molecule relaxes to a vibrational ground state within its electronically excited level. This process is known as Intramolecular Vibrational Redistribution (IVR).[106] Relaxation back to the ground state can occur via numerous radiative and non-radiative processes, which can be described in a so called Jablonski diagram.

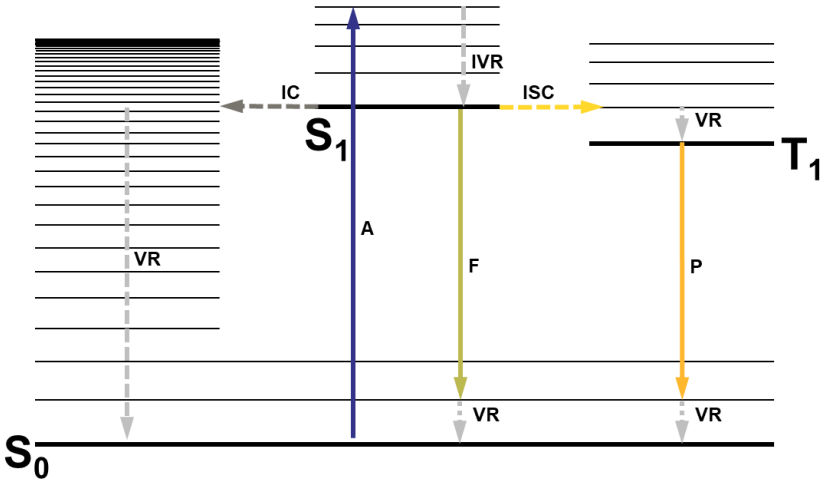

Figure 11. Jablonski diagram highlighting the primary radiative (straight arrows) and non-radiative (dashed arrows) decay pathways after excitation via absorption. Adapted from Ref [107]

Among the non-radiative pathways is the previously mentioned IVR, as well as vibrational relaxation (VR) which can involve the transfer of vibrational energy to the surrounding environment such as solvent molecules. When the vibrational levels of a ground and excited state overlap, a non-radiative transition into an isoenergetic vibrational level of a lower state can occur, this is known as internal conversion (IC).[108] Radiative relaxation from an excited singlet state S_1 into the ground state generates fluorescence as a consequence of photon emission.[109] The corresponding wavelength of the photon is proportional to the energy gap between the lowest vibrational level of the excited singlet state and a corresponding vibrational level in the singlet ground state. A molecule in an excited S_1 state can enter a process known as intersystem crossing (ISC).[110] When ISC occurs, an electron undergoes a spin forbidden transition from its singlet excited state into an excited triplet state. Molecules existing in the excited triplet state have the potential to participate in a multitude of photochemical reactions including photocycloadditions,[111] photo-initiator

cleavage[112] and photoenolization.[113] Radiative relaxation from the triplet state is also possible through a process known as phosphorescence.[114] Like fluorescence, this process includes the emission of a photon with a wavelength proportional to the energy gap between the lowest state in the excited triplet and singlet ground state.

2.2.2 Photoswitches

Photoswitches are a diverse class of molecules capable of isomerization upon absorption of light. Reversible isomerization is achieved, either upon exposure to a complimentary wavelength of light, via a thermally driven relaxation process, or both.[115] Photoswitches can be categorised based on their photochromism; a term used to define reversibility of two isomers upon photoexcitation. Two primary forms of photochromism are important for photoswitches, T- and P-type.[116] Switches that belong to the T-type exhibit thermally driven relaxation process after photoisomerization. T-type switches can additionally display photo-induced reverse isomerization, which competes with the thermal process.[117–119] P-type switches only display photo-induced reversibility and are less common than T-type switches.[120,121] The photoreversible nature of switching affords a greater degree of precision over isomerization, granting spatiotemporal control over both switching processes. Photoswitches can further be classified into E/Z and cyclisation/retro-cyclisation switches, depending on their switching mechanism.[122] Molecules that display E/Z isomerization are some of the simplest photoswitches. The most common ones include azobenzenes/stilbenes, hydrazones and indigo based compounds.[123–125] These switches are attractive due to the large conformational changes they undergo. This is often accompanied by a change in polarity between isomers.[126,127] Switches that undergo cyclisation/retro-cyclisation typically display large differences in electronic structure between their isomers. Their conformation changes can vary significantly.[128,129] For example, spiropyran displays large end-to-end length change upon isomerization when compared to diarylethene, which shows very limited length changes between two isomers.[122] The most popular E/Z and cyclization-based switches are azobenzenes and spiropyran respectively. As they were the primary photoswitches employed in this thesis, they will be the focus of the following sections.

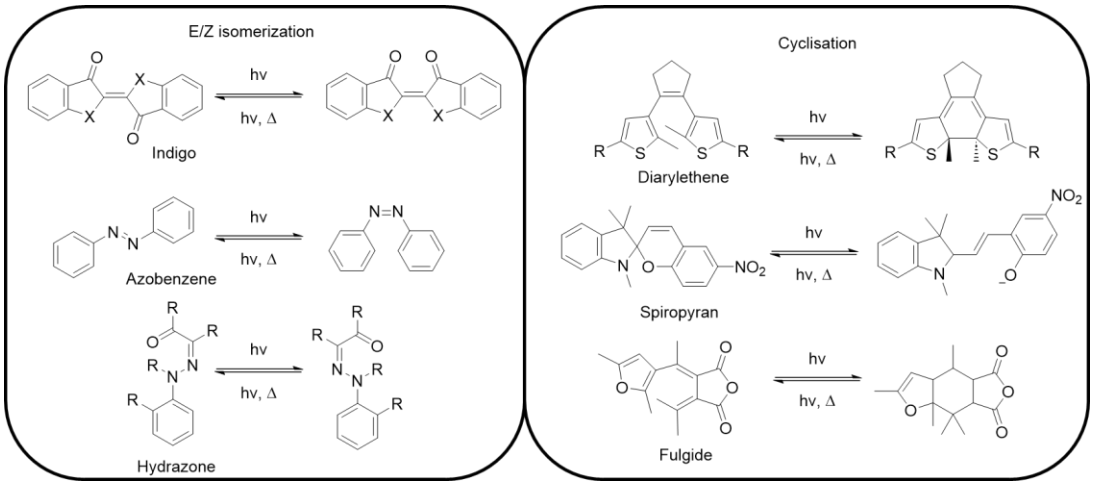

Figure 12. Different types of E/Z and cyclisation photoswitches.

2.2.3 Azobenzene

Azobenzenes are commonly used in a broad range of fields due to the disparate properties arising from its two distinct isomeric forms. Azobenzenes consist of two phenyl rings linked via a diazene bridge, with E/Z isomerization around the diazene bridge resulting in the two distinct isomers. Azobenzenes were first discovered in 1834 by Eilhard Mitscherlich and synthesised on an industrial scale in 1857 for use as clothing dyes.[130,131] In the early 20th century, the E/Z or *cis-trans* isomerization of azobenzenes was elucidated, resulting in a dramatic increase in azobenzene research.[132] The isomerization mechanism has been shown to proceed through either excitation of S^2 - S^o (π- π^*) states or via S^1 – S^o (n - π^*) excitation.[133,134] In the most basic azobenzene, *trans-cis* isomerization results in an end-to-end length reduction of ~ 3.5 Å and an increase in polarity from 0 – 3 D.[135] Isomerization occurs following excitation via one of four proposed mechanisms: rotation, inversion, concerted inversion, and inversion-assisted rotation.[136]

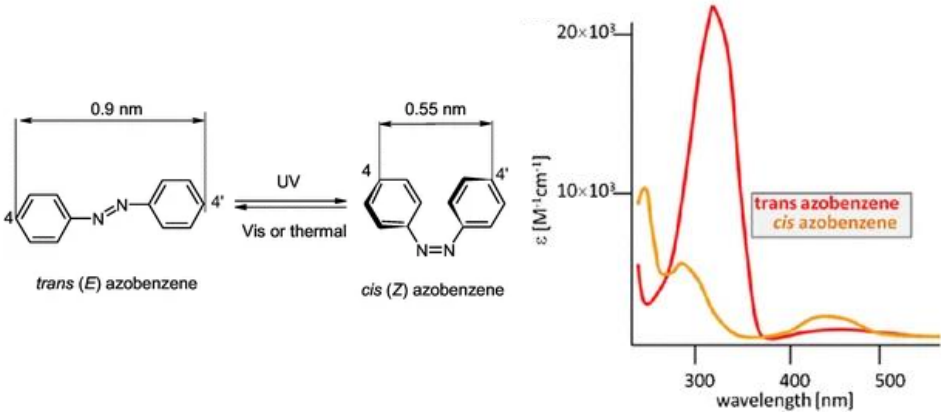

Scheme 4. *cis-trans* isomerization of an azobenzene resulting in an end-to-end length decrease and increase in polarity. Adapted from Ref **[137]**

Azobenzenes are categorised as T-type switches, whereby the reverse isomerization can be induced either photochemically or via thermal relaxation.[118,138] Several pathways for reverse isomerization have previously been proposed, yet no conclusive mechanism has been established.[139] The prevailing opinion favours a rotational mechanism. Isomerization is also highly dependent on external factors such as temperature and solvent properties, which can significantly impact the isomerization process.[140,141] An appealing aspect of azobenzene switching is an amenability to chemical modification.[142,143] With careful substitution, almost every aspect of photoswitching can be drastically modified including switching wavelengths, thermal half-lives ($t_{1/2}$) and photo stationary state compositions.[144–146] Generally, azobenzenes are classified into three different types depending on the relative energies required for excitation: azobenzene, amino-azobenzene, and pseudo-stilbene type azobenzenes (Figure 13).[144,147]

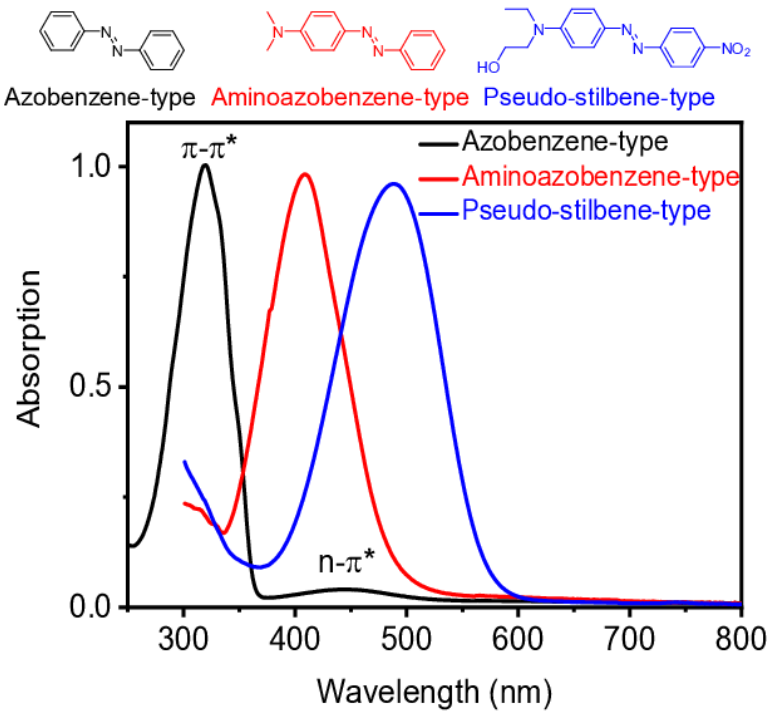

Figure 13 Azobenzene types and their corresponding UV-Vis absorption profiles. Adapted from Ref[147]

Azobenzene types typically display the most blueshifted isomerization wavelengths and the longest $t_{1/2}$. These characteristics are achieved via phenyl-substitution with alkyls, halides, carbonyls, nitrile or amides. Amino-azobenzenes are substituted with electron donating substituents such as amino or hydroxy groups. Amino-azobenzenes are more redshifted than the azobenzene class and possess faster thermal relaxation. Pseudo-stillbenes are azobenzenes which possess a push-pull substitution *para* to the azo bridge, displaying the most redshifted photoisomerization. These switches have rapid thermal relaxation often within seconds. Apart from push-pull pseudo-stillbenes, azobenzenes typically require high energy UV light to induce *trans* - *cis* isomerization. However, blue light can be detrimental to a number of applications.[148] Red-shifting the photoisomerization of azobenzenes is necessary, especially for biologically relevant fields. Utilising pseudo-stillbenes is appealing but the generated *cis* isomer rapidly relaxes thermally back into the *trans* isomer.[149] Red-shifted isomerization can be achieved via the tetra-*ortho* functionalisation of azobenzenes without sacrificing a thermally stable *cis* isomer.[148] In conventional azobenzenes, the n-π* transition of the *trans* and *cis* isomers overlaps. This means that *trans* - *cis* photoisomerization must be completed using blueshifted wavelengths of the π-π* band instead, as excitation of the n-π* will also induce *cis* – *trans* isomerization. Tetra-*ortho*-functionalisation separates the n-π* bands of the isomers by either red or blueshifting the *trans* n-π* band,

allowing for *trans-cis* isomerization with longer wavelengths without activating *cis-trans* isomerization (Figure 14).[150] Hetero-atoms are commonly employed in tetra-*ortho*-functionalisation, with halogenation and methoxy substitution being most prevalent.[151–153] Attachment of electron withdrawing groups *para* to the azo-bridge has been observed to increase the n-π* separation even further.

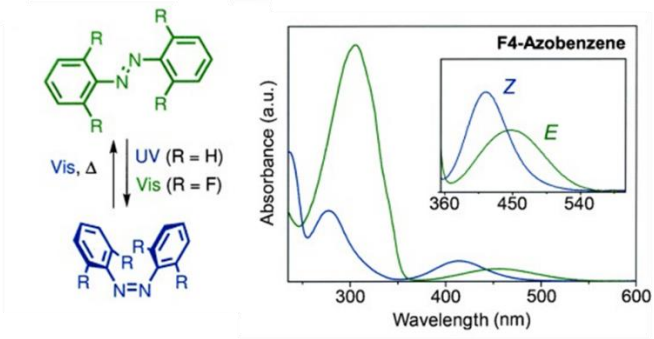

Figure 14. (Left) isomerization of a tetra-ortho-fluorinated azobenzene. (right) Corresponding absorption profile with separation of the n-π* transition band between the two azobenzene isomer. Adpated from ref[153]

Integration of azobenzenes into polymeric environments has resulted in a diverse range of photoresponsive systems through implementation as main-chain, pendant or crosslinking functionalities (Figure 15).[154–156] Azobenzene isomerization is often utilised in soft matter to induce free volume changes in a polymeric scaffold, caused by the end-to-end length reduction between the *trans* and *cis* isomers.[122]

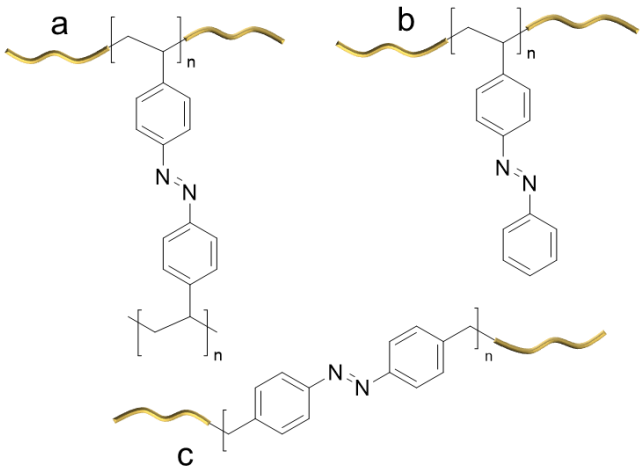

Figure 15. (a) Azobenzene as a crosslinker, (b) pendant group, (c) main chain element

The switching process of small molecule azobenzenes in solutions is typically conserved. However, increasing the steric hinderance of the surrounding environment

can impede isomerization. Diminished switching can still be observed in highly constrained polymeric environments. Valley et al. developed azobenzene-functionalized self-assembled monolayers (SAMs) tethered to gold nanoparticles. High grafting densities resulted in a reduced rate of photoisomerization and complete inhibition at 100% grafting density.[157] Introduction of spacer units restored only a moderate switching capacity compared to free azobenzene in solution. Azobenzenes are also used in polymeric liquid crystal (LC) elastomers as photoswitchable mesogens to introduce disorder upon *cis-trans* isomerization. LC elastomers containing azobenzenes exhibit significant photoresponsive, mesogenic properties. Critically, this can already be achieved with low azobenzene content. Kondo et al. showed that an increase of azobenzene content in a liquid crystalline polymer resulted in a corresponding decrease in the photoisomerization due to geometric restriction.[158] Azobenzenes are also incorporated in discrete polymeric scaffolds such as nanoparticles and micelles, with photoisomerization resulting in dynamic morphologies and functionalities. Pearson et al. developed amphiphilic polymers bearing azobenzene pendant groups that could assemble into micelles which were loaded with a hydrophobic payload of Nile red. Isomerization of the azobenzene pendant groups into the polar *cis* isomer decreased the hydrophobicity of the micelles internal structure and resulted in expulsion of the hydrophobic pay load.[159] The change in polarity between the *cis* and *trans* isomer has also been exploited to generate polymers with azobenzenes in the backbone that display light-modulated, thermo-responsive behaviour. Park et al. developed photo/thermo-responsive micelles containing an azobenzene block. The micelles displayed a lower critical solution temperature (LCST) that increased upon *trans-cis* isomerization due to an increase in polarity of the *cis* isomer.[160] Isomerization of backbone azobenzenes has also been used to specifically induce shape changes in discrete polymer systems. Dowds et al. developed a linear polymer bearing a large amount of azobenzene within the polymer backbone.[161] Photoisomerization led to a reduction in overall size, evidenced by a reduction in apparent molecular weight when analysed via SEC, and reduction in the solvo-dynamic volume in Diffusion Ordered Spectroscopy (DOSY).

2.2.4 Spiropyrans

Spiropyrans are T-type photoswitches consisting of an indolenine ring condensed to a chromene functionality via a quaternary spiro carbon. Upon irradiation the closed spiropyran upon irradiation can undergo ring-opening into its a merocyanine form. For the most basic spiropyran, irradiation leads to excitation primarily through a π-π* transition.[162] Following excitation, a dissociation of the oxygen-spiro bond occurs and generates the open merocyanine isomer in a *cis* configuration which further transforms into the more stable *trans*-merocyanine. Two resonance forms contribute to the open merocyanine, a neutral quinoidal structure and a zwitterionic structure. The zwitterionic merocyanine bears a positive charge centred on the indoline functionality and a negatively charged phenolate on the chromene.[163]

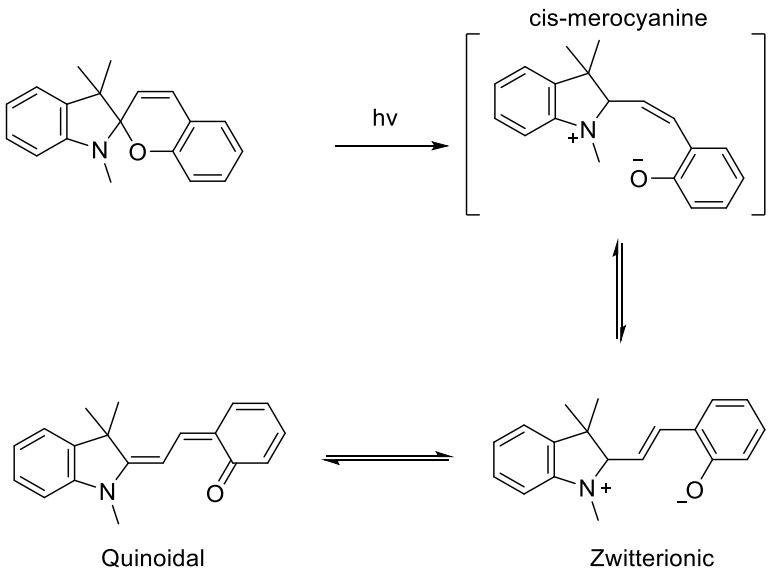

Scheme 5. Isomerization of spiropyran into the open *trans*-merocyanine forms via a *cis* intermediate

The degree of contribution each form has to the resonance structure of the merocyanine is heavily dictated by the polarity of the medium in which switching is conducted.[164,165] Polar media have been observed to stabilise the zwitterionic form over the quinoidal one with the inverse being true for non-polar media. The merocyanine is conjugated between the chromene and indolenine, afforded by a methine bridge which allows for delocalisation of charge across the molecule culminating in a redshifted transition. The open merocyanine can cyclise back into the closed spiropyran either photochemically or thermally, a process that is again highly dependent on the polarity of the solvent.[166,167] Ring closure will proceed slowly in

polar solvents due to a stabilising effect enacted on the zwitterionic structure, while rapid ring closure occurs in non-polar media. Spiropyran isomerization is also not exclusively induced via irradiation and can be activated via several stimuli including, mechanical, redox, pH and temperature.[168–171] For the sake of conciseness, this section will focus primarily on photoinduced isomerization and its correlated functions/applications. Compared to azobenzene, limited research has been conducted on tuning the spiropyran switching process, namely redshifting ring-opening and stabilising the open-isomer. Spiropyran modification typically focuses on increasing the efficiency of isomerization with UV light. To this end, substitution of the chromene functionality with a nitro group is generally performed, with the majority of spiropyrans in literature bearing a nitro substituent.[172,173] Nitro substitution results in an increase in the rate of photo-induced ring opening, facilitating isomerization by triplet states.[163,174] Due to the presence of triplet excited states, nitro substituted spiropyrans suffer from a variety of degradation mechanisms, one such involving singlet oxygen generated from the interaction between the excited spiropyran triplet state and triplet oxygen.[175] Bimolecular degradation is also prevalent, again facilitated by the excited triplet state of spiropyran. In apolar media the zwitterionic merocyanine heavily self-aggregates and the proximity further increases the rate of bimolecular degradation.[176,177] Work has shown that by increasing the electron donating character of the spiropyran, the rate of visible light ring closure increases. Installation of a methoxy substituent onto the indolenine ring of spiropyran with a nitro substituted chromene was observed to increase the rate of ring closure by an order of magnitude compared to a non-methoxy spiropyran.[178] Interestingly spiropyran with strong electron donating groups also display thermally stable open merocyanine forms.[179] The open merocyanine form can also be stabilised by complexation to suitable metal salts often in a 2:1 stoichiometry due to the charged phenolate oxygen, generated upon UV light irradiation.[180,181] As a result, spiropyran have found use as photoresponsive chemical sensors for metal detection.[182,183] Interestingly expulsion of the metal can be induced upon spiropyran recyclization with exposure to visible light, although typically not quantitatively. Reversibility is contingent on the relatively weak binding strength of the phenolate anion and can be increased and decreased as either a function of chemical modification or of metal complexability.[184] A large number of metal ions with varying oxidation states have been utilised for spiropyran metal complexation, however late transition metals with a 2^+ oxidation state are the most prevalent.[185] The

reversibility of spiropyran metal complexes upon exposure to visible light is reliant on the relatively weak strength of the spiropyran phenolate-metal bond. Selection of appropriate metals that display a sufficiently high affinity to the spiropyran phenolate anion while remaining weak enough to allow for light induced expulsion is required. This can be rationalised by Hard/Soft, Acid/Base theory (HSAB), noting that metals classified as hard acids will preferentially associate with hard bases, the same being true with soft acids and soft bases.[186] The phenolate anion of the ring opened spiropyran is considered a hard base and will thus preferentially associate with hard acids such as lanthanides, trivalent and alkali metal ions as examples.[187–189] Late transition metal species in their 2^+ oxidation states such as Ni^{2+}, Co^{2+}, Fe^{2+} and Zn^{2+} are borderline between hard and soft acids and are suitable candidates for reversible complexation, balancing affinity for spiropyran coordination while remaining sufficiently labile to decomplex upon irradiation.[190] Further functionalisation of spiropyran with additional coordinating functionalities can drastically increase the stability of the formed complexes and generate complexes that deviate from 2:1 stoichiometry.[191,192] Additionally, the ionic character of the metal species can be tuned to facilitate varied binding affinities. Metals bearing weakly coordinating ions will rapidly complex with spiropyrans, strongly coordinating ions will show a reduced binding affinity, consequently proving harder to complex.[193,194]

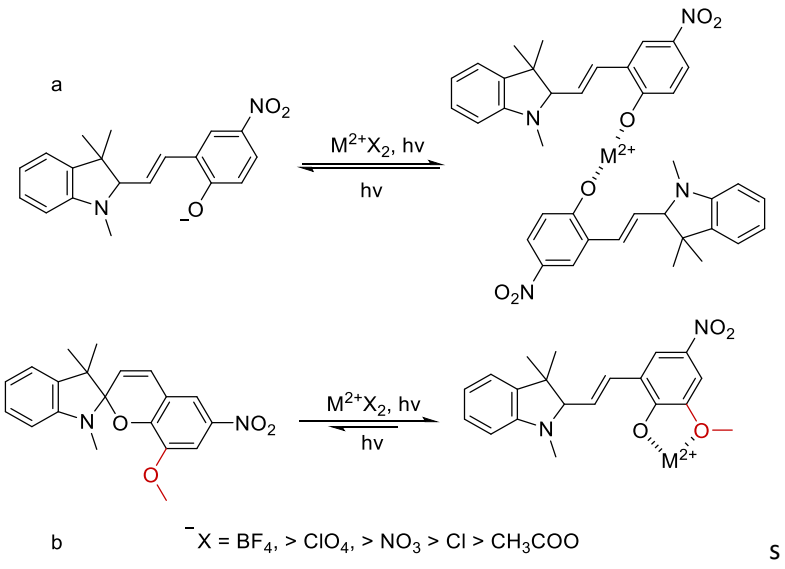

Scheme 6. (a) Metal complexation of spiropyrans, (b) possible metal salt counterions, arranged in order of weakest to strongest coordinating ability.

Spiropyrans have also been extensively incorporated into macromolecular architectures, where light induced isomerization can lead to a variety of functions. Examples include conductivity,[195] thermos-responsiveness[196] and sensing.[182] Typically, spiropyrans are used as pendant groups to decorate polymers, and the number of examples of main-chain spiropyran polymers is limited.[197] Polymers bearing pendant spiropyrans are often synthesised using controlled and un-controlled free radical techniques, through polymerization of suitably functionalised spiropyran monomers. Low conversions are often reported and moderate to high conversions typically need high concentrations of radical initiator, impacting the final dispersity of the polymer.[198,199] Poor dispersities arise from the thermally triggered ring opening into a merocyanine during polymerization which is able to abstract a hydrogen from propagating radicals.[200] This effect is more pronounced with high spiropyran content but still problematic even at low concentrations.[201] Condensed soft matter applications of polymeric spiropyran are limited. Similar to azobenzenes, large conformational changes are impeded due to increased steric hinderance.[202] Additionally, the open merocyanine shows significant self-aggregation, primarily due to π-π and dipole-dipole stacking.[203] Stacking reduces the rate of reverse isomerization into the closed spiropyran and as mentioned previously, also facilitates an increased rate of bimolecular degradation. In a polymeric matrix where free spiropyran is used as a dopant, merocyanine aggregation has the potential to severely impede and completely prevent the reverse isomerization into the spiropyran.[204] Stabilisation, covalently of a spiropyran onto a polymer backbone has been observed to reduce the negative effect of aggregation on isomerization by isolating individual spiropyran units from each other. Radu et al. compared the degree of photofatigue between spiropyrans covalently attached to polymer films and free in solution. After twelve switching cycles spiropyran films displayed a 27% reduction in photoswitching efficiency, while free spiropyran suffered from a 57% reduction.[190] It is assumed that anchoring the spiropyrans to a polymer, restricts diffusion and decreases the rate of two spiropyran meeting and aggregating, leading to a reduction in switching hysteresis. Photoswitching hysteresis of spiropyran polymers is however highly dependent on chromophore loading. Bell et al, compared the photoresponsive properties of different colloids comprised of nanoparticles grafted with either a spiropyran-methacrylate homopolymer or methyl methacrylate polymer containing 20

mol% of spiropyran. The resulting nanoparticles precipitated in toluene when exposed to UV light, generating the highly apolar merocyanine form (Figure 16).

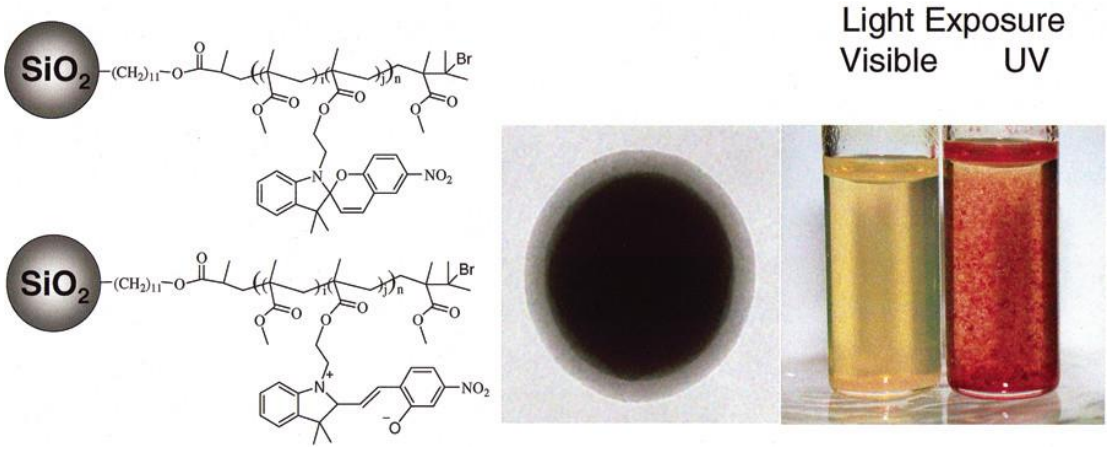

Figure 16. (left to right) Spiropyran decorated polymers grafted to silica nanoparticles, image of the nanoparticle, sedimentation of the nanoparticles after UV irradiation. Adapted from Ref[205]

The homopolymer showed significant photofatigue after only two switching cycles evidenced as a permanent decrease in the switching efficiency, whereas the 20% spiropyran polymer was cycled six times with little evidence of fatigue.[205] Specific stabilisation of the open merocyanine is not always detrimental. As mentioned previously, the merocyanine form can coordinate with metals forming stable complexes. Frequently, photoactive spiropyran polymers are used for the sensing of polluting heavy-metals, the formed complexes generating specific absorbance profiles allowing for colorimetric quantification. High reusability is reported due to the reversibility of the merocyanine-metal complexes.[206] In addition to sensing, metal complexation can be used for morphological modifications to a polymeric system. Ye et al. utilised the spontaneous complexation of copper by polymeric spiropyrans to induce micelle assembly via spiropyran, with a 2:1 stoichiometry.[207] The formed assemblies were not photoresponsive but highlight the role spiropyran metal complexation can have in morphological control. A photoresponsive system was developed by Epstein et al. who utilised polymer chains decorated with pendant spiropyran groups capable of forming SP:Co^{2+} crosslinks in a 2:1 stoichiometry.[208] Crosslinking resulted in hydrogels, which upon exposure to visible light lead to the dissociation of the spiropyran: metal crosslinks back into the closed merocyanine and subsequent degradation of the hydrogel(Figure 17). This reversibility highlights the

potential that metal-spiropyran systems have for morphology control. Such control could be applied to more diverse polymeric systems.

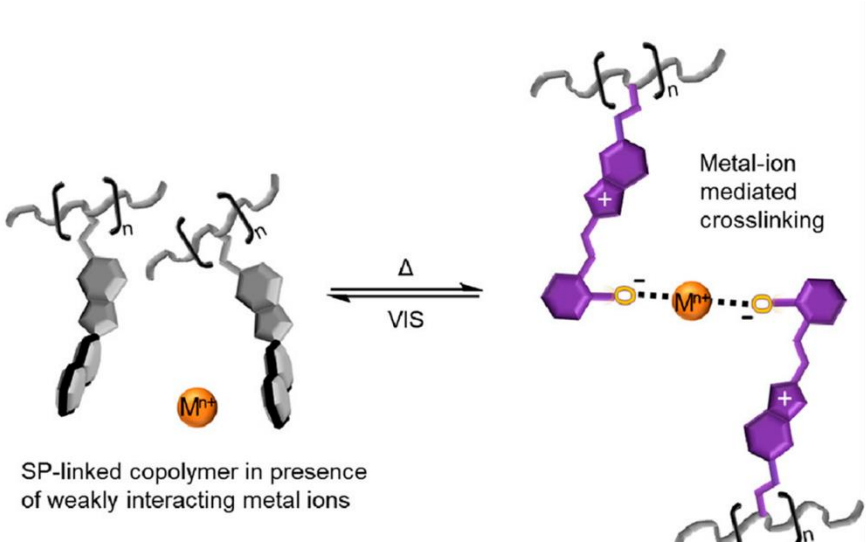

Figure 17. Spiropyran polymer crosslinking upon metal coordination to form visible light degradable hydrogels. Adapted from Ref.[208]

2.3 Single Chain-Nanoparticles

Ever since Herman Staudinger's theory of polymers in the early 20th century, it has been the goal of polymer chemists to design macromolecular systems with high precision and control over secondary and tertiary structures.[209] Precision macromolecular architectures are prevalent in nature, with proteins being responsible for a large number of biological processes, ranging from gene expression to bio-catalysis.[210] Proteins are able to perform these advanced functions in complex biological environments, whilst still retaining a high level of efficiency and selectivity. These catalytic properties of proteins, namely enzymes, are owed to their precision morphologies, and are the result of a sequence-defined primary structure comprised of amino acids. The highly defined primary structure affords macromolecules that can be folded with equally high precision. In enzymes, this results in the formation of catalytic pockets, cavities within the protein that stabilise the transition states of those substrates undergoing a bio-catalytic reaction.[211] This coordination between the polymeric scaffold of an enzyme and its catalytic pocket has served as the foundation for polymer chemists striving to develop advanced catalytic systems.[211] Early attempts using synthetic polymer techniques have been based on macromolecular architectures, which include foldamer and dendrimer-based systems and typically form spherical

morphologies. Catalytic functionalities were incorporated at the centre of the polymer structure, or attached to its dendritic branches.[212,213] Another method of forming enzyme inspired catalysts is via the intramolecular folding of single polymer chains into discrete nanoparticles in order to better emulate the folded structure of enzymes. These nanoparticles are known as Single Chain Nanoparticles (SCNP). SCNPs with catalytic functionalities are afforded with enzyme-like catalytic properties, the design rationale for which initially came from natural proteins.[7] Early SCNPs remained purely structural; simple polymers collapsed into nanoparticles via the intramolecular formation of crosslinks.[214–216] Polymer chemists were primarily interested in the physical properties of such SCNPs, namely changes in the radius of gyration as well as the intrinsic viscosity arising from nanoparticle formation.[216–220] Relevantly, catalytic SCNPs would be realised soon after this. As almost half of all enzymes in nature possess catalytic metal centres, the primary means in which catalytic properties are inferred to an SCNP is via active metal centres.[221] The first SCNPs to utilise metal centres employed them primarily as structure-forming elements to induce crosslinking, but later on, organometallic SCNPs with catalytic function were realised.[222,223] The folded structure of catalytic SCNPs can also display more specific enzyme-like properties, specifically the formation of local domains throughout the nanoparticle akin to the catalytic pockets of enzymes.[224] One advantage that SCNPs have over enzymes is the ease of modification. An SCNP can be modified iteratively from its base level, starting with monomers,[225] crosslinking chemistries[226] and the final nanoparticle morphology.[227] The same design rationale is not similarly possible with enzymes. Additionally, almost any metal can be incorporated into a catalytic SCNP with the correct selection of ligands, whereas the number of biologically suitable metal centres is limited.[228]

2.3.1 Synthesis and Characterization of SCNPs

SCNPs are formed from the folding of a linear polymer into a compacted nanoparticle due to intramolecular crosslinking. The nature of this crosslinking can be used to class SCNPs into one of two categories, selective point folding and repeat unit folding. When a linear polymer is folded via crosslinks positioned at predetermined points along the chain, the term selective point folding is used. Folding of this manner results in a specific SCNP geometry that can be formed consistently and reproducibly. Repeat unit folding leads to a randomly folded SCNP, the result of a linear pre-cursor with

statistically distributed crosslinking functionalities throughout the chain.[229] Within these two categories, SCNPs can be further classified based on the method of collapse i.e. hetero-functional, homo-functional and crosslinker mediated collapse (Figure 18).[230–232] Homo-functional collapse of a polymer into an SCNP is caused by the crosslinking of two identical reaction partners.

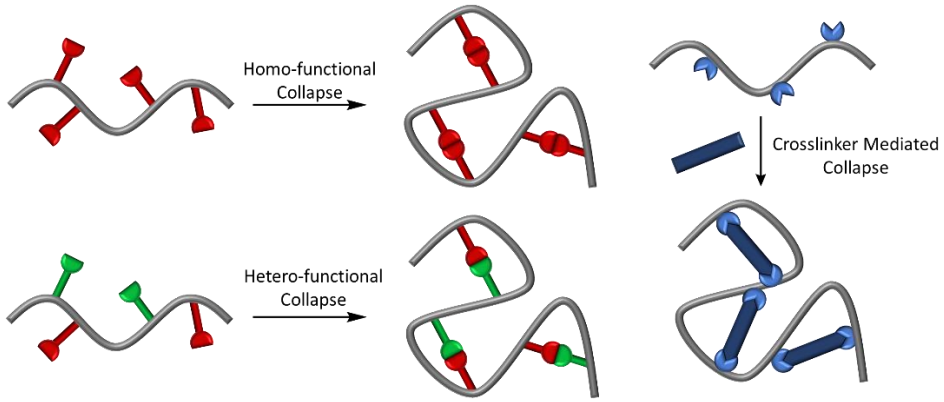

Figure 18. The three types of crosslinking in SCNPs: homo-functional collapse, hetero-functional collapse and crosslinker mediated collapse.

An early example of homo-functional collapse was the thermally induced dimerization of benzocyclobutene pendant groups placed statistically along a polymer chain.[233] Other chemistries within this class include disulfide formation,[230] homo-couplings[234] and olefin metathesis.[235] Worthy of note is also several photodimerization reactions i.e anthracene,[8] styrylpyrene[236] and coumarin.[237] Hetero-functional collapse describes the crosslinking of complimentary reactive partners along a polymer chain, with prominent examples including azide/alkyne,[238] host-guest chemistries[239,240] and a number of photoinduced heteroatom-cycloadditions.[241,242] Crosslinker mediated collapse utilises an external crosslinking agent to induce collapse upon coupling with reactive functionalities on the polymer chain. These can include covalent techniques, some of which have been listed previously,[243,244] and metal coordination.[245,246]

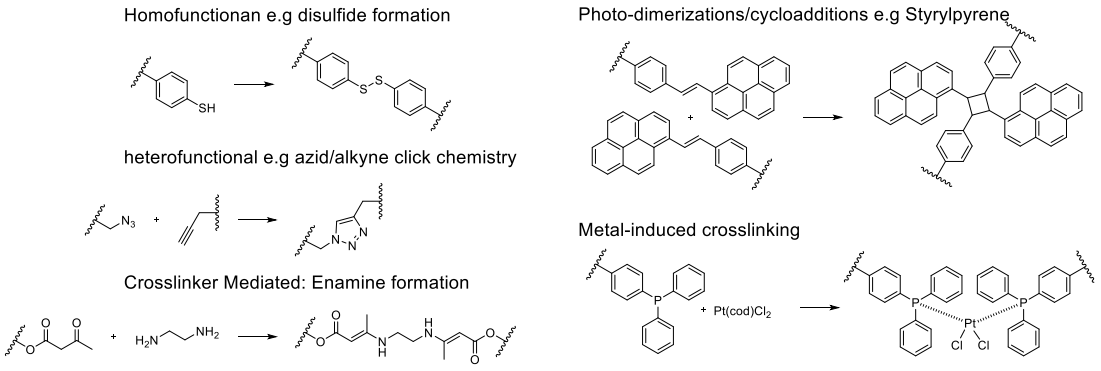

Figure 19. Representative crosslinking chemistries for linear polymer collapse into an SCNP.

In the case of the latter, catalytic functionality can simultaneously be inferred upon crosslinking. Conventional SCNP formation requires a high polymer dilution, done to ensure that linear polymer chains are isolated and intramolecularly crosslink. Typical concentrations are < 1 mg.mL^{-1}, presenting issues with scalability as a large amount of solvent is required. To address the scalability issue, techniques have been developed to decrease the necessary dilution, with some SCNPs being formed at concentrations of 100 mg.mL^{-1}.[247,248] Monitoring the collapse of a linear polymer is conducted through a variety of methods. Techniques such as SEC, Diffusion Ordered Spectroscopy (DOSY) or Dynamic Light Scattering (DLS) are used to monitor changes in size, primarily the hydrodynamic volume, and morphology resulting from SCNP formation. SEC is by far the most used technique to observe the reduction in hydrodynamic volume upon SCNP formation. SEC analysis of a linear polymer and its subsequent compacted SCNP will show an increase in retention volume and decrease in apparent molecular weight. From these values a reduction in hydrodynamic volume can be reliably assigned, assuming that any changes in mass arising due to crosslinking are insignificant.[233] DOSY is another technique used to monitor the collapse of polymers into SCNPs.[249] DOSY measurements yield the diffusion coefficient of a polymer or SCNP in a specific solvent. An increase in diffusion will be observed as the hydrodynamic radius decreases upon collapse, a phenomenon described by the Stokes-Einstein Equation.[250]

$$D = \frac{k_B T}{6\pi\eta r} \qquad \textbf{equation 12}$$

D = Diffusion Coefficient

k_B = Boltzmann Coefficient

η = Dynamic viscosity of the solvent

r = Radius of the particle

T = Absolute temperature

Dynamic Light Scattering (DLS) is also used for the determination of an SCNPs hydrodynamic radius.[251] Imaging techniques such as Atomic Force Microscopy (AFM) and Tunnelling Electron Microscopy (TEM) are also employed for the determination of an SCNPs' size and shape.[252,253] These methods are limited as imaging is typically done devoid of solvent, where samples are coated onto substrates and surfaces. A lack of solvation means that the observed values for SCNP diameter can deviate from those obtained via solution-based techniques.

Understanding the internal morphologies of an SCNP is as important as determining its relevant size. In applications such as catalysis, determining the positioning and distribution of catalytic sites through an SNCP is critical in applying them to diverse catalytic tasks.[6] Small Angle Scattering (SAS) techniques such as Single Angle Xray (SAXS) and Single Angle Neutron Scattering (SANS) have been used to determine the size and internal structures of SCNPs in solution, as well as properties such as chain flexibility.[254,255] Insights into internal SCNP morphology has been achieved using SAS techniques coupled with Molecular Dynamic simulations (MD). Pioneering work by Pomposo et al. used this method to identify two primary SCNP morphologies in solution. When an SCNP was folded in 'good' solvents such as THF where the polymer is highly soluble, linear gaussian chain like behaviour was observed and these SCNPs were labelled as "sparse SCNPs". Sparse SCNPs possess multiple domains that are locally compacted and distributed throughout the SCNP. [6,256,257] Analysis of SANS profiles showed a morphology similar to those of intrinsically disordered proteins. When SCNPs are folded in poor solvents such as water, they take on more compacted and often "globular" profiles similar to that of globular proteins such as enzymes.[258] Solvent conditions have been judicially selected by Pomposo et al. to access both sparse and globular catalytic SCNPs monitored using a SANS/MD approach.[259] Derived from an amphiphilic block co-polymer, SCNPs were initially folded in THF, resulting in the homogenous distribution of catalytic sites throughout

the polymer chain. However, when folding was performed in water and was followed by isolation and then dissolution in THF, catalytic sites clustered together forming more discrete catalytic domains (Figure 20).

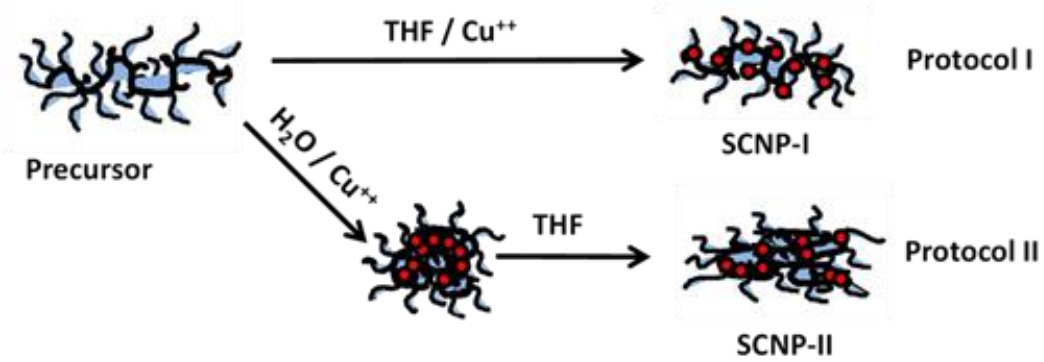

Figure 20. A sparse distribution of catalytic sites can be achieved by conducting intramolecular folding of an amphiphilic polymer in good solvents such as THF (protocol 1). Consequently, clustering of catalytic sites occurs when folding is first conducted in a poor solvent such as water, here hydrophobic/hydrophilic interaction generate localised domains of catalytic sites which are retained when the SCNP is introduced into a good solvent.(protocol 2) Adapted from Ref [240]

A concerted study into SCNP morphologies was conducted by Webb et al. who used a combined approach of machine learning and molecular dynamic simulations to yield a diverse library of single chain nanoparticles.[260] All nanoparticles were folded in good solvent conditions with respect to the precursor polymer. The average density of crosslinking functionalities as well as a varying block-like crosslinker distribution were the primary variables explored. SCNPs with a high crosslinking density, would typically always form compact globular like morphologies. When crosslinking density was low, they would form a range of diverse and sparse morphologies that showed a higher susceptibility to changes in the block like structure of the polymer. Pre-cursor polymers within these crosslinking and block parameters were earmarked as the most suitable for generating SCNPs with function specific morphologies such as for catalysis.

2.3.2 Metal Functionalised SCNPs

2.3.2.1 Synthesis and Characterization

Metal coordination can be used to form an SCNP, where a linear precursor is decorated with metal coordinating ligands. Introduction of a metal induces single chain collapse through metal chelation to the polymer anchored ligands, generating coordination complexes. [261–263] It is possible for an SCNP to be formed via non-coordinative means, and instead have metal complexes that are purely catalytic and not structural.[246]

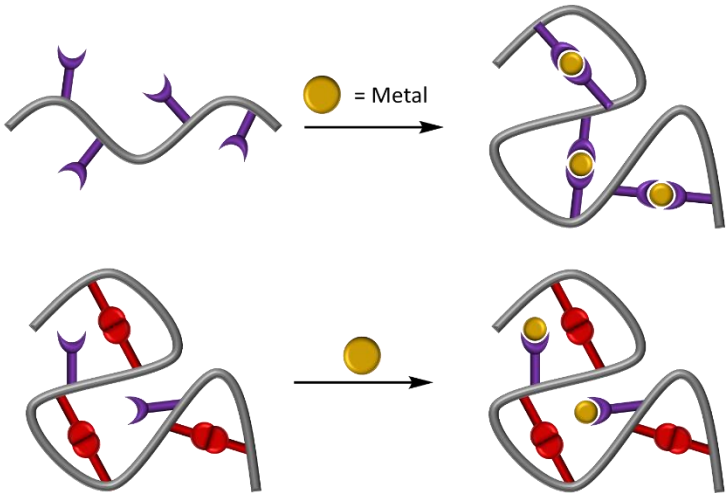

Figure 21. (top) metals used to crosslink an SCNP, (bottom) metals as purely functional elements.

Characterizing the metal centres of organometallic SCNPs is done using techniques that are applied to small molecule complexes. When applied to SCNPs, these techniques suffer from a general loss of resolution that results from the disperse nature of polymers. The structure of SCNP metal centres can be elucidated using FT-IR,[264] UV-Vis[265] as well as nuclei specific NMR experiments. [245,266] In the case of the latter, the paramagnetic nature of a number of metal complexes is often prohibitive, resulting in spectral line broadening. [267] Comparison of the data generated from these techniques can be cross-referenced against small molecule complexes for further validation.[246] Elemental analysis is often applied to organometallic SCNPs with photo emissive techniques such as Energy Dispersive X-ray Spectroscopy (EDX) and X-ray Photoelectron Spectroscopy (XPS) being the most prevalent. [268,269] The polymeric environment within an SCNP has been observed to impact the structural characteristics of embedded metal complexes. Consequently, the stoichiometries between a metal and ligands observed in small molecular counterparts are not always indicative of similar metal complexes bound in an SCNP. In these instances, a Job's plot analysis can be

helpful in determining the true coordinating structure of the metal complexes.[262,270] Structure elucidation is important as the changes in bonding between ligand and metal centre can have noticeable effects on function such as catalysis.[258]

2.3.2.2 Catalytic Organometallic SCNPs

The most common applications of organometallic SCNPs are for catalysis. Other uses exist but will not be the focus of the following section. Employing SCNPs for catalysis combines both properties from conventional homogenous and heterogenous catalysts.[258] Critically, the high activity and substrate specificity of homogenous catalysts are combined with improved recyclability of SCNPs owed to their polymeric nature allowing for isolation via precipitation or dialysis as examples.[7] The isolation and recovery of small molecular catalysts is often difficult and energy consuming, requiring high temperatures and complex solvent systems to afford high recovery yields.[271] Improving the recovery of small molecular catalysts typically involves significant chemical modification, often to achieve catalyst immobilization on heterogeneous substrates such as silica or altered solubility to afford phase based separation such as that of aqueous bi-phasic systems.[271] Immobilization can lead to the loss of the desirable catalytic properties associated with homogenous systems, as systems that utilise phase based separations are often favoured when high activity and selectivity are required.[272] A common method of achieving phase based recycling is the attachment of water soluble groups such as sulfonates or carboxylate salts to facilitate biphasic separation of the water-soluble catalyst from organic products.[273,274] Wagh et al. utilised a sulfonated triphenyl phosphine (TPPTS) coordinated to palladium able to catalyse the amination of alcohols in aqueous medium.[275]The water-soluble catalyst was quantitatively isolated from the product using standard aqueous extraction techniques. This strategy limits the range of solvents compatible with the catalyst, as water soluble groups such as sulfonates may decrease the overall solubility of the catalyst in organic solvents. Comparatively, catalytic SCNPs can display quantitative recovery in aqueous media as well as a wide variety of organic solvents owing to their polymeric structure.[276] As opposed to directly modifying a small molecular catalyst, judicious selection of co-monomers in a catalytic SCNP affords a synthetically less demanding approach to modulating the solubility for enhanced catalyst recovery. In work by Knoefel et al. a quantitative recovery of an SCNP bearing a similar phosphine-platinum complex able to catalyse

the amination of alcohols with conversions > 90% in benzene being reported.[245] Dialysis of the crude reaction mixture containing both product and SCNP in methanol afforded highly efficient recycling of the SCNP. The recovered SCNP was subsequently used in an additional catalytic cycle and displayed minimal loss of catalytic activity. The recovery and re-use of a catalytic SCNP through multiple cycles has been highlighted in work by Garmendia et al., where an organocatalytic SCNP bearing an *N*-heterocyclic carbene functionality for the condensation of benzoin was developed. The SCNP was able to be efficiently recovered via dialysis in THF and MeOH via three catalytic cycles, while showing only a minimal decrease in catalytic activity.[277] In comparative small molecular systems a loss of catalytic activity can occur owing to aggregation, solvent inhibition as well as unwanted redox process.[278] Additionally, the diffuse distribution of molecular catalyst throughout the reaction media can also increase the overall reaction time. The incorporation of catalytically active metal centres into an SCNP is shown to increase the local concentration of catalysts which together with polymeric shielding and suppression of aggregation can reduce the loss of catalytic activity.[7,279]

With judicial selection of monomers, a wide variety of possible ligands can be incorporated into an SCNP either via direct copolymerization of suitable monomers or via post functionalization. Such ligand diversity has afforded an equally diverse range of SCNPs bearing catalytically active metal centres, including Cu[280], Fe,[281] Ni,[226] Pt,[245] Pd,[282] Ru[283] as examples. Catalytic reactions such as copper catalysed azide/alkyne cycloaddition,[284] gold catalysed nucleophilic substitution of alkynes,[246] Sonogashira coupling[282] and iron catalysed living radical polymerizations[279] have all been facilitated by metal containing SCNPs. Consideration also must be given to the orthogonality of the catalyst and polymeric backbone. Metal centres that catalyse functionalities residing on the polymer backbone can lead to potentially unwanted polymer centred side-reactions. For example, a polymer generated from ROMP bearing alkene functionalities may not be compatible with metals that catalyse the nucleophilic substitution of un-saturated carbon bonds such as gold or platinum.[285] While a specific combination of polymer architecture and metal centre may be incompatible, the diverse range of polymerization techniques and co-monomers means that a suitable combination of polymer architecture and metal can be found.[6,7,286]

The polymeric scaffold of an SCNP has the potential to infer substrate selectivity in an enzyme like manner. Pomposo et al. synthesised an SCNP via copper complexation to β-ketoester functionalities.[222] The metal complexes formed both the crosslinks and a catalytic functionality that facilitates the oxidative coupling of acetylene derivatives. High selectivity was observed for an acetylene derivative that bore a small aliphatic side chain, while catalytic activity was barely observed for almost all other substrates. Additionally, in competitive substrate experiments, the copper SCNP showed selective homo-coupling for the aliphatic substrate where no hetero-coupling was observed. The selectivity was attributed to the ability of the polymeric environment to preferentially stabilise the transition state of the specific substrate during the reaction; a result of complimentary geometries between substrate and SCNP akin to that of an enzymes catalytic pocket.[287–289] As mentioned previously, enzyme-like SCNPs are often synthesised from amphiphilic polymers folded in poor solvents such as water, resulting in globular enzyme-like morphology. Globular SCNPs have been synthesised by Sathyan et al. by folding an amphiphilic polymer in water consisting of hydrophilic jeffamine and hydrophobic n-dodecyl and 1,3,5-tricarboxamide (BTA) pendant groups.[290] To provide catalytic functionality, nitrogen and phosphine ligands able to complex with palladium were covalently attached, facilitating the depropargylation of substrates. The use of n-dodecyl and BTA pendant groups resulted in the formation of a centralised catalytic, hydrophobic pocket. A clear relationship was observed between the increase in catalytic activity and an increase in the hydrophobicity of the substrates used. Additionally, when palladium was incorporated into the SCNP, the polymeric scaffold provided a shielding effect to catalytic sites from deactivating species when employed in complex biological media like Dulbecco's Modified Eagle Medium (DMEM). Comparatively, free palladium salts exhibited reduced catalytic activity arising from interactions from these deactivating species. Polymer shielding of catalytic sites in complex biological media has also been reported by Garcia et al.[291] Amphiphilic block polymers self-assembled into SCNPs with hydrophobic catalytic cores were developed. The SCNPs were functionalised with ruthenium complexes allowing for the ruthenium catalysed cleavage of allyl carbamates. The SCNPs displayed higher conversions then the small molecule counterpart in Phosphate Buffered Solution (PBS) and DMEM. The same catalytic tests were also carried out in HeLa cell lysate, in which the small molecule catalyst showed slightly higher conversions than the SCNP. The reduced catalytic efficiency of the SCNP was

hypothesized to be the result of partial unfolding of the polymer chain. Retention of the polymer environment in more complex media likely would require the use of covalent crosslinks to ensure the compacted structure is maintained. Developing SCNPs to mimic the catalytic properties of enzymes is integral to progress in the field. However, attention should also be focused on developing catalytic SCNPs with added properties not possible with enzymes, one such property being photoresponsive catalysis. Using light to control the catalytic process has a number of benefits, primarily milder reaction conditions and temporal control.[292] A limited number of examples of photoresponsive catalytic SCNPs exist. Many of these SCNPs utilise photo-redox catalysts or photosensitisers,[293–295] the bulk of which are organic functionalities. Here photoresponsivity is restricted by the catalytic functionality and remains separate to the rest of the polymer architecture. As such, only a limited number of metals/functionalities that display photocatalytic properties can be used. A more appealing concept is the use of light to dynamically alter the overall SCNP morphology and enact catalytic control through changes to the polymeric scaffold.[7] An optimal design would be the use of light to fold and unfold a linear polymer and SCNP respectively. Tooley et al. used the photodimerization of anthracene to fold an SCNP bearing a single iron metal complex, acting as a hydrogenase mimic.[281] While the photodimerization of small molecule anthracene is reversible, the same was not observed in an SCNP, consistent with previous work by the same group.[8] This loss of reversibility has been explained in studies looking at the reversible photodimerization of styrylpyrene units in confined environments such as SCNPs.[236,296] Limited diffusion of styrylpyrene units away from each-other upon light induced cyclo-reversion prevents unfolding. A photostationary state forms where the majority of styrylpyrene remains crosslinking the polymer as dimers. Identifying photoreversible chemistries that retain their reversibility in confined environments is critical to achieving photoreversible morphology in catalytic SCNPs.

2.3.3 Photodynamic SCNPs

Photodynamic SCNP morphologies are still uncommon in literature, with reversible folding and unfolding considered as particularly difficult. Common photoreversible, covalent chemistries such as styrylpyrene, anthracene and coumarin dimerization,

display photostationary states that are highly skewed towards the dimer when placed in confined polymer environments, making them unsuitable for reversible folding.[296] Partially photoreversible SCNP folding has been achieved by Maag et al, who folded linear polymers with light degradable bimane units as external crosslinkers.[297] Folding/crosslinking with bimane units was completed thermally while irradiation with 415 nm light cleaved the crosslinkers, regenerating the original linear polymer. The regenerated linear polymer could be re-folded upon the addition of bimane crosslinkers and the light induced unfolding repeated. Using light as a single step in folding/unfolding of an SCNP was also achieved by Kodura et al. who utilised the photocycloaddition between a triazolinedione (TAD) crosslinking agent and naphthalene pendant groups to generate an SCNP.[298] The cycloadduct is thermally unstable and reverts to the TAD and naphthalene units in the dark, forming the linear polymers. The two mentioned strategies are limited in that photoresponsiveness is unidirectional, to either unfold or fold the polymer and SCNP respectively. While the use of photocycloadditions/dimerization to reversibly crosslink linear pendant groups on a polymer has not yet been achieved, chain ligation has. Frisch et al. utilised the photodimerization of anthracene pendant groups and a styrylpyrene end group in one polymer to orthogonally control folding into an SCNP and chain ligation respectively.[9] Anthracene dimerization generated the SCNP with 330 nm light, a wavelength previously established to revert styrylpyrene dimerization. Chain ligation to a PEG polymer using styrylpyrene end groups could be performed at 455 nm without inducing anthracene dimerization. Critically, chain ligation could be reverted using 330 nm light, resulting in highly efficient splitting of the two polymers with simultaneous anthracene dimerization into the SCNP. The photostationary state mentioned previously is not applicable to the end group styrylpyrene dimerization. Both polymer chains are able to freely diffuse away from eachother upon 330 nm irradiation as no other bonds are holding them in close proximity. The reversible ligation doesn’t result in unfolding or alteration of the SCNPs intramolecular compaction but does constitute reversible morphological control of an SCNPs tertiary structure.

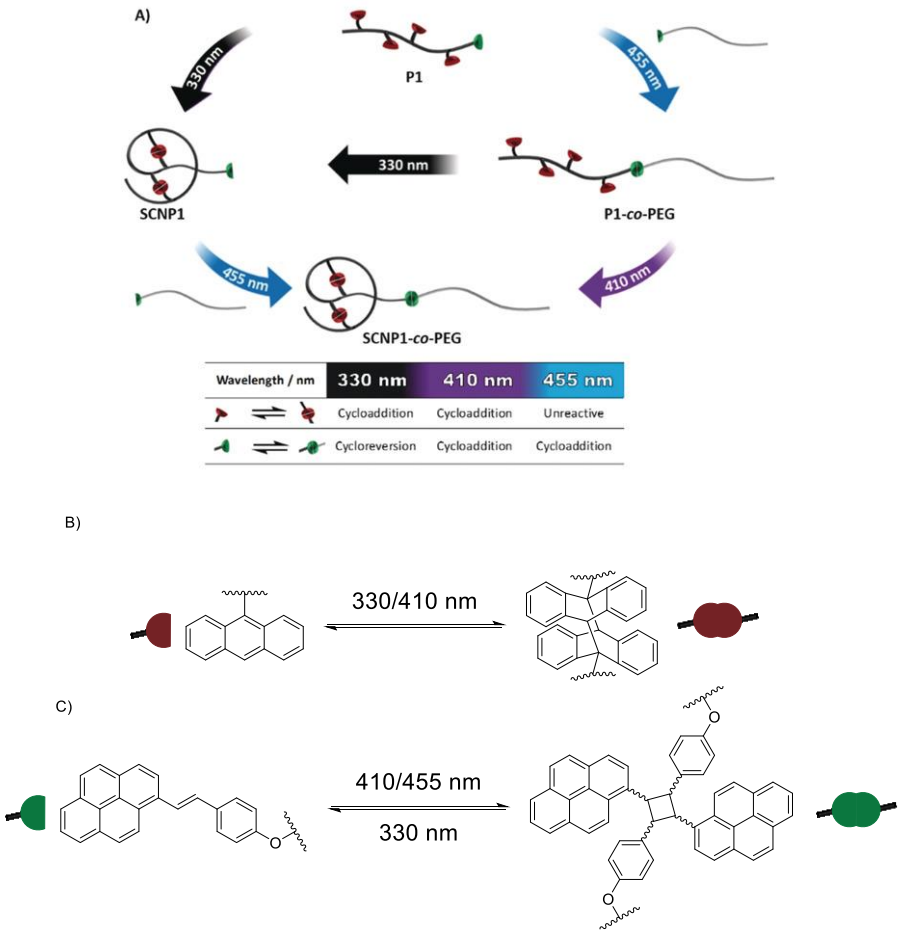

Figure 22. A) Selective, photo-induced chain ligation via B) intramolecular crosslinking using anthracene pendant groups (330 nm) and C) styrylpyrene dimerization (455 nm). Adapted from Ref [9]

Photoswitches which have been addressed in earlier chapters are an appealing candidate for inferring photo-induced morphological control over an SCNP. A highly conserved switching mechanism even in polymeric environments means that minimal hysteresis is often observed.[200,299,300] While implemented in a number of non-SCNP polymeric environments, SCNPs bearing photoswitches are limited. Wen et al. utilised the photodimerization of stilbenes to generate an SCNP containing azobenzene pendant groups, undergoing reversible E/Z isomerization with 360 and 520 nm light respectively.[301] The nanoparticles were imaged using TEM and revealed tubular morphologies prior to irradiation, after UV exposure (360 nm), the morphology changed to become spherical and increased in size. Irradiation with complementary visible light (520 nm), restored the original tubular morphology. Azobenzenes display a large change in free volume upon isomerization in addition to polarity,[302,303] both properties were used to describe the observed morphological changes. The change in free volume induced liquid crystal phase-transitions within the polymeric

environment, leading to the tubular morphologies arising from the stacking of *trans* azobenzenes in the SCNPs. *Cis* isomerization leads to spherical morphologies due to an increase disorder in the LC structure, restored upon visible light irradiation. The higher polarity of the *cis* isomer also leads to an overall increase in the hydrophilicity resulting in increased polymeric solvation and swelling. This reversible morphology is limited to using secondary effects from photoisomerization i.e. crystallinity and polarity changes for morphological control, owing to the implementation of azobenzenes as side chain functionalities. Incorporation of photoswitches not as pendant groups, but as main-chain units, makes use of photoisomerization to directly induce morphological changes via the primary structure of a polymer chain. Mutlu et al. utilised bis-imine photoswitches, capable of Z/E isomerization, as main chain elements of a linear polymer.[304] Upon Z/E isomerization with UV light, the linear polymer folded into an SCNP with reduced hydrodynamic volume, evidenced by DOSY, DLS and SEC. Complete recovery of the linear polymer was achieved after thermal relaxation of the photoswitch to its stable Z isomer (Figure 23). Recovery of the Z isomer with a complementary wavelength of light was shown on a small molecule model but was not attempted on the polymer. The end-to-end length of the bis-imine photoswitch was calculated to increase upon Z/E isomerization, the simple explanation that isomerization leads to polymer compaction was therefore not appropriate. The folding of the linear polymer was instead attributed to an increase in the overall chain flexibility induced upon photoisomerization. Interestingly, metal coordination leading to the compacted SCNP was possible via introduction of palladium ions, capable of coordinating to the Z isomer of the bis-imine. The formation of the bis-imine-palladium complexes lead to a secondary pathway to generate an SCNP, with clear compactions observed via DLS and SEC. The use of photoswitchable units as structure forming elements of an SCNP as well as metal coordination highlights an appealing system for future catalytic SCNPs that display reversible morphology and catalytic control.

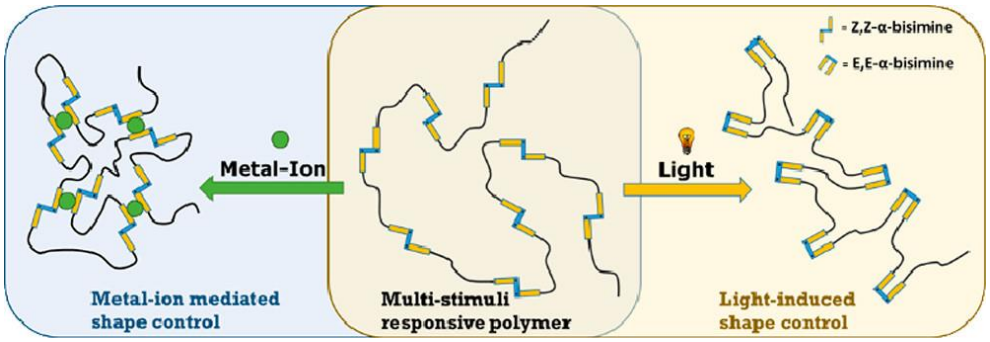

Figure 23. Two SCNP morphologies generated from main-chain photoisomerization of a bis-imine photoswitch and metal coordination. Adapted from Ref [271]

3 Research Aims and Objectives

A large number of SCNPs with an equally diverse number of catalytically active metal centres have been developed.[222,245,280] The presence of a polymeric scaffold around embedded catalytic sites within the SCNP have the potential to afford enhanced selectivity over substrates through complementary physical properties between substrate and the SCNP morphology. Consequently, the ability to control SCNP catalysis may arise from the dynamic control over the morphology, which may perhaps be realised through the unfolding and folding of an SCNP or through morphology changes to a formed SCNP. An appealing concept is the use of light to reversibly change the structure of an SCNP, leading to temporal control over an SCNPs catalysis, a concept that is yet to be achieved.[7] Reversible folding and unfolding of SCNPs has been attempted using photo-induced dimerization such as that of anthracene and styrylpyrene crosslinks.[8,281,296] However, the confinement of these species within an SCNP environment severely impedes the cycloreversion of the formed dimers, resulting in a relatively unchanged morphology. An appealing design concept is the use of photo switches such as azobenzenes embedded within an SCNP to enact morphological control, where the highly reversible photo switching process is retained even in confined environments. The incorporation of photoswitches within an SCNPs structure is relatively uncommon in literature, yet has been shown to enable reversible SCNP morphology control.[301,304] Critically lacking, however, is the combination of photoswitches and catalytically active metal species into the same SCNP, where

morphological changes arising from photoisomerization lead to indirect changes to the catalytic properties. A possible SCNP design would utilise photoswitches such as azobenzenes already incorporated into an SCNP bearing catalytically active metal centres. Photoisomerization of the SCNP-bound azobenzenes would result in reversible morphological changes i.e compaction, compartmentalization or expansion to the SCNPs structure. Azobenzenes are particularly appealing due to their conserved switching process, tuneable switching wavelengths, amenability to chemical modification as well as the distinct geometric and electronic properties that arise from the two photoisomers.[136,142,147] Such unprecedented catalytic control can also be envisioned by exploiting direct interactions between photoswitches where photoisomerization leads to reversible metal complexation. Spiropyran photoswitches are known to complex with metal ions upon photoisomerization into their merocyanine isomer, a process that is reversible with visible light irradiation.[184] Reversible spiropyran metal complexation is a known process in both small molecule and polymeric examples,[181,189,208] enabling crosslinking in the latter via the coordination of multiple spiropyrans to one metal ion. The same process, however, has not been utilised for the light triggered folding or unfolding of an SCNP from a spiropyran functionalised linear polymer. Such a system would constitute a highly appealing method of simultaneous light induced SCNP collapse and metal complexation, while also potentially affording photocontrol over SCNP unfolding.

3.1 Research Objectives

- Incorporate spiropyran photoswitches into linear polymer precursors and form SCNPs upon simultaneous spiropyran photoisomerization and metal complexation.
- Probe the reversible unfolding of SCNPs formed from the metal:spiropyran complexation into linear polymers using light as a stimuli.
- Develop an SCNP bearing both catalytic metal centres and azobenzene into its final structure.
- Investigate the impact of azobenzene photoisomerization on SCNP morphology and the subsequent effect on the catalytic properties of the same SCNP.

4 Photoswitchable, Catalytic SCNP via Azobenzene Crosslinks

4.1 Objective

Intramolecularly folded single chain polymers that exhibit dynamic control over secondary and tertiary structures are one of the ultimate design goals of polymer chemists working in the field of functional SCNP systems.[7] Proteins and enzymes, which inspired the first SCNP designs, display precisely ordered primary structures, and dynamic secondary and tertiary structures which are central to their function.[1,305,306] Achieving precise ordering in the primary structure of synthetic polymers is typically limited to small scales. However, the ability to impart dynamic changes to an SCNPs secondary and tertiary structure is still possible.[307–310]

Early dynamic SCNP morphologies have been achieved using reversible disulfide crosslinks[311] and host-guest chemistries that facilitate the folding and unfolding of an SCNP upon exposure to chemical stimuli.[312] Following these early studies, dynamic morphologies emerged. These were addressable using photochemical techniques, dynamic covalent pathways, and strong secondary bonding interactions, amongst other techniques.[9,298,313–315] The manipulation of tertiary structures has also been achieved using irreversible chemistries. Such examples include amine/anhydride cross-linking and subsequent thiol–ene chemistry,[311] as well as multicomponent reaction (MCR) based folding followed by hydrazino turn folding.[316]

A promising method of achieving truly dynamic control over the tertiary structure of an SCNP is via the incorporation of photoswitches into the polymer scaffold. Photoswitches have gained widespread usage in complex polymeric architecture, namely with azobenzene, bis-imine, spiropyran, and diarylethene switches.[317–320] Only a few examples exist of photoswitches being incorporated directly into SCNPs.[304] Typically photoswitches are relegated to pendant groups decorating a polymer as opposed to being incorporated as crosslinks or main chain elements.[155,301,321,322] Azobenzenes are by far the most utilised photoswitching motif in polymeric systems.[323–325] Ease of synthesis and the ability to finely tune the switching wavelengths via chemical modification make azobenzenes suitable

candidates for dynamic SCNP systems.[125,142] Combining such properties with catalytic functionalities would be a steppingstone to controlling the catalysis of an SCNP with light induced morphological changes.

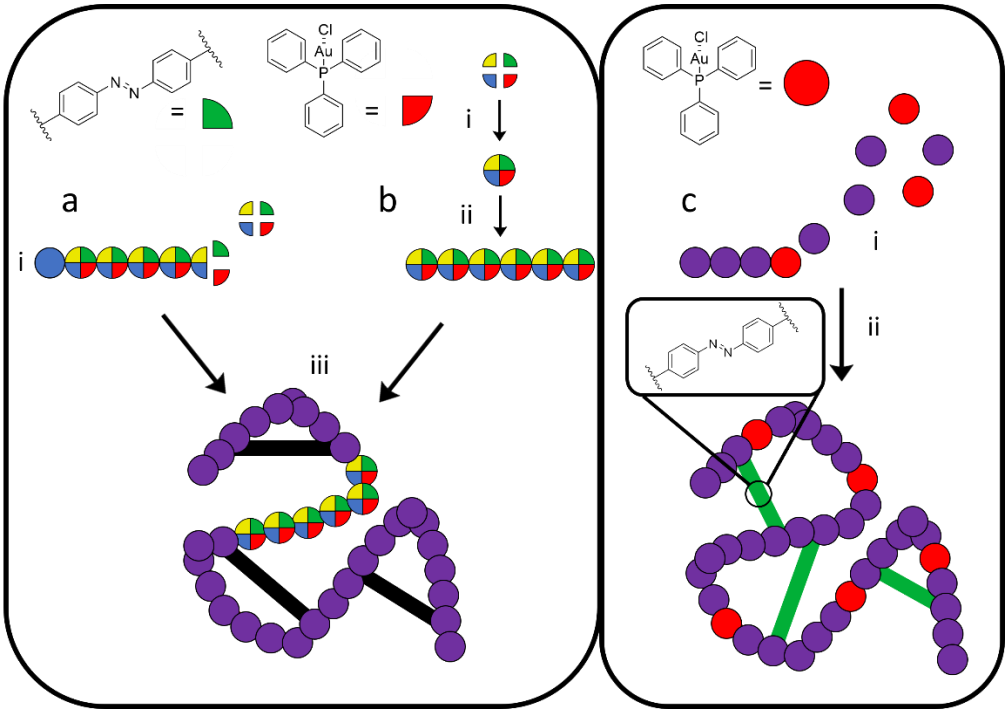

Scheme 7. a;i) incorporation of main chain azobenzenes into a sequence defined polymer block along with catalytically active Ar_3PAuCl groups via a multicomponent reaction, **(b;i)** a multicomponent reaction is used to make a photoswitchable/catalytic monomer, **(b;ii)** the monomer is polymerised into a polydisperse block. **(a&b;iii)** the photoswitchable catalytic block is then propagated into a block copolymer able to crosslink into an SCNP, **(c;i)** a polydisperse linear polymer is generated containing Ar_3PAuCl pendant groups, **(c;ii)** the polymer is crosslinked into an SCNP via external azobenzene crosslinkers.

In the current chapter an SCNP system addressable with two disparate wavelengths of light is introduced, resulting in reversible changes to the overall hydrodynamic volume and polarity (Scheme 7). Photoswitchable azobenzene crosslinks were implemented to fold a linear polymer decorated with triphenyl phosphine pendant groups, enabling the loading of catalytically active Au^I centres. The Au^I phosphine complex is further capable of catalysing intramolecular hydroamination reactions. The combination of photoswitchable crosslinks with catalytic properties in an SCNP highlights the potential for further advancements in the control of thermal catalysis by photochemical means.

Two synthetic strategies are initially discussed to develop such an SCNP system with azobenzene functionalities in the polymer backbone using multicomponent reactions. Inconclusive results led to the third synthetic strategy discussed in this chapter, which resulted in the successful development of a catalytically active photoswitchable SCNP (Scheme 7, **c**). The folding of the linear polymer into the SCNP with external azobenzene crosslinkers is also outlined. The current chapter also details the morphological characterization of the light induced switching of the SCNP and its preliminary results for employment as a catalyst in hydroamination reactions.

4.2 Sequence Defined Main Chain Photoswitchable SCNP Design

The insertion of photoswitches into the backbone of a linear polymer has been shown to induce significant morphological changes, namely a reduction in hydrodynamic volume. In the current section, we target a photoswitchable-catalytic SCNP generated from an ABA block copolymer. The B block consists of a sequence defined main chain-photoswitchable catalytic block generated using a multicomponent Ugi-polycondensation reaction. Conducted using a carbonyl, amine, isocyanide, and carboxylic acid, the Ugi reaction has previously been utilised for the development of highly functionalised polymer architectures.[326] Propagation of the cross linkable A blocks could be completed using Ring Opening Metathesis Polymerization (ROMP) and serves to irreversibly collapse the polymer into an SCNP.

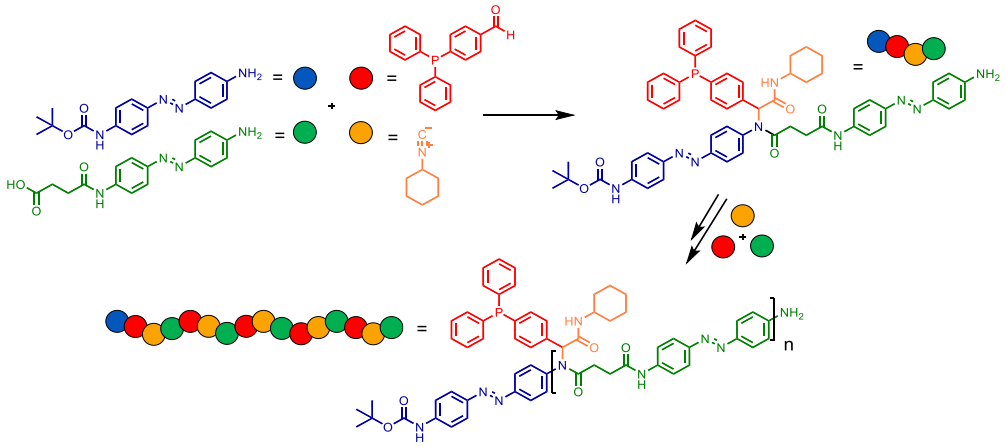

Scheme 8. Proposed Ugi-polycondensation for the formation of a sequence defined catalytic block bearing photoswitchable azobenzenes as main chain elements.

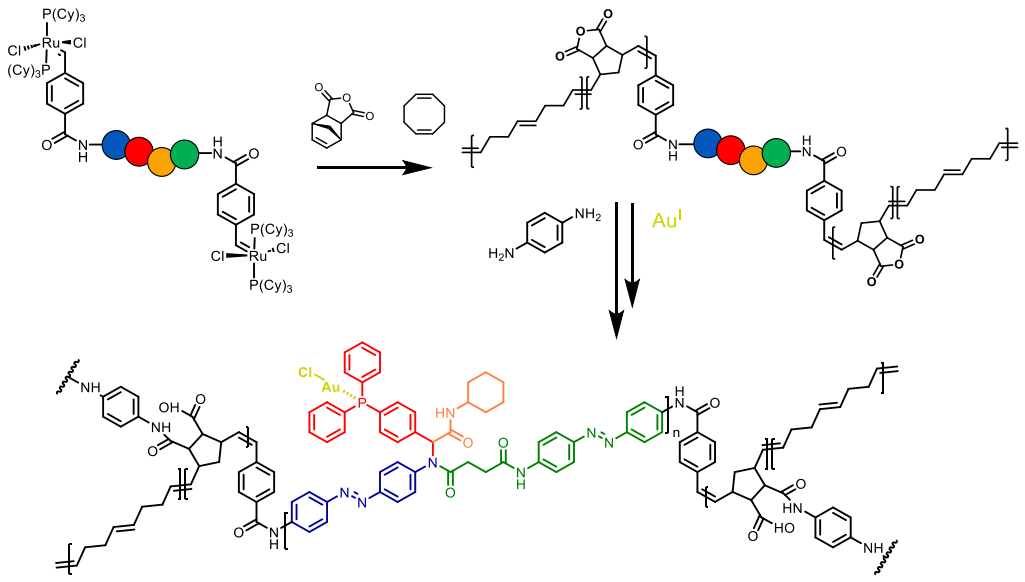

Scheme 9. Formation of a hybrid ROMP bis-initiator used to propagate the cross linkable A blocks from the catalytic B block.

Azobenzenes functionalised at the 4,4 positions with relevant functionalities for Ugi reactions are critical for the generation of a photoswitchable catalytic block. 4, 4 diamino azobenzene is asymmetrically protected by a Boc group and is used as the first point of propagation for sequential Ugi reactions with an acid, aldehyde, and isocyanide. The acid component is an azobenzene asymmetrically substituted with an amine and a carboxylic acid, the carbonyl; a triphenylphosphine functionalised with an aldehyde for Au^{I} loading and the isocyanide component consists of a commercially available linear isocyanide.

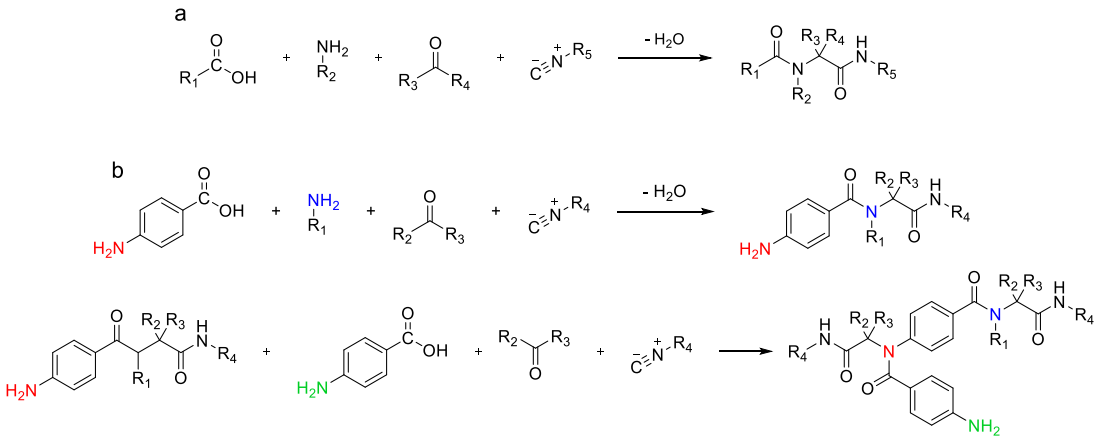

Scheme 10. (a) The Ugi multicomponent reaction. (b) polycondensation of sequence defined polymer via sequential Ugi reactions

The first Ugi adduct generates a free amine, which subsequently serves as the point of propagation for the next acid, aldehyde and isocyanide (Scheme 10). Repetition of this process can be completed until the catalytic block is of a suitable size (Scheme 8). Boc deprotection of the final propagated Ugi block would yield two free amines, which exchange with the styrene ligand of a Grubbs catalyst and generate a hybrid ROMP bis-initiator (Scheme 9). The hybrid initiator would be able to propagate norbornene anhydride from both sides of the catalytic block, affording the desired ABA block co-polymer structure. The resulting anhydride functionalities were to be crosslinked via ring opening with a suitable amine, forming an irreversible compaction into the SCNP. Gold loading of the phosphine pendant groups imbue the SCNP with its catalytic properties. The reversible isomerization of the photoswitchable B block was to be achieved by irradiation with two separate wavelengths of light.

4.2.1 Synthesis of the Boc Protected Amino Azobenzene

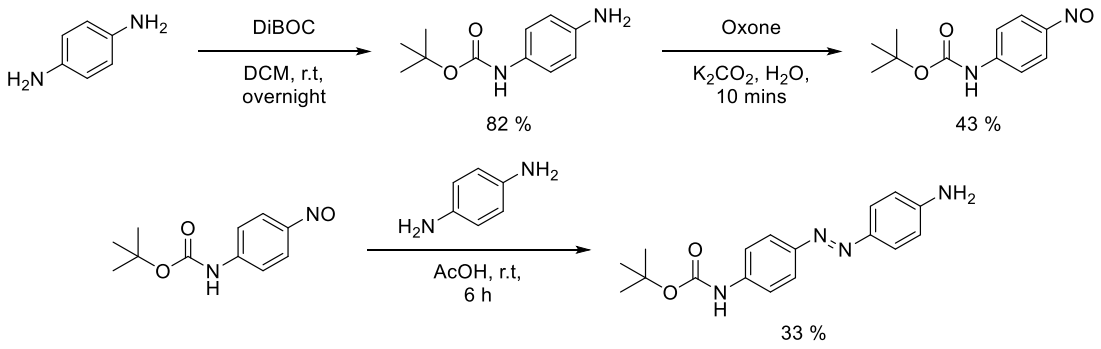

Scheme 11. Synthetic route to afford the asymmetrically Boc protected amino azobenzene.

The amine component was realised in a three-step procedure, beginning with the asymmetric Boc protection of phenylenediamine. Following a literature procedure, an excess of diamine was required to avoid the formation of the double protected diamine, residual amine was removed via column chromatography affording the Boc protected amine.[327] A common method of forming azobenzenes is via the condensation of an amine and nitroso group known as the Mills reaction.[142] The nitroso component can be formed via the oxidation of an aromatic amine using oxidising agents such as peroxymonosulfuric acid (caro's acid) or potassium peroxymonosulfate (Oxone), the latter is often favoured due to its easier handling. Using a modified literature procedure, the Boc protected amine was converted to the nitroso using Oxone in a solvent mixture of THF and water.[328] Conventionally conducted in water, the

oxidation of the hydrophobic Boc amine required the addition of THF with minimal impact on the reaction. The oxidation of the amine group into the nitroso variant meant that the product could be precipitated from solution with the addition of a large amount of water and used for the next step without the need for purification. The Mills condensation of the two components was subsequently carried out using a modified literature procedure in acetic acid and THF for only 5 hours, commonly conducted overnight.[328] The sensitivity of the Boc group to the acidic reaction conditions was considered and a test reaction was performed. Stirring the nitroso group in acetic acid, simple TLC analysis showed only the presence of the starting material suggestive of an intact Boc group. Likely, the Mills reaction could be carried out for longer periods of time to increase the yield of the final novel amine ugi component. ^{1}H NMR spectroscopy revealed the asymmetric protection of the azobenzene, highlighted by the characteristic signal attributed to the *tert*-butyl resonances of the Boc group (δ = 1.5 ppm). Furthermore, the asymmetric splitting of the azobenzene aromatic hydrogens into 4 separate resonances (*c,d,e,f* - Figure 24) validates the asymmetric Boc protection of the azobenzene (for detailed synthesis refer to Experimental section **8.2.1**, associated spectra, Appendix section **10.1.1)**.

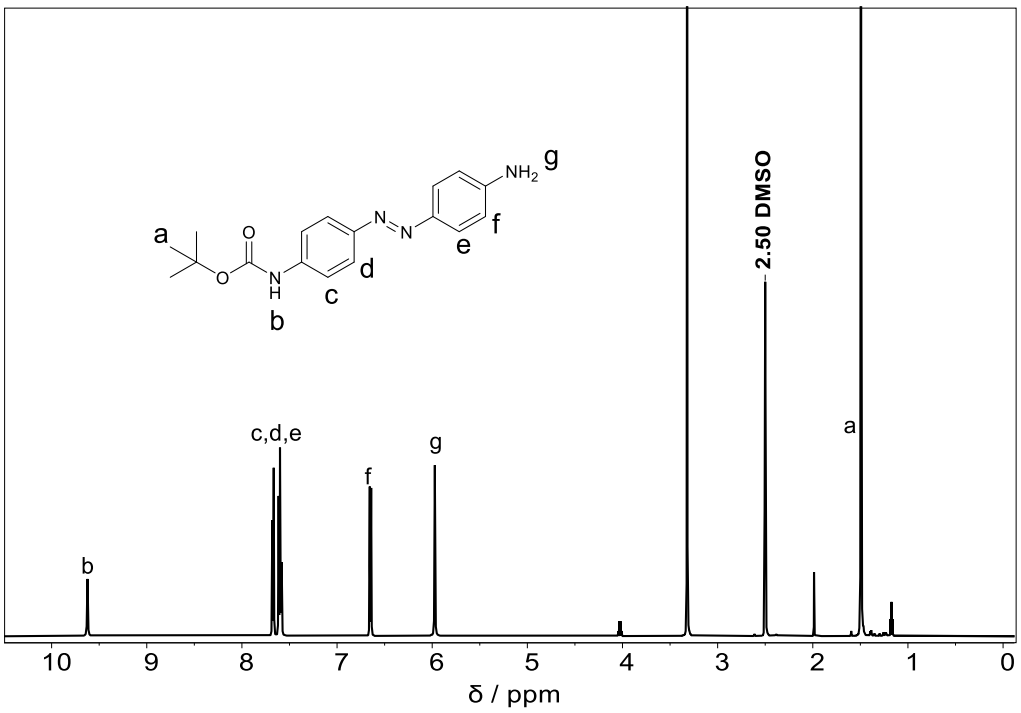

Figure 24. ^{1}H NMR spectrum of the Boc protected azobenzene in DMSO.

4.2.2 Synthesis of the Amine/Carboxylic Azobenzene

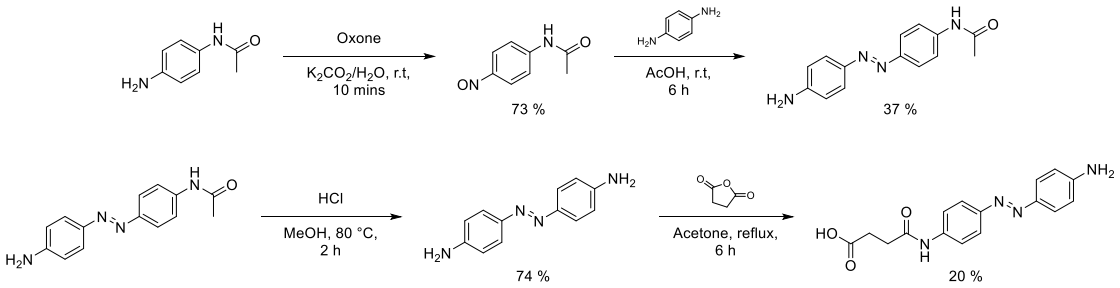

Scheme 12. Synthesis route to afford the bi-functional acid/amine azobenzene component.

The first three steps of the synthesis procedure (Scheme 12) were completed following a modified procedure by Ge et al.[328] Acetanilide was converted into the nitroso derivative using Oxone as the oxidising agent. Like the synthesis of the Boc protected azobenzene completed previously, the nitro group was condensed with p-phenylenediamine to afford an asymmetric azobenzene with a free primary amine. 4,4-Diamino azobenzene was subsequently generated by the acidic hydrolysis of the acetanilide functionality, and an increase in pH precipitated the crude product, which was then purified via column chromatography. Ring opening of succinic anhydride was used to install a carboxylic acid functionality onto the azobenzene following a modified literature procedure.[329] Achieving the novel mono-functionalised product proved difficult, as the doubly functionalised adduct consistently formed. Lowering the concentration of succinic anhydride could have been used to prevent this impurity from forming at the cost of a reduced yield of the desired product. Separation of the mono functionalised product from the bis functionalised impurity was partially achieved using a mixture of MeOH/DCM with 1% triethyl amine. Many fractions contained both species, enough of the desired product was however isolated. ^{1}H NMR resonances (Figure 25) belonging to the propanoic acid chain are clearly visible (δ = 2.6-2.5 ppm), indicating the attachment of the acid functionality. Additionally, the resonance attributed to the amide bond generated upon ring opening is clearly visible at (δ = 10.2 ppm)(for detailed synthesis refer to Experimental section **8.2.2**, associated spectra, Appendix section **10.1.2)**.

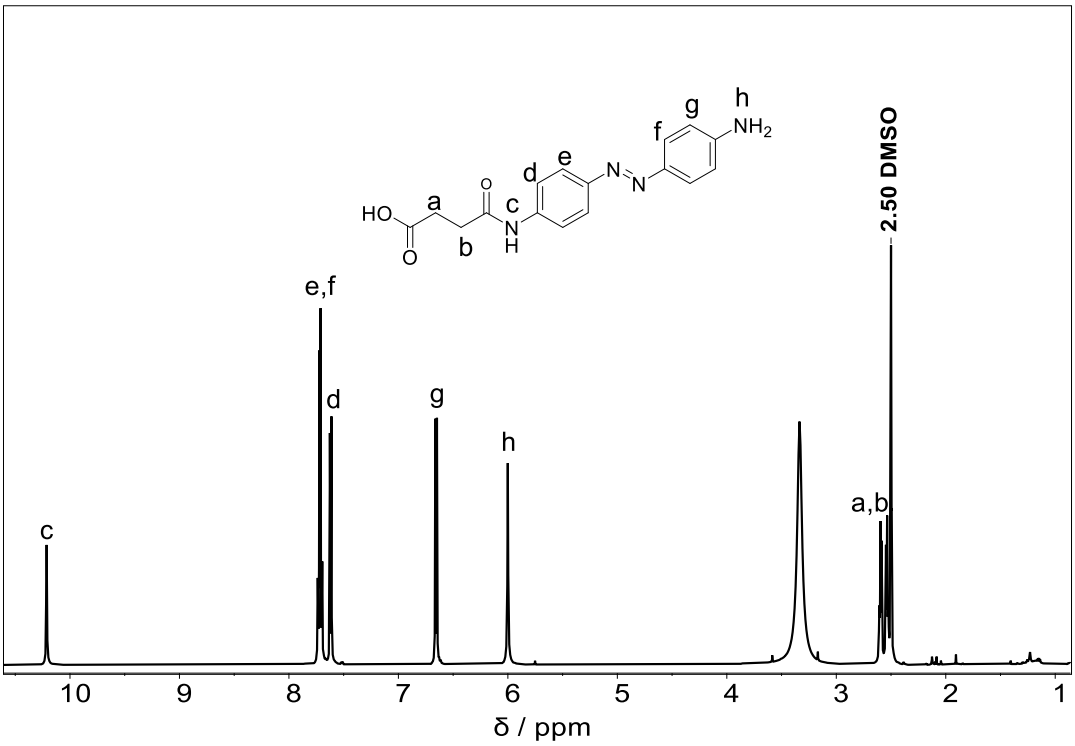

Figure 25. [1]H NMR spectrum of the bi-functional acid/amine azobenzene in DMSO.

4.2.3 Synthesis of the Aldehyde Triphenylphosphine

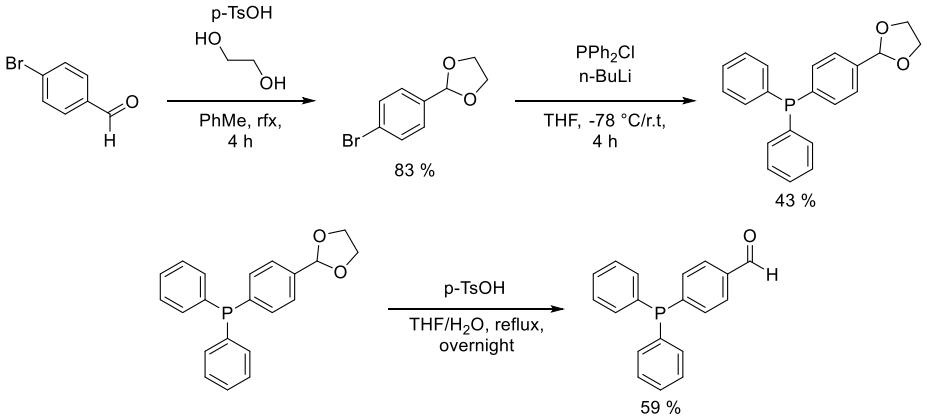

Scheme 13. Synthetic route to afford aldehyde functionalised triphenyl phosphine.

Catalytic properties were to be imparted into the SCNP via triphenylphosphine coordinated with a gold centre. A three-step procedure to functionalise triphenylphosphine with an aldehyde was completed,[330] constituting the carbonyl component of the Ugi reaction. Ethylene glycol was used to protect 4-bromo benzaldehyde in toluene. The protection was completed using a dean stark apparatus driving the reaction to a high yield of 83% after 16 hours. The aldehyde impurity was

removed from the reaction mixture via subsequent washes with saturated sodium bisulfite, where the aldehyde is converted into a water-soluble charged sulphite species that is taken up in the water layer.[331] The product was isolated without the need for column chromatography and used for the next step. The protected aldehyde was subsequently converted into the corresponding triphenylphosphine with chlorodiphenyl phosphine, facilitated by a halogen exchange reaction using n-butyllithium. The triphenyl phosphine was formed, however oxidation of phosphine was pervasive as evidenced by ^{31}P NMR. No oxidation was visible in the starting material, suggesting that oxidation was occurring during the reaction. While the reaction was completed under dry conditions and an argon atmosphere, residual oxygen and/or peroxide radicals in the THF may have resulted in oxidation of the phosphine. The reaction was then completed with THF sourced from a solvent purifier system (SPS) and was extensively degassed via N_2 sparging, resulting in a small amount of oxidation that was tolerated as an un-avoidable impurity. The acetal protected triphenyl phosphine was readily isolated via precipitation in cold methanol overnight. Deprotection of the aldehyde was completed using catalytic amounts of toluenesulfonic acid to generate the final aldehyde functionalised triphenylphosphine, precipitated using cold methanol. ^{31}P NMR spectroscopy shows the characteristic resonance of free tri aryl phosphines and a minimal amount of phosphine oxide, ^{1}H NMR spectroscopy shows a resonance at (δ = 10 ppm), characteristic of an aldehyde hydrogen (for detailed synthesis refer to Experimental section **8.2.3**, associated spectra, Appendix section **10.1.3)**.

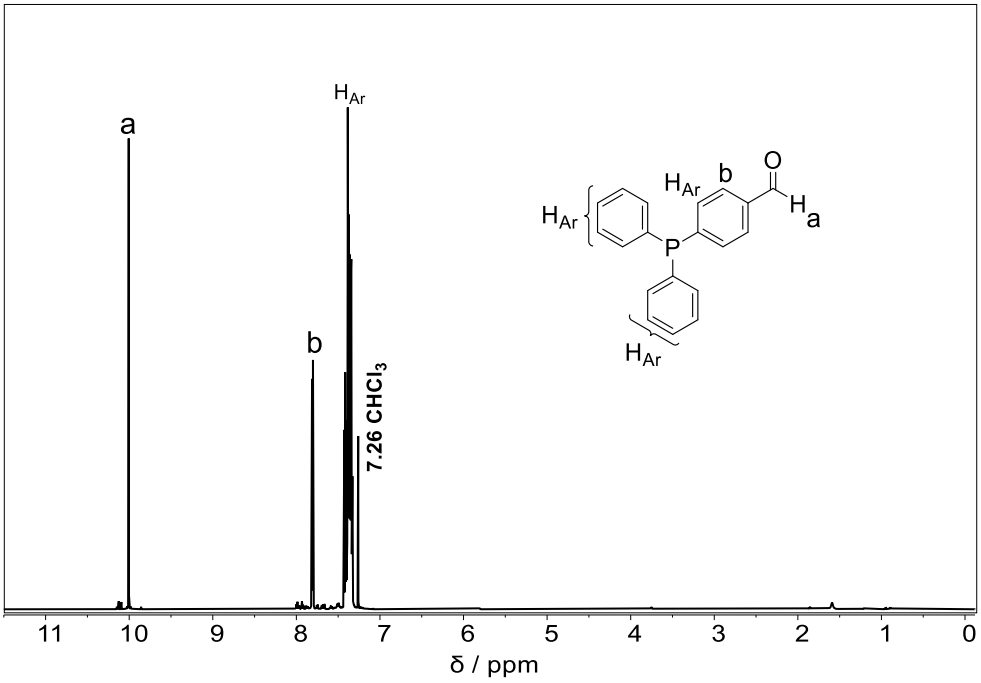

Figure 26. ^{1}H NMR spectrum of the aldehyde triphenylphosphine in $CDCl_3$.

4.2.4 Attempted Ugi Reaction

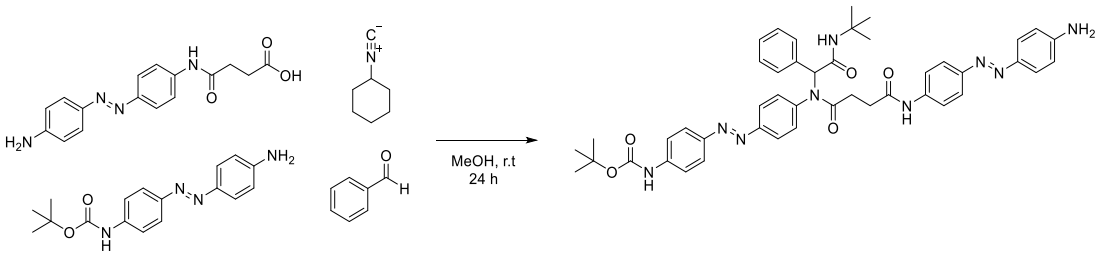

Scheme 14. Attempted test Ugi reaction between the carboxylic acid and amine azobenzenes with benzaldehyde and cyclohexyl isocyanide.

Ugi test reactions were initially completed without the triphenylphosphine aldehyde component, instead benzaldehyde was used as a model substrate. The amine and aldehyde components were combined and stirred for 2 hours, subsequently the carboxylic acid and isocyanide were added to the reaction mixture in succession. An orange precipitate formed after 4 hours of stirring at room temperature. Ugi reactions are regularly conducted in methanol,[332] often inducing precipitation of the typically apolar Ugi adduct. TLC analysis showed a large amount of starting material was present even after three days of stirring. The reaction was stopped, the orange precipitate collected, and the reaction mixture concentrated under reduced pressure.

LC-MS analysis of the concentrated reaction mixture revealed a small amount of the desired Ugi adduct, a large amount of starting material, and unidentifiable side products. A large peak in the chromatogram was attributed to the competitive Passerini multicomponent reaction. The Passerini reaction is a three component reaction, proceeding without the amine. The formation of the Passerini adduct is suggestive of either a slow forming or weakly basic imine intermediate in the Ugi reaction (Scheme 15).

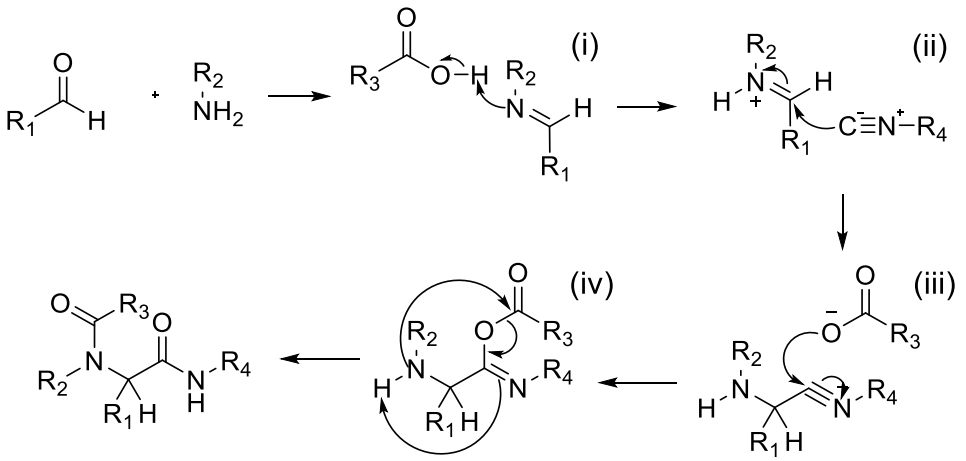

Scheme 15. Generally accepted mechanism for the Ugi reaction, (i) imine formation and protonation, (ii) nucleophilic trapping of the isocyanide, (iii) substitution of the carboxylate, (iv) Mumm rearrangement.

A ^{1}H NMR spectrum was hard to analyse due to a multitude of overlapping resonances. Characteristic resonances attributed to the amide proton of the amine starting material at (δ = 10.16 ppm), as well as a large resonance at (δ = 8.71 ppm) potentially belonging to the imine intermediate (Figure 27). (for detailed synthesis refer to Experimental section **8.2.3.4)**.

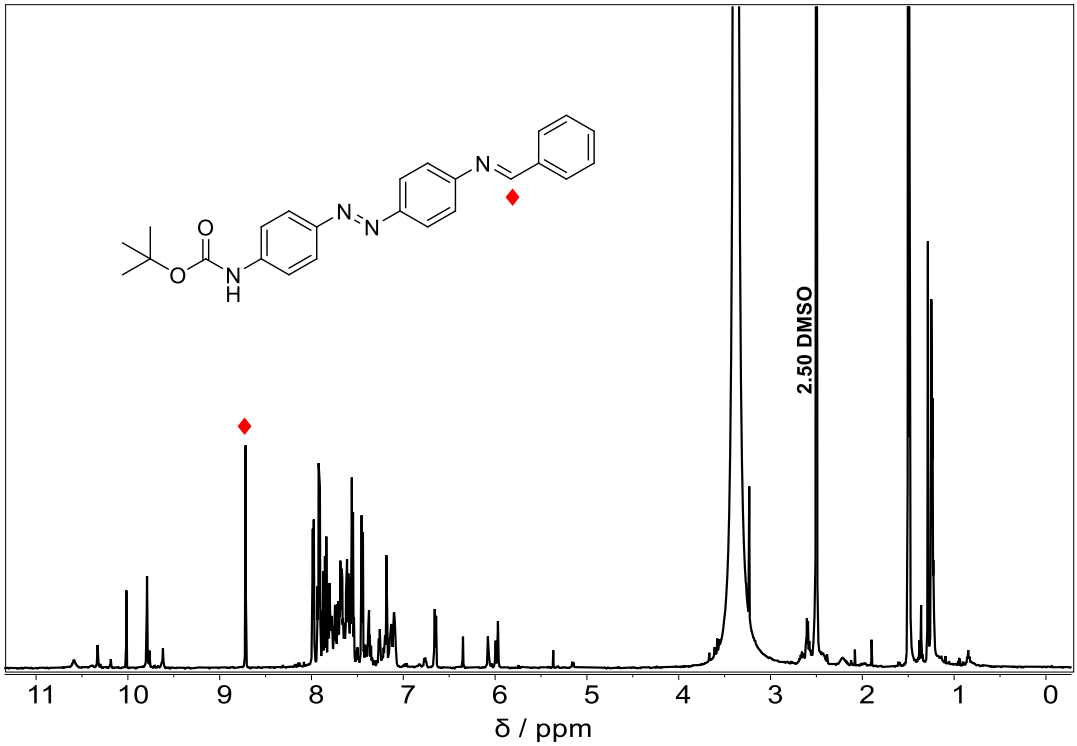

Figure 27. ^{1}H NMR spectrum of the crude Ugi reaction in DMSO, possible imine proton highlighted by a red diamond.

Furthermore, the precipitate did not contain the Ugi adduct as indicated by LC-MS analysis and ^{1}H NMR spectroscopy. Starting material could not be assigned in the NMR spectrum, the collected precipitate was also only soluble in $CDCl_3$, while both azobenzene starting materials were soluble in DMSO. LC-MS analysis revealed only carboxylic acid starting material. It is possible that the bulk of the precipitate was comprised of an apolar species that elutes very late in the reverse phase, acetonitrile/water mixture LC-MS method. A longer chromatogram or amended method facilitating an apolar substrate may have supported this conclusion. The Ugi reaction was re-run using a solvent mixture of THF:MeOH. Ugi reactions using THF are not commonly described in literature but examples exist, particularly when apolar Ugi components are used.[333] Furthermore, if the triphenylphosphine aldehyde component were utilised it would not be soluble in pure MeOH, and a second co-solvent such as THF would be required. The amine and aldehyde were initially reacted to form the imine followed by the addition of the carboxylic acid and isocyanide. TLC analysis of the reaction mixture containing only the amine and aldehyde components showed a new orange spot attributed to the imine forming after an hour of stirring. An

additional hour of stirring was completed, and the carboxylic acid and isocyanide added with no precipitate forming. LC-MS analysis revealed only starting material and un-identifiable side products with absorption profiles similar to that of an azobenzene. The presence of larger amounts of the aldehyde and amine components suggests that the Ugi reaction did not proceed to/or past the imine formation step.

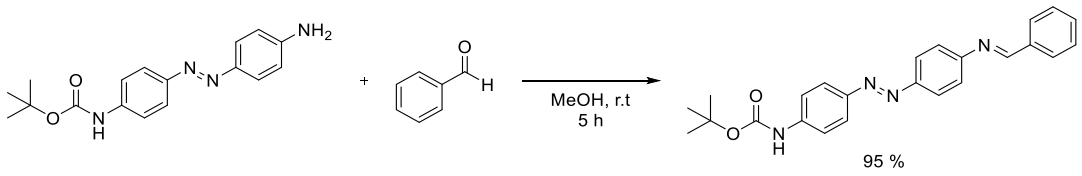

Scheme 16. One step reaction to convert the Boc protected azobenzene into an imine.

Isolating the imine intermediate was subsequently attempted (Scheme 16). Combining the aldehyde and amine component in pure methanol resulted in a new spot forming after 1 hour. After 5 hours, ^{1}H NMR analysis confirmed the formation of the imine with a characteristic resonance at (δ = 8.71 ppm), the same resonance was observed in the crude Ugi ^{1}H NMR spectrum.

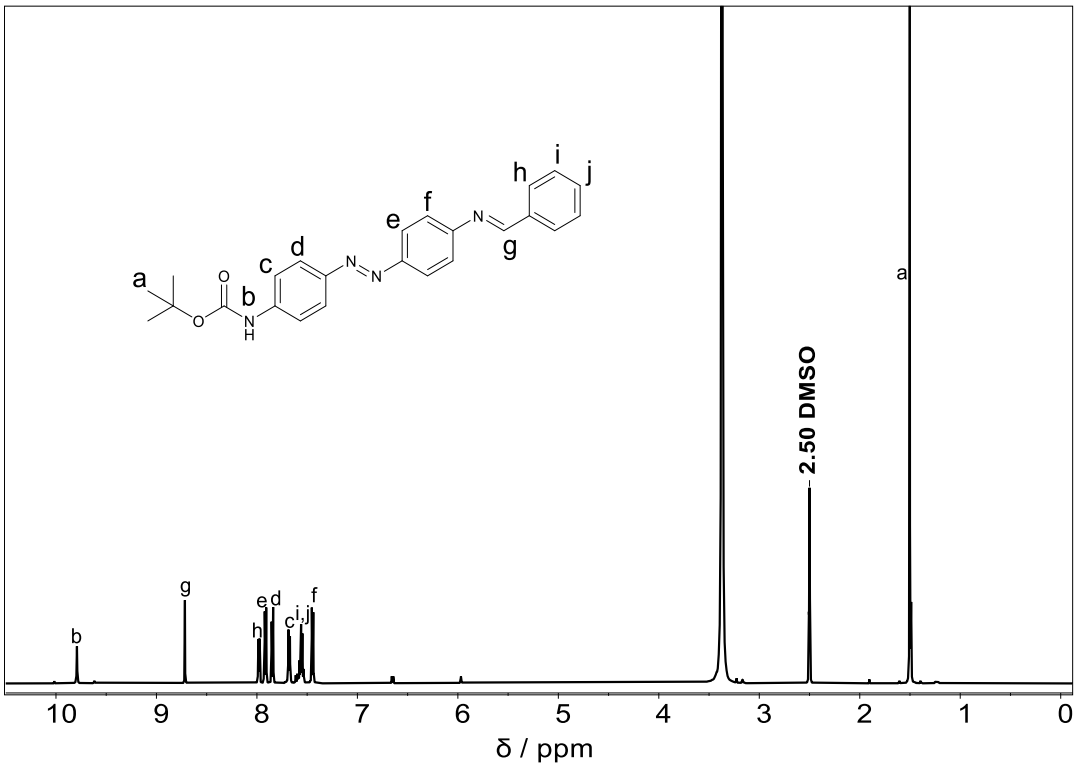

Figure 28. ^{1}H NMR spectrum of the imine in DMSO.

Only the amine and a very small amount of the imine product was observed in LC-MS, identified as imine hydrolysis by the acidic conditions of the column. Based on these findings it is likely that the imine is able to form, it is however relatively unreactive and unable to deprotonate the carboxylic acid in the subsequent step. The azo-bridge in *para*-position to the imine acts as a withdrawing group reducing the basicity of the imine, furthermore the aromaticity of benzaldehyde may favour imine formation but will further reduce its basicity (for the detailed synthesis refer to Experimental section **8.2.1.3** associated spectra **10.1.1.4)**..[334,335] To remedy this problem, a more reactive amine and consequently imine were envisioned.

4.2.5 Fmoc/Boc Orthogonally Protected Reactive Amine

The acidity of the aromatic amine of the previously synthesised azobenzenes prevents the resulting imine from being able to deprotonate the carboxylic acid component. A new three step procedure was developed to generate an azobenzene bearing an aliphatic amine. 4-Amino benzylamine was asymmetrically protected using Fmoc-chloride following a literature procedure.[336] Isolation of the resulting product via column chromatography proved difficult. The product was identified using ^{1}H NMR spectroscopy and LC-MS, however 4-amino benzylamine still remained in the sample as an impurity. The difficulty of isolating the product meant it was used with impurities for the next step. The Mills reaction was again used to condense the free amine of the Fmoc protected compound with the nitroso group of the Boc protected compound employed to make the earlier Boc protected amino azobenzene. Combined in acetic acid and left overnight, the novel Boc-Fmoc protected azobenzene was synthesized and readily purified using column chromatography, removing impurities from the Fmoc protection still present in the reaction mixture. Analysis with ^{1}H NMR spectroscopy shows a characteristic signal at (δ = 1.6 ppm) attributed to the *tert*-butyl fragment of the Boc group. Additionally, the resonance attributed to the aliphatic hydrogens of the benzyl amine functionality (*f*: δ = 4.46 ppm) display the correct integral ratios with the characteristic methyl and fluorenyl resonances (*g*: δ = 4.5 ppm and *h*: δ = 4.3 ppm) indicating successful attachment of the Fmoc group (see Figure 29 for alphabetic resonance assignments).

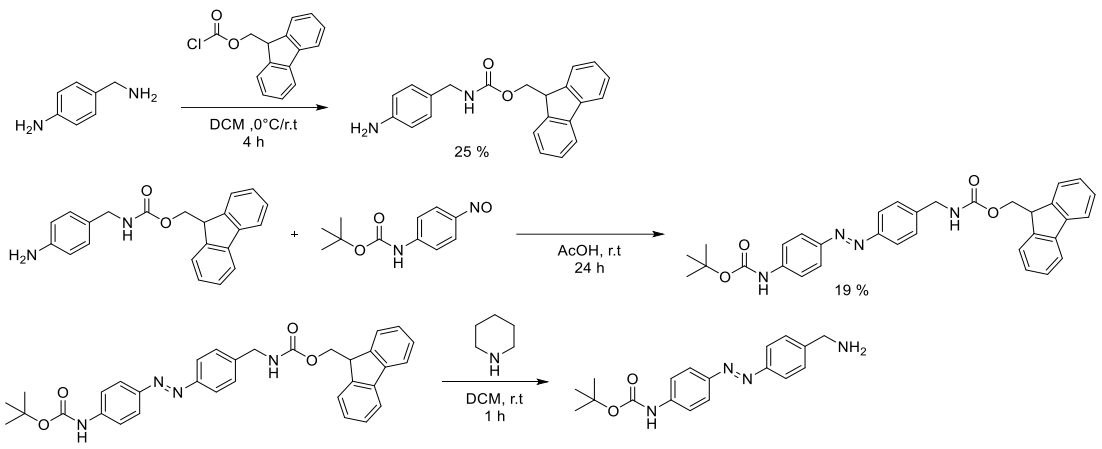

Scheme 17. Synthetic route to afford the benzylamine azobenzene via orthogonal Fmoc/Boc protection and subsequent Fmoc deprotection.

A test deprotection of the Fmoc group to generate the free aliphatic amine was completed, using piperidine in DCM. Deprotection was completed over an hour and TLC analysis indicated that deprotection had occurred within the first 10 minutes and the reaction could have been stopped sooner. The crude reaction mixture was concentrated under reduced pressure and a bright orange solid was generated. LC-MS analysis of the crude reaction mixture showed the deprotected amine product and an abundance of the expected piperidine/fluorenyl adduct. The reaction was not scaled up and the product was not purified from the piperidine/fluorenyl adduct. However, the procedure resulted in the formation of the desired aliphatic amine functionalised azobenzene (for the detailed synthesis refer to Experimental section **8.2.1**, associated spectra, Appendix section **10.1.1)**.

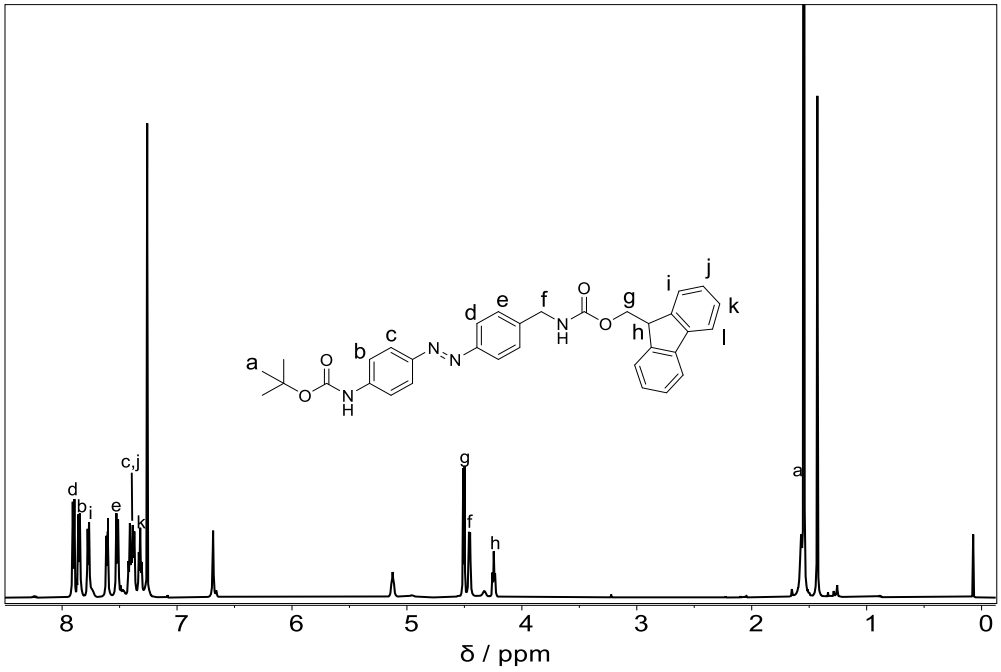

Figure 29. ^{1}H NMR spectrum of the orthogonally protected azobenzene in $CDCl_3$.

4.2.6 Conclusions

This strategy was intended to use sequential Ugi reactions to construct a sequence defined catalytic B block of an SCNP with an ABA block structure. Three Ugi components were synthesised, a Boc protected amino azobenzene, a 4,4 amino carboxy azobenzene, and an aldehyde functionalised triphenylphosphine. The two azobenzene components were combined with aldehyde and a commercial isocyanide in test Ugi reactions. LC-MS and ^{1}H NMR spectroscopic analysis of the test reactions revealed a large amount of starting material and the presence of the imine intermediate, the first step of the Ugi reaction. An adduct belonging to the competitive Passerini reaction was also identified using LC-MS. A subsequent experiment was completed combing the amino azobenzene and the aldehyde to form the imine. The imine formed in an appreciable amount of time and was characterized via ^{1}H NMR. Based on the ease of imine formation, the large amount of starting material and the Passerini adduct, it was assumed that the formed imine was too unreactive to take part in the Ugi reaction. A new amine component was synthesized utilizing an orthogonal Boc/Fmoc protection strategy to generate an azobenzene bearing an aliphatic amine, subsequently able to form a more reactive imine. Deprotection of this new component was completed but further experiments were not. The synthetic effort required to continue

with this strategy may not have been feasible. A new reactive amine/carboxylic component would also need to be synthesised. Additionally, the effect of the aldehyde triphenyl phosphine on the Ugi reaction is unknown. It is possible that an imine formed with triphenylphosphine would have decreased reactivity owing to increased delocalisation across the phenyl rings, a new aldehyde component may then also be needed. Significant time had been taken to already to synthesise all the components and would require more time for the new reactive components. Sequential Ugi reactions, Grubbs catalyst functionalisation and ROMP polymerization was still yet to be completed. To pursue a sequence defined system a less complicated reaction would be needed. Poly-condensation using a basic esterification reaction with suitably functionalised azobenzenes would be more realistic. Post functionalisation of the azobenzene catalytic block with triphenylphosphine could afford the polymeric block with the desired photoswitchable catalytic properties. Foregoing a sequence defined block, a new strategy was envisioned that was synthetically easier to achieve while still affording a similar final SCNP.

4.3 Polydisperse Main Chain Photoswitchable SCNP Design

The second approach to incorporating azobenzenes into the backbone of an SCNP utilizes an Ugi reaction to synthesise a single monomer, which entails both the catalytic phosphine and photoswitchable azobenzene. The monomer makes use of the isocyanide and aldehyde components employed in the first strategy, requiring a new bis carboxyl substituted azobenzene and alkene capped linear amine. The combination of these components would culminate in a single monomer functionalised with two phosphine ligands and a central azobenzene unit that bears linear alkenes for ADMET polymerization. The targeted polymer lacks the monodisperse nature of the SCNP attempted in the first strategy yet would be less synthetically demanding.

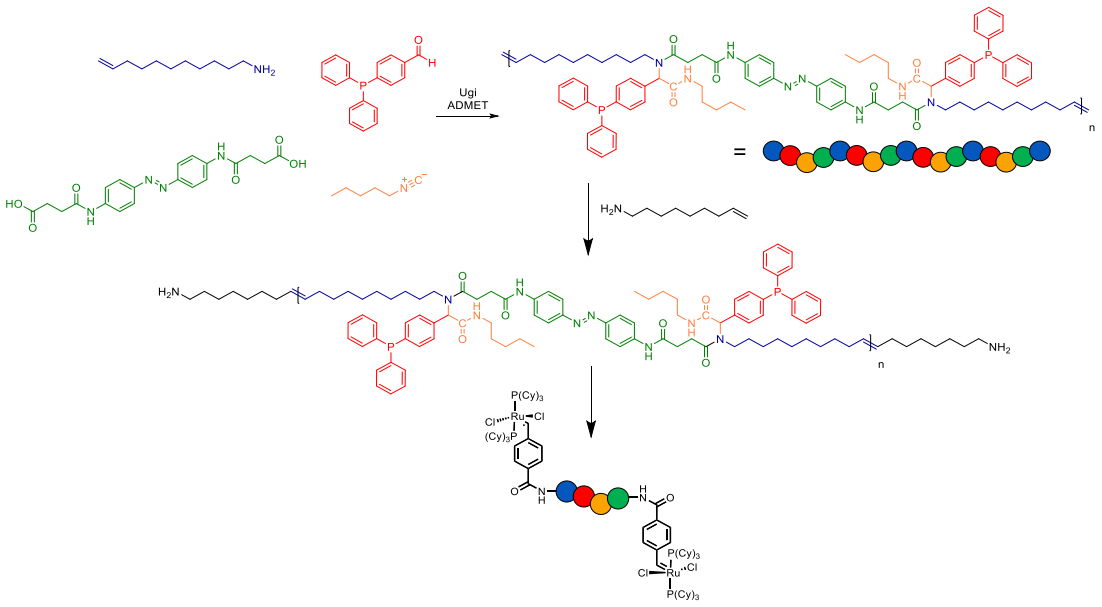

Scheme 18. Use of the Ugi reaction to first generate a monomer polymerized into via ADMET followed by functionalisation into a hybrid-bis initiator for ROMP propagation of cross linkable A chains.

ADMET polymerization is used to form the catalytic B block of the SCNP system. Amine chain stoppers could cap the propagating chain, followed by the same procedure discussed in the first strategy. The catalytic block would be exchanged with a Grubbs catalyst, forming a hybrid bis-initiator for ROMP. The hybrid initiator propagates norbornene anhydride, which can be crosslinked using a suitable amine to generate the compacted SCNP which is loaded with catalytic gold complexes.

4.3.1 Synthesis of amine

The amine component of this Ugi reaction bears the polymerizable alkene functionality at the end of an 11-carbon chain, necessary for ADMET polymerization. The amine was synthesised following a literature procedure starting from 10 undecenoic acid,[304] by initially converting the acid into the acid chloride, using thionyl chloride as both a reagent and solvent. The bulk of thionyl chloride was removed by distillation, affording the acid chloride which was then taken to the next step. The acid chloride was converted to the primary amide, using ammonia to substitute the chloride. Finally, the amide was reduced to the corresponding primary amine using $LiAlH_4$, yielding a ^1H NMR spectrum matching that of literature. [304] The product was deemed pure and further purification of this product was not completed (for detailed synthesis refer to Experimental section **8.2.5**, associated spectra, Appendix section **10.1.5)**

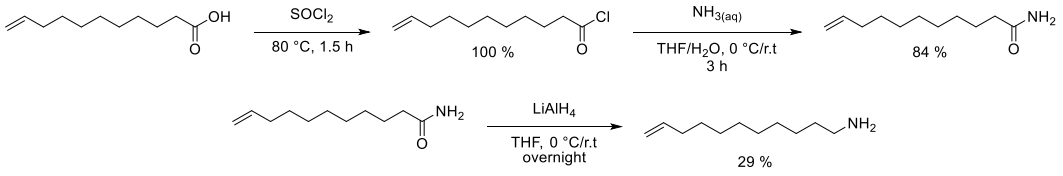

Scheme 19. Synthetic route to afford the linear amine capped with a terminal alkene.

4.3.2 Synthesis of the Disubstituted Carboxylic Acid Azobenzene

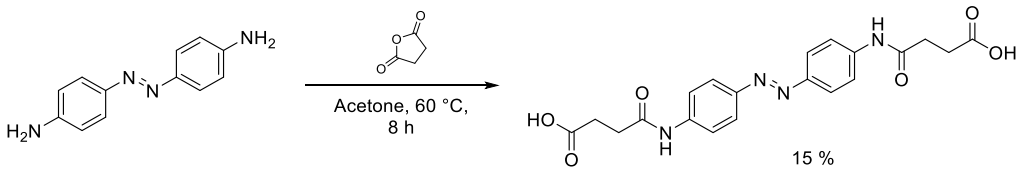

Scheme 20. One step reaction to convert diamino azobenzene into a di-acid azobenzene.

The novel di-acid component was subsequently synthesized using a modified synthetic procedure, from the previous diamino azobenzene used for the synthesis of the sequence defined Ugi components.[329] Succinic anhydride in excess was used to generate the dicarboxylic azobenzene. A small amount of the mono-functionalised azobenzene was observed along with residual succinic anhydride, suggesting the reaction should have been left to react for a longer period. Column chromatography to purify the product was not attempted owing to the carboxylic functionalities and recrystallisation was instead conducted. Finding a suitable solvent for recrystallization was challenging, as the capacity of the carboxylic acids to hydrogen bond with themselves made the product highly insoluble in many solvents. However, the product was able to be re-crystallised from a mixture of water and EtOH. Two overlapping aromatic resonances with a combined integral attributed to 8 H each was visible in the aromatic region of the ^{1}H NMR spectrum suggesting a symmetrically functionalised azobenzene with the carboxylic acid functionalities. The alkyl hydrogens of the propanoic acid substituents was also present as two distinct signals in the aliphatic region of the spectrum (for detailed synthesis refer to Experimental section **8.2.4.1**, associated spectra, Appendix section, **10.1.4.1)**.

4.3.3 Ugi Reaction

The individual Ugi components already display solubility in a limited range of solvents and this is exacerbated when all components are combined. The aldehyde functionalised triphenyl phosphine is insoluble in polar solvents such as MeOH and DMSO and soluble in DCM and THF. Inversely, the di-carboxylic acid is soluble in only the most polar solvents at room temperature such as DMF or DMSO and sparingly soluble in MeOH. Consequently, the Ugi reaction needed to be completed in a mixture of DMSO and DCM, such combination of an apolar and polar solvent in place of pure MeOH has been reported for Ugi reactions.[337] The linear amine and aldehyde functionalised triphenyl phosphine were combined in a solvent mixture of 1:2 DCM:DMSO, allowing for complete dissolution of both components. This was followed again by the addition of carboxylic acid and isocyanide components. No precipitate formed and the crude reaction mixture was instead concentrated under reduced pressure. The Ugi adduct was not identified using LC-MS, even a method tailored specifically for a polar compound did not show any Ugi product and only starting material was observed. An ^{1}H NMR spectrum of the crude mixture contained many overlapping signals making useful analysis highly challenging. The same reactivity problem that was used to explain the lack of product formation for the sequence defined Ugi procedure would not explain the absence of product, the linear amine being highly nucleophilic. As mentioned previously, an imine formed between an amine and triphenylphosphine may not be suitably reactive for the further steps of the reaction. The Ugi reaction, while possible in a variety of solvents, favours polar solvent and low yields are reported in solvent mixtures,[338] as such DCM:DMSO may not be a suitable solvent mixture for this ugi reaction (for detailed synthesis refer to Experimental section **8.2.5.4**, associated spectra, Appendix section **10.1.5.4)**.

4.3.4 Conclusion

The strategy to develop a polydisperse main-chain switchable SCNP envisioned a single monomer formed by the Ugi reaction able to propagate via ADMET polymerization. This monomer would consist of an azobenzene central unit functionalised at the 4’4-positions with linear alkenes and further functionalised with a triphenyl phosphine unit. A di-carboxylic azobenzene and linear amine terminated with an alkene were synthesized. Combining these two components with the aldehyde functionalised triphenylphosphine and a commercial isocyanide failed to form the ugi adduct. Owing to the disparate solubilities of the components, solvent mixtures potentially not conducive to an Ugi reaction were required and this may have affected product formation. A linear aliphatic amine was used, fault cannot be placed on an unreactive amine as it was in the first strategy. It was however possible that an imine formed with triphenylphosphine is still too unreactive. Subsequent test reactions should be completed where the amine/alkene and carboxy/azobenzene components are iteratively reacted with simple Ugi components before being combined together. Due to the failure of this Ugi reaction and the significant amount of work required in both testing the viability of the Ugi reaction as well further steps, a third simpler strategy was envisioned. The Ugi reaction proving problematic, was to be removed all together in place of a conventional free radical polymerization. A poly disperse statistical copolymer is generated with catalytic functionality and crosslinked with azobenzenes.

4.4 Photoswitchable, Catalytic SCNP via Azobenzene Crosslinks

Incorporating azobenzenes as crosslinking agents for a catalytic linear polymer is a more realistic way of affording a photoswitchable catalytic system. A non-defined SCNP system was envisioned where light induced morphological changes are the result of isomerization of azobenzene crosslinks as opposed to isomerization of the backbone incorporated azobenzenes. Catalytic phosphine units and azobenzene crosslinks are treated as separate units rather than being combined in one highly complex monomer or repeat unit. A statistical copolymer distribution also replaces the desired ABA structure of the first two strategies helping to reduce the overall complexity of the system while still affording a catalytic SCNP with light addressable morphologies. Synthetically, this strategy is divided into three parts, the free radical

polymerization of a suitable linear polymer, synthesis of the azobenzene crosslinker and subsequent light induced morphology/catalytic testing. Discussed in the current section, is the copolymerization of styrene via Nitroxide Mediated Polymerization (NMP) with vinylic derivatives of triphenyl phosphine and benzyl substituted styrene's for catalysis and crosslinking, respectively. Aswell as the development of suitable crosslinking strategies to incorporate azobenzene crosslinks while retaining the functionality of the polymer.

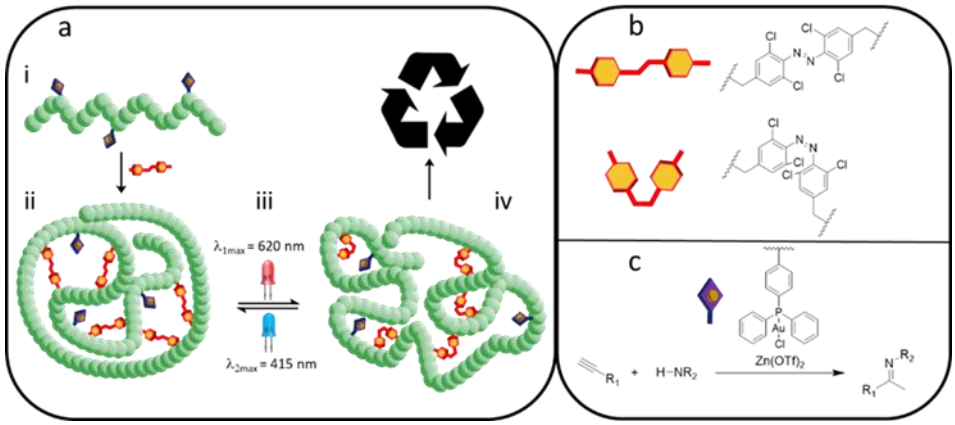

Scheme 21 (i) linear polymer bearing [Ar_3PAuCl] as a potential catalytic site; (ii) compaction of the linear polymer into an SCNP using an external azobenzene cross-linkers; (iii) reversible light-induced switching of the azobenzene crosslinks alters the SCNP morphology; (iv) azobenzene isomerization restricts access to the gold catalyst, (b) azobenzenes used to crosslink the linear polymer, irradiation yields *cis* and *trans* isomers, (c) catalytic functionality is provided by Ar_3PAuCl for the hydroamination of alkynes.

4.4.1 Synthesis of Linear Polymer and Crosslinking

Vinyl benzyl chloride was initially copolymerised with styrene to generate a 14,000 g mol^{-1} test polymer without the phosphine pendant groups to establish the SCNP crosslinking conditions (NMP procedure, Experimental section **8.3.1.1**, ^{1}H NMR spectra and SEC elugrams, Appendix section **10.2.1)**. A one step oxidative coupling of 4-nitrobenzoic acid afforded 4,4-dicarboxy azobenzene[339] (Azobenzene synthesis, Experimental section **8.2.8**, ^{1}H NMR spectra, Appendix section **10.1.8.1)**, which was subsequently used to collapse the linear polymer by substituting two benzyl chloride pendant groups in the presence of potassium carbonate. SEC/RI coupled measurements of the azobenzene crosslinked polymer show an apparent decrease in the molecular weight of the polymer, seen as a shift to longer retention volumes when compared to the linear polymer This increase in retention volume is not attributed to a loss in molecular mass but rather a reduction in the hydrodynamic volume of the linear

test polymer upon crosslinking with azobenzenes. Overlapping the RI traces generated from SEC for both the linear polymer and the azobenzene crosslinked SCNP visually highlights this compaction as a distinct separation of the two traces, evidencing the formation of an SCNP (Figure 30).

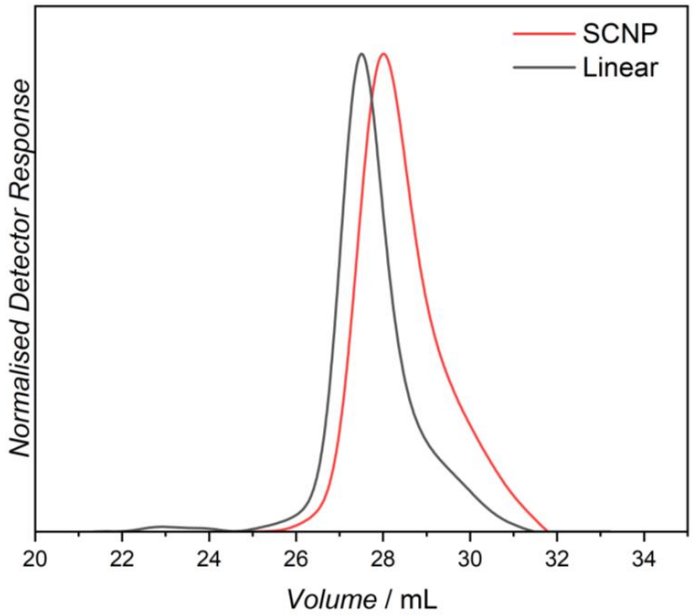

Figure 30. Overlayed RI traces of the linear benzyl chloride test polymer (black) and the polymer after intramolecular crosslinking with azobenzene crosslinkers into an SCNP (red), measured in THF (polystyrene calibration standards). The separation of the SCNP RI trace to a higher retention volume upon crosslinking is representative of intramolecular crosslinking and a reduction in hydrodynamic volume.

^{1}H NMR spectroscopy also showed the successful incorporation of the azobenzene as resonances belonging to the two aromatic proton environments of the azobenzene. (Crosslinking procedure, Experimental section **8.3.2.1**, ^{1}H NMR spectra, Appendix section **10.4.1)**

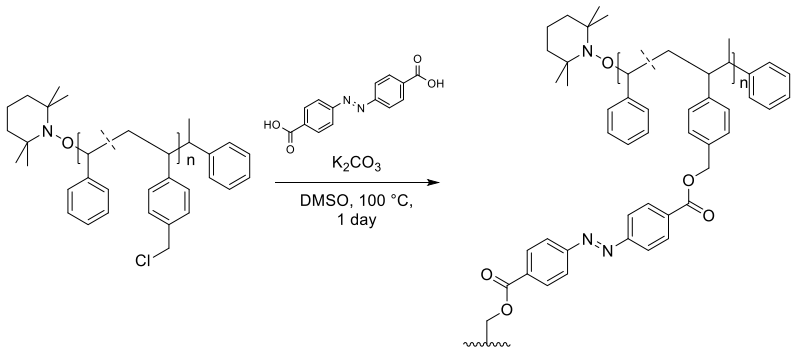

Scheme 22. Crosslinking of a non-catalytic linear polymer into an SCNP via a benzyl chloride substitution with an azobenzene crosslinker.

With a crosslinking strategy established, a new polymer bearing Ar_3P pendant groups for Au metal loading was required. Attempts to polymerise the free phosphine with vinyl benzyl chloride proved challenging, due to the formation of phosphonium salts at the high temperatures (>110 °C) required for NMP. Instead, the Ar_3P monomer was converted into Ar_3PAuCl using AuCl(tht) synthesised in a one-step reaction between tetrahydrothiophene (tht) and chloroauric acid, a procedure adapted from Harper et al. (Ar_3PAuCl procedure, Experimental section **8.2.6.4** and **8.2.6.5**, associated spectra, Appendix section **10.1.6.4)**.[340] The Ar_3PAuCl monomer was copolymerised with vinyl benzyl chloride, preventing the formation of the phosphonium salt while proving resistant to the high temperatures required for NMP. (NMP procedure, Experimental section **8.3.1.3**, ^1H NMR spectra and SEC elugrams, Appendix section **10.2.2)** Attempts to crosslink this new polymer with 4,4-carboxy azobenzene were unsuccessful. The crosslinking conditions established with the styrene/vinyl benzyl chloride polymer resulted in the degradation of the Ar_3PAuCl pendant groups. Subsequent ^1H NMR spectroscopy revealed triphenylphosphine oxide and colloidal gold was present as purple solids in the reaction mixture. A milder crosslinking strategy was required involving lower temperatures and milder reagents (For the crosslinking procedure refer to **8.3.2.2**, ^1H NMR spectra and SEC elugrams, Appendix section **10.4.2)**.

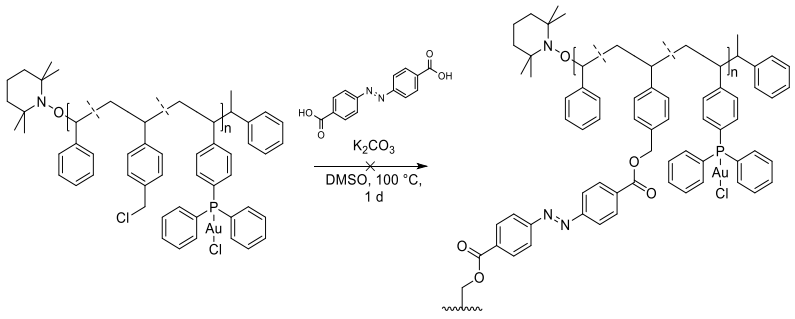

Scheme 23. Attempted crosslinking of a non-catalytic linear polymer into an SCNP via a benzyl chloride substitution with an azobenzene crosslinker

Benzylic alcohol was used instead of benzyl chloride as the crosslinking functionality decorating the linear polymer. Vinyl benzyl chloride was converted into the acetate ester to then be hydrolysed into vinyl benzyl alcohol following a literature procedure (for experimental procedures refer to experimental section **8.2.6**, associated spectra, Appendix section **10.1.6)**.[341] Using NMP, vinyl benzyl alcohol was polymerised with styrene and 4-diphenylphosphine styrene to yield a polymer bearing free triphenyl

phosphine and cross linkable alcohols. Using the above strategy two polymers were synthesised, i.e. **P-13** and **P-23**, differing – primarily – in their benzyl alcohol content determined via ^{1}H NMR, the number average molecular weights (M_n) of the polymers were determined via SEC (Scheme 24). By utilizing the free phosphine instead of the gold complexed derivative, consideration had to be taken in avoiding triphenyl phosphine oxidation. However, no oxidation was observed during the polymerization and its work up. Generation of the catalytically active linear polymers **Au-P-13** and **Au-P-23** via the addition of AuCl(tht) followed, the monomer composition and M_n values determined via ^{1}H NMR spectroscopy and SEC respectively are tabulated in Table 1.(for polymer procedures refer to experimental section **8.3.1**, associated spectra and elugrams, Appendix section **10.2)**.

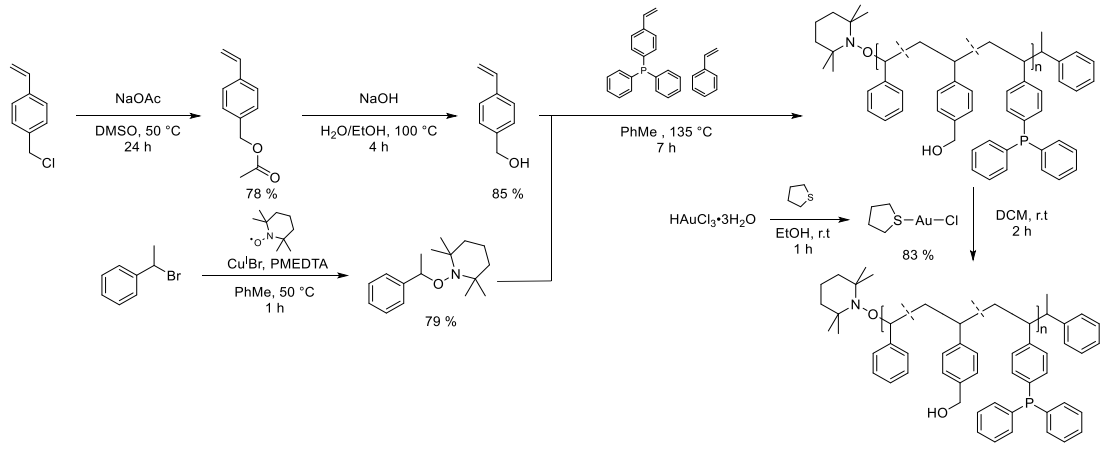

Polymer	mol % OH	mol % Ar_3PAuCl	M_n / g mol^{-1}	$Đ$
Au-P-13	13 %	7 %	21 000	1.25
Au-P-23	23 %	6 %	26 000	1.51

Scheme 24. Nitroxide Mediated Polymerization of styrene derivatives to afford a catalytically active linear polymer.

Table 1. Composition characteristics of the two linear polymers after gold complexation.

^{31}P NMR spectroscopy (Figure 31) showed exclusively a resonance at (δ = 32 ppm) belonging to the gold complexed phosphine, with an absence of oxidation signal, shifted upfield from the free phosphine at (δ = -4 ppm the absence of oxidation signals at (δ = 28 ppm). The ^{1}H NMR spectrum also showed a downfield shift in the signals attributed to the aromatic rings of the phosphine, indicative of the gold chloride

complexation (Figure 31). A correlated increase in the number average molecular weight of the polymers was observed arising from the additional mass gained from gold complexation as determined via SEC analysis (Figure 31, bottom).

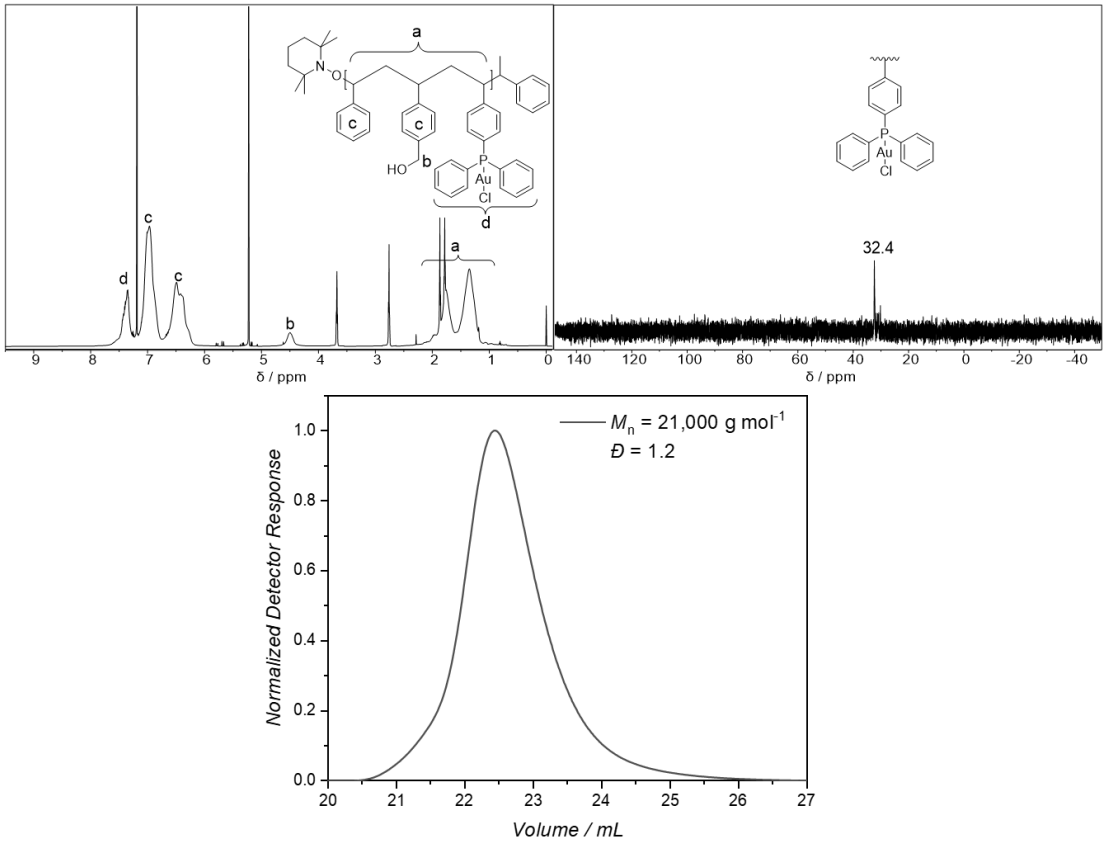

Figure 31. (Top left) ^{1}H NMR spectrum of **Au-P-13** in $CDCl_3$, (Top right), ^{31}P NMR of **Au-P-13** in $CDCl_3$, (Bottom) SEC elugram of **Au-P-13** measured in THF (polystyrene calibration standards) revealing a number average molecular weight of 21,000 g mol^{-1}, an increase of 2,000 g mol^{-1} compared to the non-gold complexed polymer **P-13**.

4.4.2 Synthesis of a Visible Light Reactive Crosslinker

A mild crosslinking strategy was envisioned, utilising an azobenzene functionalised with activated esters at the 4,4 ends. This substitution allows ester linkages to form with the benzylic alcohol pendant groups decorating the gold complexed linear polymers. 4-Nitro benzoic acid was oxidatively coupled to form a 4,4-dicarboxylic substituted azobenzene following the literature procedure utilised in the previous section (Azobenzene synthesis, Experimental section **8.2.8**, ^{1}H NMR spectra, Appendix section **10.1.8.1)**.[339] The dicarboxylic azobenzene was largely insoluble in most solvents due to increased H-bonding between the carboxylic acids, making further modifications difficult. Addition of thionyl chloride as solvent followed by heating converts the carboxylic acids to acid chlorides resulting in gradual dissolution. The acid chloride serves as the handle to attach suitable crosslinking functionalities to. Both carbonyldiimidazole (CDI) and pentafluoro phenyl (PFP) esters were considered for functionalisation via nucleophilic substitution to the acid chloride. Attempts to make the CDI functionalised azobenzene failed due to the susceptibility of the ester to spontaneous hydrolysis. The novel PFP ester azobenzene however, was able to be isolated via recrystallization. PFP esters are known to display an increased resistance to spontaneous hydrolysis resulting in a more stable ester.[342] ^{19}F NMR spectroscopy of the crystallised PFP-azobenzene shows three distinct singlets attributed to the fluorines *ortho*, *meta* and *para*, to the ester linkage proving a successfully attachment of the PFP unit (for azobenzene synthesis refer to Experimental section **8.2.8.3**, associated spectra, Appendix section **10.1.8.3)**.

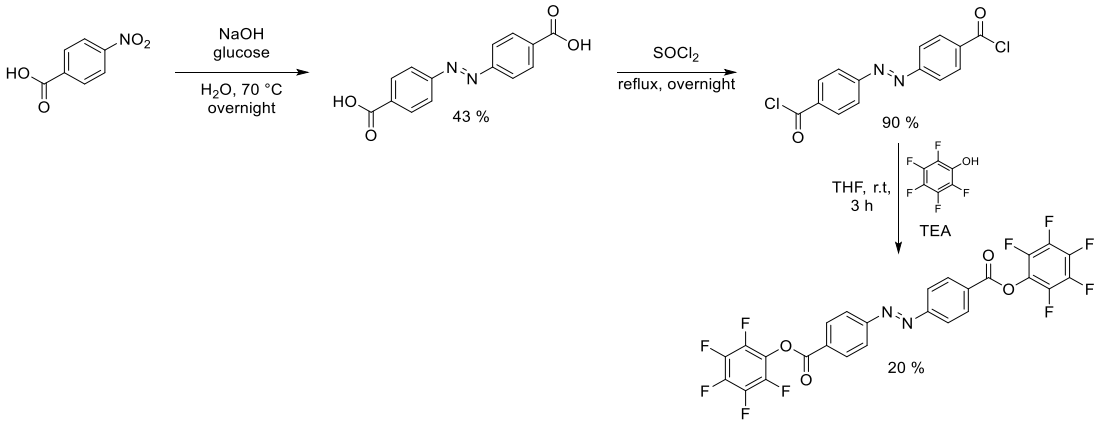

Scheme 25. Synthetic route to afford the PFP-functionalised azobenzene crosslinker.

Preliminary test reactions with stoichiometric amounts of DMAP showed ester formation between the PFP-azobenzene and benzylic alcohol, reaching ~60% conversion after overnight stirring. SCNP folding was first attempted on the polymer bearing a non-gold-coordinated phosphine ligand. The polymer and DMAP were dissolved together in toluene, while the azobenzene was dissolved separately in toluene. Slow addition of the polymer/DMAP solution to the azobenzene solution at 60 °C was completed over a 24 hour period and further left to stir. Subsequent analysis of the polymer via ^{31}P NMR spectroscopy revealed that a large amount of phosphine was oxidised into triphenylphosphine oxide (TPPO) indicated by a resonance at (δ = 29 ppm). To prevent the oxidation from occurring, the polymers containing gold complexed triphenylphosphine were used; complexation proving to be suitable at protecting against phosphine oxide formation. SCNP formation could be successfully completed, evidenced by an increase in the retention volume in SEC analysis. Additionally, the characteristic sharp resonance of the gold-complexed aryl phosphine hydrogens is visible at (δ = 7.8 ppm) in the ^{1}H NMR spectrum (for the SCNP crosslinking procedure refer to Experimental section **8.3.2.3**, associated spectra and elugrams, Appendix section **10.4.3)**. Due to the change in end-to-end length of the azobenzene arising from UV triggered *trans* to *cis* isomerization, a size compaction observable as a shift to longer retention volumes in as SEC chromatogram was expected. No additional compaction was observed in the consequent chromatograms, due to the fast thermal relaxation from *cis* to *trans* of the azobenzene after UV irradiation and low *cis* content photostationary state (for the SEC elugram refer to Appendix section **10.6.5**).[136]

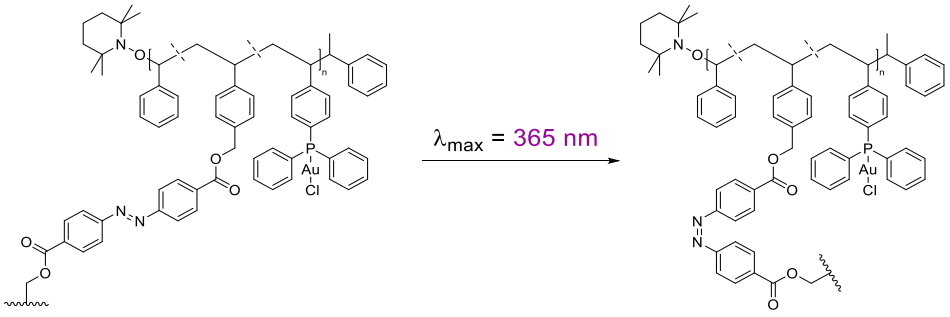

Scheme 26. Proposed isomerization of **Azo-Au-SCNP** azobenzene crosslinks upon irradiation with 365 nm light.

The lack of photoresponsivity was further corroborated with NMR-studies, where only the *trans* isomer of the azobenzene was observed, even after extensive irradiation (Figure 32). To improve the isomerization efficiency and slow the thermal relaxation, *ortho*-tetra chlorination was considered.

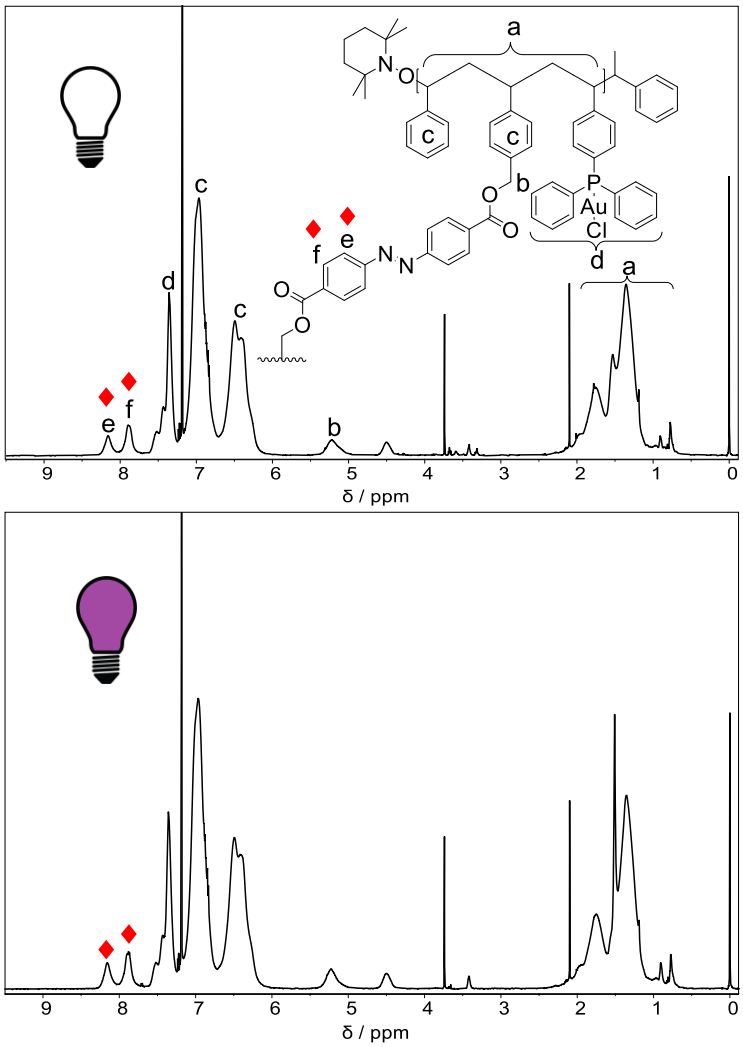

Figure 32. (Top) **Azo-Au-SCNP** prior to irradiation. (Bottom) Irradiation of **Azo-Au-SCNP** in $CDCl_3$ with a 365 nm LED.

Ortho-tetra chlorination of azobenzenes is known to increase the thermal half-life of the *cis* isomer while also redshifting the wavelength required to generate it.[150,151] Palladium catalysed late-stage tetra chlorination of the azobenzene was envisioned utilising formed azobenzenes as opposed to chlorinated starting material. Selective chlorination at positions *ortho* to the azobenzene diazo bridge is achieved via the coordination of a palladium catalyst which facilitates *ortho* chlorination.[151] Initially, tetra chlorination was completed on the 4,4 dicarboxylic substituted azobenzene using

NCS and $Pd(OAc_2)$ at high temperatures adapted from a literature procedure.[150] However, partial chlorination was always observed in the ^1H NMR spectrum, seen as a mixture of multiple aromatic resonances. For successful tetra-chlorination only one aromatic resonance should be visible. Increasing catalyst and NCS concentrations still resulted in a mixture of substitute products. Hydrogen bonding between the carboxylic acid groups resulted in poor solubility in most solvents, possibly contributing to the mixture of chlorinated products. Chlorination was attempted with the ethyl ester derivative to improve solubility, still yielding a mixture of chlorinated products (for the NCS chlorination refer to Experimental section **8.2.9.1**, associated spectra, Appendix section **10.1.9.1)**.

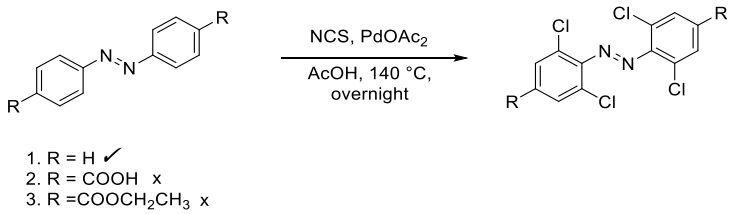

Scheme 27. Chlorination of unsubstituted azobenzene and ester/carboxy 4'4 substituted derivatives with N-chlorosuccinimide and palladium acetate.

Considering both the mixture of chlorinated products and the solubility, a stronger chlorinating procedure was adapted from Liu et al,[343] i.e. trichloro cyanuric acid (TCCA) in conjunction with potassium persulphate ($K_2S_2O_8$) as an oxidiser was utilised. Two hours of heating at 110 °C yielded the *tetra* chlorinated azobenzene with a yield of 43.4 %. Hydrolysis of the ester afforded the di-carboxy derivative, converted into the acid chloride by reactive dissolution in thionyl chloride. PFP substitution of the formed acid chloride yielded the novel *o*-tetra chlorinated azobenzene (Scheme 28). Tetra-chlorination could be evidenced by the presence of a single aromatic resonance (δ = 7.8 ppm) in the subsequent ^1H NMR spectrum assigned to the hydrogens *ortho* to the ester linkage (Figure 33) (for the azobenzene synthesis refer to Experimental section **8.2.9**, associated spectra, Appendix section **10.1.9)**.

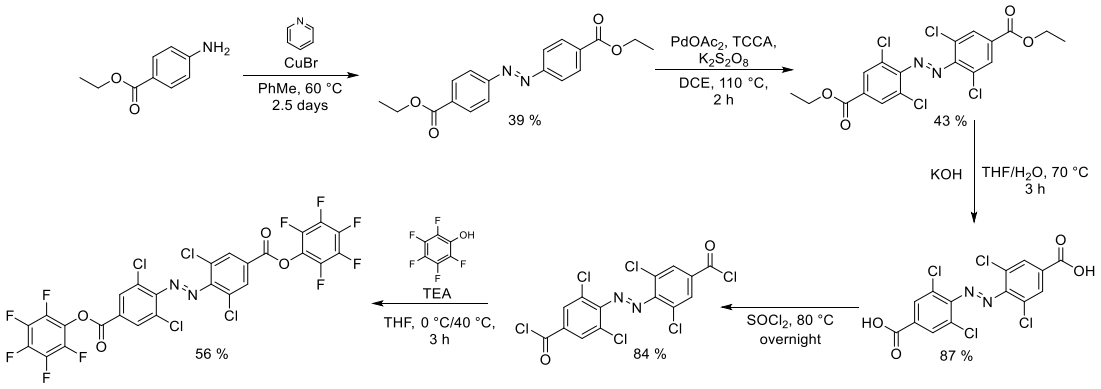

Scheme 28. Synthetic route to afford an *ortho*-tetra chlorinated, PFP functionalised azobenzene crosslinker.

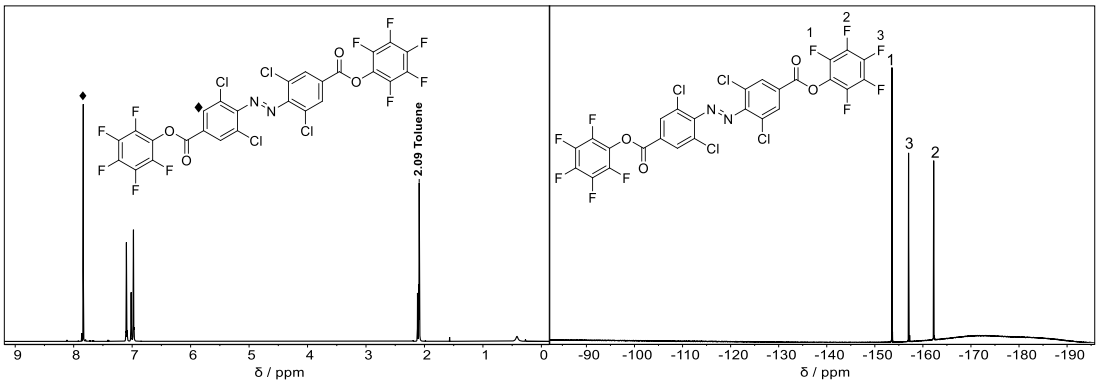

Figure 33.(Left) ^{1}H NMR spectrum of the *ortho*-tetra chlorinated PFP azobenzene in toluene d_8, (Right) ^{19}F NMR spectrum in toluene d_8.

Isomerization of the 4,4 dicarboxylic azobenzene into the *cis* isomer was performed using 620 nm irradiation, which upon irradiation with 415 nm light successfully converted the azobenzene back into the *trans* isomer. This was evidenced by the separation of the distinct symmetry forbidden n−π* transition of the *cis* isomer with a λ_{max} of 440 nm in the UV-Vis spectrum upon irradiation with 620 nm light from the *trans* isomer (for UV-Vis spectra refer to Appendix section **10.6.2)**.

4.4.3 Synthesis of Visible light Switchable Single Chain Nanoparticles

The catalytic linear polymer was folded using the tetra chlorinated azobenzene functionalised with PFP esters (**PFP-*o*-AzoCl$_4$**). Folding followed the same procedure as for the non-chlorinated azobenzene attempted in the previous section (**4.4.1**). Crosslinking with **PFP-*o*-AzoCl$_4$** yielded **AzoCl$_4$-Au-SCNPs** compacted by 24 % and 46 % for the 13 % and 23 % OH containing polymers respectively evidenced by DOSY (for primary DOSY data refer to Appendix section **10.7**) and SEC (Figure 34). By overlaying the refractive index trace from SEC with the SEC UV-Vis trace, an exact overlap can be observed, confirming that the high absorbing **AzoCl$_4$** crosslinks are responsible for the compaction (refer to Appendix section **10.4.4**).

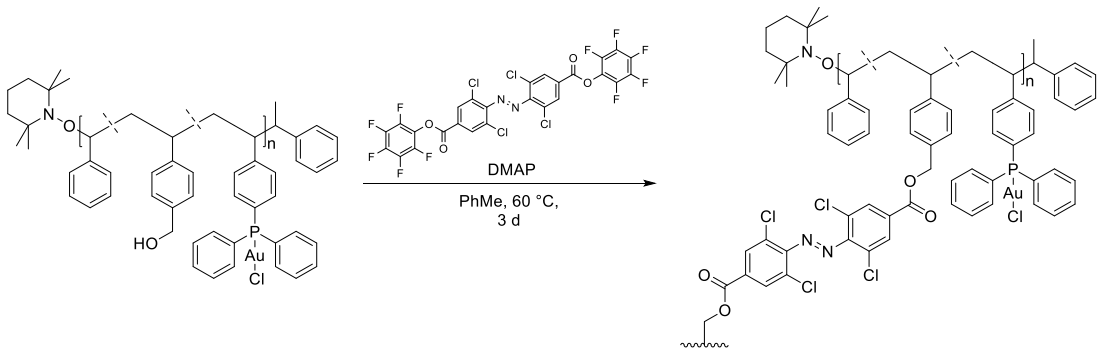

Scheme 29. Crosslinking of the gold complexed linear polymer with **PFP-AzoCl$_4$** into an SCNP (**AzoCl$_4$-Au-SCNP**)

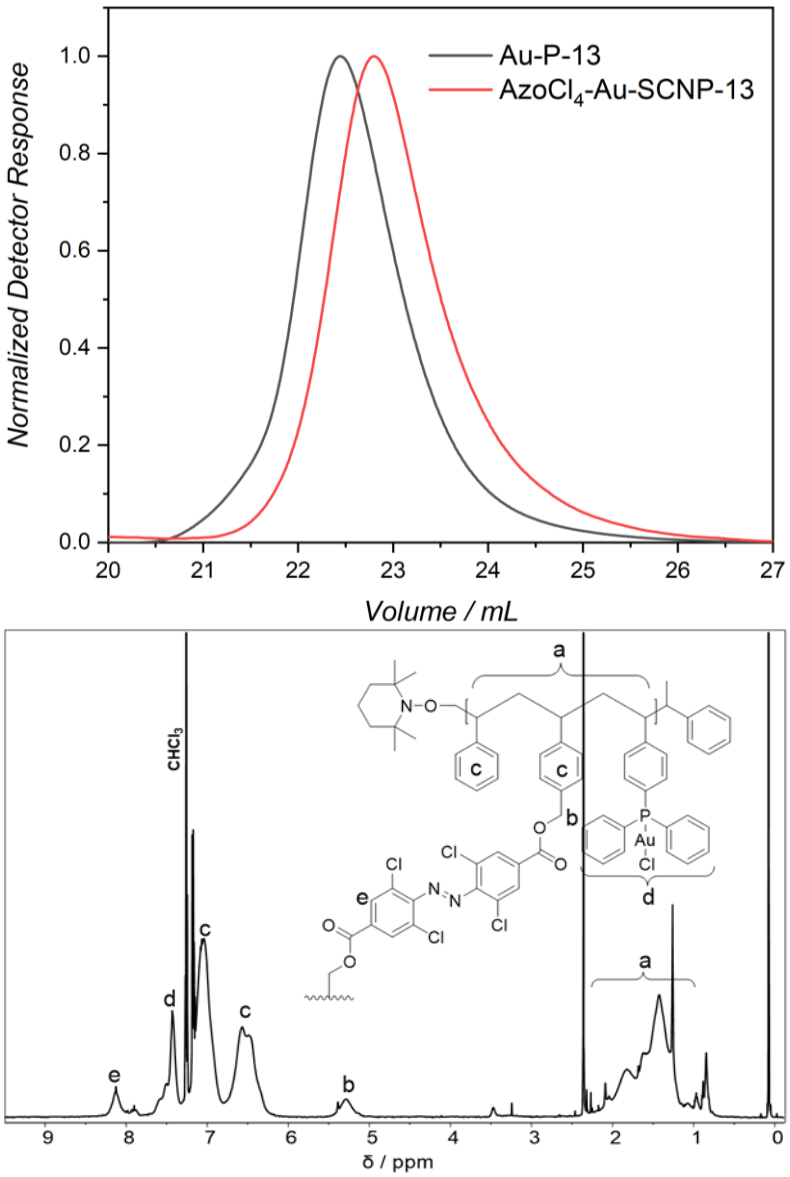

Figure 34. (Top) SEC elugram of **Au-P-13** and **AzoCl₄-Au-SCNP-13** measured in THF (polystyrene calibration standards). (Bottom) ^{1}H NMR spectrum of **AzoCl₄-Au-SCNP-13** in $CDCl_3$ (corresponding data for **AzoCl₄-Au-SCNP-23** can be found in Appendix section **10.4.4**)

^{1}H NMR spectroscopy was also used to observe the folding of the SCNPs. Upon esterification with the PFP crosslinkers (Figure 34), a clear downfield shift of the hydrogen atoms belonging to the benzylic alcohol pendant groups (δ = 4.5 ppm) converting to benzylic esters (δ = 5.3 ppm) is observed. Protons on the azobenzene crosslinks are also observed as a single broad resonance at (δ = 8.1 ppm) attributed to the symmetric protons at the α-position to the ester functionality. DOSY analysis was also employed to measure the reduced hydrodynamic radius of the SCNPs compared to the parent polymers. DOSY spectra ($CDCl_3$) of the parent polymers were recorded and compared to the spectra of the SCNPs, and diffusion coefficients were determined

and used to calculate the % compactions of the SCNPs. The SCNP containing 13 mol% of crosslinker compacted by 35 %, 2.59 nm to 1.68 nm, while a compaction of 44% was observed for the 23 mol% SCNP, 2.99 nm to 1.68 nm. Compaction of the linear gold-OH polymers into the **AzoCl$_4$-Au-SCNPs** affords a light responsive particle, addressable with orthogonal wavelengths of light (for primary DOSY data refer to Appendix section **10.7**).

4.4.4 Visible light induced Photoreversibility within the SCNP

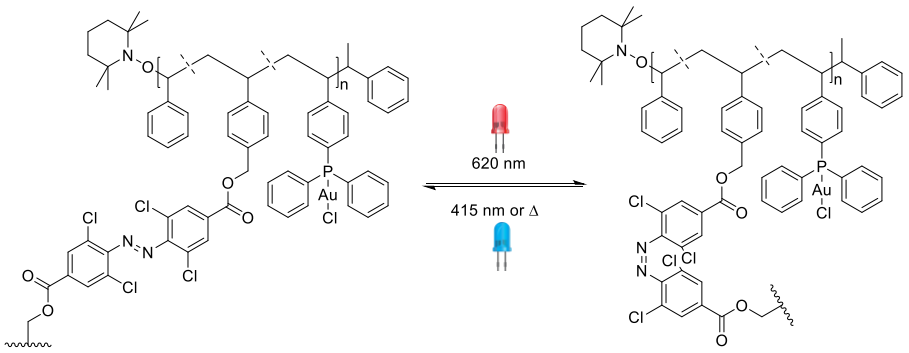

Scheme 30. Reversible visible light switching of the **AzoCl$_4$-Au-SCNP**.

Azobenzene photoswitches display a high resistance to repeated photoinduced isomerization and are often implemented in functions where a high switching cyclability is required, such as in liquid crystal devices, molecular motors and optical sensors.[344–346] Critically, they display a conserved switching mechanism even in constrained environments,[347] which constitutes an important property when integrating the azobenzenes into the confined polymeric environment of an SCNP. **AzoCl$_4$-Au-SNP-13** was used primarily as the model system for the determination of the photoresponsive properties arising from azobenzene isomerization. UV-Vis spectra of the SCNPs both after 620 nm and subsequent 415 nm irradiation displayed the characteristics absorption bands of azobenzene *cis* and *trans* isomer respectively (Figure 35). 620 nm irradiation resulted in the increase and separation of the n–π* band centred at 440 nm, after 1 hour of irradiation no additional increase in the intensity of this band was observed. 415 nm irradiation for 30 minutes decreased the n–π* band and restored the *trans* isomer content to the level prior to 620 nm irradiation. High resistance to photofatigue is particularly important for photoresponsive catalytic SCNPs, where the goal is to recycle and reuse them through multiple catalytic cycles with minimal photo and catalytic hysteresis. **AzoCl$_4$-Au-SCNP-13** was irradiated with

620 nm and 415 nm light through multiple cycles (for the emission spectra of the LED and the irradiation setup refer to Experimental section **8.4)**. UV-Vis spectroscopy was used to monitor this increase and subsequent decrease in the absorption of the visible light band at 440 nm between the two isomers upon 620 and 415nm irradiation respectively (Figure 35). It was clear that after multiple irradiation cycles little change in the absorptivity profiles of both *cis* and *trans* isomers occurred suggesting a visible light responsive nanoparticle with a highly conserved switching process.

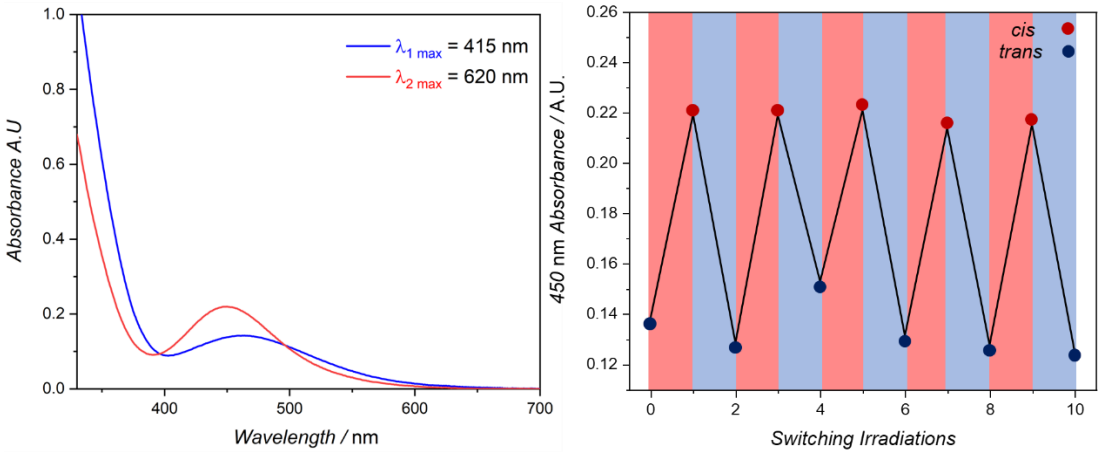

Figure 35.(Left) UV−Vis analysis depicting the increase in absorption of the 440 nm visible band upon irradiation of **AzoCl$_4$-Au-SCNP-13** with 620 nm light (red) and recovery of the 440 nm band with 415 nm light (blue). (**Right**) Cycling 620 and 415 nm light irradiation of **AzoCl$_4$-Au-SCNP-13** with no hysteresis.

To further evidence the *cis-trans* isomerization of the nanoparticles, ^{1}H NMR spectroscopy was employed. The *trans* and *cis* isomers display noticeably different electronic properties from each other, reflected as changes in the ^{1}H NMR spectra. A change in the alignment of the electron cloud arising from *trans-cis* isomerization results in an anisotropic effect that shifts the aromatic proton signals associated with the relevant isomer.[348] Consequently, resonances associated with the *cis* isomer are located comparatively upfield of those belonging to the *trans* isomer. The *ortho*-tetra chlorination of the azobenzene crosslinkers contained within **AzoCl$_4$-Au-SCNP-13** results in a single aromatic proton resonance corresponding to the four protons located on the ring, prior to visible light irradiation this resonance is observed at (δ = 8.1 ppm). Subsequent irradiation with 620 nm light results in a shift up field to (δ = 7.8 ppm), indicative of the isomerization of the crosslinks into the *cis* isomer. An incomplete conversion from *trans* to *cis* is observed after 1 hour of irradiation. Comparison of the integrals between the two isomers resonances reveals a photostationary state

comprised of a *cis*:*trans* ratio of 7:3 (Figure 36), in agreement with similar values observed in the literature for tetra chlorinated azobenzenes.[150] Irradiation with 415 nm light results in the complete reversion of the *cis* isomer back to the *trans* isomer providing a direct observation of the structural change occurring in the **AzoCl$_4$-Au-SCNP-13**. The *cis* isomer of azobenzenes will gradually revert over time into the thermally more stable *trans* isomer. For certain applications, a fast thermal relaxation is desired,[145] for catalytic applications, where noticeable changes are observed between the *cis* and *trans* isomer, a lower energy *cis* isomer and consequently slower thermal relaxation is desired.

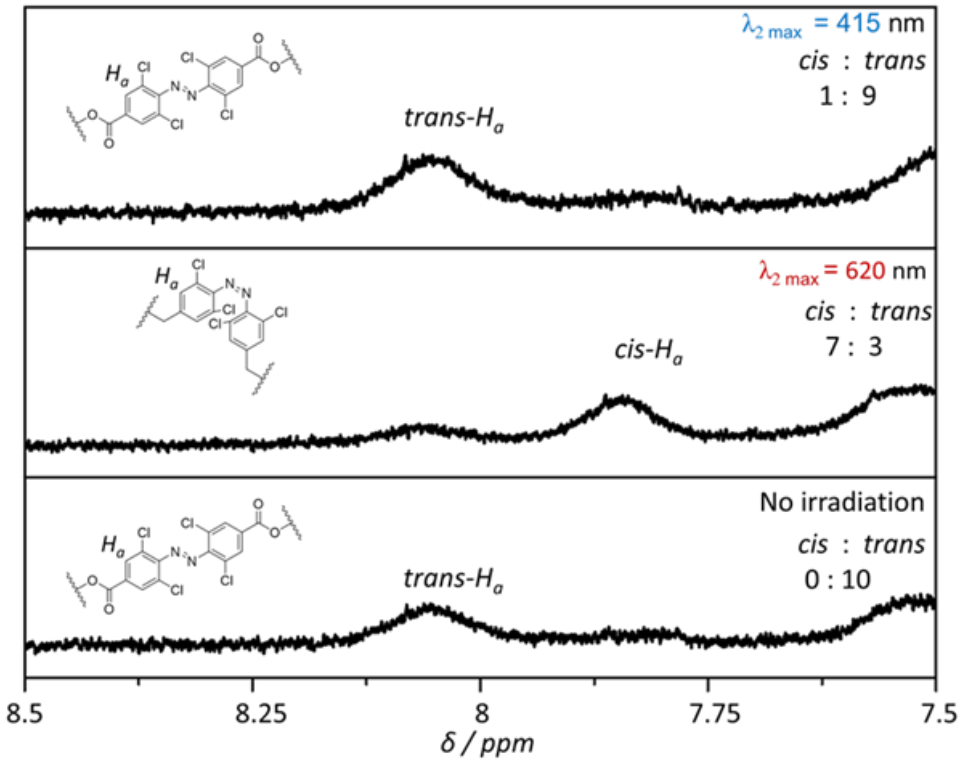

Figure 36. Switching of **AzoCl$_4$-Au-SCNP-13** upon irradiation with 620 and 415 nm light, monitored with ^{1}H NMR spectroscopy.

Critically, ^{1}H NMR spectroscopy can be used to monitor the gradual downfield shift of aromatic resonances attributed to the *cis* isomer upon thermal relaxation to the *trans* isomer. After irradiation with 620 nm light, the aromatic resonances associated with *cis* isomer are observed to slowly shift downfield to (δ = 8.1 ppm), representing a gradual increase in the *trans* isomer fraction. After 16 hours, approximately 40% of all crosslinks exist as the *cis* isomer suggesting a $t^{1/2}$ < 16 hours (Figure 37). The slow

thermal relaxation affords a large catalytic window, where any desired changes in catalysis can occur owing to the high percentage of crosslinks existing as the *cis* isomers.

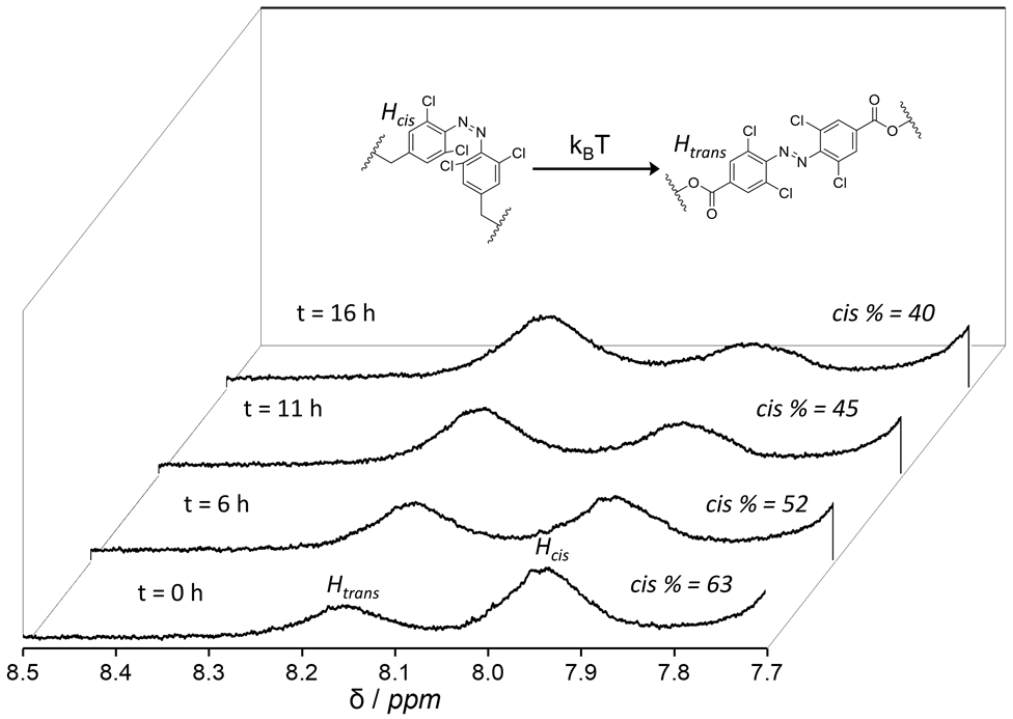

Figure 37. Thermal relaxation of *cis*-azobenzene crosslinks in **AzoCl$_4$-Au-SCNP-13** monitored by ^{1}H NMR spectroscopy.

Azobenzene isomerization results in an end-to-end length reduction between the 4,4' positions, a process that can be amplified in suitable environments to enact size changes of much larger assemblies such as in linear polymers.[161,304] It was envisioned that the isomerization of the ***o*-AzoCl$_4$** crosslinks into the *cis* isomer would result in an overall reduction in size of the formed SCNPs, observed primarily as an increase in retention volume of the chromatogram generated from SEC. Irradiation of **AzoCl$_4$-Au-SCNP-13** with 620 nm light resulted in a small compaction, revealed by an overall increase in the retention volume. Critically, complementary irradiation with 415 nm light reverts the compaction, yielding an SEC trace identical to the non-irradiated SCNP confirming the photoreversible nature of the SCNP. Triplicate experiments consisting of 620 nm irradiation of **AzoCl$_4$-Au-SCNP-13** followed by irradiation with 415 nm light were conducted. Peak molecular weight (M_p) values were utilised to confirm the observed shift in retention volume. An average of the three triplicate

experiments was taken and an apparent shift to lower molecular weight of 1,000 g mol^{-1} was observed. Similarly, an average was also taken of the reverse process, where the *cis*-**AzoCl$_4$** crosslinks are reverted to the *trans* isomer upon 415 nm irradiation. A 900 g mol^{-1} increase in apparent molecular weight was observed upon irradiation with 415 nm light, closely matching the initial non-irradiated SCNP (for triplicate SEC elugrams refer to Appendix section **10.6.1).**

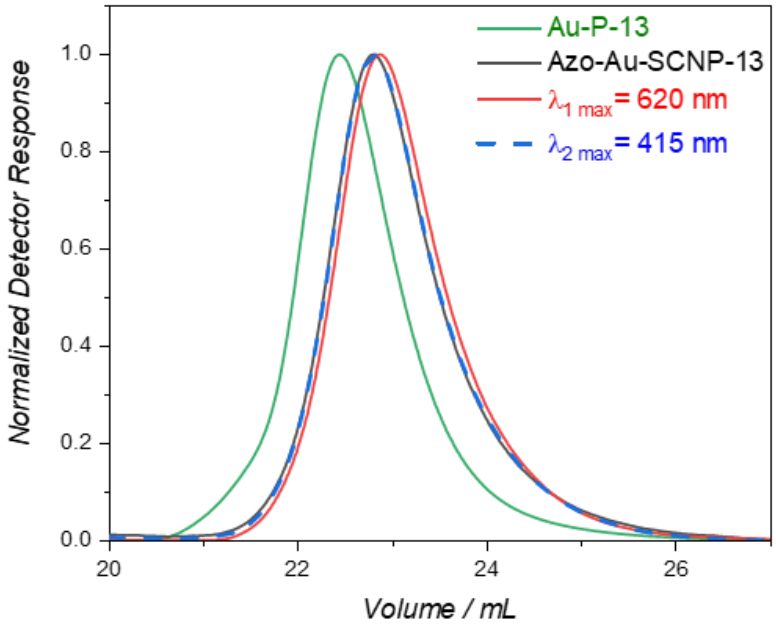

Figure 38. SEC analysis of the linear polymer (**Au-P-13**) (**green**), compaction into the SCNP (**AzoCl$_4$-Au-SCNP-13**) (**black**) followed by irradiation with λ_1, max = 620 nm light (**red**) and subsequent irradiation with λ_2, max = 415 nm light (**blue dotted**).

A second SCNP with almost double the crosslinking density, **AzoCl$_4$-Au-SCNP-23**, was synthesized with the intention of increasing the compaction upon visible light irradiation. **AzoCl$_4$-Au-SCNP-13** displayed a larger overall compaction then **AzoCl$_4$-Au-SCNP-23**. While the switching process is conserved with the **AzoCl$_4$-Au-SCNP-23** crosslinks, evidenced by ^{1}H NMR, the increased crosslinking density may result in a more constrained environment (for **AzoCl$_4$-Au-SCNP-23** ^{1}H NMR and SEC switching data spectra refer to Appendix section **10.4.4)**. Movement of the polymer chain may be diminished, as such a smaller compaction compared to **AzoCl$_4$-Au-SCNP-13** could be expected. An important aspect of azobenzene switching that accompanies geometric changes, is an increase in net dipole moment from the *trans* to the *cis* isomer measured as 0 D to 3 D respectively for basic azobenzenes.[135] Due to this change in polarity it is that the degree of SCNP compaction is dependent on the

solvent in which it is carried out. In solvents such as THF, used in this work, relatively small compactions were observed as increased solvation facilitates a nanoparticle having a higher hydrodynamic radius, larger compactions could be expected in low polar solvents such as chloroform or toluene.[161] Catalytic applications relying on the size change of the **Azo-Au-SCNPs** may be highly dependent on the solvent in which catalysis is carried out. To maximise the effect that light induced morphological changes have on catalysis, **Azo-Au-SCNPs** need to be applied in suitable solvent conditions. Furthermore, suitable substrates must also be used, as physical factors such as steric bulk and polarity will impact how the substrate interacts with different SCNP morphologies.

4.4.5 Catalysis

Having synthesised a photoswitchable single chain nanoparticle bearing catalytic functionalities, its catalytic properties were investigated. The switch between the isomerized *cis* and *trans* form of the **AzoCl$_4$-Au-SCNP-13** was hypothesised to display different catalytic properties as a consequence of the resulting morphological and physical changes. These arise from the *trans* to *cis* isomerization of the **AzoCl$_4$** crosslinks. Due to the thermally regulated relaxation of the *cis*-**AzoCl$_4$** crosslinks, room/low temperature catalysis is required. Elevated temperatures would favour the *trans* isomer of **AzoCl$_4$** crosslinks drastically increasing the rate of thermal relaxation from the *cis* isomer, constituting in a much smaller window for photoreversibly controlled catalysis to occur. Gold (I) complexes such as Ar$_3$PAuCl are well known for their ability to facilitate the electrophilic activation of unsaturated carbon-carbon bounds, particularly alkynes towards nucleophiles.[285,349] Alkyne activation occurs via the formation of an alkyne-gold π-complex. The high Lewis acidity of the gold (I) centre draws electron density away from the alkyne, leading to increased susceptibility towards substitution with a range of nucleophiles. Gold (I) complexes are highly resistant to redox process such as oxidative additions, as such no change in oxidation state occurs during this catalytic process (Figure 39). To investigate the potential for room temperature, photo-controlled catalysis, **AzoCl$_4$-Au-SCNP-13** was utilized as the gold (I) catalyst for hydroaminations between an alkyne and a primary amine.

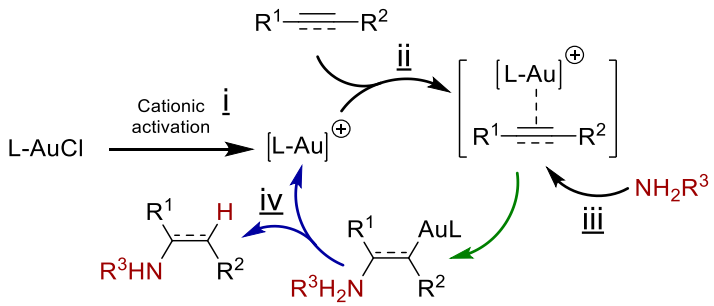

Figure 39. Generalised mechanism for the hydroamination of alkynes via cationically activated Au^{I} catalysts. (i) Activation of catalyst, (ii) coordination of an alkyne to the cationic gold centre, withdrawing electron density from the triple bond, (iii) Nucleophilic attack of an amine on the electron deficient alkyne-gold complex occurs, resulting in a vinylic intermediate (iv) internal proton transfer from the original nucleophile to the L-Au centre forms the final anti-Markovnikov adduct and the regenerated catalyst.

4.4.5.1 Intramolecular Hydroamination

Bohlen et al. have conducted room temperature intramolecular hydroaminations with Au^{I} functionalised SCNPs resulting in high conversions and fast kinetics.[246] The same intramolecular reaction was employed in the current thesis to test the benchmark catalysis of the formed SCNP. First, a nitrile intermediate was synthesised according to a procedure adapted from Jiang et al.[350] The tertiary carbon of diphenyl acetonitrile was deprotonated with in-situ formed LDA, followed by the addition of 1-bromo-2-pentyne. Additional purification beyond washing was not necessary for this step due to the absence of impurities evidenced by ^{1}H NMR spectroscopy. The nitrile functionality was subsequently reduced into a primary amine through the use of $LiAlH_4$ according to a literature procedure.[246] Impurities generated at this step were likely caused from the over reduction of the alkyne into an alkene; a difficult impurity to separate via column chromatography. Milder reaction conditions were then employed, lowering the yield of the nitrile reduction but preventing the reduction of the alkyne, where the nitrile starting material proved easier to remove. The result of the above two-step process was a linear substrate consisting of a 7-carbon backbone, bearing an internal alkyne, and a primary amine with diphenyl beta-substituents (for the experimental procedure refer to Experimental section **8.2.7**, ^{1}H NMR spectra Appendix section **10.1.7)**

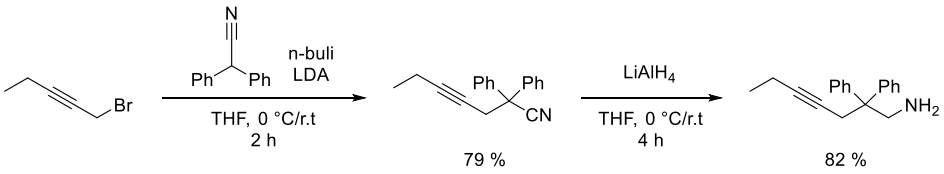

Scheme 31. Synthesis of the intramolecular hydroamination substrate bearing a primary amine and internal alkyne.

1-Bromo-2-pentyne can be substituted with a variety of *iso*-nitrile derivatives. Diphenylacetonitrile was used due to the steric bulk that the diphenyl substitution exerts on the linear backbone of the final substrate. Bulky groups along the backbone can significantly enhance intramolecular ring closure reactions. This is known as the Thorpe-Ingold or Angle Compression effect and describes how two bulky substituents will move to maximise the angle between themselves and consequently decrease the angle between reactive partners situated on the same molecule.[351] In the current context, this pre-arrangement is between an internal alkyne and a primary amine. To determine suitable conditions for further catalytic testing, a benchmark catalysis was completed with the small molecule ArP_3AuCl. ArP_3AuCl was synthesized in a two-step procedure by first generating the pre-catalyst AuCl(tht) and then exchanging it with Ar_3P, affording the final catalyst (for the synthetic procedure refer to Experimental section **8.2.6**, associated spectra, Appendix section **10.1.6)**. Catalytic tests at 2 mol% catalyst loading were carried out in a Young's NMR tube that was prepared in a glove box. $Zn(OTF)_2$ was employed for the cationic activation of Ar_3PAuCl, shown to successfully generate the catalytically relevant Au^+ species in phosphine gold complexes.[246,285] Anisole was used as the internal standard and the reaction was carried out in dry $CDCl_3$ at 20 °C. A conversion of 90% was reached after 16 hours, with 80% reached within the first 7 hours. The small molecule catalyst was then replaced with the catalytically active linear polymer, the molar amount of which was calculated to maintain the same catalyst loading of 2 mol%. 90% conversion was reached within 3 hours and quantitative conversion after approximately 8 hours.

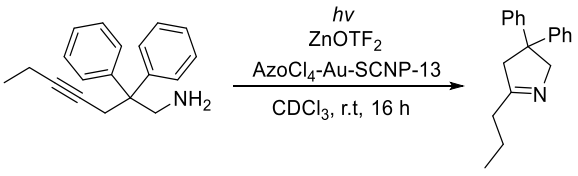

Scheme 32. Conditions to test the viability of **$AzoCl_4$-Au-SCNP-13** as a catalyst for intramolecular hydroamination reactions, anisole was used the internal standard.

AzoCl$_4$-Au-SCNP-13 was irradiated for 5 minutes with 415 nm light to ensure that all azobenzene crosslinks were present in the more open *trans* form. The open SCNP showed similar conversion to the linear polymer, reaching 90% conversion after 4 hours and near quantitative conversion after 11 hours (for the catalytic experiments procedures, Experimental section **8.5.1.1)**. The same catalytic experiment was replicated with **AzoCl$_4$-Au-SCNP-13** after irradiation with 620 nm light. A marginal reduction in conversion was observed, reaching 90% after 5.5 hours (for the ^{1}H NMR spectra of the catalytic experiments refer to Appendix section **10.5)**. Ar$_3$PAuCl functionalised SCNPs have been utilised by Bohlen et al. for the hydroamination of the same intramolecular substrate, using similar catalyst loadings of 2 mol%.[246] Here SCNPs were crosslinked using the metal coordination of yttrium to carboxylic acid units and were folded from larger precursors then **AzoCl$_4$-Au-SCNP-13.** Fast conversions were also reported, 90% after 2 hours, faster than the conversions reported for **AzoCl$_4$-Au-SCNP-13** catalysis. The gold catalysed hydroamination reported in this thesis and in literature using Ar$_3$PAuCl functionalised SCNPs with the same intramolecular substrate, suggests a catalytic process that is mostly conserved even in differing polymer environments. The small change in catalytic rates observed after 620 nm irradiation of **AzoCl$_4$-Au-SCNP-13** may be attributed to the morphological change in the SCNP as the azobenzene crosslinks isomerised. A reduction in the overall size of the nanoparticle and increase in steric hinderance around the catalytic sites may prevent substrate access. The polarity increase could also have affected the encapsulation of the substrate within the SCNP as the *cis* isomer content increased. For a polar substrates this could manifest as a decrease in catalytic rates and inversely as an increase in polar substrates.

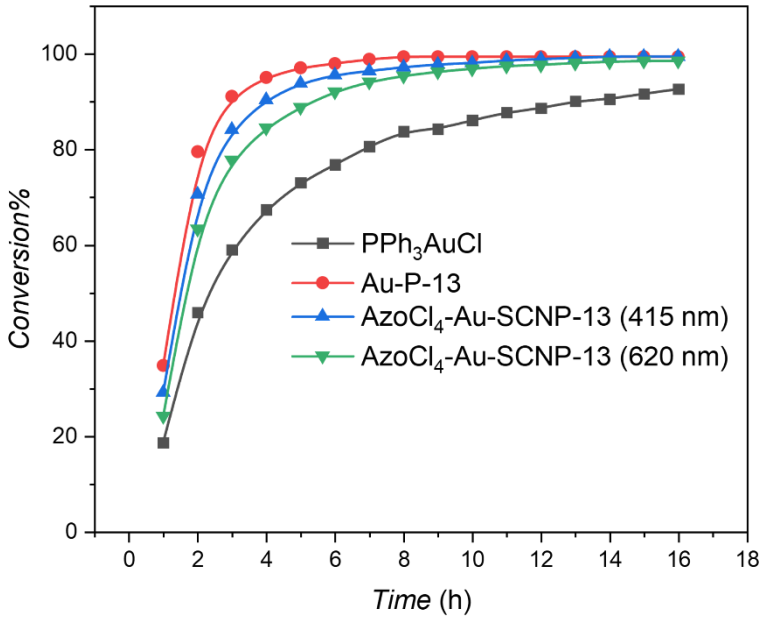

Figure 40. Catalytic and photocatalytic testing of the small molecule, linear polymer catalysts and irradiated SCNP respectively.

A gradual reduction in yield was observed in subsequent catalytic tests, which attempted to reproduce the high catalytic conversions achieved in the first experiments where the SCNP was irradiated (Figure 40). Under the same conditions the conversion decreased from quantitative – observed in the first experiments – to 19 % after 16 hours for later tests (for the conversion vs time graphs and the associated ^{1}H NMR spectra refer to Appendix section **10.5.1**). It is possible that this discrepancy arose from degradation of the co-catalyst $Zn(OTF)_2$ used to activate the gold complex. Improper storage may have resulted in an accumulation of water hydrolysing the triflate into triflic acid. The low conversion was observed even with the small molecule catalyst, further suggesting that problems with the SCNP are not responsible for loss of catalysis. A more stable, water tolerant co-catalyst NaBARF replaced $Zn(OTF)_2$ in subsequent tests to identify suitable candidates for room temperature hydroamination reactions. The intramolecular ring closure of the diphenyl substituted substrate displayed fast reaction kinetics even at room temperature. Changes in catalysis induced by the open and closed SCNP may have even been more visible on slower intramolecular reactions. In order to produce a slower ring closure than that of the previous substrate, a new linear substrate was synthesised bearing a terminal alkyne and a primary amine with no substituents along the backbone. A Gabriel synthesis adapted from a literature procedure was used to synthesise this molecule.[352]

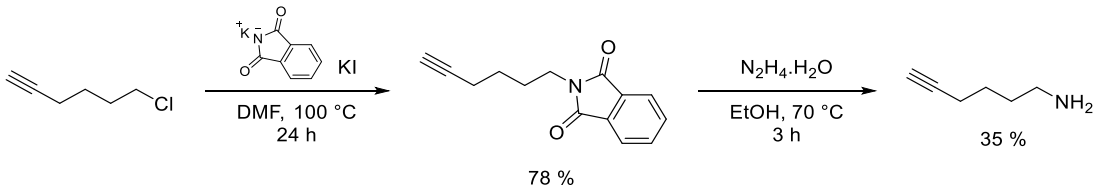

Scheme 33. Synthesis of the linear intramolecular hydroamination substrate with a terminal alkyne.

6-chloro-heptyne was substituted with potassium phthalimide and subsequently hydrolysed with hydrazine monohydrate to yield the primary amine, yielding a ^{1}H NMR spectrum that matched literature (for the Gabriel synthesis refer to Experimental section **8.2.7**, ^{1}H NMR spectra, Appendix section **10.1.7)**. The small molecule ArP_3AuCl catalyst was employed to test the new substrate. Using the same catalyst loadings as the previous tests, a 65 % conversion was achieved after heating to 40 °C. Attempts to complete this catalysis at room temperature would have resulted in lower conversions, ruling out the substrate for further tests. (for the associated ^{1}H NMR spectra of the catalytic experiments refer to Appendix section **10.5.2).**

4.4.5.2 Intermolecular Hydroamination

To further explore the potential of using the **AzoCl$_4$-Au-SCNP-13** as light responsive catalysts, a variety of intermolecular hydroamination reactions were also considered. The changes between the *trans* and *cis* form of the **AzoCl$_4$-Au-SCNP-13** may have a more noticeable effect on intermolecular substrates, particularly if the substrates differ significantly from each other in steric bulk and/or polarity.

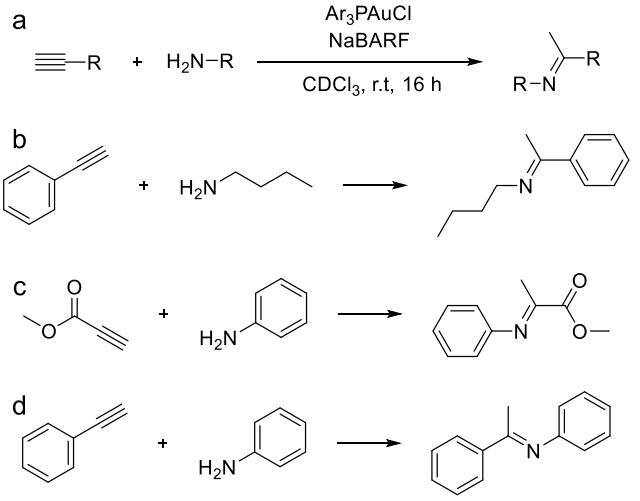

Scheme 34. Substrates fielded as potential candidates for intermolecular hydroamination reactions, anisole was used as an internal standard.

Intermolecular substrates were initially tested on the small molecular catalyst (Ar_3PAuCl) to determine suitable reaction conditions (for the catalytic experiments procedures, Experimental section **8.5.2**). Low yields or no product formation was observed in all the small molecular tests. Only the reaction between aniline and phenylacetylene gave 9% conversion after 17 hours at room temperature (Figure 41), increasing to 20 % when heated at 40 °C. Intermolecular hydroamination reactions using ArP_3Au^+ as a catalyst often require elevated temperatures and few examples exist of reactions occurring quantitively at room temperature, without niche substrates/conditions.[349,353–355]

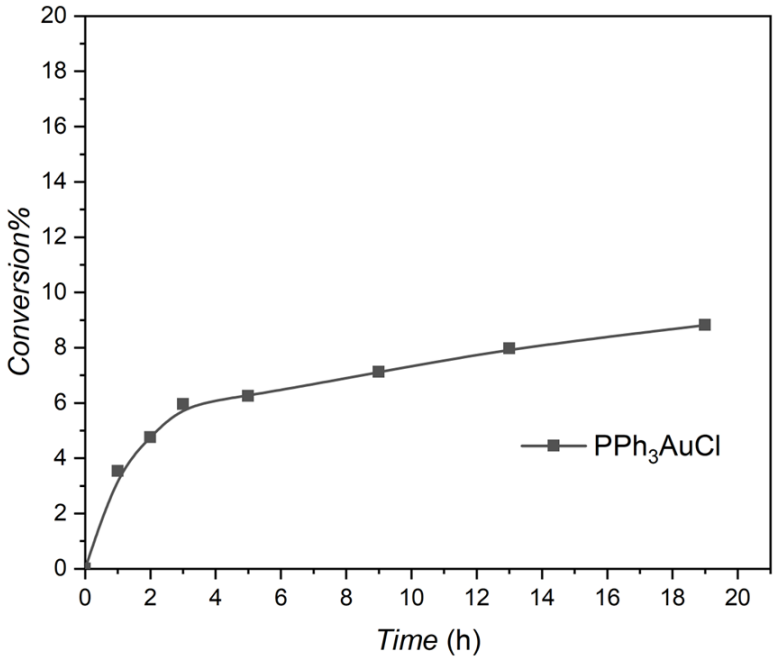

Figure 41. Room temperature catalysis of aniline and phenylacetylene by NaBARF activated Ar_3PAuCl.

To avoid increasing temperature, the nucleophilicity of the amine component was increased to better facilitate nucleophilic attack on the gold-coordinated alkyne. Butylamine was used in place of aniline constituting a more nucleophilic amine, while phenylacetylene was still used as the alkyne component. No reaction took place between the two substrates, while competitive coordination of butylamine to the gold complex is likely increased, owing to the higher Lewis basicity accompanying the increase in nucleophilicity. High affinity of the amine component prevents the coordination of the alkyne and activation by the gold complex.[356] In a second experiment, a more electron deficient alkyne was used to possibly increase the affinity

of coordination to the gold centre. Methyl propiolate was employed in place of phenyl acetylene and added to aniline. Characteristic resonances for the anti-Markovnikov product were not observed in the ^{1}H NMR spectrum, instead unidentifiable products formed which gradually increased throughout the course of the reaction. Total consumption of methyl propoliate was still low at 24% after 17 hours, higher than the comparative phenyl acetylene reactions but still not high enough to justify further catalytic tests. (For ^{1}H NMR spectra of the catalytic runs refer to Appendix section **10.5.3).**

4.4.6 Conclusions: Catalysis

AzoCl$_4$-Au-SCNP was employed as a catalyst for the intramolecular hydroamination of alkynes. Preliminary catalytic tests showed the **AzoCl$_4$-Au-SCNP** retained its catalytic activity when used for the ring closure of a substituted intramolecular substrate. A high conversion was observed, reaching quantitative yields after 11 hours. Irradiation of the reaction mixture with 620 nm light resulted in a slight decrease in conversion compared to the non-irradiated reaction. Further catalytic testing was not possible due to the gradual loss of catalytic activity attributed to the degradation of the co-catalyst, Zn(OTf)$_2$. Intermolecular substrates were fielded with a small molecular catalyst (Ar$_3$PAuCl) using a new stable co-catalyst, NaBARF, to identify potential substrates that would display a larger difference in conversion when catalysed by the "open" and "closed" **AzoCl$_4$-Au-SCNP**. Low conversions were observed in all tests which ruled out the possibility of using intermolecular substrates suggesting intramolecular substrates are required. A library of intramolecular substrates with a large variation in polarity and steric bulk should be investigated. Using intramolecular substrates ensures that high enough conversions are reached, varying the polarity and steric bulk of the substrates should increase the impact that isomerization of **AzoCl$_4$-Au-SCNPs** has on catalysis, as those same properties change within the SCNP upon isomerization. Additionally, catalysis should be attempted using **AzoCl$_4$-Au-SCNPs** with higher percentages of azobenzene content. Increasing the content of azobenzenes within the SCNPs should also increase the magnitude of the change in physical properties associated with isomerization, such as polarity. The associated physical change should then result in a greater change in catalytic properties between the "open" *cis* and "closed" *trans* form of the **AzoCl$_4$-Au-SCNPs**.

4.5 Conclusions

In the present chapter a single chain nanoparticle is introduced displaying photoreversible compaction and polarity changes upon exposure to two distinct colours of visible light. Photoresponsive SCNPs were obtained via the intramolecular collapse of linear polymer chains with chlorinated azobenzene crosslinkers, able to isomerize upon 620 and 415 nm irradiation. The linear polymer precursor is generated via nitroxide mediated polymerization of styrene monomers, utilizing triphenylphosphine and benzyl alcohol derivatives for catalytic properties (Ar_3PAuCl) and crosslinking respectively. Compaction of the linear polymer into the SCNP was observed via DOSY and NMR spectroscopy as well as SEC measurements, clearly demonstrating an overall size reduction of 44% for the SCNP with the highest crosslinking density. A small, reversible compaction of the SCNP was observed upon exposure to visible light irradiation, indicated by a small shift in the SEC trace to longer retention times. Reversible morphological changes in the SCNP were corroborated with UV-Vis and ^{1}H NMR spectroscopy, the latter of which allowed for the direct quantification of the *cis*:*trans* content of the SCNPS after visible light irradiation. After 1 hour of irradiation with 620 nm light, a maximum of ~ 70% of azobenzene crosslinks can be switched into the *cis* isomer. ^{1}H NMR spectroscopy also revealed that the azobenzene crosslinks in the *cis* configuration display a slow thermal relaxation $t_{1/2} > 16$ hours, affording a large window for photoresponsive catalysis to occur. Reversible switching of the crosslinks between the *cis* and *trans* isomers was repeated five times and monitored with UV-Vis revealing hysteresis free switching. The SCNP decorated with triphenylphosphine pendant groups coordinated with catalytically active Au-Cl-complexes, was employed as a catalyst for the intramolecular hydroamination of an internal alkyne and amine. Small changes in catalytic properties arising from photoreversible morphological changes in the SCNP were observed.

5 Light-Driven Folding of Single Polymer Chains via Metal-Complexation

5.1 Objective

SCNP technology is a constantly evolving field, finding relevance for a number of soft material applications, significantly in catalysis.[280,290,293] The earliest SCNPs were inspired by enzymes, a large portion of which utilise metals for bio-catalysis. It is fitting that the majority of catalytic SCNPs are organometallic, using active metal centres for catalysis.[7] Several design strategies make SCNPs appealing polymeric catalyst for diverse chemical systems namely hydrophilic/hydrophobic pockets, increased surface area, and high functional density. [265,357,358] While organometallic, catalytic SCNPs are yet to recreate the catalytic properties of their natural counterparts and may well never, macromolecular engineering can assist in installing advanced functions to SCNPs not possible with enzymes, such as stimuli-responsiveness. Enzymes also possess a relatively restricted number of compatible metals, with specific organometallic tailoring, SCNPs can be functionalised with almost any metal species. However, current systems require specific ligand designs to facilitate the complexation of desired metal species. Ligands such as phenanthroline and bipyridine, that can accommodate many metals species are highly appealing in organometallic SCNPs.[261,359] Additionally, simultaneous metal complexation and chain folding into the SCNPs often affords milder reaction conditions then covalent chemistries.[226,284,360] Even milder conditions can be realised with photochemical processes, with the added benefit of inferring temporal control over chain folding.[361] Combining the two aforementioned processes of metal induced SCNP folding with photochemical triggers constitutes a mild and effective strategy for generating light-responsive organometallic SCNPs.

In the following chapter spiropyran functionalised polymers are investigated as light-responsive ligands for the binding to late transition metals in the 2^+ oxidation state. These specific metal ions are conventionally used in a diverse range of catalytic process.[362] However, their catalytic properties were not a primary factor in the

decision to implement them. The specific metals were chosen primarily for their ability to form stable enough yet reversible complexes with the spiropyran functionalities.

The spiropyrans – behaving as photoswitches – isomerise into a ring opened form, able to coordinate with metals as multidentate complexes, forming SCNPs through intramolecular spiropyran-metal crosslinks. The diversity of the spiropyran as a metal ligand is exemplified by SCNPs formed with a variety of late transition metals. The reversible nature of the spiropyran crosslinks was also investigated, however – currently – yielding inconclusive results.

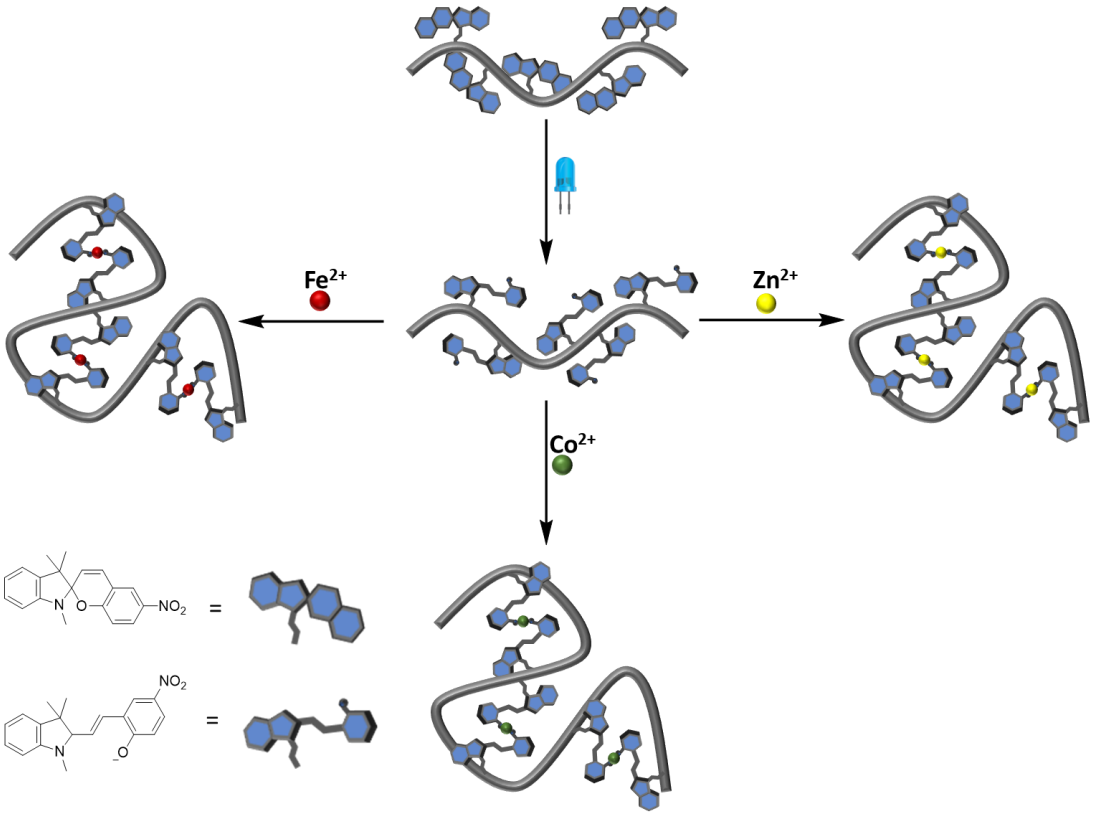

Figure 42. Schematic overview of SCNP formation via light induced metal complexation of linear polymers decorated with spiropyran pendant groups.

In the current thesis, linear polymers were envisioned to bear spiropyran pendant groups. RAFT polymerization was employed to generate narrow dispersity polymers, and methyl methacrylate functionalised spiropyran was copolymerised with methyl-methacrylate derivatives, selected for solvent compatibility to generate statistical copolymers. Light induced ring opening of the pendant spiropyran groups yielding the charged open form was to be achieved with UV-B irradiation. Complexation to the open form with late transition metals would induce chain collapse and SCNP

formation. The reversible photochromism displayed by spiropyrans potentially affords SCNPs with reversible folding upon irradiation with visible light. Consequently, the current chapter is divided into three sections relating to the synthesis of the linear polymer, the light induced crosslinking and the reversible folding attempts.

5.2 Synthesis of Spiropyran Polymers

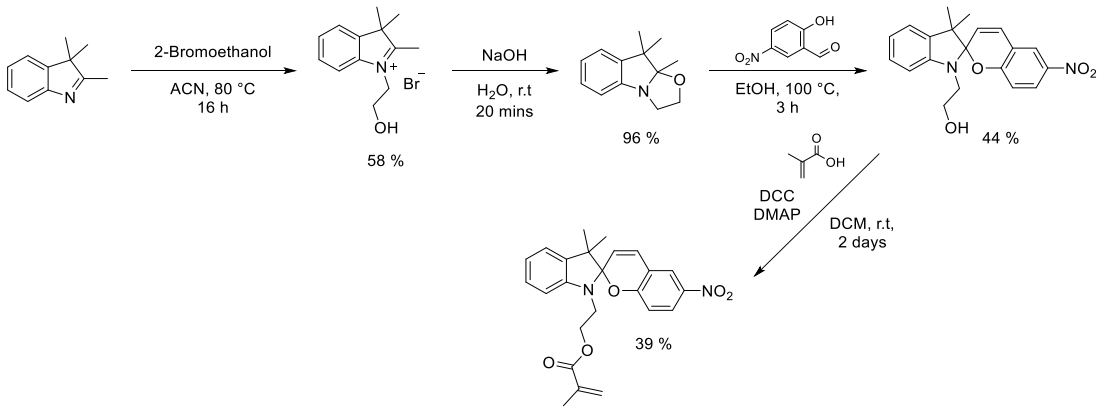

Figure 43. Synthetic route to afford methyl methacrylate spiropyran.

The methacrylate spiropyran was realised in a four-step synthesis, followed according to literature procedures. Starting with 2,3,3 trimethyl indolenine, bromo-ethanol was used to electrophilically alkylate the nitrogen centred on the indolenine. Overnight reflux was followed by simple trituration with ethyl acetate to generate fine crystals that were used for the next step. The alkylated indolenine was subsequently converted into an oxazole derivative using sodium hydroxide.[363] The oxazole was then used without purification and condensed with 5-nitrosalicahyde. A purple-coloured solution rapidly formed, and after 3 hours the reaction mixture was concentrated.[363] Recrystallization was achieved using a two solvent combination of ethyl acetate and n-hexane, affording the ethanol substituted spiropyran compound. The final step was the attachment of the methacrylate functionality. Nucleophilic substitution of the ethanol group to methacroyl chloride was attempted followed by collum chromatography, yet low yields were always observed < 15%. A possible explanation is the spontaneous ring opening of the spiropyran by acid formed during the reaction.[364] Degradation may occur via substitution of the negatively charged phenolate in the open form to methacroyl chloride. DCC coupling was performed instead, using methacrylic acid and pyridine as a catalyst adapted from Chen et al.[365] The resulting product was purified using column chromatography as well as a

recrystallization. Purple coloured material remained on the silica of the column after elution of the product suggesting a large amount of starting material and side product was present. Nonetheless a higher yield of close to 40% was achieved affording the methacrylate functionalised spiropyran **SP-MMA.** Attachment of the methacrylate functionality is visible as the presence of new resonances at 6.1, 5.5 and 1.9 ppm attributed to the acrylate and methyl functionalities respectively (Figure 44) (for the detailed synthesis description refer to Experimental section **8.2.10**, associated spectra **10.1.10**).

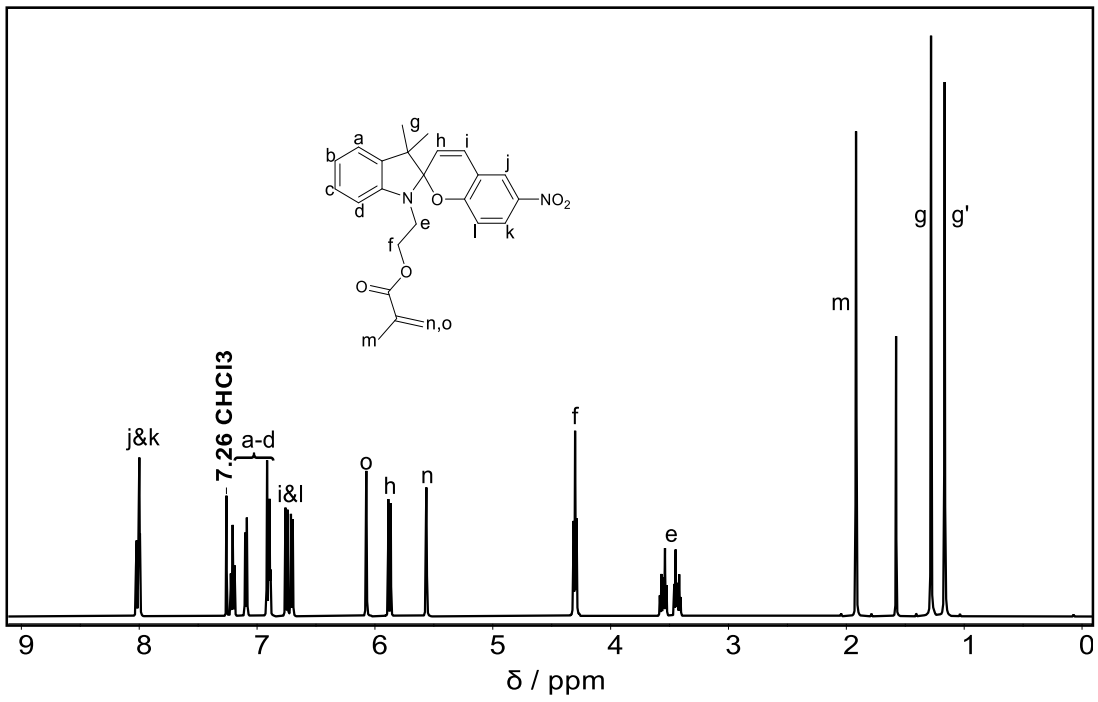

Figure 44. ^{1}H NMR spectrum of **SP-MMA** in $CDCl_3$.

SP-MMA was initially copolymerised with methyl methacrylate using ABCN as the radical initiator, with a feed ratio of 60:300 **SP-MMA** to MMA, resulting in a polymer possessing a spiropyran content of 20 mol% (**SP-20-MMA**).

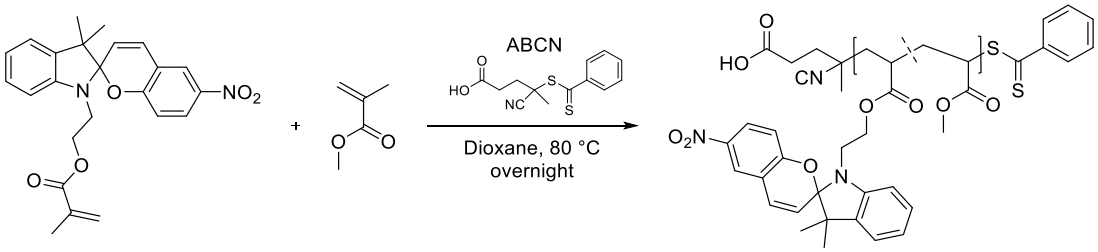

Figure 45. Copolymerization of **SP-MMA** and MMA via RAFT.

SP-20-MMA displayed poor solubility in polar solvents, known to favour the open zwitterionic form of spiropyran, due to the MMA co-monomer. The thermal stability of the open spiropyran is drastically reduced in less polar solvents such as chloroform and THF, rapidly reverting back to the closed form in minutes.[366] A long-lived open form is beneficial for the complexation of metal ions, and thus polymerizing **SP-MMA** with polar comonomers may yield better SCNPs.[367] (for the detailed polymerization descriptions refer to Experimental section **8.3.3.1**, associated data **10.3.3**)

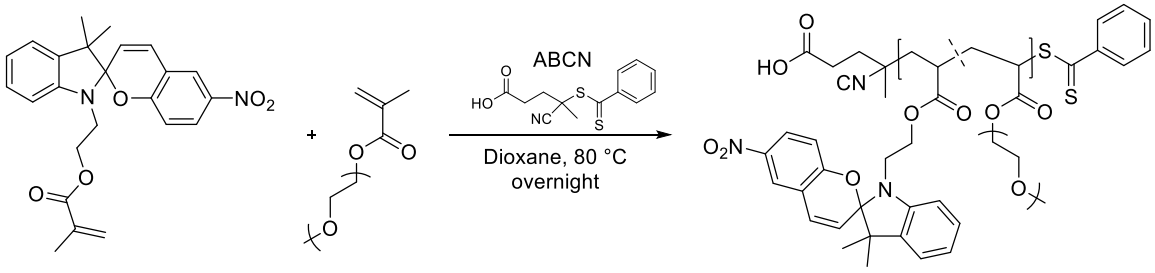

Figure 46. Copolymerization of **SP-MMA** and PEGMEMA via RAFT.

To facilitate better solubility, **SP-MMA** was copolymerised with polydisperse polyethylene glycol methyl ether methacrylate (PEGMEMA, Mn 300). Initially, a polymer consisting of 36 mol% spiropyran was generated (**SP-36-PEGMEMA**). However, a second polymer with a 15 mol% spiropyran content (**SP-15-PEGMEMA**) was prepared with the intention of comparing the compaction between high and low crosslink density. The resulting polymers displayed better solubility in polar solvents such as acetonitrile and methanol. However, **SP-36-PEGMEMA** required the addition of small amounts of dioxane to remain soluble in methanol arising from increased amount of the apolar closed spiropyran (for the detailed polymerization descriptions, refer to Experimental section **8.3.3.2**, associated data **10.3**).

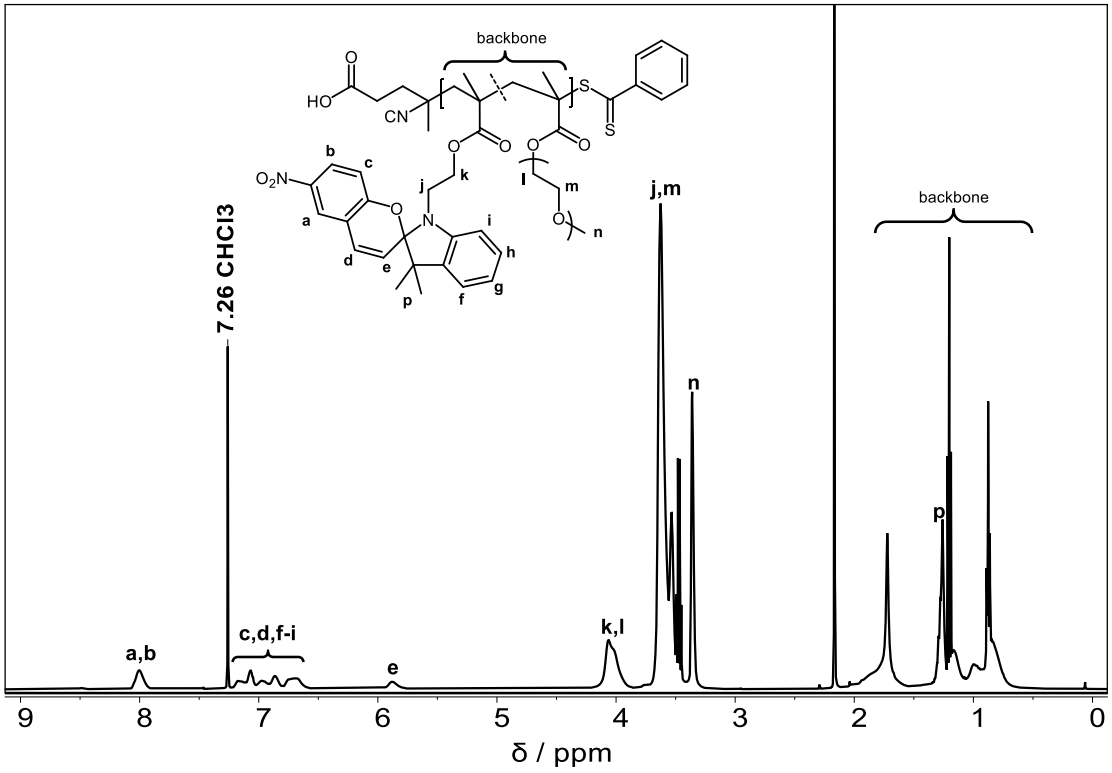

Figure 47. ^{1}H NMR spectrum of **SP-36-PEGMEMA** in $CDCl_3$.

Low conversions (15 %) were observed similar to the MMA based polymer; this was more pronounced when attempting polymerization with a feed ratio high in **SP-MMA** content. To reach the reported conversions, polymerizations were typically conducted for longer than 18 hours, with a gradual decrease in propagation observed after 20 hours. Doubling of the initiator content resulted in an increased rate of propagation, however high molecular weight-material began appearing after 20 hours. The broad molecular weight distributions were likely explained by the presence of the open form of the spiropyran during the course of the reaction. While ring-opening is photochemically driven at room-temperature, in polar solvents at elevated temperatures thermally induced ring opening occurs.[165] This effect not only arises from the polarity of the solvent, but is likely also due to the polarity of the co-monomer, here the polar PEG chains. The open form is in resonance with its quinoidal form,[163] suspected as being capable of α-hydrogen abstraction from a propagating radical, resulting in slow polymerizations and high dispersities.[200,201] A test polymer consisting of only PEGMEMA reached high conversions after 9 hours, further validating the inhibitory effect of the spiropyran (for the polymerization procedure refer to **8.3.3.3** associated elugrams and spectra, Appendix **10.3.4**). To decrease the

spontaneous ring-opening of spiropyran, toluene was used instead of dioxane. However, low conversions and high dispersity still occurred likely due to an increased rate of spiropyran bimolecular degradation.[176] The low conversions were accepted, and the polymers were used for subsequent photo-characterization and SCNP compactions.

SP-36-PEGMEMA was dissolved in EtOH (1 mg.mL^{-1}) and was irradiated for varying amounts of time with 365 nm light to determine suitable irradiation dosages. The formation of the open merocyanine upon irradiation is evidenced by an increase in the absorption band centred at 555 nm. Irradiation of ≥ 2 mins lead to similar intensities of the merocyanine band, with 1 minute of irradiation resulting in a lower amount of merocyanine forming (Figure 48, left). The thermal relaxation of the polymer **SP-36-PEGMEMA** was measured in EtOH after being irradiated for 3 minutes with a 365 nm LED to generate the maximum amount of merocyanine. The decrease of the band at 555 nm associated with the open merocyanine was used to track the thermal reverse isomerization into the closed spiropyran. After 9 minutes, close to 50 % of the formed merocyanine had thermally reverted, and after 60 minutes almost quantitative conversion to the spiropyran had occurred (Figure 48, right).

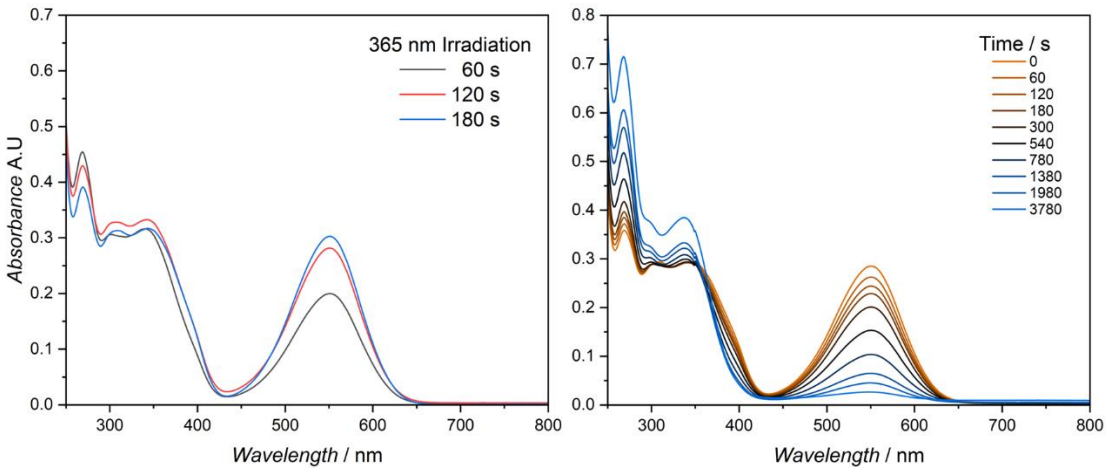

Figure 48. (left) Dosage experiments of **SP-36-PEGMEMA**, (right) thermal relaxation of **SP-36-PEGMEMA** in EtOH.

As spiropyrans are prone to photodegradation arising from oxidative as well as bimolecular degradation, it is important to establish the degree that this degradation results in photofatigue of the spiropyran switching process. The degree of spiropyran photodegradation is impacted significantly by factors relating to the polymeric

environment as well as the solvent.[177,368] Cyclic irradiation of a solution containing 1 mg.mL^{-1} of **SP-36-PEGMEMA** with 3 minutes of 365 nm light and 1 minute of white light was performed. By tracking the absorption of the 555 nm merocyanine band, hysteresis could be observed after the first irradiation cycle. A steady decrease in intensity of the band occurred over an additional 4 cycles with almost a 50% reduction in absorption by the last cycle (Figure 49, right). The increased photofatigue was expected due to the high spiropyran content of the polymer, which increases bimolecular degradation. Additionally, the sample was not degassed prior to irradiation and oxidative degradation likely occurred, which is probably only a minor contributor to hysteresis.[176]

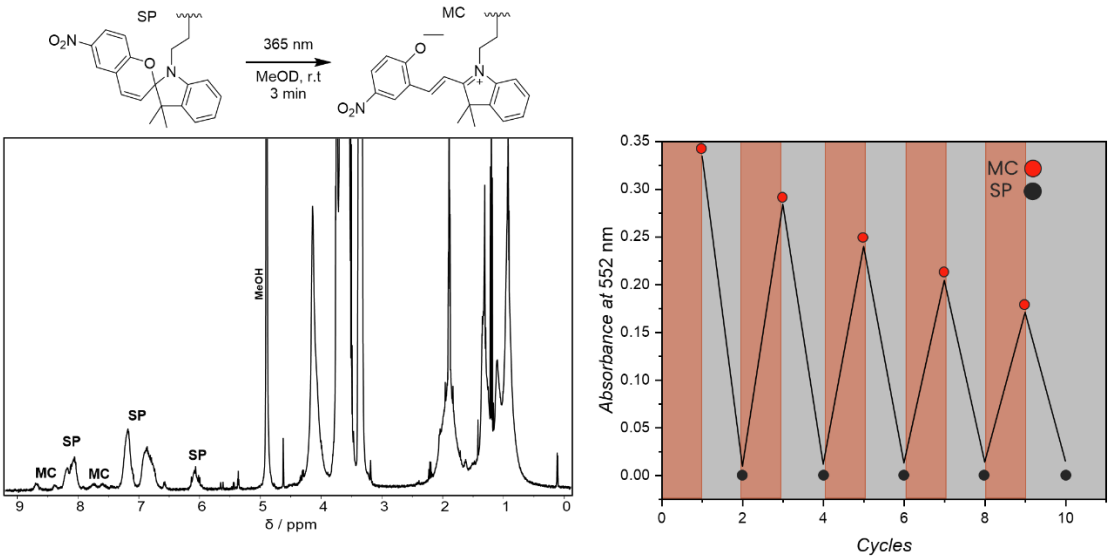

Figure 49.(Left) ^{1}H NMR spectrum of **SP-36-PEGMEMA** after 365 nm irradiation in MeOD, (right) cyclic irradiation of **SP-36-PEGMEMA** with 365 nm and white light.

The increased thermal half-life of the open merocyanine in polar solvents such as MeOD meant that photoisomerization was able to be evidenced by ^{1}H NMR spectroscopy (Figure 49, left). Merocyanine (MC) resonances between (δ = 7.5 - 7.8 ppm) and (δ = 8.4 – 8.7 ppm) were visible after 3 mins of irradiation with a 365 nm LED. Close to 8% of the spiropyran (SP) is converted to merocyanine based of the resonance integrals. Spiropyrans often display low isomerization efficiency with photostationary states consisting of < 20% being commonly observed in polar solvents.[369,370] Thus, the observed relatively low merocyanine content was expected. Furthermore, in the time taken to prepare and analyse the sample (ca. 10 mins), significant thermal reversion could occur even in polar solvents such as MeOH.[366]

5.3 Light induced Metal Coordination

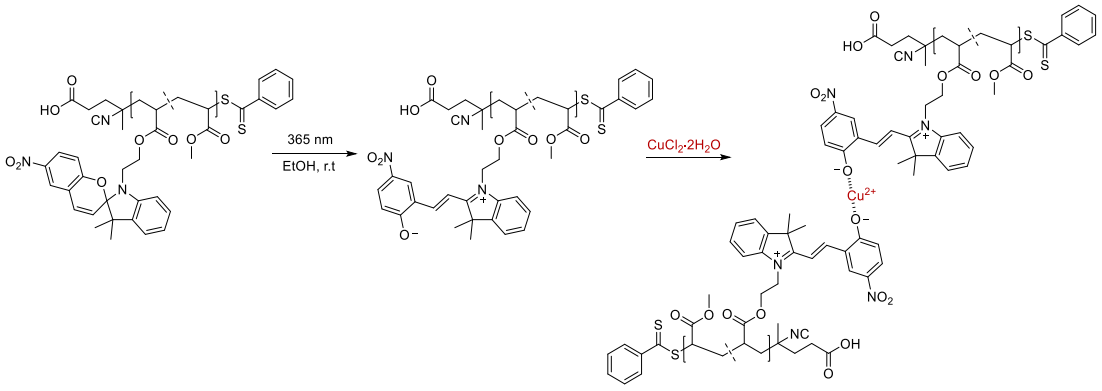

Figure 50. Light induced, metal coordination of **SP-MMA-20** forming merocyanine: copper crosslinks.

The Lewis acidity of the metal species was considered when determining possible spiropyran-metal crosslinking strategies. Late transition metals in the 2^+ oxidation state were chosen for complexation with the spiropyran containing polymers due to them possessing a Lewis acid character between soft and hard. These metal species were envisioned to have a high enough affinity for the spiropyran phenolate anion - a hard base - while still retaining a weak enough metal-oxygen bond for potential light induced reversibility. SCNP folding was attempted initially on **SP-20-MMA**. Due to the poor solubility of the polymer in polar solvents, the following experiments were conducted in a solvent mixture of acetonitrile and chloroform. The polymer was dissolved (1 mg mL^{-1}) in a photo vial, which was pulse irradiated in cycles with 1-minute pulses of 365 nm light, followed by 10 minutes in the dark under stirring, repeated 10 times over the course of 110 minutes. It was expected that a significant amount of thermal relaxation would occur in the 10 minutes of dark time between pulses. During the course of the irradiations, a slow and continuous addition of 1 eqv of $CuCl_2{\cdot}2H_2O$ (to each spiropyran) was completed. Continuous irradiation over the full 110 minutes of addition would result in extensive photofatigue/degradation, thus the above noted pulse irradiations were used. Slow addition was selected to keep that relative concentration of copper to merocyanine low, ensuring that 2:1 merocyanine:Cu^{2+} crosslinks formed as opposed to 1:1 merocyanine:Cu^{2+} complexes.[208] After the 110 minutes of pulse irradiations and continuous addition, the combined solutions were allowed to stir for one hour to allow for thermal relaxation of non-complexed merocyanine. Isolation of the polymer from the metal proved

difficult, as the crude reaction mixture could not be concentrated owing to uncontrolled crosslinking due to residual copper. Removing excess copper was achieved by the addition of DCM followed by aqueous washes and concentration of the organic layer to afford the polymer (for experimental procedures refer to **8.3.4**). Comparison of the SEC chromatograms of the polymer before and after addition of copper and irradiation when overlayed with eachother revealed overlapping RI traces with almost identical retention volumes, suggesting no SCNP had formed (for the associated elugrams refer to **10.4.6**). Failure to form the SCNP is attributed to the low concentrations of both the polymer (1 $mg.mL^{-1}$) and copper – 1 equivalent of copper to 1 equivalent of spiropyran. Increasing the concentration of the polymer above 1 $mg.mL^{-1}$ increases the probability of intermolecular crosslinks forming. Thus – instead – the amount of metal added was increased to 4 eqv. Repeating the SCNP formation resulted in a clear intramolecular compaction as evidenced by a shift to higher retention volumes in the SEC chromatogram (Figure 51). Critically, the reversibility of the folding was also investigated. The SCNPs were dissolved in THF and irradiated with white light, which resulted in a partial reversion of the folding as evidenced by a shift to lower elution volumes during SEC analysis. Additionally, leaving the SCNP overnight in THF also resulted in an almost identical shift.

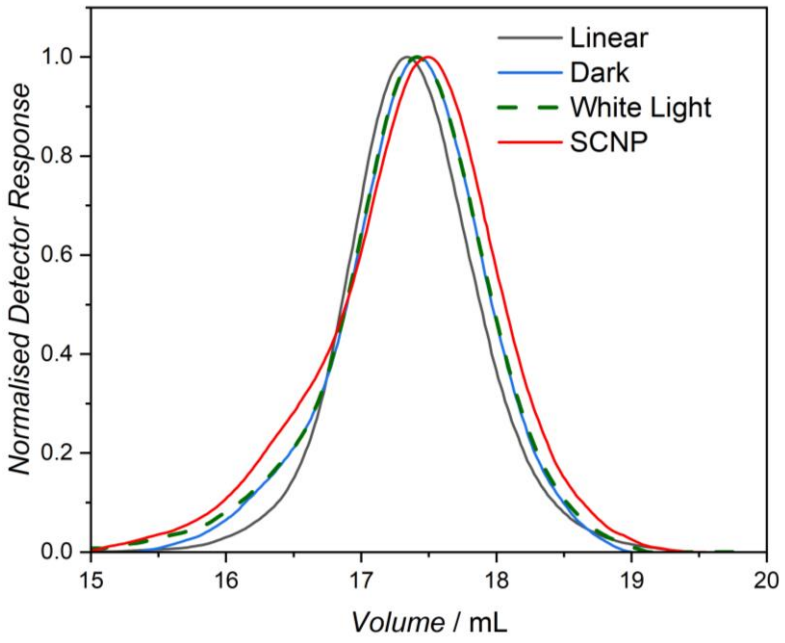

Figure 51. SEC chromatogram of **SP-MMA-20** (black) after simultaneous irradiation with 365 nm and slow addition of copper forming an SCNP (red), partial unfolding of the SCNP after white light irradiation (green) and comparative relaxation in the dark (blue).

The partial reversion was attributed to irreversible crosslinking of the polymer due to non-coordinative processes. Cu^{2+} has been shown to irreversibly dimerise spiropyrans via an oxidative coupling mechanism. The degree of dimerization was highly dependent on the ratio of copper to spiropyran, with the effect being most dramatic with 3 equivalents of copper.[371] A portion of crosslinking could have been the result of such a dimerization, with photoreversibility limited to the fraction of crosslinks remaining non-dimerized. It was also suspected that photofatigue may be a factor, where photo-induced bimolecular degradation of the merocyanine might also lead to irreversible crosslinking. Therefore, being able to reduce the amount of pulse irradiations required to form the SCNPs was considered. A more polar solvent would stabilise the open merocyanine and increases its thermal half-live. The effect of the increased thermal half-life is that a lower amount of irradiation would be required to generate a sufficiently high merocyanine concentration to complex with metal ions over the course of the reaction. Thus, **SP-PEGMEMA** polymers were developed, displaying increased solubility in polar solvents.

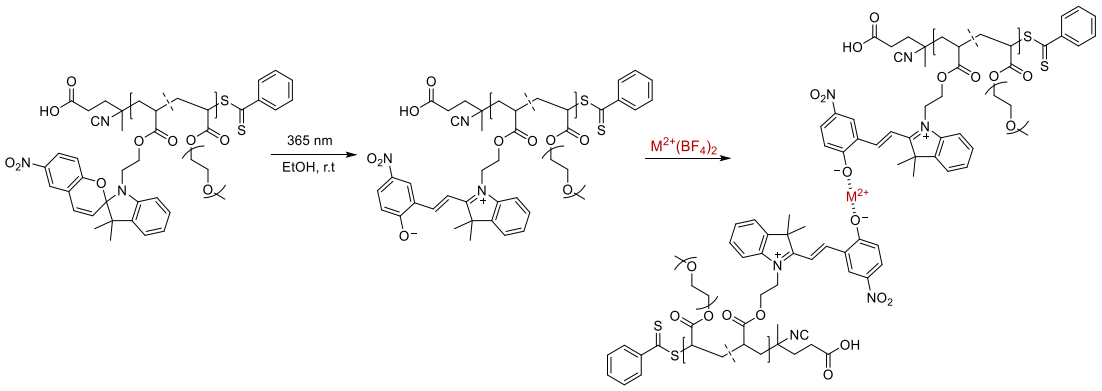

Figure 52. Light induced, metal coordination of **SP-36-PEGMEMA** forming merocyanine: copper crosslinks.

SP-36-PEGMEMA dissolved in ethanol was employed for further testing, using less irradiation and different metal species. Focus was primarily given to the formation of SCNPs as opposed to their reversibility. A series of metal salts with weakly coordinating BF_4^- ions were used to facilitate better complexation with spiropyran and afford larger compactions. Crosslinking was completed in a similar manner to that of **SP-MMA-20**, with continuous addition of a metal species to an ethanol solution containing **SP-36-PEGMEMA** being irradiated in pulses. The polymer solution was irradiated six times for 1 minute – as opposed to 10 – with 15-minute intervals of

darkness between each pulse. In addition to reduced irradiation time, a lower concentration of polymer (0.5 mg.mL^{-1}) was used to limit intermolecular crosslinking and solutions were degassed with N_2 prior to irradiation. After six cycles of irradiation, the combined polymer/metal solutions were left in the dark for one hour to allow for thermal relaxation of any non-complexed merocyanine. No work-up was completed and the crude samples were diluted in THF and analysed via SEC. Three metals were investigated for folding, i.e. zinc, cobalt, and nickel. Comparison of M_p values for each metal revealed reproducible compactions for $Co(BF_4)_2$ and $Zn(BF_4)_2$ represented by an apparent molecular weight reduction of 10,000 g mol^{-1} and 3,000 g mol^{-1} respectively, while a compaction of < 1000 g mol^{-1} was observed for $Ni(BF_4)_2$ (Figure 53).

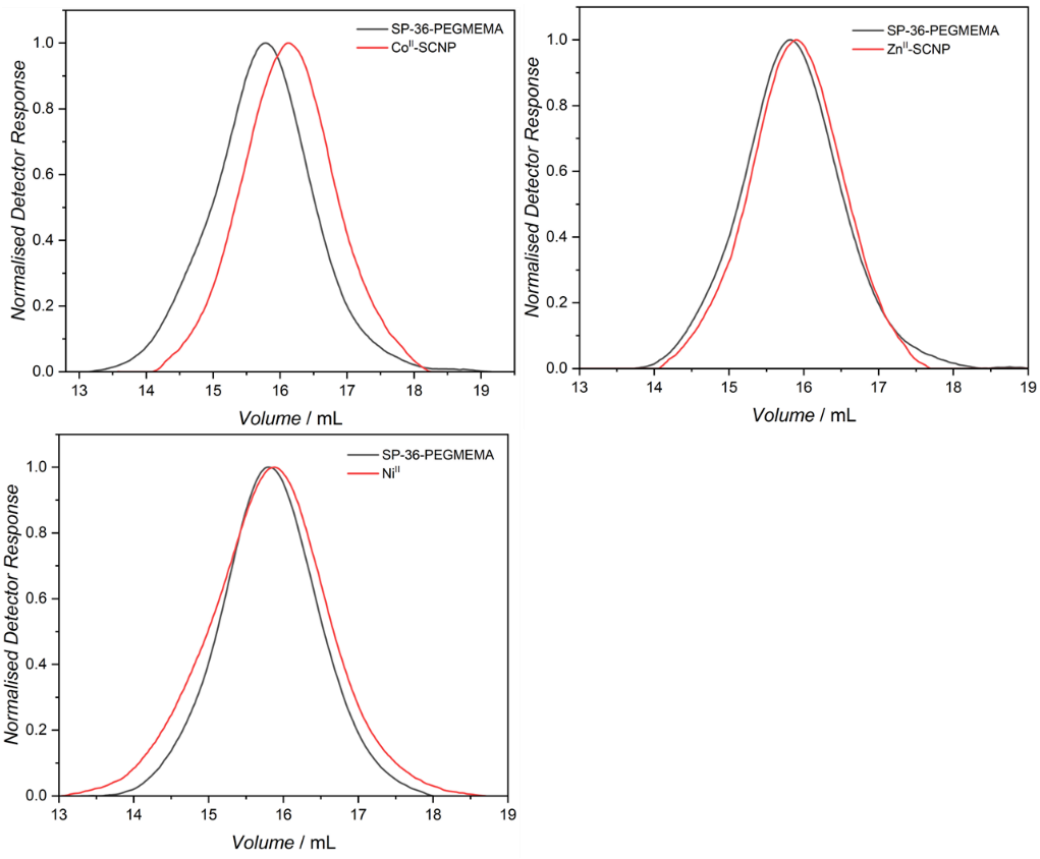

Figure 53. SEC chromatograms of **SP-36-PEGMEMA** (0.5 mg.mL^{-1}) after 365 nm irradiation and addition of tetrafluoroborate metals (4 eqv) (top left) **SP-36-PEGMEMA**, cobalt complexation, (top right) **SP-36-PEGMEMA**, zinc complexation, (bottom left) **SP-36-PEGMEMA**, nickel complexation

The degree of compaction was assumed to correlate to the relative binding affinities of each metal to the open merocyanine. A study examining the spectroscopic

properties of spiropyran bound to a surface revealed a reactivity series of $Ni^{2+} < Co^{2+} < Zn^{2+} < Cu^{2+} = Fe^{2+}$.[372] This reactivity series supports the observation of the nickel compaction experiments, but does not necessarily support the large compaction of cobalt compared to zinc. According to this series, the highest compaction should be observed for SCNPs formed using $Zn(BF_4)_2$, as it should show the highest affinity for the merocyanine isomer. Instead, SCNPs formed using $Co(BF_4)_2$ displayed the greatest compaction. The polymeric architecture in spiropyran polymers is known to stabilise merocyanine: metal complex via additional coordination to comonomers and other functionalities such as the ester group of acrylate based monomers(Figure 54).[373,374]

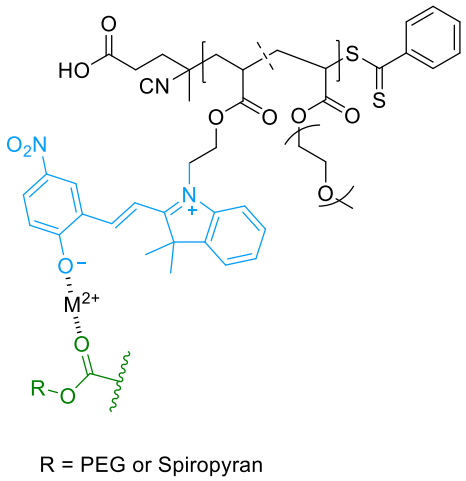

Figure 54. Possible coordination between the spiropyran phenolate anion (blue) and a polymer bound acrylate functionality (green) to a divalent metal centre.

It is likely that higher coordinated complexes are formed in the SCNPs arising from the coordination between multiple spiropyrans and ester units (Figure 55). Thus, the aforementioned reactivity series, which only analysed di-coordinated merocyanine: metal complexes may not be viable.

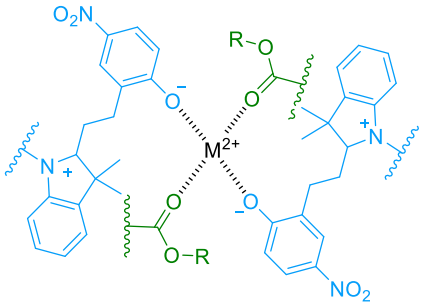

Figure 55. Additional coordination sites may be provided by ester functionalities along the polymeric backbone. A deviation from the standard 2:1 merocyanine:M^{2+} stoichiometry may occur leading to higher coordinated crosslinks within the SCNPs.

Other studies have shown differing reactivity series for polymeric spiropyran, suggesting that metal binding may be dependent on the polymeric environment and should be individually determined for each system.[181,375] Compaction experiments were also completed on **SP-15-PEGMEMA**, however only cobalt and iron were assessed, as they were expected to display the largest compactions. Iron was selected due to the number of free orbitals available for coordination in its valence shell, a property that has been related to the ease of formation of spiropyran metal complexes.[181] Interestingly, only minimal compaction was observed when using cobalt and a moderate compaction was observed for iron, suggesting that forming spiropyran metal complexes is reliant on a high molar percentage of spiropyran pendant groups (for relevant elugrams, Appendix section **10.4.7** and **10.4.8**). It is clear from these experiments that judicial selection of metal ions is required for suitable SCNP formation. Additionally, the effect of the counterion is a contributing factor and will likely impact the potential reversibility of the merocyanine-metal crosslinks.

5.4 Reversible folding experiments

Being able to recover the linear polymer by removal of metal from the crosslinks, would mean that the same polymer sample could be complexed with multiple metal centres. In a broader context, a single SCNP that displays this property could be imbued with a plethora of functions, normally only obtainable by making multiple different SCNPs. Due to the weakly coordinating nature of the BF_4^- counterion, $M^{2+}(BF_4)_2$ complexes display increased affinity to open merocyanine. The increased stability of the resulting complexes prohibits the reverse isomerization via thermal and photochemical means.[193] Thus, herein, the focus was on chemical methods for

removing the metal complex from the merocyanine constituting the intramolecular crosslinks of the SCNPs. Quantitative methods of metal removal were required as it has been shown that in circumstances of reversible crosslinks, compacted SCNP morphologies will remain intact even when a small number of residual crosslinks is present. The SCNP formed using $Zn(BF_4)_2$ was treated using ethylenediaminetetraacetic acid (EDTA), with the intention of decomplexing zinc from the merocyanine crosslinks (Figure 56). SEC analysis of the SCNP before and after EDTA treatment showed no noticeable change to retention volumes, with the EDTA treated sample's trace overlapping perfectly with the initial SCNP trace. It is possible that instead of selectively removing the zinc from merocyanine, the EDTA cooperatively forms a stable complex with the zinc-merocyanine species resulting in an unchanged SCNP morphology (For description of all unfolding experiments refer to Experimental section **8.3.4**).

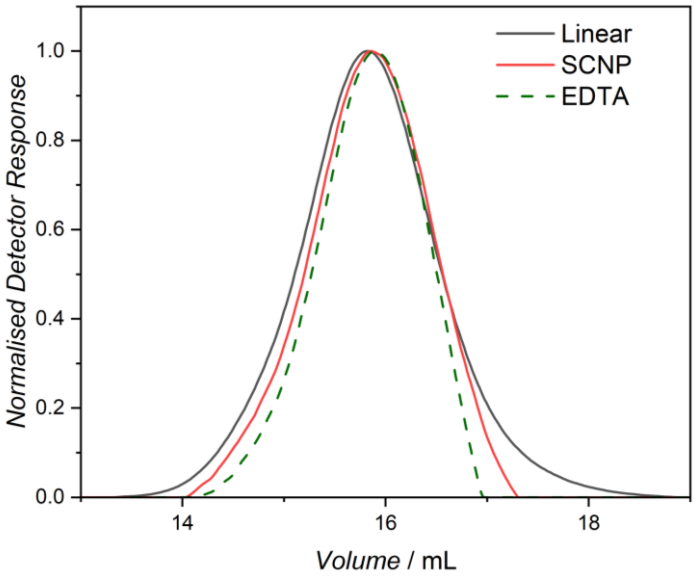

Figure 56. SP-36-PEGMEMA, (black) a zinc containing SCNP formed with 365 nm irradiation and continuous addition of 4 equivalents of $Zn(BF_4)_2$ (red), attempted decomplexation using EDTA, (4 eqv) (green).

To prevent the possibility of a new complex forming between the merocyanine:zinc-crosslinks, a new strategy was employed to precipitate the Zn^{2+} ions from solution as ZnS by the addition of thioacetamide (TAM) in basic conditions to the SCNP solution followed by light heating (Figure 57). Precipitation of a solid occurred, followed by the formation a yellow-coloured solution. The precipitate was assumed to be ZnS, highly insoluble in ethanol, the solvent used for SCNP formation. Subsequent analysis

via SEC showed that unfolding did not take place and instead an increase in retention volume was observed indicative of additional compaction.

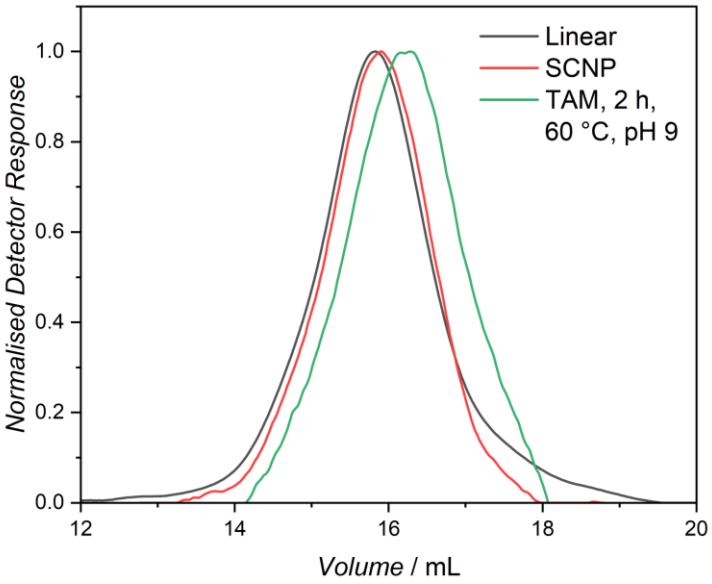

Figure 57. SP-36-PEGMEMA, (black) a zinc containing SCNP formed with 365 nm irradiation and continuous addition of 4 equivalents of $Zn(BF_4)_2$ (red), attempted decomplexation using 3 equivalents of thioacetamide to zinc at pH 9 with heating to 60 °C(green).

Test experiments were completed on a polymer containing only PEG side chains and no spiropyran units. The tests were conducted to determine whether or not the PEG side chain are cleaved off the polymer under the thioacetamide complexation conditions, leading to a decrease in the apparent molecular weight of the polymer. Additionally, it was considered that the PEG chains may also be able to encapsulate the Zn^{2+}, possibly resulting in irreversible compaction.[376] Thus, the conducted test experiments served two purposes. SEC analysis, however, indicated no difference between the untreated-polymer and the polymer treated with Zn^{2+} and thioacetamide (Figure 58, right). No shift to higher retention volumes was observed in the chromatogram which would have been indicative of a loss of mass due to PEG chain cleavage or compaction due to zinc encapsulation. Treatment of **SP-36-PEGMEMA**, without prior 365 nm irradiation, with thioacetamide also did not result in additional compactions, with the SEC trace matching non-treated **SP-36-PEGMEMA** (Figure 58**,** left)**.**

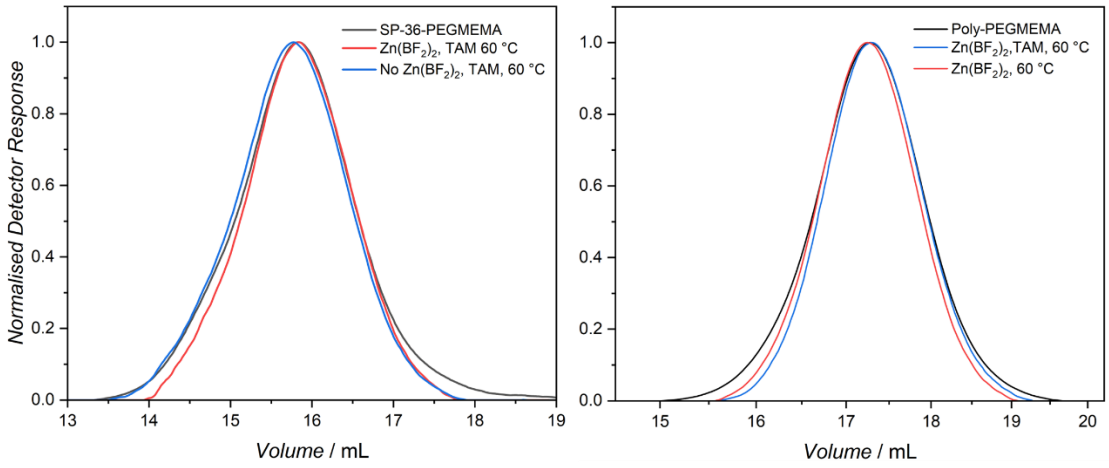

Figure 58. (left) Control experiment performed on **SP-36-PEGMEMA**, (right) control experiment performed on a PEGMEMA test polymer.

On the basis of these test experiments, it was concluded that thioacetamide likely only impacted the open merocyanine form and not the PEG chains or closed spiropyran. The compactions observed when attempting to reverse the SCNPs may be due to the open merocyanine forms reacting with the sulphide ions generated from the thioacetamide. As trapping of the merocyanine form is achieved using a variety of nucleophiles, it is possible that the same process is occurring with sulphide ions leading to permanently open spiropyran adducts (Figure 59).[377–379] Disulfide bridge formation between spiropyran could potentially occur from either of these adducts resulting in the observed increase in compaction.

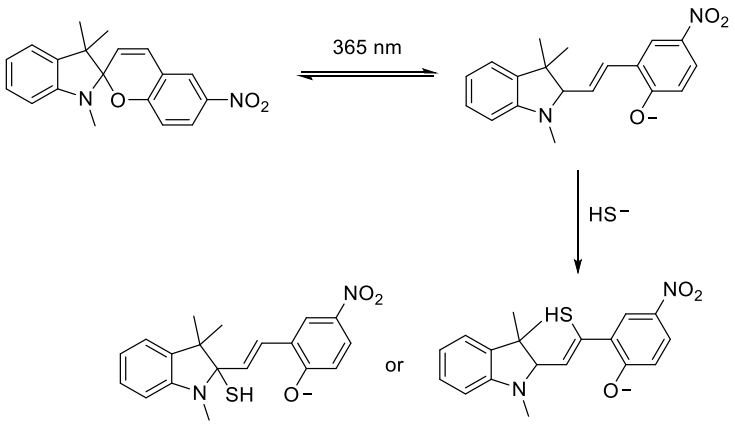

Figure 59. Nucleophilic trapping of the open merocyanine with sulphide ions.

Reversible folding was also attempted on the SCNPs formed from $Co(BF_4)_2$. A small amount of ammonia in methanol was added to the SCNP solution after being allowed to stir in the dark for one hour. An hour after the addition of the ammonia solution, a partial unfolding of the SCNP occurred as shown by a decrease in the retention volume of the corresponding SEC chromatogram, yet a further hour of stirring lead to no additional unfolding (Figure 60, blue and green trace). Co^{2+} salts will readily precipitate from solution as $Co(OH)_2$ when reacted with aqueous ammonia, however this is not a quantitative method for removing cobalt. A large amount of cobalt remains complexed with the merocyanine forming the SCNP crosslinks.

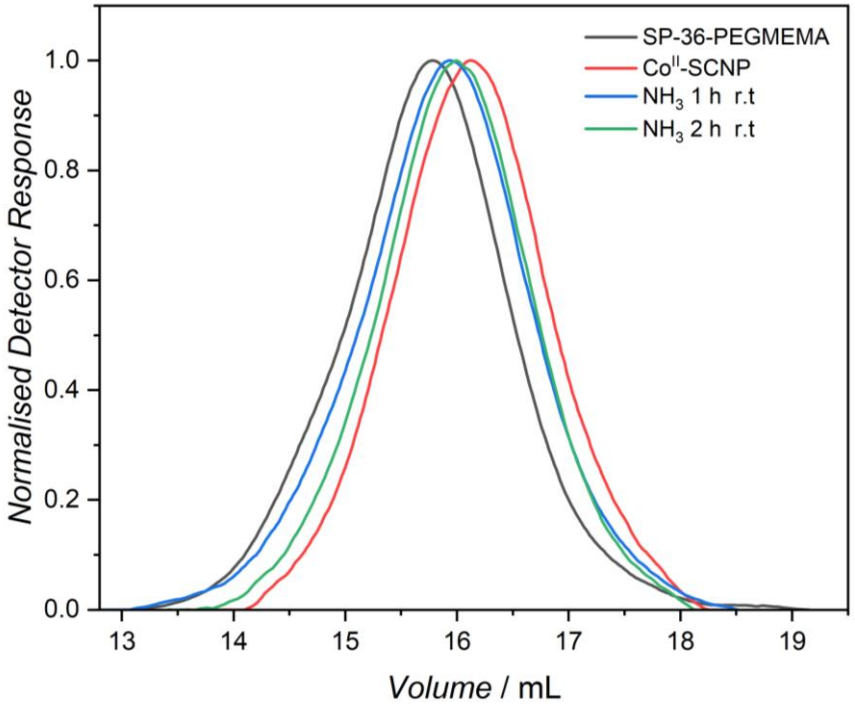

Figure 60. SP-36-PEGMEMA, (black) a cobalt containing SCNP formed with 365 nm irradiation and continuous addition of 4 equivalents of $Co(BF_4)_2$ (red), attempted decomplexation using a large excess of ammonia to zinc (~35 eqv) (green).

For true reversibility, new methods of chemical de-complexation are required that lead to quantitative, or close to, removal of metals from the merocyanine crosslinks are required. Finding such methods is also highly dependent on the metal species in question as metals such as Co^{2+} can be decomplexed comparatively easier than Zn^{2+}.

5.5 Conclusion

In the current chapter, SCNPs were generated using spiropyran containing polymers, able to form stable complexes with a range of late transition metals upon exposure to 365 nm light. The linear polymers were synthesised using RAFT polymerization, yielding a range of polymers with varying spiropyran content, and differing co-monomers enabling solubility in a variety of polar and apolar solvents. Experimental parameters including solvent, irradiation time and metal species were varied to facilitate SCNP formation. Polymers bearing polar PEGMEMA side chains were found to constitute a versatile pre-cursor polymer able to form SCNPs with iron, zinc and cobalt tetrafluoroborate salts. Polymers constituted of methyl methacrylate co-monomers were of limited use due to their poor solubility in polar solvents. Light and chemical stimuli were employed in preliminary un-folding experiments, attempting to decomplex metals from the SCNPs and recover the linear polymer. Partial un-folding was observed in some cases, yet due to the sensitivity of the spiropyran pendant groups to a variety of photo and chemical degradation pathways, un-folding was incomplete. The work contained in the current chapter constitutes a novel method of folding linear polymers via metal complexation into organometallic SCNPs via a mild photochemical trigger. Future potential lies within application in dynamic morphology control and catalysis.

6 Conclusion

The present thesis demonstrates two photoresponsive organometallic SCNPs over two chapters that make use of metal centres as either catalytic functionalities or as purely structural elements of the SCNP morphology. Photoresponsivity is imparted to the SCNPs via the incorporation of photoswitches as intramolecular crosslinks. Two separate crosslinking strategies were employed for both SCNPs, affording photoresponsive morphologies. Azobenzenes used as external crosslinking agents were able to fold a catalytic linear polymer upon substitution with benzylic alcohol pendant groups on the polymer. Azobenzene substitution afforded SCNPs that showed light-induced control over their folded structure via azobenzene isomerization, which in turn appeared to have an impact on their catalytic functionality due to compaction and polarity changes to the SCNP environment. The second system utilised a linear polymer with spiropyran pendant groups, able to intramolecularly crosslink via complexation with a diverse range of transition metals upon photoisomerization. Conclusions were provided at the end of each chapter but will be summarised in the following section.

The azobenzene crosslinked **AzoCl$_4$-Au-SCNP** was discussed in the fourth chapter of the current thesis. Reversible compaction arising from the *cis*/*trans* isomerization of tetra chlorinated azobenzene crosslinks was achieved using two wavelengths of visible light, 620 and 415 nm respectively. Azobenzenes tetra-chlorinated *ortho* to the azo bridge were functionalised at the 4,4 positions with pentaflurophenyl esters to facilitate intramolecular crosslinking via pendant alcohol groups on the polymer chain. Catalytic functionality was provided by triphenylphosphine-gold complexes capable of catalysing the hydroamination of alkynes. The folding of the linear polymer was evidenced by SEC measurements and DOSY-NMR spectroscopy, showing a clear reduction in apparent molecular weight and hydrodynamic volume. The photoswitching properties of the **AzoCl$_4$-Au-SCNP** were analysed using UV-Vis and ^{1}H NMR spectroscopy, revealing efficient switching of the azobenzene crosslinks into the *cis* isomer with a long thermal half-life. Photoswitching was also able to be performed over multiple irradiation cycles with minimal hysteresis. SEC measurements revealed a small compaction of the SCNP after irradiation with 620 nm

light. Critically, this small compaction could be reversed with complimentary 415 nm irradiation to revert the azobenzenes to their *trans* isomer. Preliminary catalytic tests employing **AzoCl$_4$-Au-SCNP** as a catalyst for the intramolecular hydroamination of an alkyne revealed a small change in substrate conversion upon irradiation with 620 nm light and subsequent photoisomerization. The change in conversion was attributed to a change in polarity and internal SCNP morphology arising from *cis* to *trans* isomerization.

The second SCNP systems introduced in the fifth chapter of the current thesis uses photoresponsive spiropyran-metal crosslinks for intramolecular collapse. Upon 365 nm irradiation, a spiropyran attached to linear polymers isomerises into an open, charged merocyanine form. The charged phenolate ion of the merocyanine was used to form coordination complexes with late transition metals. Copolymers of spiropyran methyl methacrylate and PEGMEMA side chains were found to be the most suitable polymer design for photo-induced complexation due to increased solubility in solvents stabilising spiropyran isomerization. SCNPs were formed using iron, zinc and cobalt centres bearing weakly coordinating tetrafluoroborate salts, chosen due to their high affinity towards the merocyanine isomer. The reversible nature of the merocyanine/metal crosslinks was investigated. Partial unfolding was observed for some SCNPs upon exposure to several photo and chemical stimuli. The sensitivity of the spiropyran pendant groups prevented complete unfolding due to their tendency to degrade upon exposure to those same stimuli.

Metal centres provide critical functionality to SCNP morphologies. Combining such organometallic SCNPs with photoresponsivity culminates in advantages over natural analogous. The systems introduced in the present thesis highlight these possibilities, with catalytic and morphology control being at the forefront of the design considerations. The use of photoswitchable elements incorporated in the polymeric structure of SCNPs allowed for versatile morphological transformations to be performed, not as readily realised using more conventional photochemical techniques. Hopefully, the SCNPs introduced in the thesis aid in the development of more advanced photoresponsive metal based SCNPs displaying diverse functionalities and greater morphological changes.

7 Outlook

The loss of catalytic activity that was observed when employing **AzoCl$_4$-Au-SCNP-13** as a catalyst for the intramolecular hydroamination of alkynes, could potentially have arisen from either the degradation of the gold species or the co-catalyst. Analysis of the SCNP post catalysis with techniques such as ^{31}P NMR or XPS could be used in determining the cause behind the loss of catalytic activity. ^{31}P NMR would be useful in determining the status of the phosphine species through distinct shifts in the phosphine resonance dependant on the nature of the species attached to it. Loss of catalytic activity could be evidenced by the formation of phosphine oxide, a common by-product of phosphine-gold degradation with a distinct resonance in ^{31}P NMR (δ = 29 ppm). XPS could also yield valuable insights into the nature of the gold species, particularly its oxidation state. The reduction of gold (I) into gold (0) is a common degradation pathway in gold catalysis[380] and could be easily identified via XPS.[381] The degradation of the co-catalyst zinc triflate was also considered, occurring possibly through hydrolysis into triflic acid. This degradation could be confirmed via ^{19}F NMR experiments, a techniques that has been used to identify distinct resonances for either the metal coordinated triflate anions or free triflic acid.[382] It was envisioned that due to the *trans-cis* isomerization of the azobenzene crosslinks and subsequent compaction of the SCNP, that access to catalytic sites would be limited. A significant difference between catalytic conversions between the two isomers of the azobenzene would then occur, effectively constituting photo-controllable catalysis. While a slight reduction in conversion was observed, to be considered a truly photoresponsive catalyst **AzoCl$_4$-Au-SCNPs** require further development. Additional work in characterising the composition of the **AzoCl$_4$-Au-SCNP** is required to fully realise the photo-catalytic responsivity of the system. Better understanding the photoswitching properties of the SCNPs is critical to applying them for photoresponsive catalysis. While a variety of techniques can be utilised as they were in the respective chapter, to verify the switching and overall compaction of the SCNP, observation of the SCNPs internal morphology would yield key insights into how azobenzene isomerization affects catalysis. Characterization including Single Angle Scattering (SAS) techniques could be used in conjunction with molecular dynamic simulations (MD) to determine the spatial distributions of catalytic sites throughout the SCNP.[383] Subsequently, a combined

SAS and MD approach could be used to show how the spatial distribution might change upon irradiation and isomerization of azobenzene crosslinks. Identifying how catalytic sites are distributed throughout the **AzoCl$_4$-Au-SCNPs** may guide design strategies of how to make them more photo-catalytically responsive. As an example, if the catalytic sites were sparsely distributed throughout the SCNPs, then isomerization may have a lesser effect on catalysis due to less defined catalytic pockets throughout the SCNP. The inverse effect on catalysis could be true for a more globular SCNP, where catalytic sites are internalised within a central pocket within the particle. Insights gathered from such characterization can inform synthetic strategies to afford SCNPs that display the aforementioned morphologies. Several SCNPs could then be synthesised with morphologies that range from sparse to globular. The morphology dependence on catalysis could subsequently be assessed in a more methodical way, allowing for better optimisation of the desired photo-catalytic properties.

In addition to a more detailed characterization of the **AzoCl$_4$-Au-SCNP** morphology, effort is required to identify suitable substrates for **AzoCl$_4$-Au-SCNP** catalysis. More diverse intramolecular substrates should also be investigated with varying polarities and steric bulk as these two properties vary within the SCNP morphologies upon switching. For example, highly polar substrates may show a higher binding affinity for the isomerised and more polar *cis*-**AzoCl$_4$-Au-SCNP**, which may decrease upon switching into the less polar *trans*-**AzoCl$_4$-Au-SCNP**. Sterically bulky substrates may be better able to access catalytic sites in the open *trans*-**AzoCl$_4$-Au-SCNP** as opposed to the more compacted *cis* form. An extensive substrate screening is required to reveal these SCNP/substrate affinities. Identifying substrates that display marked differences in affinity and consequently conversions between *cis* and *trans*-**Azo-Au-SCNP** could allow for the development of complex tandem substrate catalysis systems. Two substrates could be combined in one reaction which display high affinity for one of the two configurations of the **AzoCl$_4$-Au-SCNP**. The affinity of the SCNP between the two substrates switching depending on the colour of light irradiating the sample, consequently resulting in a decrease in conversion of one of the substrates and an increase in the other (Figure 61).

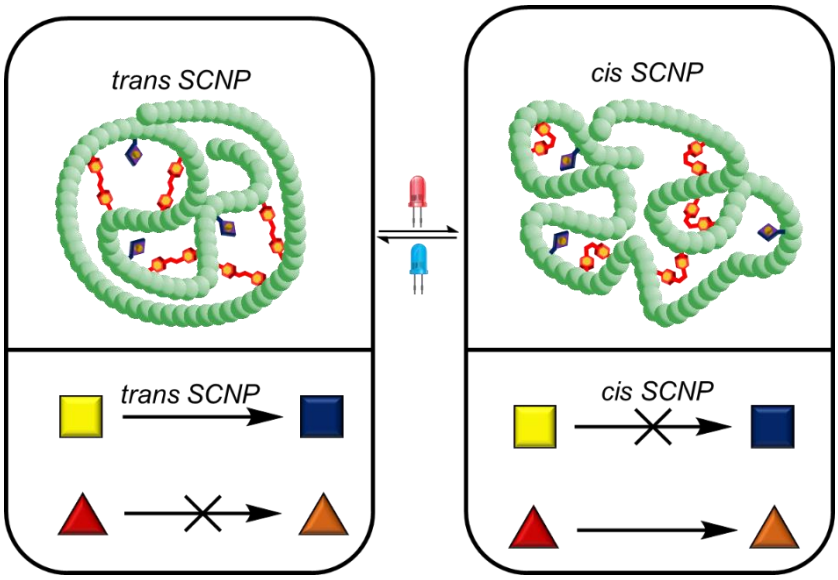

Figure 61. Example of selective substrate catalysis using the two "isomers" of **AzoCl$_4$-Au-SCNPs**, (left) in the *trans* isomer configuration the SCNP could display higher conversion for one of the substrates (yellow →blue), upon exposure to 620 nm light and switching to the *cis* isomer configuration, selectivity switching to the other substrate (red →orange)

Similarly, the **AzoCl$_4$-Au-SCNPs** could be applied for tandem catalytic systems with a second catalyst. A single substrate could be converted into one of two products facilitated by either the **AzoCl$_4$-Au-SCNP** or the complementary catalyst in a competitive process. Increased/decreased binding of the substrate to the **AzoCl$_4$-Au-SCNP** would vary depending on the SCNP *cis/trans* configuration upon light irradiation, resulting in a direct decrease/increase for the binding to the second complementary catalyst. The change in substrate affinity would be reflected in the yields/rates of two possible products formed by either the SCNP or the second catalyst, constituting light-controlled product selectivity.

A property of the azobenzene switching discussed in the respective chapter is the increase in polarity as *trans* azobenzene isomerises into the *cis* configuration. This light induced change in polarity has been utilised for modulating thermoresponsive properties of azobenzene containing polymers, notably the tuning of Upper Critical Solution Temperature (UCST).[384,385] Often isomerization of azobenzenes bound to polymers that display UCST results in a decrease in the cloud point temperature (T_{CP}) as the *cis* isomer increases the overall polarity of the polymer.[386,387] Potentially, solvent systems exists where the **AzoCl$_4$-Au-SCNP** displays UCST behaviour and the cloud point temperature can be decreased upon irradiation with light because of *trans*

to *cis* isomerization, increasing the overall polarity of the SCNP. Catalysis could be conducted at a temperature just below the cloud point of the non-irradiated **AzoCl$_4$-Au-SCNP**, with substrates that remain soluble both above and below the T_{CP}. Irradiation of the mixture at this temperature could induce catalytic control not only from morphology changes to the SCNP but through phase transitions, as the T_{CP} of the **AzoCl$_4$-Au-SCNP** is decreased below the temperature of catalysis. Catalytic control has been achieved using thermoresponsive SCNPs displaying UCST behaviour,[388] however light-induced control of the UCST resulting in catalytic control would be a very appealing system. Identifying the solvents systems in which *cis* and *trans* **AzoCl$_4$-Au-SCNPs** display sufficiently large differences between UCST would be difficult but if found could represent an additional photo-induced thermoresponsive catalytic process.

The spiropyran:metal based SCNPs would benefit from characterization via spectroscopic techniques such as IR/Raman and allow for the binding strength of the merocyanine: metal complexes to be calculated.[372] Determining relative bond strengths provides useful insights into the stability of the merocyanine: metal complexes and by extension, the SCNPs. Conducting such analyses on a variety of metal species with varying counter ions would assist in identifying possible metals able to be reversibly decomplexed using mild stimuli such as light. Achieving both light induced folding and un-folding of the developed spiropyran polymers is critically dependant on the experimental conditions as much as it is on the employed metal species.[367] Most significant is the effect of solvent on the stability of the merocyanine: metal crosslinks. Polar solvents show a stabilising effect, inhibiting reversion, while apolar solvents destabilise the merocyanine and facilitate the ring closure in the spiropyran.[166] A combination of a polar solvent to form the complexes followed by isolation and uptake in an apolar solvent to decomplex could be used to realise such a light-responsive system. Achieving light reversible complexation and consequently unfolding of the SCNPs with two respective colours of light would be an important milestone in SCNP design.[389] The ideal application of the SCNP system reported in the respective chapter, would be in dynamically controlled catalytic processes. A catalytic functionality could be combined with the reversible folding and unfolding and – once established – afford dynamic control over SCNP driven catalysis. There is a lack of literature utilising spiropyran metal complexes for catalysis, [191,390] a

substantial task would thus be the identification of possible catalytic reactions. Many catalytic reactions require redox active metal centres, such a change in the oxidation state of a spiropyran coordinated metal may have an impact on the complex's overall coordination structure. This may not be detrimental to the overall structure of an SCNP utilising such spiropyran: metal complexes as crosslinks, as spiropyrans are able to form complexes with metal species in varying oxidations states (1^+, 2^+, 3^+).[181,187,391] A possible use of the Co^{2+} based SCNP for catalysis may be as a catalyst for the hydration of alkenes using phenyl silane and molecular oxygen.[392] Conventionally, this reaction utilises the cobalt complex $Co(acac)_2$ which bears a resemblance to the structure of the polymer-spiropyran complex highlighted earlier in figure (Figure 55) where cobalt is coordinated in addition to the spiropyran phenolate to the carbonyls of the pendant ester linkages.

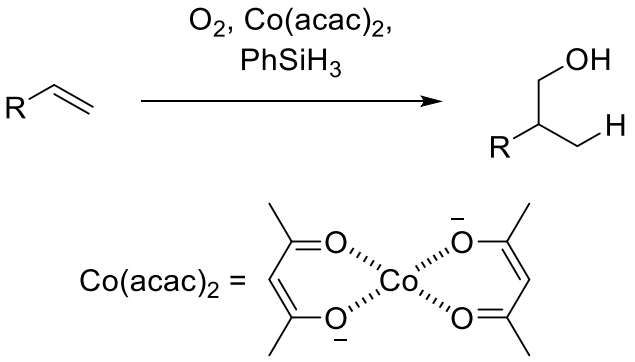

Figure 62. Hydration of alkenes utilising $Co(acac)_2$ as a catalyst, reports of the reaction mechanism are conflicted but typically involve the redox cycling of the Co^{2+} centre into Co^{3+}.[393]

The cobalt centre in this catalytic cycle undergoes oxidation from Co^{2+} to Co^{3+}.[393] Embedded within a spiropyran SCNP crosslink, such a change in the oxidation state and Lewis acid character would likely lead to an increase in the binding strength of the bond between the metal and spiropyran phenolate. Accompanying this may also be an increase in the degree of coordination to the metal arising from additional polymeric ester coordination. Thus, the state of the metal centre would need to be analysed post catalysis via spectroscopic techniques such as FT-IR and XPS as well as the morphology of the SCNP via techniques such as SEC. If a catalytic system using the metal-spiropyran SCNPs reported could be identified and reversible light induced decomplexation and unfolding achieved, catalytic functionality and SCNP formation could be simultaneously achieved upon irradiation and as easily removed (Figure 63).

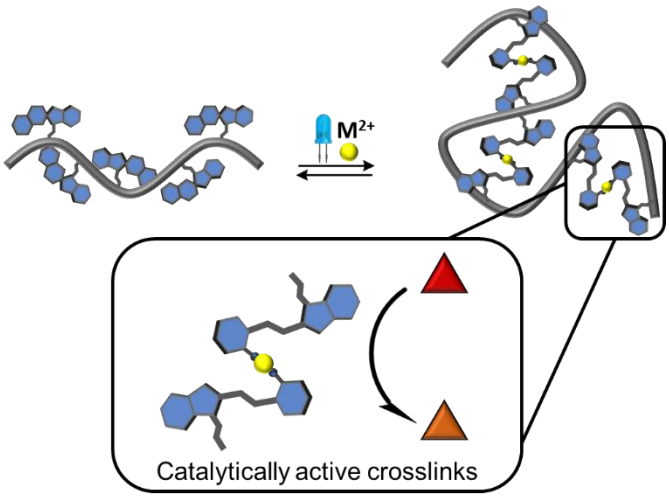

Figure 63. Identification of catalytically active merocyanine: metal complexes (inset) could lead to SCNPs that display simultaneous light-controlled folding and catalysis.

8 Experimental

8.1 Instrumentation

8.1.1 Liquid chromatography–mass spectrometry

Liquid chromatography–mass spectrometry (LC-MS) measurements were performed on an UltiMate 3000 UHPLC System (Dionex, Sunnyvale, CA, USA) consisting of a pump (LPG 3400SZ), autosampler (WPS 3000TSL) and a temperature-controlled column compartment (TCC 3000). Separation was performed on a C18 HPLC column (Phenomenex Luna 5µm, 100 Å, 250 × 2.0 mm) operating at 40 °C. Water (containing 5 mmol L-1 ammonium acetate) and acetonitrile were used as eluents. A gradient of acetonitrile: H_2O 5:95 to 100:0 (v/v) in 7 min at a flow rate of 0.40 mL·min^{-1} was applied. The flow was split in a 9:1 ratio, where 90 % of the eluent was directed through a DAD UV-detector (VWD 3400, Dionex) and 10 % was infused into the electrospray source. Spectra were recorded on an LTQ Orbitrap Elite mass spectrometer (Thermo Fisher Scientific, San Jose, CA, USA) equipped with a HESI II probe. The instrument was calibrated in the *m*/*z* range 74-1822 using premixed calibration solutions (Thermo Scientific). A constant spray voltage of 3.5 kV, a dimensionless sheath gas and a dimensionless auxiliary gas flow rate of 5 and 2 were applied, respectively. The capillary temperature and was set to 300 °C, the S-lens RF level was set to 68, and the aux gas heater temperature was set to 100 °C.

8.1.2 Size-exclusion chromatography (SEC) THF ‘normal mode’

The Size-exclusion chromatography (SEC) measurements were conducted on a PSS SECurity^2 system consisting of a PSS SECurity Degasser, PSS SECurity TCC6000 Column Oven (35 °C), PSS SDV Column Set (8x150 mm 5 µm Precolumn, 8x300 mm 5 µm Analytical Columns, 100000 Å, 1000 Å and 100 Å) and an Agilent 1260 Infinity Isocratic Pump, Agilent 1260 Infinity Standard Autosampler, Agilent 1260 Infinity Diode Array and Multiple Wavelength Detector (A: 254 nm, B: 360 nm), Agilent 1260 Infinity Refractive Index Detector (35 °C). HPLC grade THF, stabilized with BHT, is used as eluent at a flow rate of 1 mL·min^{-1}. Narrow disperse linear poly(styrene) (M_n 266 g·mol^{-1} to 2.52·10^6 g·mol^{-1}) standards (PSS ReadyCal) were used as calibrants.

All samples were passed over 0.22 µm PTFE membrane filters. Molecular weight and dispersity analysis was performed in PSS WinGPC UniChrom software (version 8.2).

8.1.3 Bruker 600 MHz NMR

^{1}H, ^{13}C, ^{19}F and ^{31}P NMR -spectra were recorded on a Bruker System 600 Ascend LH, equipped with a BBO-Probe (5 mm) with z-gradient (^{1}H: 600.13 MHz, ^{13}C 150.90 MHz,^{19}F 564.63 MHz, ^{31}P 242.92 MHz). Resonances are reported in parts per million (ppm) relative to tetramethylsilane (TMS). The δ-scale was calibrated to the respective solvent signal of $CHCl_3$ or DMSO for ^{1}H spectra and for ^{13}C spectra on the middle signal of the $CDCl_3$ triplet, the DMSO quintet or the ACN septet. The annotation of the signals is based on HSQC-, COSY- and DEPT-experiments.

8.1.4 Bruker 500 MHz NMR

^{1}H, ^{13}C, and ^{31}P NMR -spectra were recorded on a Bruker Ultrashield plus 500 spectrometer (^{1}H: 500.28 MHz, ^{13}C 125.81 MHz, ^{31}P 202.51 MHz). Resonances are reported in parts per million (ppm) and calibrated to the 4 respective solvent signal of $CHCl_3$ in ^{1}H spectra and for ^{13}C spectra to the $CDCl_3$ triplet relative to tetramethyl silane (TMS) as $\delta = 0$ ppm. Diffusion Ordered NMR Spectroscopy (DOSY) of the SCNPs and their precursor polymers were recorded on a Bruker Avance 400 with the probe type PA BBO 400S1 BBF-H-D-05 Z. Diffusion coefficients were measured using bipolar gradient pulse pair with longitudinal eddy current delay (ledbpgp2s).

8.1.5 Bruker 400 MHz NMR

^{1}H, ^{13}C, ^{31}P NMR as well as DEPT 135, COSY and HSQC-spectra were recorded on a Bruker Ultrashield 400, equipped with a QNP-Probe (5 mm) with z-gradient (^{1}H: 400 MHz, ^{13}C 100.66 MHz, ^{31}P 161.33 MHz). Resonances are reported in parts per million (ppm) relative to tetramethylsilane (TMS). The δ-scale was calibrated to the respective solvent signal of $CHCl_3$ or DMSO for ^{1}H spectra and for ^{13}C spectra on the middle signal of $CDCl_3$ triplet, the DMSO quintet or ACN septet. The annotation of the signals is based on HSQC-, COSY- and DEPT-experiments.

8.1.6 Diffusion Ordered NMR Spectroscopy DOSY

DOSY experiments based on ^{1}H NMR were performed in $CDCl_3$ at 301 K on a Bruker 400 UltraShield spectrometer equipped with a Quattro Nucleus Probe (QNP) with an operating frequency of 400 MHz (^{1}H). A sequence with longitudinal eddy current delay (LED) using bipolar gradients was employed in order to compensate eddy currents. Bipolar gradient δ and a diffusion delay Δ were determined separately for each sample. Gradient strength was linearly incremented from 2% at 0.96 G to 95% at 45.7 G in 16 steps. The obtained data was processed with TopSpin 4.0.6 and Dynamics Center 2.5.3.

After Fourier transform of the 1D spectra, the signal decay along the gradients G was fitted to

$$f(G) = I_0 * e^{-D*G^2*\gamma^2*\delta^2*\left(\Delta-\frac{\delta}{3}\right)} * 10^4$$

with the gyromagnetic ratio γ and the full signal intensity I0.

Hydrodynamic diameters, d_H, were calculated from the Stokes-Einstein equation:

$$d_H = \frac{k_B * T}{3 * \pi * \eta * D}$$

Where k_B is the Boltzmann constant, T the temperature and η the solvent viscosity ($CDCl_3$: 0.537 mPa·s).[394]

8.1.7 Shimadzu UV-VIS

UV-Vis spectra were recorded on a Shimadzu UV-2700 spectrophotometer equipped with a CPS-100 electronic temperature control cell positioner. Samples were prepared in solvent THF with a concentration of 0.5 mg mL^{-1} and measured in Z cuvettes at 25 °C.

Cuvettes:

- BrandTech disposable UV cuvettes

- Hellma Analytics quartz high precision cell

8.1.8 LED Characterisation

LED emission spectra were recorded using an Ocean Insight Flame-T-UV-Vis spectrometer, with an active range of 200-850 nm and an integration time of 10 ms. LED output energies were recorded using a Thorlabs S401C thermopile sensor, with an active area of 100 mm^2 and a wavelength range of 190 nm – 20 µm, connected to a Thorlabs PM400 energy meter console. The emitted power from each LED was measured for 60 s at a fixed distance from the sensor, after which the mean and standard deviation of the emission could be determined. LEDs were cooled during measurement to minimise any thermal effects on the emission power or sensor performance.

8.2 Synthetic Procedures.

8.2.1 Sequence Defined Main Chain Amine

8.2.1.1 Boc Protected Phenylenediamine

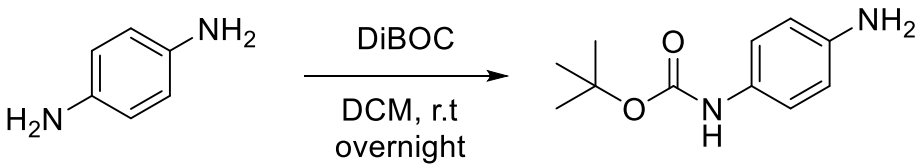

p-Phenylenediamine (2.63 g, 24.36 mmol, 3 eqv) was dissolved in degassed anhydrous DCM (250 ml) and cooled to 0 °C using an ice salt bath. Separately DiBoc (2 g, 8.12 mmol, 1 eqv) was dissolved in DCM (5 mL) and then added dropwise to the first solution at 0 °C with rapid stirring. After the addition was completed, the ice bath was removed and the reaction mixture was allowed to heat to room temperature and left to stir overnight. The reaction was monitored for completion by TLC, following which the solvent was removed and the product was purified using column chromatography (6:4, EtOAc:CH). Yield = 1.385 g (82 %)

^{1}H NMR (600 MHz, $CDCl_3$) δ 7.06 (d, *J* = 7.7 Hz, 2H), 6.58 – 6.54 (m, 2H), 6.19 (s, 1H), 3.46 (s, 2H), 1.43 (s, 9H). see appendix section 10.1.1.1

HRMS (ESI): m/z calculated for $[C_{11}H_{16}N_2O_2+H]^+$ 209.1285; found 209.1289, Δppm =1.9127.

8.2.1.2 Boc Protected Nitrosobenzene

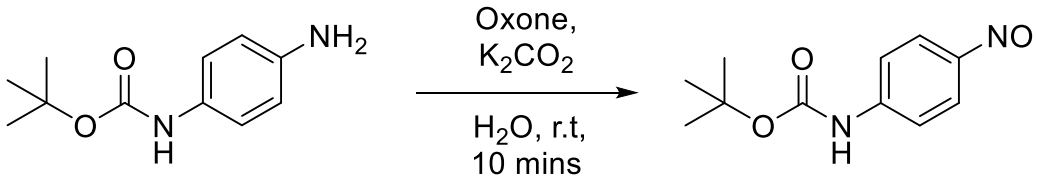

The Boc protected diamine (1 g, 4.80 mmol, 1 eqv) was dissolved in water (53 mL) and THF (5 mL), separately Oxone (4.426 g, 14.4 mmol, 3 eqv) was also dissolved in water (86 mL) and subsequently neutralised to a pH of approximately 6 using potassium carbonate. To the first solution the Oxone solution was added quickly with rapid stirring. A lime green precipitate formed, and after 10 minutes the precipitate

was filtered off and dried under vacuum at 40 °C, yielding a lime green solid. Yield = 0.461 g (43 %).

^{1}H NMR (600 MHz, $CDCl_3$ δ 7.88 (d, *J* = 8.3 Hz, 2H), 7.62 – 7.54 (m, 2H), 6.86 (s, 1H), 1.55 (s, 9H). see appendix section 10.1.1.2.

HRMS (ESI): m/z calculated for $[C_{11}H_{14}N_2O_3+H]^+$ 223.1077; found 223.1078, Δppm = 0.4482.

8.2.1.3 Boc Protected Imine Azobenzene

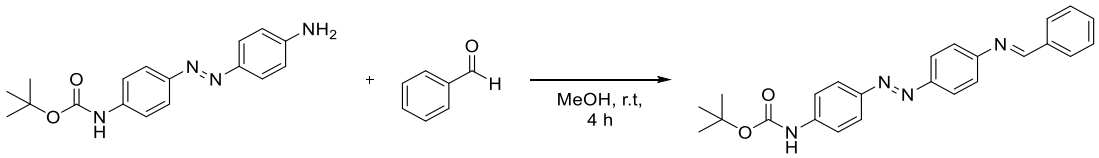

The amino azobenzene (0.016mmol, 1 eqv) was dissolved in MeOH (2 mL), to this benzaldehyde (0.016 mmol, 1 eqv) was added and the reaction was stirred for 4 hours at room temperature. The product was concentrated under reduced pressure affording an orange solid. Crude Yield = 0.006 g (95 %).

^{1}H NMR (600 MHz, DMSO-d_6) δ 9.79 (s, 1H), 8.72 (s, 1H), 8.00 – 7.96 (m, 2H), 7.94 – 7.89 (m, 2H), 7.87 – 7.82 (m, 2H), 7.70 – 7.66 (m, 2H), 7.58 – 7.53 (m, 3H), 7.47 – 7.43 (m, 2H), 1.50 (s, 9H). see appendix section 10.1.1.4.

HRMS (ESI): m/z calculated for $[C_{24}H_{24}N_4O+H]^+$ 401.1972; found 401.1971, Δppm = 0.2492.

8.2.1.4 Boc Protected Amino Azobenzene

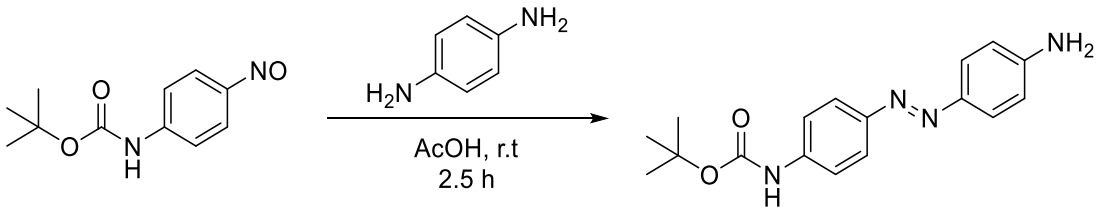

p-Amino aniline (0.729 g, 6.75 mmol, 3 eqv) was dissolved completely in glacial acetic acid (10 mL). To this solution the Boc protected nitroso (0.5 g, 2.25 mmol, 1 eqv), dissolved in THF (3 mL) was added dropwise with rapid stirring over a 1 hour period at room temperature. The reaction was monitored by TLC and after 1.5 hours

the reaction mixture was then poured onto ice and neutralised with sodium hydroxide to a basic pH. The product was then extracted using DCM (3*10 mL), the combined organic layers were dried over magnesium sulphate and concentrated under reduced pressure. The crude product was purified using column chromatography to afford the product as an orange solid (4:6, EtOAc:CH). Yield = 0.231 g (33 %).

^{1}H NMR (600 MHz, DMSO-d_6) δ 9.62 (s, 1H), 7.70 – 7.65 (m, 2H), 7.63 – 7.57 (m, 4H), 6.67 – 6.63 (m, 2H), 5.97 (s, 2H), 1.49 (s, 9H). see appendix section 10.1.1.3.

HRMS (ESI): m/z calculated for $[C_{17}H_{20}N_4O_2+H]+$ 313.1659; found 313.1660, Δppm = 0.3193.

8.2.1.5 Fmoc Protected Diamine

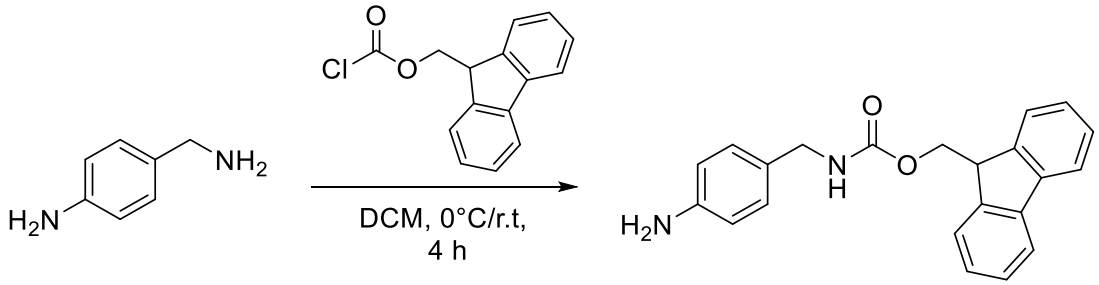

The benzylamine (0.8 g, 6.55 mmol, 1 eqv) was dissolved in DCM (100 mL), and once dissolved, Fmoc-chloride (2.03 g, 7.86 mmol, 1.2 eqv) was added. Triethylamine (0.43g, 4.25mmol, 1.1 eqv) was added dropwise to this solution with stirring. The reaction was then allowed to stir for 4 hours at room temperature resulting in a yellow solution. Once completed, the product was purified using column chromatography, resulting in the impure product as a light brown solid (4:6, EtOAc:CH). Yield = 0.56 g (25 %).

The ^{1}H NMR spectrum was compared to literature and characteristic resonances were observed.[395] ^{1}H NMR (600 MHz, DMSO-d_6) δ 7.89 (d, J = 7.5 Hz, 2H), 7.70 (d, J = 7.5 Hz, 2H), 7.42 (t, J = 7.6 Hz, 2H), 7.34 – 7.31 (m, 2H), 6.90 (d, J = 8.0 Hz, 2H), 6.53 – 6.48 (m, 2H), 4.94 (s, 2H), 4.31 (d, J = 7.0 Hz, 2H), 4.22 (t, J = 7.1 Hz, 1H), 4.01 (d, J = 6.1 Hz, 2H). see appendix section 10.1.1.5.

HRMS (ESI): m/z calculated for $[C_{22}H_{20}N_2O_2+H]^+$ 345.1598; found 345.1598, Δppm = 0.

8.2.1.6 Fmoc/Boc Protected Azobenzene

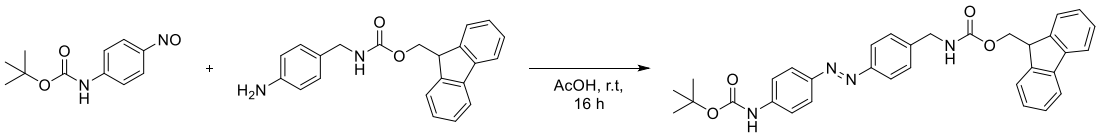

The nitroso (0.248 g, 1.1 mmol, 1 eqv) and amine (0.381 g, 1.1 mmol, 1 eqv) were dissolved separately in 6 ml and 8 ml of acetic acid respectively at room temperature and the nitroso compound was added dropwise to the amine solution. THF (2 mL) was added to the final volume of the reaction mixture. The reaction was allowed to stir at room temperature for 16 hours. The reaction mixture was diluted with water (25 mL), resulting in a precipitate. EtOAc was added to extract the product (3*10 mL) and the combined organic layers were washed with brine and dried over magnesium sulphate. The product was then concentrated under reduced pressure and purified using column chromatography (3:7, EtOAc:CH). Yield = 0.115 g (19 %).

^{1}H NMR (600 MHz, $CDCl_3$) δ 7.83 (d, *J* = 8.8 Hz, 2H), 7.80 – 7.76 (m, 2H), 7.70 (d, *J* = 7.6 Hz, 2H), 7.54 (d, *J* = 7.5 Hz, 2H), 7.45 (d, *J* = 8.6 Hz, 2H), 7.36 – 7.29 (m, 3H), 7.25 (t, *J* = 7.4 Hz, 2H), 6.61 (s, 1H), 5.05 (s, 1H), 4.43 (d, *J* = 6.7 Hz, 2H), 4.38 (d, *J* = 6.1 Hz, 2H), 4.17 (t, *J* = 6.8 Hz, 1H). see appendix section 10.1.1.6.

HRMS (ESI): m/z calculated for $[C_{33}H_{32}N_4O_4+H]^+$ 549.2496; found 549.2486, Δppm = -1.82.

8.2.1.7 Deprotection - Fmoc Azobenzene

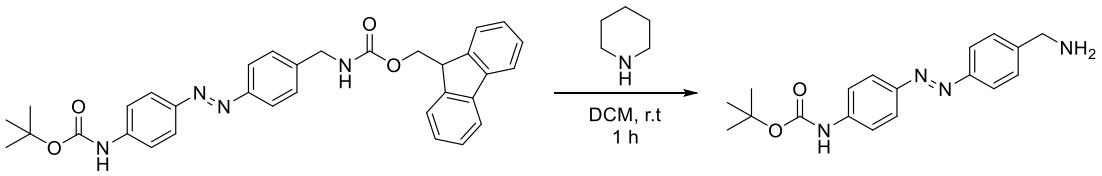

The Fmoc/Boc protected azobenzene (0.030 g, 0.054 mmol, 1 eqv) was dissolved in DCM (4.5 mL). To this solution was added piperidine (1.88 mL) dropwise over the course of 5 mins. The combined reaction mixture was then stirred for a further 40 minutes. The solvent was removed under reduced pressure, affording an orange solid that was then dried under vacuum overnight. ^{1}H NMR spectroscopy was not conducted.

Crude Yield = 0.020 g

8.2.2 Sequence Defined Main Chain Acid

8.2.2.1 Nitroso Acetanilide

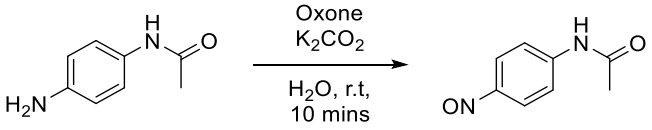

Oxone (60 mmol, 3 eqv) was dissolved in water (36 mL) and to this solution potassium carbonate was added slowly, neutralising the solution to a pH of approximately 6. Simultaneously p-amino acetanilide (3.00 g, 20 mmol, 1 eqv) was dissolved in water (60 mL). To this solution the Oxone solution was added quickly and with rapid stirring. The reaction mixture turned dull green and a green precipitate formed. After 10 minutes the precipitate was filtered off washed with water and dried under vacuum at 40 °C, affording the product as a dull green solid which was used immediately for the next step. Yield = 1.779 g (73 %).

The ^{1}H NMR spectrum was compared to literature and characteristic resonances were observed.[396] ^{1}H NMR spectroscopy indicated a nitro impurity was present. ^{1}H NMR (600 MHz, DMSO-d_6) δ 10.62 (s, 1H), 10.54 (s, 1H), 8.20, 7.90 (q, J = 8.4 Hz, 4H), 2.14 (s, 3H). see appendix section 10.1.2.1.

8.2.2.2 Acetanilide Azobenzene

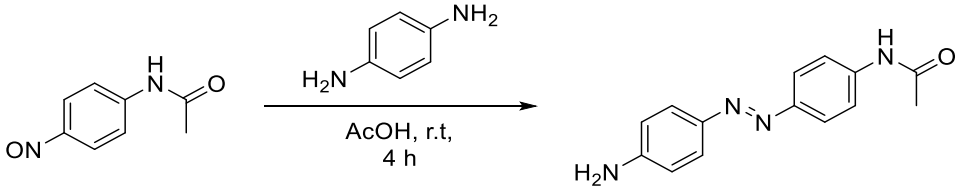

p-Aminoaniline (3.93 g, 36.33 mmol, 4 eqv) was dissolved completely in glacial acetic acid (20 mL). With rapid stirring, the nitroso species (1.50 g, 9.08 mmol, 1 eqv) dissolved in THF: acetic acid (1:1, 20 mL) was added dropwise over approximately 1 hour, the reaction was monitored by TLC and was stopped after 3 hours. The reaction mixture was poured onto ice and then neutralised to a basic pH of approximately 9 with sodium hydroxide. The product was then extracted using DCM (3*20 mL), dried over magnesium sulphate and concentrated under reduced pressure. The crude product

was then purified using column chromatography, affording the product as a yellow solid (3.7, EtOAc:CH). Yield = 0.8547g (37 %).

The ^{1}H NMR spectrum matched literature.[397] ^{1}H NMR (600 MHz, DMSO-d_6) δ 10.16 (s, 1H), 7.74 – 7.69 (m, 4H), 7.64 – 7.60 (m, 2H), 6.68 – 6.64 (m, 2H), 6.00 (s, 2H), 2.08 (d, J = 1.0 Hz, 3H). see appendix section 10.1.2.2.

HRMS (ESI): m/z calculated for $[C_{14}H_{14}N_4O+H]^+$ 255.1240; found 255.1243, Δppm = 1.1758.

8.2.2.3 Diamino Azobenzene

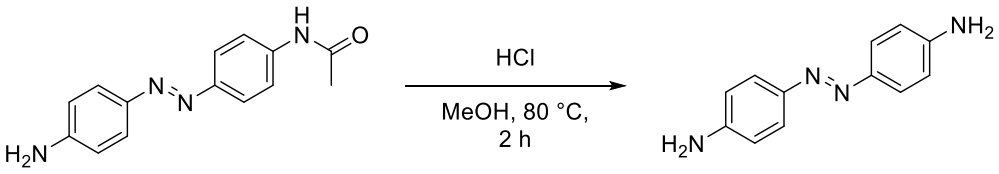

The acetylated azobenzene (1.09 mmol) was added to MeOH (12 mL) and allowed to dissolve. To this solution, HCl (3M, 6 ml) was added and the solution was heated to 80 °C and allowed to stir for 2 hours. Once completed the reaction mixture was diluted with water, poured onto ice and neutralised with sodium hydroxide to a basic pH. The product was then extracted with DCM (3*10 mL) washed with brine, dried over magnesium sulphate and concentrated under reduced pressure to afford the product as an orange solid. Yield = 170. 94 g (74 %).

The ^{1}H NMR spectrum matched literature.[398] ^{1}H NMR (600 MHz, DMSO-d_6) δ 7.55 – 7.50 (m, 4H), 6.65 – 6.61 (m, 4H), 5.73 (s, 4H). see appendix section 10.1.2.3.

HRMS (ESI): m/z calculated for $[C_{12}H_{12}N_4+H]^+$ 213.1135; found 213.1138, Δppm = 1.4077.

8.2.2.4 Amino/Carboxy Azobenzene

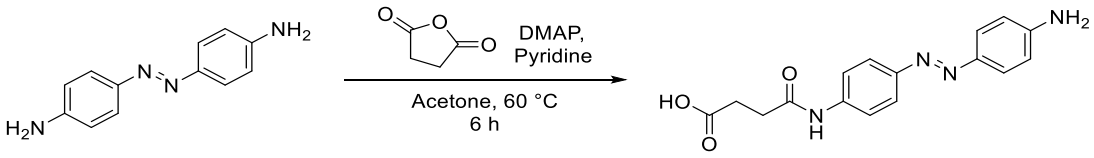

Diamino azobenzene (0.133 g, 0.62 mmol, 3 eqv), DMAP (0.00256 g, 0.0209 mmol, 0.1 eqv), and pyridine (0.016 g, 0.418 mmol, 2 eqv) were dissolved in acetone (25 mL) under an inert atmosphere. Succinic anhydride (0.021 g, 0.209mmol, 1 eqv) was dissolved separately in acetone (5 mL) and was added dropwise to the first solution. The combined solution was then heated to 60 °C and allowed to stir for 6 hours. The reaction mixture was then allowed to cool to room temperature. The product was concentrated under reduced pressure and dried on a Schlenk line overnight. The product was purified using column chromatography, yielding the product as an orange solid (1:9, MeOH:DCM). Yield = 0.013 g (20 %).

^{1}H NMR (600 MHz, DMSO-d_6) δ 10.21 (s, 1H), 7.75 – 7.68 (m, 4H), 7.64 – 7.60 (m, 2H), 6.68 – 6.63 (m, 2H), 2.62 – 2.52 (m, 4H). See appendix section 10.1.2.4.

HRMS (ESI): m/z calculated for $[C_{16}H_{16}N_4O_3+H]^+$ 313.1295; found 313.1288, Δppm = -2.2354.

8.2.3 Sequence Defined Main Chain Aldehyde

8.2.3.1 Acetal protected Benzaldehyde

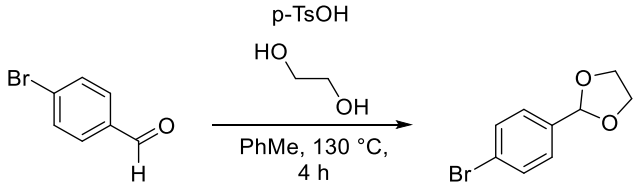

Benzaldehyde (5.26 g, 28.43 mmol, 1 eqv) was dissolved in toluene (50 mL), to which ethylene glycol (3.88 g, 62.54 mmol, 2.2 eqv) and p-tolueneulfonic acid monohydrate (1.22 mmol, 0.043 eqv) were added. A dean stark apparatus and condenser were attached to the flask, and the reaction mixture was refluxed at 130 °C under argon for 4 hours. The reaction was then allowed to cool to room temperature, to which MeOH (100 mL) was then added. The product was then concentrated under reduced pressure and washed with a saturated solution of sodium bisulfite (20 ml). The product was then extracted with DCM (3*10 mL), dried over magnesium sulphate, concentrated under

reduced pressure, and dried overnight on a Schlenk line to afford the product. Yield = 5.4 g (83 %).

The ^{1}H NMR spectrum matched literature.[399] ^{1}H NMR (600 MHz, $CDCl_3$) δ 7.46 – 7.42 (m, 2H), 7.30 – 7.27 (m, 2H), 5.70 (s, 1H), 4.06 – 3.94 (m, 4H). See appendix section 10.1.3.1.

HRMS (ESI): m/z calculated for $[C_9H_9BrO_2+H]^+$ 228.9859; found 228.9853, Δppm = -2.6202.

8.2.3.2 Acetal Protected Phosphine

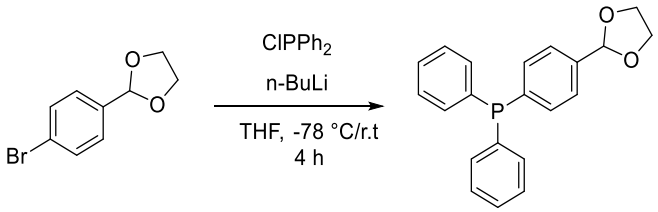

To oven-dried glassware under argon, the protected aldehyde (5.43 g, 23.70 mmol, 1 eqv) was added, followed by the addition of dry and degassed THF (50 mL). The solution was then cooled to approximately -78 °C using an EtOAc /liquid nitrogen bath. n-Buli (10.5 mL, 2.5M) was then added dropwise to the solution resulting in a yellow colour change and the reaction was allowed to stir for 1 hour at -78 C. Chlorodiphenylphosphine (5.49 g, 24.88 mmol, 1.05 eqv) was then added at -78 °C slowly and allowed to heat slowly to room temperature. After 3 hours of stirring the reaction was quenched with saturated ammonium chloride (10 mL). The organic layer was then collected and washed with water (2*10 ml) and brine (10 ml). The crude product was then concentrated under reduced pressure, affording an oil. MeOH (30 mL) was added, and the crude product was placed overnight in the freezer, resulting in a precipitate. This was consequently filtered off and washed with ice cold MeOH, affording product as a cream coloured solid. Yield = 3.41 g (43 %).

The ^{1}H NMR spectrum matched literature.[399] ^{1}H NMR (600 MHz, $CDCl_3$) δ 7.49 – 7.46 (m, 2H), 7.35 (dddd, *J* = 15.4, 7.9, 4.2, 2.1 Hz, 12H), 5.83 (s, 1H), 4.17 – 4.04 (m, 4H). See appendix section 10.1.3.2.

^{31}P NMR (243 MHz, CDCl3) δ -5.64 (p, *J* = 7.3 Hz).

HRMS (ESI): m/z calculated for $[C_{21}H_{19}O_2P+H]^+$ 335.12217 ; found 335.1195, Δppm = 6.5648.

8.2.3.3 Phosphine Aldehyde

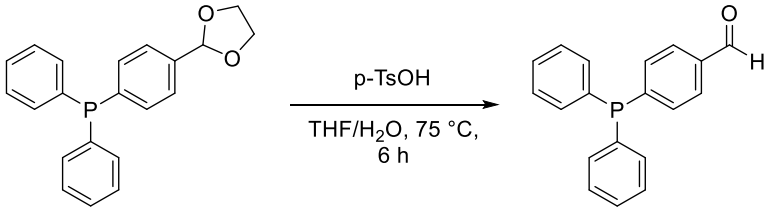

The phosphine (3 g 8.97 mmol, 1 eqv) was dissolved in water (9 mL) and degassed THF (28 mL), p-toluenesulfonic acid (0.046 g, 0.269 mmol, 0.03 eqv) was added and the combined reaction mixture refluxed under inert conditions. The reaction was stopped after 6 hours. The crude product was concentrated under reduced pressure resulting in a yellow oil. MeOH (20 mL) was added, and the crude product was left overnight in the freezer, resulting in a precipitate that was filtered off and washed with ice cold MeOH. This afforded the product as a light-yellow solid. Yield = 1.534 g (59 %).

The ^{1}H NMR spectrum matched literature.[399] ^{1}H NMR (600 MHz, $CDCl_3$) δ 10.03 (s, 1H), 7.84 – 7.82 (m, 2H), 7.46 – 7.34 (m, 12H). See appendix section 8.2.3.3.

^{31}P NMR (243 MHz, CDCl3) δ -4.32 (p, *J* = 7.1 Hz).

HRMS (ESI): m/z calculated for $[C_{19}H_{15}OP+H]^+$ 291.0933; found 291.0956, Δppm = 7.9012.

8.2.3.4 Ugi Reaction

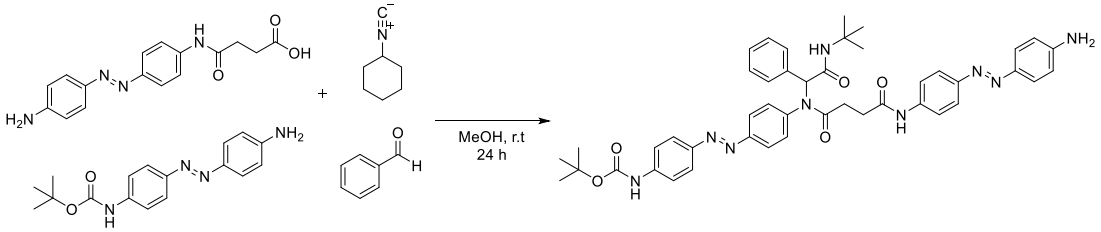

The Boc-protected amino azobenzene (0.005 g, 0.016 mmol, 1 eqv) and benzaldehyde (0.0017 g, 0.016 mmol, 1 eqv) were dissolved in MeOH (5 mL) and allowed to stir for 1 hour at room temperature. The acid azobenzene (0.005 g, 0.0016 mmol, 1 eqv) was

then added and allowed to stir for 10 minutes, followed by the addition of the isocyanide (0.0013 g, 0.0016 mmol, 1 eqv). The reaction was then allowed to stir for 24 hours at room temperature. An orange precipitate formed, which was collected and taken for analysis. The filtrate was then concentrated under reduced pressure and analysed.

8.2.4 Polydisperse Main Chain Acid

8.2.4.1 Di-butanoic Acid Azobenzene

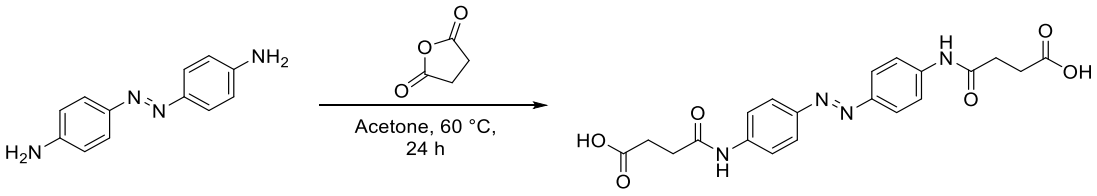

Diamino azobenzene (0.25 g, 1.18 mmol, 3 eqv), DMAP (0.028 g, 0.236 mmol, 0.2 eqv), and pyridine (0.018 g, 2.36 mmol, 2 eqv) were dissolved in acetone (50 mL). Once completely dissolved succinic anhydride (0.353 g, 3.53 mmol, 3 eqv) was added, the reaction was heated to 60 °C and allowed to stir for 24 hours. An orange precipitate formed. The precipitate was collected and washed with ice-cold acetone. The orange solid was recrystallised from EtOH/H_2O 1:1 to afford the product as fine orange crystals.

Yield = 0.072 g (15 %)

^{1}H NMR (600 MHz, DMSO-d_6) δ 10.31 (s, 2H), 7.85 – 7.77 (m, 8H), 2.61 (t, J = 6.6 Hz, 4H), 2.54 (t, J = 6.6 Hz, 4H). See appendix section 10.1.4.1.

HRMS (ESI): m/z calculated for $[C_{20}H_{20}N_4O_6+H]^+$ 413.1456; found 413.1445, Δppm = -2.6625.

8.2.5 Polydisperse Main Chain Amine

8.2.5.1 Undecenoyl chloride

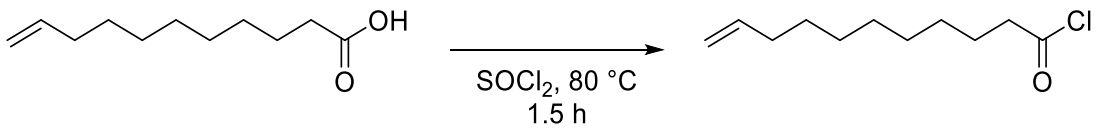

The carboxylic acid (4.00 g, 21.17 mmol, 1 eqv) was added to a flask and dissolved in thionyl chloride (19.62 g, 11.97 mL, 164.97 mmol, 7.6 eqv) under an inert atmosphere.

The reaction was then heated to reflux and allowed to stir for 1.5 hours. The reaction was then allowed to cool to 40 °C, with excess thionyl chloride then being distilled off under vacuum. Residual thionyl chloride was removed by dissolving the product in EtOAc and concentrating it under reduced pressure. The product was then stored at 5 °C under argon and used the next day. Yield = Quantitative.

The ^{1}H NMR spectrum matched literature.[304] ^{1}H NMR (600 MHz, $CDCl_3$) δ 5.81 (ddt, *J* = 16.9, 10.2, 6.7 Hz, 1H), 4.99 (dq, *J* = 17.1, 1.7 Hz, 1H), 4.93 (dq, *J* = 10.2, 1.4 Hz, 1H), 2.88 (t, *J* = 7.3 Hz, 2H), 2.04 (tdd, *J* = 8.1, 6.0, 1.5 Hz, 2H), 1.71 (q, *J* = 7.3 Hz, 2H), 1.42 – 1.24 (m, 12H). See appendix section 10.1.5.1.

8.2.5.2 Undecene amide

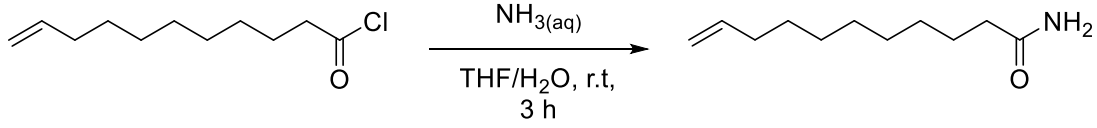

The acid chloride (9.87 mmol, 1 eqv) was added to dry THF (40 mL) and cooled to 0 °C, to which 30% ammonia$_{(aq)}$ solution (40 mL) was added dropwise. Once the addition was completed, the ice bath was removed, and the reaction was allowed to heat to room temperature and stirred for 3 hours. The reaction was then diluted with water and extracted with EtOAc (2*30 ml). The combined organic layers were washed with brine (10 mL), dried over sodium sulphate and concentrated under reduced pressure. The product was then recrystallised from EtOH and water, affording the product as a light yellow powder. Yield = 1.67 g (84 %).

The ^{1}H NMR spectrum matched literature.[304] ^{1}H NMR (600 MHz, $CDCl_3$) δ 5.80 (ddt, *J* = 16.9, 10.2, 6.7 Hz, 1H), 4.98 (dq, *J* = 17.1, 1.8 Hz, 1H), 4.94 – 4.89 (m, 1H), 2.23 – 2.18 (m, 2H), 2.05 – 1.99 (m, 2H), 1.62 (p, *J* = 7.5 Hz, 2H), 1.39 – 1.24 (m, 10H). See appendix section 10.1.5.2.

HRMS (ESI): m/z calculated for $[C_{11}H_{21}NO+H]^{+}$ 184.1696; found 1844.1694, Δppm = -1.0859.

8.2.5.3 Undecene Amine

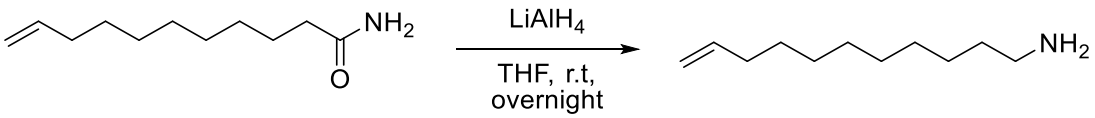

Lithium aluminium hydride (0.9 g, 23.73 mmol, 2.9 eqv) was suspended in dry THF (15 mL) under inert conditions and cooled to 0 °C. The carboxamide (1.50 g, 8.18 mmol, 1 eqv) was dissolved separately in dry THF (20 mL) under an inert atmosphere and added dropwise to the first solution via cannula. Once the addition was completed, the combined reaction mixture was allowed to heat to room temperature and stirred overnight. The reaction was then cooled back to 0 °C and quenched with a slow dropwise addition of water until gas evolution stopped. Following this NaOH (1 M, 30 mL) was added slowly. The reaction mixture was then filtered, and the filtrate concentrated under reduced pressure and dissolved in Et_2O (20 mL). The organic layer was then washed with brine (10 mL) and dried over sodium sulphate and concentrated under reduced pressure, affording the product as a yellow oil. Yield = 0.389 g (28 %).

The ^{1}H NMR spectrum matched literature.[304] ^{1}H NMR (600 MHz, $CDCl_3$) δ 5.83 (ddt, *J* = 16.9, 10.2, 6.7 Hz, 1H), 5.01 (dq, *J* = 17.1, 1.7 Hz, 1H), 4.95 (ddt, *J* = 10.2, 2.4, 1.3 Hz, 1H), 2.74 – 2.67 (m, 2H), 2.06 (tdd, *J* = 8.1, 6.0, 1.5 Hz, 2H), 1.69 – 1.61 (m, 2H), 1.42 (dq, *J* = 40.1, 7.1 Hz, 4H), 1.31 (q, *J* = 4.6, 3.4 Hz, 10H). See appendix section 10.1.5.3.

HRMS (ESI): m/z calculated for $[C_{11}H_{23}N+H]^+$ 170.1903; found 170.1901, Δppm = -1.1751.

8.2.5.4 Ugi Reaction

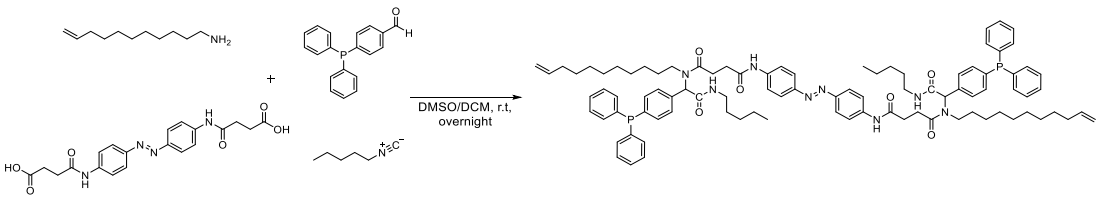

The amine-alkene (0.01g, 0.068 mmol, 1eqv) and phosphine-aldehyde (0.017 g, 0.068 mmol, 1 eqv) components were dissolved in a 1:1 mixture of degassed DCM:DMSO (5 mL) and allowed to stir for 1 hour at room temperature. The acid component (0.025 g, 0.068 mmol, 1eqv) was then added, and the combined mixture was allowed to stir

for 10 mins before the isocyanide (0.006 g, 0.068 mmol, 1 eqv) was added. The reaction was left to stir at room temperature overnight. A small aliquot of the reaction mixture was then taken, dried under vacuum and light heating, affording a light-yellow oil used for subsequent analysis. For ^{1}H NMR spectra, see appendix section 10.1.5.4.

8.2.6 Catalytic SCNP via Azobenzene Crosslinks: Monomers

8.2.6.1 Vinyl Benzyl Acetate

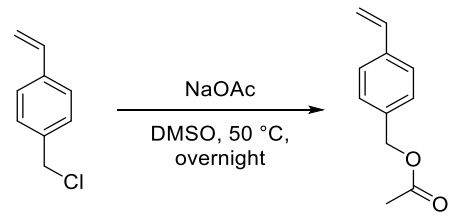

4-Vinylbenzyl chloride (15 g, 98.28 mmol, 1 eqv) and sodium acetate (12.09 g, 147.42 mmol, 1.5 eqv) were dissolved in DMSO (60 mL) under an argon atmosphere, heated to 50 °C and allowed to stir for 24 h. The reaction mixture was then allowed to cool to ambient temperature and subsequently transferred to a separating funnel, to which water (70 mL) was added. The product was extracted with EtOAc (3*100 mL), dried over sodium sulphate and concentrated under reduced pressure to afford the crude product as a light-yellow oil. This was taken to the next step without purification. Yield: 13.523 g crude (78 %).

The ^{1}H NMR spectrum matched literature.[341] ^{1}H NMR (600 MHz, $CDCl_3$) δ 7.43 – 7.38 (m, 2H), 7.34 – 7.28 (m, 2H), 6.71 (dd, *J* = 17.6, 10.9 Hz, 1H), 5.76 (dd, *J* = 17.6, 0.9 Hz, 1H), 5.26 (dd, *J* = 10.9, 0.8 Hz, 1H), 5.09 (s, 1H), 2.10 (s, 3H). See appendix section 8.2.6.1.

8.2.6.2 Vinyl Benzyl Alcohol

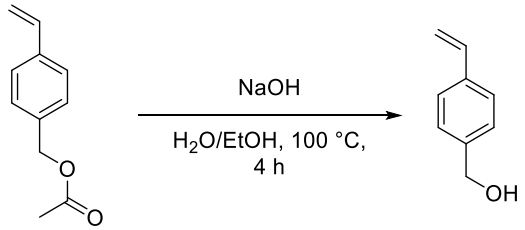

4-vinylbenzyl acetate (13 g, 85.101 mmol, 1 eqv) was dissolved in EtOH (50 mL), to which was added NaOH (5.104 g, 167.08 mmol, 1.96 eqv) in water (50 mL). The reaction mixture was heated at reflux for 4 hours. The mixture was subsequently allowed to cool to ambient temperature. The crude product was extracted using EtOAc

(3*20 mL) and the combined organic layers were washed with water (70 mL) and brine (70 mL) and subsequently dried over $MgSO_4$. The organic layer was the concentrated under reduced pressure, affording a dark brown liquid. The product was then purified using column chromatography (8:2, CH: EtOAc), affording the product as a light red oil. Yield: 9.778 g (85 %).

The ^{1}H NMR spectrum matched literature.[400] ^{1}H NMR (600 MHz, $CDCl_3$) δ 7.43 – 7.39 (m, 2H), 7.35 – 7.30 (m, 2H), 6.72 (dd, *J* = 17.6, 10.9 Hz, 1H), 5.75 (dd, *J* = 17.6, 0.9 Hz, 1H), 5.25 (dd, *J* = 10.9, 0.9 Hz, 1H), 4.68 (s, 2H). See appendix section 8.2.6.2.

8.2.6.3 Nitroxide Initiator

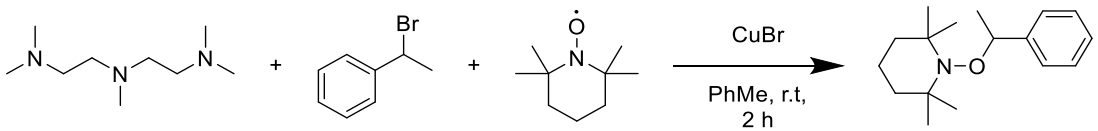

Copper (I) bromide (0.837 g, 5.84 mmol, 1 eqv), PMEDTA (1.01 g, 5.84 mmol, 1 eqv) and dry toluene (15 mL) were added to a dried Schlenk flask placed under argon and allowed to stir at ambient temperature for 10 min. In a separate dried Schlenk tube, TEMPO (0.835 g, 5.35 mmol) bromoethyl-benzene (0.9 g, 4.86 mmol) and dry toluene (15 mL) were added and stirred for 15 min. The contents of the second flask were added to the first via slow cannula addition, followed by stirring at 50 °C for 1 hour. Solid material was filtered off and the subsequent filtrate was concentrated under reduced pressure. The product was purified via column chromatography (9:1, CH: EtOAc) affording a clear oil which was scratched with a spatula to result in the final product of white crystals. Yield: 1.01 g (79 %).

The ^{1}H NMR spectrum matched literature.[401] ^{1}H NMR (600 MHz, $CDCl_3$) δ 7.29 – 7.22 (m, 4H), 7.21 – 7.14 (m, 1H), 4.72 (q, *J* = 6.7 Hz, 1H), 1.49 (s, 1H), 1.43 (d, *J* = 6.7 Hz, 4H), 1.32 (s, 2H), 1.24 (s, 4H), 1.11 (s, 3H), 0.97 (s, 3H), 0.61 (s, 3H). See appendix section 10.1.6.3.

8.2.6.4 Gold Catalyst Pre-complex

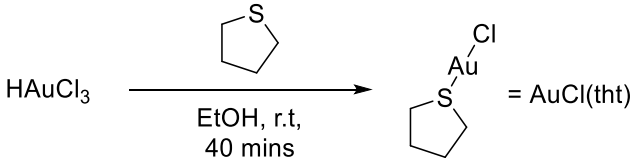

Gold tetrachloroaurate (0.3 g, 0.716 mmol, 1eqv) was dissolved in EtOH (3 mL), with vigourous stirring, tetrahydrothiophene (0.141 g, 1.6 mmol, 2.1 eqv) was added dropwise. A white precipitate formed, and the reaction was allowed to stir for 40 minutes. The white precipitate was then collected, washed with EtOH, and dried under vacuum, affording a fine white powder. Yield = 0.24 g (83 %).

8.2.6.5 Phosphine Gold Catalyst

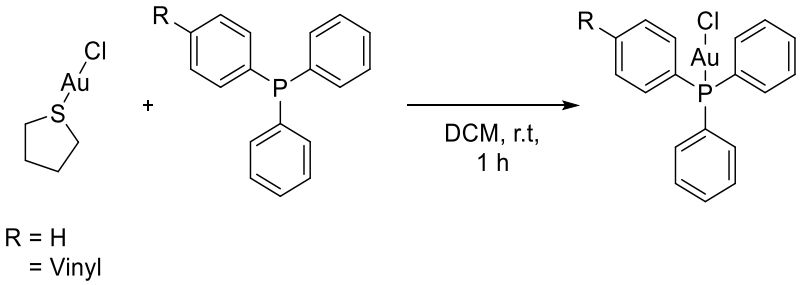

The relevant phosphine (0.489 mmol, 1 eqv) and AuCl(tht) (0.134 g, 0.514 mmol, 1.05 eqv) were dissolved separately in DCM (1.5 mL). AuCl(tht) was added dropwise to the phosphine solution with stirring. After complete addition, the combined reaction mixture was stirred for one hour. The crude reaction mixture was then concentrated under reduced pressure and recrystallised using a two solvent system of DCM and EtOH, affording fine white crystals. For all spectra, see appendix section 10.1.6.4 and 10.1.6.5.

R = H; Yield = 0.152 g (63%).

^{1}H NMR (600 MHz, $CDCl_3$) δ 7.56 – 7.50 (m, 9H), 7.49 – 7.45 (m, 6H).

^{31}P NMR (243 MHz, $CDCl_3$) δ 33.18.

R = Vinyl; Yield = 0.192 g (71 %).

^{31}P NMR (243 MHz, $CDCl_3$) δ 32.54.

8.2.7 Catalytic SCNP via Azobenzene Crosslinks: Hydroamination Substrates

8.2.7.1 Substituted Intramolecular Substrate Nitrile

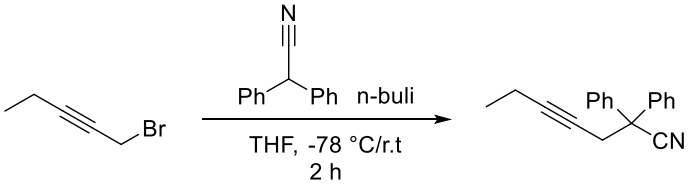

Diisopropylamine (0.688 g, 6.80 mmol, 1 eqv) was dissolved in anhydrous THF (7 mL) and cooled to -78 °C under argon. To this solution, 2M *n*-BuLi in hexane (3.4 mL, 6.80 mmol, 1 eqv) was added dropwise under stirring. The combined solution was subsequently allowed to stir at -78 °C for 30 min. Diphenyl acetonitrile (1.31 g, 6.80 mmol, 1 eqv) dissolved in anhydrous THF (6 mL) was then added dropwise to the solution and was allowed to stir for a further 1.5 hours at -78 °C, resulting in a yellow solution. 1-Bromo-2-pentyne (1 g, 6.80 mmol, 1 eqv) was added dropwise to the solution which was allowed to stir for 10 min at -78 °C. The combined reaction was subsequently allowed to slowly warm to ambient temperature and stir for 16 hours. DCM (30 mL) was added to the reaction, transferred to a separating funnel and washed with HCl (1M, 2*30 mL) and brine (30 mL). The organic layer was dried over sodium sulphate and concentrated under reduced pressure, affording the product as a viscous yellow oil that was used without further purification. Yield = 1.44 g (82 %)

The ^{1}H NMR spectrum matched literature.[246] ^{1}H NMR (600 MHz, $CDCl_3$) δ 7.42 – 7.29 (m, 10H), 3.20 (td, *J* = 2.4, 0.7 Hz, 2H), 2.13 – 2.06 (m, 2H), 1.03 (td, *J* = 7.5, 0.7 Hz, 3H). See appendix section 10.1.7.1.

8.2.7.2 Substituted Intramolecular Substrate Amine

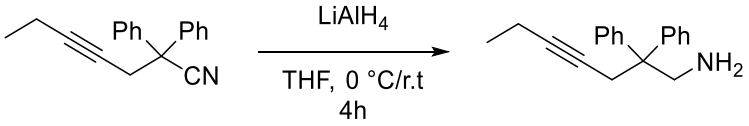

$LiAlH_4$ (0.701 g, 4.62 mmol, 1 eqv) was suspended in anhydrous Et_2O (18 mL) at 0 °C with an ice bath under argon. To this solution, 2,2-diphenylhept-4-yn-1-amine (1.2 g, 18.51 mmol, 4 eqv) dissolved in anhydrous Et_2O (18 mL) was added dropwise. Upon complete addition, the ice bath was removed, and the reaction was allowed to heat to ambient temperature and stirred for 16 hours. The reaction was subsequently

cooled to 0 °C with an ice bath and carefully quenched with cold water (10 mL). It was then allowed to warm to ambient temperature and subsequently stirred for 15 min. A solution of sodium hydroxide (2 M, 10 mL) was added, and the reaction mixture stirred for a further 15 min. The product was then extracted from the aqueous layer with Et_2O (3 * 30 mL), with the combined organic layer being washed with brine (40 mL), dried over sodium sulphate and concentrated under reduced pressure. The product was purified using column chromatography (7:3, CH: EtOAc) affording the product as a viscous oil. Yield = 2.15g (79 %).

The ^{1}H NMR spectrum matched literature.[246] ^{1}H NMR (600 MHz, $CDCl_3$) ^{1}H NMR (600 MHz, $CDCl_3$) δ 7.29 (t, *J* = 7.8 Hz, 4H), 7.24 – 7.18 (m, 6H), 3.54 – 3.49 (m, 2H), 2.99 (dt, *J* = 2.4, 1.2 Hz, 2H), 2.08 – 2.02 (m, 2H), 1.00 (td, *J* = 7.5, 0.8 Hz, 3H). See appendix section 10.1.7.2.

8.2.7.3 Intramolecular Substrate Linear Phthalimide

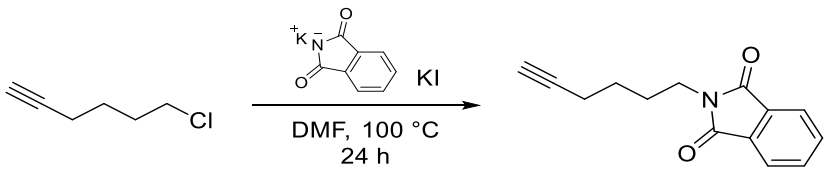

6-Chloro-1-heptyne (1.00 g, 8.58 mmol, 1 eqv) was dissolved in DMF (30 mL), to which potassium phthalimide (2.38 g12.87 mmol, 1.5 eqv) was added. The reaction mixture was then heated to 100 °C and allowed to stir for 24 hours. The reaction was then allowed to cool, diluted with water (40 mL) and extracted using EtOAc (3*10 mL). The combined organic layers were then dried over sodium sulphate and concentrated under reduced pressure. The product was then purified using column chromatography (2:8 EtOAc: CH), affording the product as a light orange solid. Yield = 1.52 g (78 %).

The ^{1}H NMR spectrum matched literature.[352] ^{1}H NMR (500 MHz, $CDCl_3$) δ 7.84 (dd, *J* = 5.4, 3.1 Hz, 2H), 7.71 (dd, *J* = 5.5, 3.0 Hz, 2H), 3.72 (t, *J* = 7.1 Hz, 2H), 2.25 (td, *J* = 7.0, 2.6 Hz, 2H), 1.94 (t, *J* = 2.7 Hz, 1H), 1.86 – 1.77 (m, 2H), 1.63 – 1.53 (m, 2H). See appendix section 10.1.7.3.

8.2.7.4 Intramolecular Substrate Linear Amine

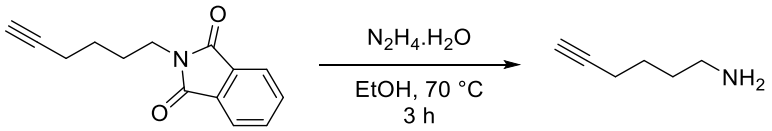

6-Phthalimido-1-heptyne (0.200 g, 0.880 mmol, 1 eqv) was dissolved in EtOH (10 mL), to which hydrazine monohydrate was added dropwise. The reaction mixture was then heated to 70 °C for 3 hours. The reaction was allowed to cool to room temperature and was diluted with water. Hydrochloric acid (1 M, 10 mL) was then added to the solution, the precipitate filtered, and the solution cooled. This was subsequently basified using sodium hydroxide (1 M) and the product was extracted using DCM (3*5 mL). The combined organic layers were then dried over sodium sulphate and concentrated under reduced pressure, affording a yellow oil. Yield = 0.03g (35 %).

The ^{1}H NMR spectrum matched literature.[352] ^{1}H NMR (500 MHz, $CDCl_3$) δ 2.72 (q, *J* = 4.7, 3.4 Hz, 2H), 2.21 (dp, *J* = 5.7, 2.8 Hz, 2H), 1.95 (t, *J* = 2.7 Hz, 1H), 1.57 (p, *J* = 3.5 Hz, 4H), 1.49 (s, NH_2). See appendix section 10.1.7.4.

8.2.8 Catalytic SCNP via Azobenzene Crosslinks: PFP Azobenzene

8.2.8.1 Di-Acid Azobenzene

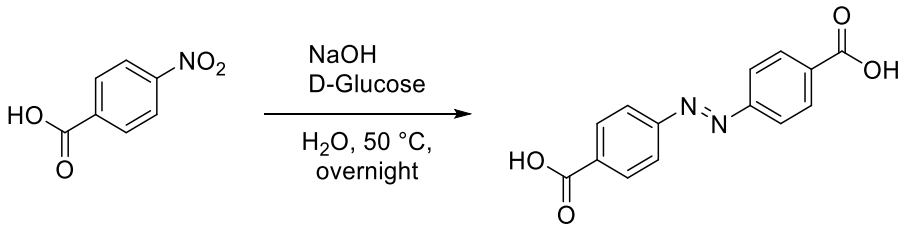

4-Nitrobenzoic acid (13 g, 77.8 mmol, 1 eqv) was added to sodium hydroxide solution (50 g in 250 mL, 1250 mmol, 16 eqv) at 50 °C. To this solution was added D-glucose (100 g, 555 mmol, 7 eqv) dissolved in water (150 mL), dropwise over a 1 hour period. The brown reaction mixture was subsequently cooled to ambient temperature and bubbled with air for 12 hours with stirring, giving a viscous dark brown mixture. The solution was then acidified with glacial acetic acid to a of pH 6–7, resulting in a yellow precipitate. The solid was filtered and dried affording an orange solid. Yield = 9.2 g (43 %).

The ^{1}H NMR spectrum reasonably matched literature.[402] ^{1}H NMR (600 MHz, $CDCl_3$) δ 8.16 (d, *J* = 8.5 Hz, 2H), 8.00 (d, *J* = 8.5 Hz, 2H). See appendix section 10.1.8.1.

8.2.8.2 Di-acid Chloride Azobenzene

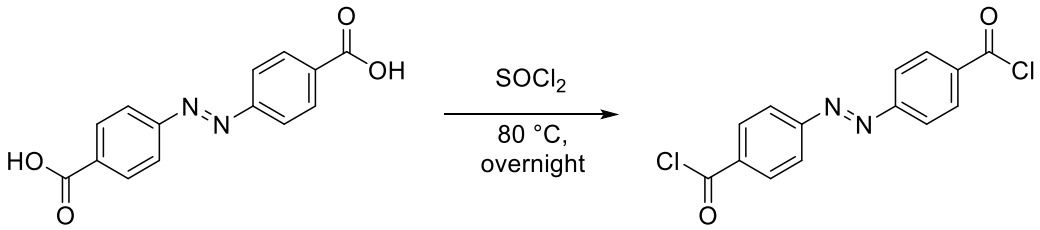

4,4-Di-acid azobenzene (1.5 g, 5.55 mmol, 1 eqv) was dissolved in thionyl chloride (30 mL), The reaction mixture was then heated to reflux and allowed to stir overnight. Thionyl chloride was removed via distillation and the resulting orange solid was collected and stored in the fridge under argon. Yield = 1.53 g (90 %).

The ^{1}H NMR spectrum reasonably matched literature.[402] ^{1}H NMR (600 MHz, $CDCl_3$) δ 8.34 – 8.29 (m, 4H), 8.09 – 8.04 (m, 4H). See appendix section 10.1.8.2.

8.2.8.3 PFP-Ester Azobenzene

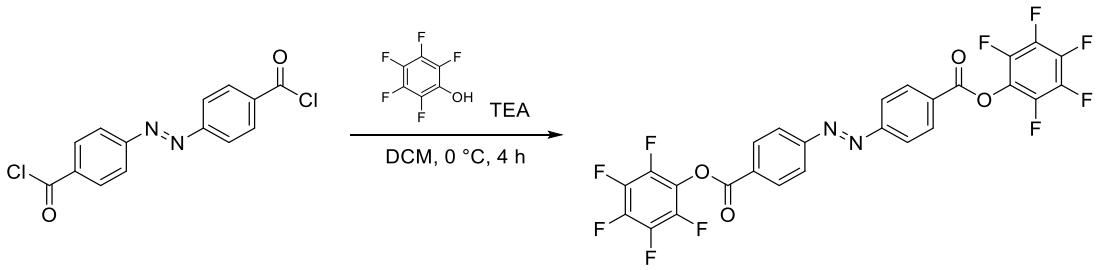

4,4-Di-acid chloride azobenzene (0.1 g, 0.23 mmol, 1 eqv) was dissolved in anhydrous THF (10 mL), placed under argon and cooled to 0 °C in an ice salt bath. In a separate flask, pentafluorophenyl alcohol (0.132 g, 0.718 mmol, 3.20 eqv) was dissolved in dry THF (1.5 mL) and added dropwise to the first solution under rapid stirring. The combined solutions were allowed to stir for 10 min at 0 °C. Triethylamine (0.048 g, 0.470 mmol, 0.109 mL, 2.10 eqv) was added dropwise to the reaction, resulting in an orange precipitate. The reaction was subsequently allowed to stir at 0 °C for a further 10 min, after which it was heated to 40 °C for 4 hours. The reaction was diluted with DCM (10 mL) and filtered to remove any salt. The reaction mixture was further diluted with toluene (10 mL) and transferred to a separating funnel. The mixture was then washed with sodium bicarbonate (2*20 mL), brine (20 mL) and concentrated under

reduced pressure. The crude product was recrystalized from a minimal amount of toluene, affording the product as a light orange powder. Yield = 0.043 g (20%).

^{1}H NMR (600 MHz, Tol-d_8) δ 8.16 – 8.11 (m, 1H), 7.84 – 7.79 (m, 1H). ^{19}F NMR (565 MHz, Tol) δ -153.51 – -153.85 (m), -157.73 (t, J = 22.1 Hz), -162.41 – -162.87 (m). See appendix section 10.1.8.3.

8.2.9 Catalytic SCNP via Azobenzene Crosslinks: Chlorinated Azobenzene

8.2.9.1 NCS Azobenzene Chlorination

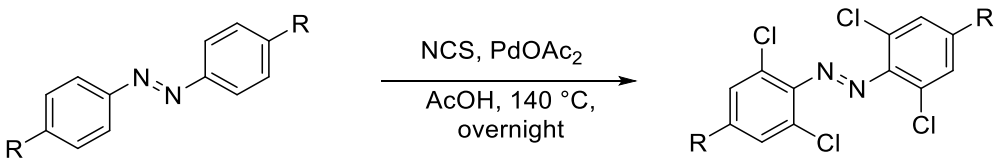

1. R = H
2. R = COOH
3. R = $COOCH_2CH_3$

In a Schlenk tube, the appropriate azobenzene (1.37 mmol, 1 eqv) was dissolved in glacial acetic acid (10 mL) with palladium acetate (0.030 g, 0.137 mmol, 0.1 eqv) and N-chlorosuccinimide (0.915 g, 6.80 mmol, 5 eqv). The Schlenk tube was sealed, and the reaction mixture was heated to 140 °C and stirred overnight. Acetic acid was then removed under reduced pressure, the crude solid was dissolved in EtOAc and washed with sodium carbonate (10 mL), brine (10 mL) and dried over sodium sulphate.

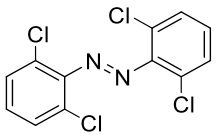

Yield = 0.39 g (89 %).

^{1}H NMR (600 MHz, DMSO-d_6) δ 7.71 (d, J = 8.2 Hz, 2H), 7.55 – 7.50 (m, 1H). See appendix section 10.1.9.1.

8.2.9.2 Di-Ester Azobenzene

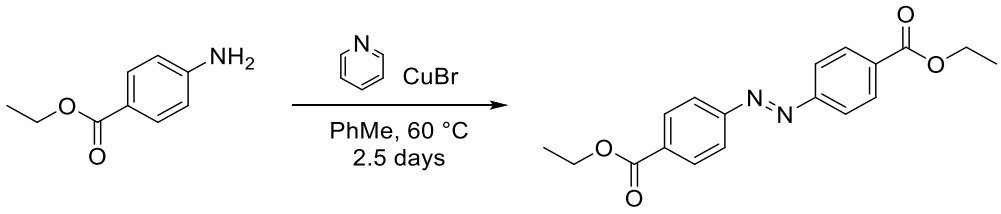

Benzocaine (9.79 g, 59.26 mmol, 1 eqv) and copper (I) bromide (255.04 mg, 1.78 mmol, 0.03 eqv) were dissolved in toluene (250 mL) and stirred for 15 minutes at ambient temperature. Pyridine (468.79 mg, 5.93 mmol, 477.39 µL, 0.10 eqv) was subsequently added and the reaction mixture was heated to 60 °C for 2 days. The reaction was allowed to cool to ambient temperature and solids were filtered off. The crude product was concentrated under reduced pressure dissolved in EtOAc (300 mL) and washed with water (2*100 mL), HCl (1 M, 100 mL) and brine. The product was subsequently purified via recrystallization from EtOAc and CH (2:8). The NMR spectral data appeared to match literature.[403] Yield = 3.764 g (38.9 %). For all spectra, see appendix section 10.1.9.2.

^{1}H NMR (600 MHz, $CDCl_3$) δ 8.24 – 8.19 (m, 2H), 8.01 – 7.96 (m, 2H), 4.43 (q, *J* = 7.1 Hz, 2H), 1.43 (t, *J* = 7.1 Hz, 3H).

^{13}C NMR (151 MHz, $CDCl_3$) δ 140.74, 137.28, 136.79, 127.50, 126.68, 114.17, 65.27.

HRMS (ESI): m/z calculated for $[C_{18}H_{18}N_2O_4+H]^+$ 327.1339; found 327.1333, Δppm = -1.834.

8.2.9.3 Tetra Chlorinated Di-Ester Azobenzene

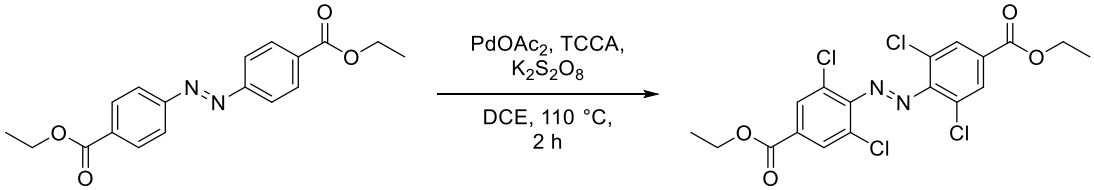

The chlorinated di-ester azobenzene was synthesised according to a modified procedure. The di-ester azobenzene (1.36 g, 4.168 mmol, 1 eqv), TCCA (1.938 g, 8.326 mmol, 2 eqv), potassium persulphate (1.349 g, 5.001 mmol, 1.2 eqv) and palladium acetate (93.49 mg, 0.042 mmol, 0.10 eqv) were added to a Schlenk flask and dissolved in DCE (50 mL). The flask was purged with argon for approximately 15 minutes. The flask was then closed to argon, the reaction mix heated to 110 °C behind

a blast shield and allowed to stir for 2 hours. A dark red solution formed during the reaction. After 2 hours, the reaction was allowed to cool to ambient temperature and was subsequently diluted with DCM (30 mL). The reaction mixture was filtered to remove solid impurities and the filtrate concentrated under reduced pressure. The crude product was purified via column chromatography (EtOAc: CH 1:9) affording the product as a dull red solid. Yield = 0.838 g (43.4 %). For all spectra, see appendix section 10.1.9.3.

^{1}H NMR (600 MHz, $CDCl_3$) δ 8.12 (s, 4H), 4.47 – 4.36 (q, 4H), 1.46 – 1.37 (q, 6H).

^{13}C NMR (151 MHz, $CDCl_3$) δ 163.77, 150.31, 131.92, 130.47, 127.23, 62.12, 14.26.

HRMS (ESI): m/z calculated for $[C_{18}H_{14}N_2O_4+H]^+$ 462.9780; found 462.9787, Δppm = 1.5119.

8.2.9.4 Tetra Chlorinated Di-carboxy Azobenzene

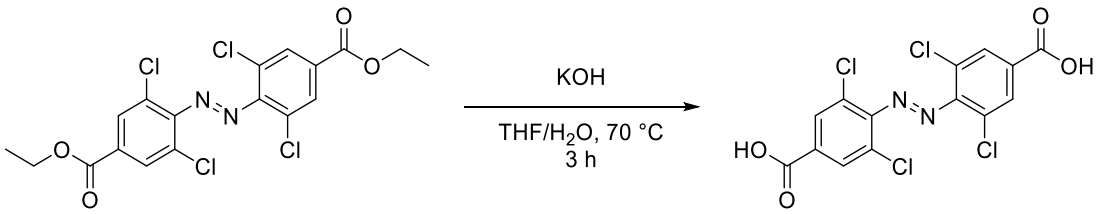

Tetra chlorinated di-ester azobenzene (0.7g, 1.51 mmol, 1 eqv) and potassium hydroxide (0.381g, 6.79 mmol) were dissolved in a 1:1 THF/water mixture (30 mL) and the reaction mixture was heated to 70 °C and allowed to stir for 3 hours after which the reaction was allowed to cool to ambient temperature. The crude product was subsequently concentrated under reduced pressure and recrystalized from a minimal amount of water to afford the product as pink/red crystals. Yield = 0.534g (86.8 %). For all spectra, see appendix section 10.1.9.4.

^{1}H NMR (600 MHz, DMSO-d_6) δ 7.95 (s, 4H).

^{13}C NMR (151 MHz, DMSO-d_6) δ 165.1, 148.7, 135.9, 130.6, 126.4.

HRMS (ESI): m/z calculated for $[C_{14}H_6Cl_4N_2O_4-H]-$ 404.9009; found 404.9008, Δppm = -0.2469.

8.2.9.5 Tetra Chlorinated Di-acid Chloride Azobenzene

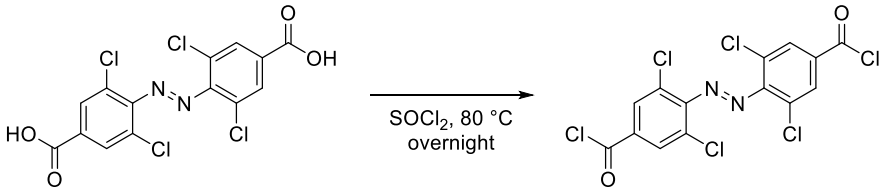

The di-carboxy azobenzene (0.450 g, 1.23 mmol, 1 eqv) was dissolved in thionyl chloride (30 mL) and allowed to stir at reflux overnight. The reaction mixture was allowed to cool to ambient temperature, thionyl chloride was removed via distillation and the remaining red solid was dissolved in dry toluene (20 mL) and filtered. The filtrate was subsequently placed under argon and the product was allowed to recrystalize overnight in the freezer, affording the product as dark red crystals. Yield = 0.359 g (84 %). For all spectra, see appendix section 10.1.9.5.

^{1}H NMR (600 MHz, toluene-d_8) δ 7.62 (d, J = 0.8 Hz, 4H).

^{13}C NMR (151 MHz, $CDCl_3$) δ 165.71, 151.60, 134.27, 131.71, 127.75.

8.2.9.6 Tetra Chlorinated PFP-ester Azobenzene

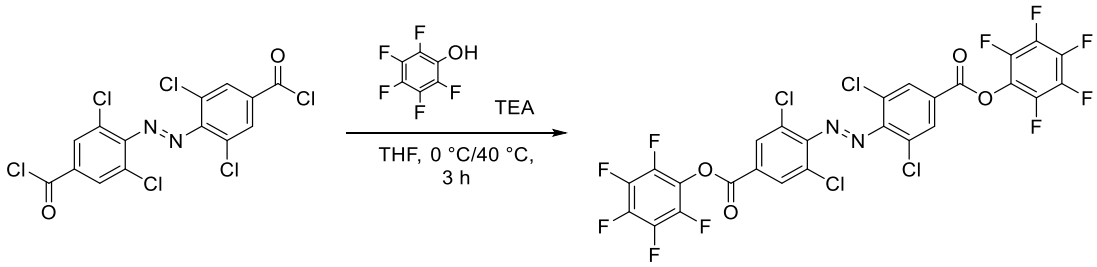

The di-acid chloride azobenzene (0.3 g, 0.67 mmol, 1 eqv) was dissolved in anhydrous THF (25 mL), placed under argon, and cooled to 0 °C in an ice salt bath. In a separate flask, pentafluorophenyl alcohol (0.396 g, 2.154 mmol, 3.20 eqv) was dissolved in dry THF (5 mL) and added dropwise to the first solution under rapid stirring. The combined solutions were allowed to stir for 10 min at 0 °C. Triethylamine (0.143 g, 1.411 mmol, 0.328 mL, 2.10 eqv) was added dropwise to the reaction, resulting in an orange precipitate. The reaction was subsequently allowed to stir at 0 °C for a further 10 min, after which it was heated to 40 °C for 3 hours. The reaction was diluted with DCM (40 mL) and filtered to remove any salt. The reaction mixture was further diluted with toluene (30 mL), transferred to a separating funnel and washed twice with sodium bicarbonate (20 mL), brine (20 mL) and concentrated under reduced pressure. The

crude product was recrystalized from a minimal amount of toluene, affording the product as maroon crystals. Yield = 0.469 g (56.4 %). For all spectra, see appendix section 10.1.9.6.

^{1}H NMR (600 MHz, toluene-d_8) δ 7.83 (s, 4H)

^{19}F NMR (565 MHz, toluene-d_8) δ -153.4 – -153.8 (m), -156.8 – -157.4 (m), -162.1 – -162.5 (m)

8.2.10 Light-Driven Folding via Metal-Complexation

8.2.10.1 Hydroxyethyl Indolenine

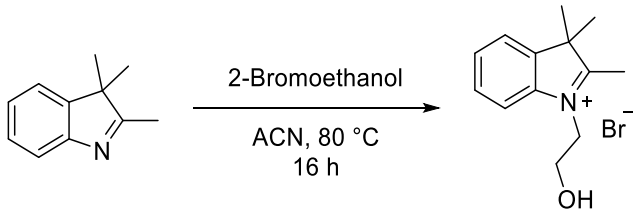

2,3,3 Trimethyl indolenine (2.5 g, 15.7 mmol, 1 eqv) was dissolved in ACN (35 mL) and placed under N_2 atmosphere, to which 2-bromoethanol (2.16 g, 17.27 mmol, 1.1 eqv) was added dropwise. The mixture was then heated to reflux overnight, MeOH was added (10 mL) and the reaction was further stirred at reflux for 30 minutes. The reaction was then allowed to cool to room temperature before being concentrated to a volume of 10 mL. Cold EtOAc (30 mL) was then added, and the resulting purple precipitate was filtered and washed with cold EtOAc before being air dried. This afforded a purple powder that was used immediately for the next step. Yield = 2.58 g (58 %).

8.2.10.2 Oxazole Indolenine

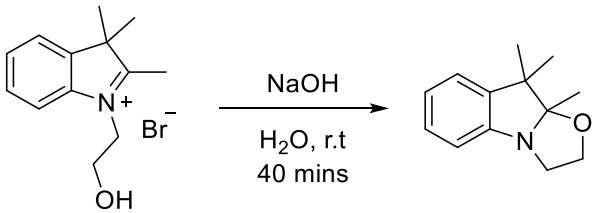

Hydroxyethyl indolenine (2.5 g, 8.8 mmol, 1 eqv) was dissolved in water (50 mL). Separately, potassium hydroxide (0.9 g) was dissolved in water (50 mL) and added to the solution. The combined solutions were stirred at room temperature for 40 minutes.

The resulting product was then extracted with DCM (3*15 mL) and concentrated under reduced pressure, affording a yellow oil that was used without further purification. Yield = 1.71 g (96 %)

^{1}H NMR (500 MHz, $CDCl_3$) δ 7.14 (td, *J* = 7.6, 1.4 Hz, 1H), 7.07 (dd, *J* = 7.5, 1.3 Hz, 1H), 6.92 (td, *J* = 7.4, 1.0 Hz, 1H), 6.76 (d, *J* = 7.9 Hz, 1H), 3.84 (td, *J* = 7.4, 3.0 Hz, 1H), 3.72 (ddd, *J* = 11.4, 7.1, 3.1 Hz, 1H), 3.63 – 3.48 (m, 2H), 1.43 (s, 3H), 1.39 (s, 3H), 1.18 (s, 3H). See appendix section 10.1.10.1.

8.2.10.3 Hydroxyethyl Spiropyran

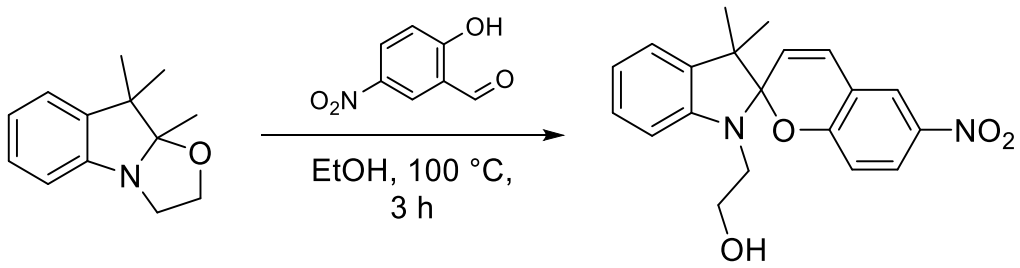

The oxazole (1.2 g, 8.85 mmol, 1 eqv) was dissolved in EtOH (15 mL) and placed under N_2 atmosphere. To this was added 5-nitro salicaldehyde (1.48 g, 8.85 mmol, 1.5 eqv) and the combined reaction mixture was heated to 100 °C for 3 hours. The combined solution was then allowed to cool to room temperature, before being concentrated under reduced pressure. The resulting dark purple solid was then purified using a two solvent recrystallization with n-hexane and EtOAc, affording fine purple crystals. Yield = 0.91 g (44 %). For all spectra, see appendix section 10.1.10.2.

The ^{1}H NMR spectrum matched literature.[363] ^{1}H NMR (500 MHz, $CDCl_3$) δ 8.06 – 7.96 (m, 2H), 7.20 (td, *J* = 7.7, 1.3 Hz, 1H), 7.10 (dd, *J* = 7.3, 1.3 Hz, 1H), 6.94 – 6.87 (m, 2H), 6.76 (d, *J* = 8.9 Hz, 1H), 6.67 (d, *J* = 7.8 Hz, 1H), 5.89 (d, *J* = 10.4 Hz, 1H), 3.94 – 3.61 (m, 2H), 3.54 – 3.23 (m, 2H), 1.29 (s, 3H), 1.20 (s, 3H).

^{13}C NMR (126 MHz, $CDCl_3$) δ 159.69, 147.36, 141.55, 136.21, 128.66, 128.25, 126.38, 123.17, 122.31 (d, *J* = 2.2 Hz), 120.40, 118.92, 115.92, 107.30, 61.26, 53.23, 46.51, 26.29, 20.41.

8.2.10.4 Spiropyran-Methyl Methacrylate (SP-MMA)

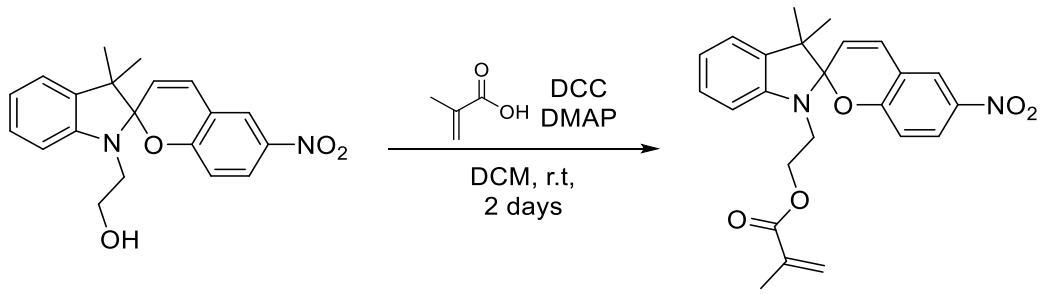

Dicyclohexylcarbodiimide (0.843 g, 4.09 mmol, 1.2 eqv) was dissolved in dry DCM (10 mL) and cooled to 0 °C. To this was then added methacrylic acid (0.340 g, 3.95 mmol, 1.16 eqv) dropwise, followed by stirring for 10 mins at 0 °C. Dimethyl amino pyridine (0.05 g, 0.408 mmol, 0.12 eqv) was then added. Separately, hydroxyethyl spiropyran (1.20 g, 3.41 mmol, 1 eqv) was dissolved in dry DCM (10 mL) and subsequently added dropwise to the first solution at 0 °C. The combined solution was then allowed to warm to room temperature and stirred for two days. The reaction mixture was then filtered, and the white solid was washed with DCM. The filtrate was collected and concentrated under reduced pressure, affording a purple gum. The product was purified first using silica chromatography (7:3 hexane: EtOAc). The resulting fractions were concentrated and the light-yellow solid was recrystalised from MeOH, affording the product as fine, light yellow crystals. Yield = 0.572 g (39 %). For all spectra, see appendix section 10.1.10.3.

The ^{1}H NMR spectrum matched literature.[365] ^{1}H NMR (500 MHz, $CDCl_3$) δ 8.05 – 7.98 (m, 2H), 7.21 (td, *J* = 7.7, 1.3 Hz, 1H), 7.09 (dd, *J* = 7.2, 1.2 Hz, 1H), 6.93 – 6.87 (m, 2H), 6.75 (d, *J* = 8.8 Hz, 1H), 6.70 (d, *J* = 7.8 Hz, 1H), 6.07 (t, *J* = 1.3 Hz, 1H), 5.88 (d, *J* = 10.3 Hz, 1H), 5.57 (q, *J* = 1.5 Hz, 1H), 4.30 (t, *J* = 6.3 Hz, 2H), 3.55 (dt, *J* = 14.9, 6.7 Hz, 1H), 3.43 (dt, *J* = 15.1, 5.9 Hz, 1H), 1.92 (t, *J* = 1.3 Hz, 3H), 1.28 (s, 3H), 1.17 (s, 3H).

^{13}C NMR (126 MHz, $CDCl_3$) δ 167.35, 159.53, 146.79, 141.21, 136.17, 135.83, 128.44, 127.99, 126.09 (d, *J* = 6.9 Hz), 122.92, 121.94 (d, *J* = 4.2 Hz), 120.07, 118.55, 115.70, 106.89, 106.66, 62.77, 52.94, 42.56, 25.98, 19.97, 18.50.

8.3 Polymers

8.3.1 Styrene Polymers

8.3.1.1 NMP of Vinyl Benzyl Chloride and Styrene

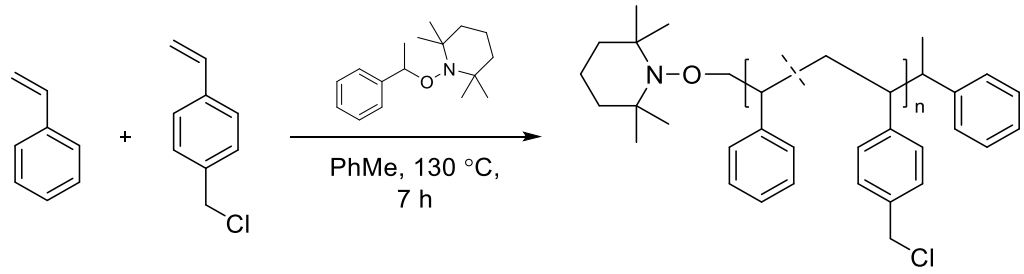

Vinyl benzyl chloride (0.54 g, 8.03 mmol, 60 eqv), styrene (2.79 g, 53.56 mmol, 400 eqv) and the nitroxide initiator (0.017 g, 0.067 mmol, 1 eqv) were added to a Schlenk tube and dissolved in dry toluene (1 mL). The combined reaction mixture was subjected to three freeze pump thaw cycles and subsequently heated to 130 °C for 7 hours. The reaction mixture was then quenched by cooling in liquid nitrogen and exposure to air. The polymer was precipitated three times into ice cold methanol and dried at 40 °C in a vacuum oven, affording the polymer as a light-yellow solid.

8.3.1.2 NMP of Vinyl Benzyl Chloride, Diphenylphosphine Styrene and Styrene

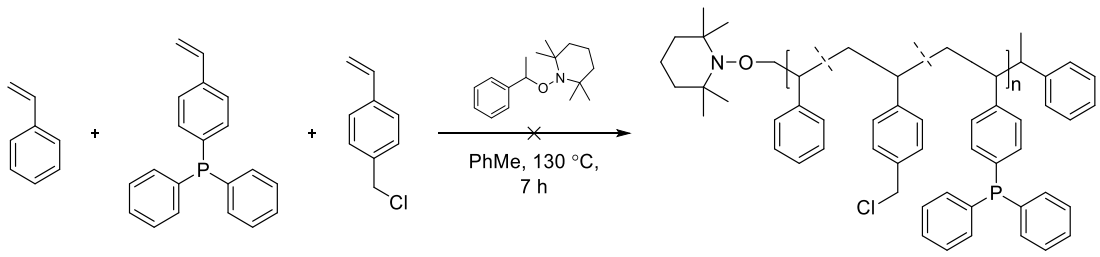

4-(Diphenylphosphino)styrene (0.58 g, 2.01 mmol, 30 eqv), vinyl benzyl chloride (0.54 g, 8.03 mmol, 60 eqv), styrene (2.79 g, 53.56 mmol, 400 eqv) and the nitroxide initiator (0.017 g, 0.133 mmol, 1 eqv) were added to a Schlenk tube and dissolved in dry toluene (1.5 mL). The combined reaction mixture was subjected to three freeze pump thaw cycles and subsequently heated to 130 °C for 7 h. The reaction mixture formed a yellow gel after 3 hours due to phosphonium salt formation.

8.3.1.3 NMP of Vinyl Benzyl Chloride, Gold Complexed Diphenylphosphine Styrene and Styrene

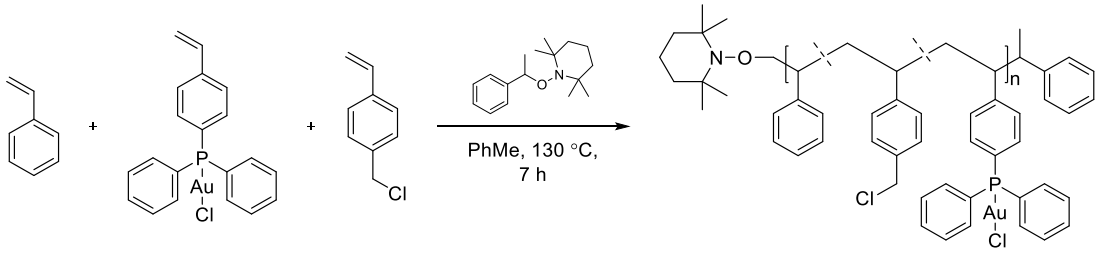

Gold chloride complexed 4-(Diphenylphosphino)styrene (0.139 g, 0.27 mmol, 15 eqv), vinyl benzyl chloride (0.122 g, 0.0.80 mmol, 45 eqv), styrene (0.559 g, 5.37 mmol, 300 eqv) and the nitroxide initiator (0.004 g, 0.0017 mmol, 1 eqv) were added to a Schlenk tube and dissolved in dry toluene (0.5 mL). The combined reaction mixture was subjected to three freeze pump thaw cycles and subsequently heated to 130 °C for 7 hours. The reaction mixture was then quenched by cooling in liquid nitrogen and exposure to air. The polymer was precipitated three times into ice cold MeOH and dried at 40 °C in a vacuum oven, affording the polymer as an off white solid.

8.3.1.4 NMP of Vinyl Benzyl Alcohol, Diphenylphosphine Styrene and Styrene (P-13 and P-23)

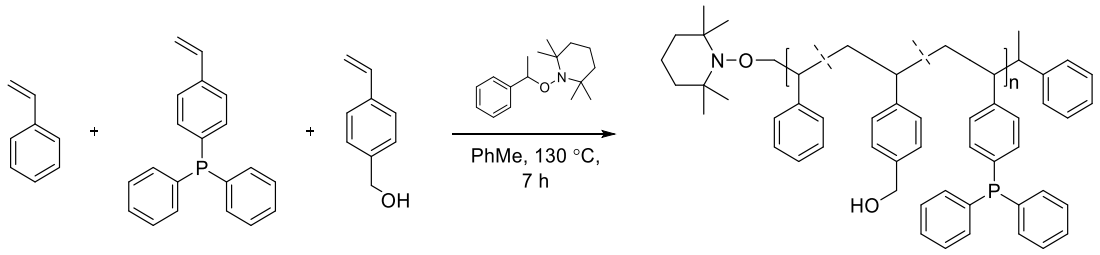

4-(Diphenylphosphino)styrene (1.16 g, 4.02 mmol, 30 eqv), vinyl benzyl alcohol (1.08 g, 8.03 mmol, 60 eqv-120 eqv for **P-23**), styrene (5.58 g, 53.56 mmol, 400 eqv) and the nitroxide initiator (0.035 g, 0.133 mmol, 1 eqv) were added to a Schlenk tube and dissolved in dry toluene (1.5 mL). The combined reaction mixture was subjected to three freeze pump thaw cycles and subsequently heated to 130 °C for 7 hours. The reaction mixture was then quenched by cooling in liquid nitrogen and exposure to air. The polymer was precipitated three times into ice cold MeOH and dried at 40 °C in a vacuum oven, affording the polymer as a light-orange solid.

8.3.1.5 Gold Loading of P-13 and P-23

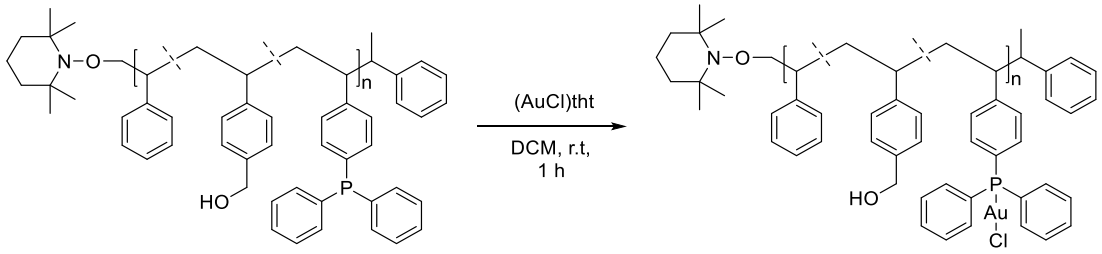

AuCl(tht) (0.060g, 0.000187 mol)) was added to a solution of either **Au-P-13** or **Au-P-23** (0.5g) in DCM (10 mL) in a Schlenk flask under argon, followed by stirring at ambient temperature for 1 hour. The crude product was concentrated under reduced pressure, redissolved in a minimal amount of DCM and precipitated from cold MeOH. The precipitate was then filtered and washed with cold EtOH, affording the gold complexed polymer as a cream coloured solid.

8.3.2 Azobenzene SCNP Procedures

8.3.2.1 Benzyl Chloride Crosslinking

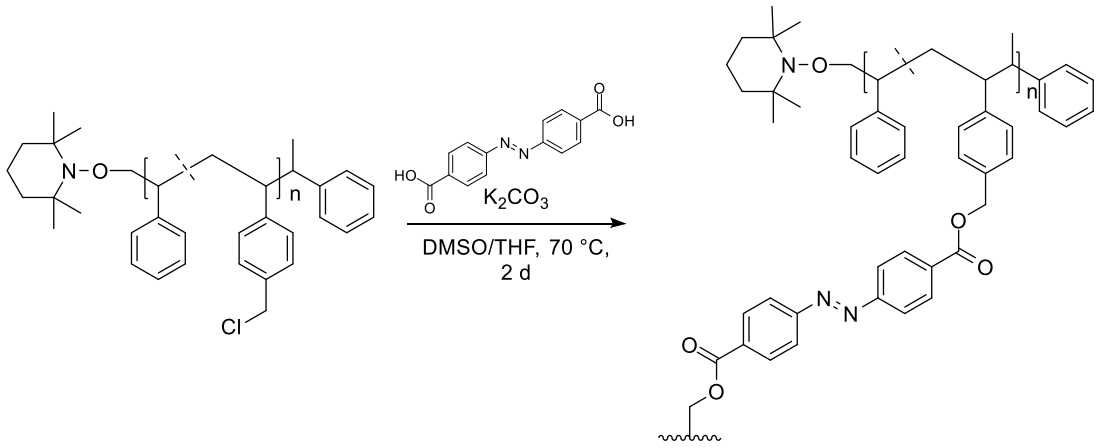

The benzyl chloride polymer (0.05g, 0.0036 mmol, 1 eqv) was dissolved in DMSO (20 mL) and THF (3 mL). Separately, 4,4-dicarboxy azobenzene (0.108 g, 0.400mmol, 15 eqv) and potassium carbonate (0.083 g, 0.6 mmol 22.5 eqv) were dissolved in DMSO (30 mL) and THF (4.5 mL) and heated to 70 °C. The polymer solution was then added dropwise using a syringe pump at a rate of 1 mL/hr. After complete addition the combined solution was then allowed to stir for an additional day. The reaction mixture was then allowed to cool to room temperature, before being filtered to remove

the formed precipitate. The polymer was extracted using EtOAc (3*10 mL) and washed extensively with water (5*10 mL), dried over sodium sulphate and concentrated under reduced pressure. The crude polymer was then taken up in minimal amount of DCM and precipitated into cold MeOH, affording the SCNP as a light orange solid.

8.3.2.2 Gold Chloride Benzyl Chloride Crosslinking

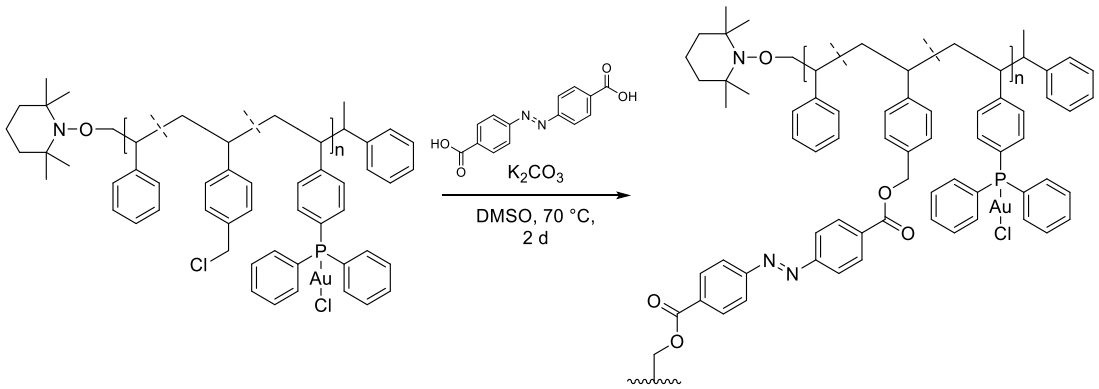

The benzyl chloride polymer (0.040 g, 0.0033 mmol, 1 eqv) was dissolved in DMSO and THF (1:1, 20 mL). Separately, 4,4-dicarboxy azobenzene (0.108 g, 0.4mmol, 15 eqv) and potassium carbonate (0.083 mg, 0.6 mmol, 22.5 eqv) were dissolved in DMSO (30 mL) and THF (4.5 mL) and heated to 70 °C. The polymer solution was then added dropwise using a syringe pump at a rate of 1 mL/hr. After complete addition a purple precipitate formed attributed to colloidal gold and the combined solution was then allowed to stir for an additional day. The reaction mixture was then allowed to cool to room temperature, before being filtered to remove the formed precipitate. The polymer was extracted using EtOAc (3*10 mL), washed extensively with water (5*10 mL), dried over sodium sulphate and concentrated under reduced pressure. The crude polymer was then taken up in minimal amount of DCM and precipitated into cold MeOH, affording the SCNP as a light orange solid.

8.3.2.3 PFP Ester Crosslinking

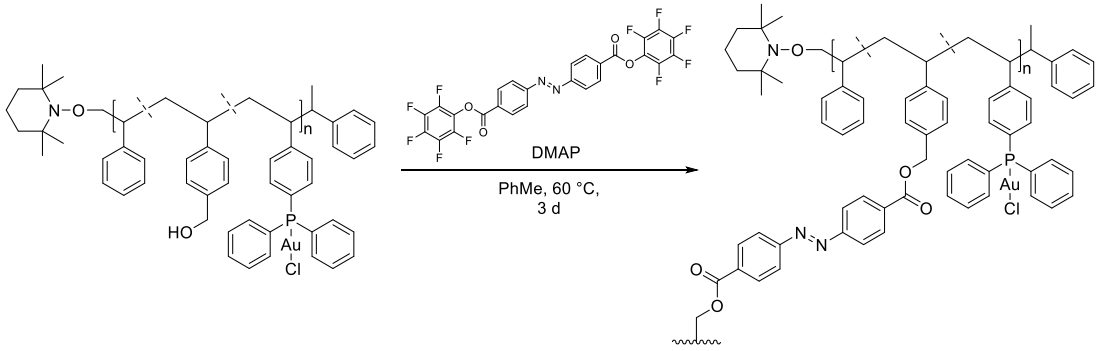

The azobenzene crosslinker (0.089g, 0.149 mmol, 7 eqv) was dissolved in dry toluene (35 mL) under argon, and sparged with argon for 20 min. Separately, the polymer **Au-P-13** (0.045 g, 0.00213 mmol, 1 eqv) and DMAP (0.036 g, 0.2988 mmol, 140 eqv) were dissolved in dry toluene (15 mL) under argon and similarly sparged. The solution containing the azobenzene crosslinker was heated to 60 °C, to which the polymer containing solution was added dropwise at a rate of 0.75 mL/hr. After complete addition of the polymer, the solution was allowed to stir for a further 2 days at 60 °C. To quench the excess of azobenzene crosslinker, butylamine (0.222 g, 0.3 mL, 3 mmol) was added to the solution at 60 °C and allowed to stir for 3 hours. The reaction mixture was subsequently cooled in an ice bath and the resulting precipitate was filtered off using a syringe filter. The filtrate was concentrated under reduced pressure, redissolved in a small amount of DCM and precipitated three time from ice cold MeOH, affording the SCNP as a light orange powder.

8.3.2.4 Tetra chlorinated PFP Ester Crosslinking

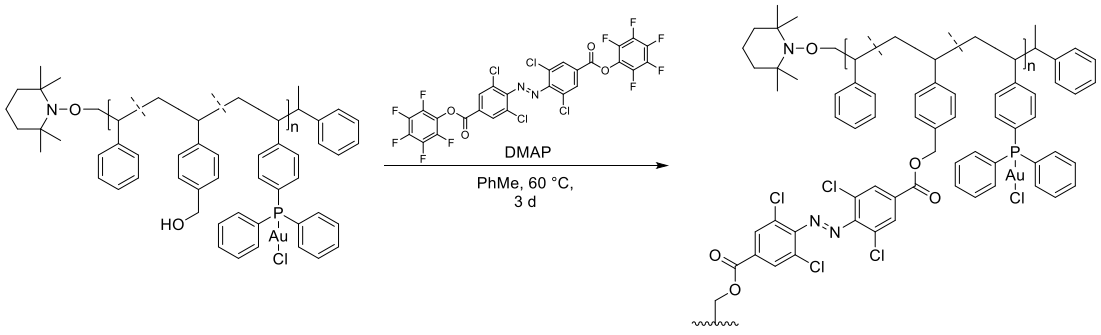

The azobenzene crosslinker (0.110g, 0.149 mmol, 7 eqv) was dissolved in dry toluene (35 mL) under argon, and sparged with argon for 20 min. Separately, the polymer **Au-**

P-13 (0.045 g, 0.00213 mmol, 1 eqv) and DMAP (0.036 g, 0.2988 mmol, 140 eqv) were dissolved in dry toluene (15 mL) under argon and similarly sparged. The solution containing the azobenzene crosslinker was heated to 60 °C, to which the polymer containing solution was added dropwise at a rate 0.75 mL/hr. After complete addition of the polymer, the solution was allowed to stir for a further 2 days at 60 °C. To quench the excess of azobenzene crosslinker, butylamine (0.222 g, 0.3 mL, 3 mmol) was added to the solution at 60 °C and allowed to stir for 3 hours. The reaction mixture was subsequently cooled in an ice bath and the resulting precipitate was filtered off using a syringe filter. The filtrate was concentrated under reduced pressure, redissolved in a small amount of DCM and precipitated three time from ice cold MeOH, affording the SCNP as a red powder.

For AzoCl$_4$-Au-SCNP-23. The same general synthetic procedure was followed, instead using 0.192 g of the azobenzene crosslinker, 0.063 mg of DMAP and 0.6 mL of butylamine.

8.3.3 Methacrylate Polymers

8.3.3.1 RAFT Polymerization of SP-MMA and MMA

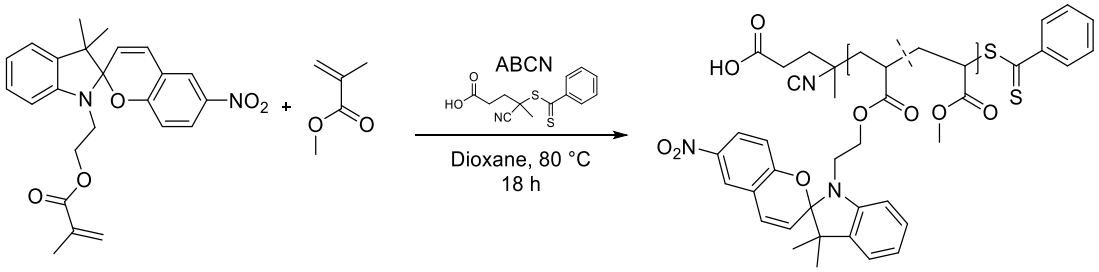

Methyl methacrylate and dioxane were purified over a short plug of basic aluminium oxide to remove inhibitors. De-inhibited methyl methacrylate (0.155 g, 1.56 mmol, 300 eqv) and dioxane (0.275 mL) were added to a vial containing chain transfer agent, 4-cyano-4-(phenylcarbonothioylthio)-pentanoic acid (0.00145 g, 0.0052 mmol, 1 eqv) and methyl methacrylate functionalised spiropyran (SP-MMA) (0.130 g, 0.311 mmol, 60 eqv). Separately a stock solution of 1,1-azobis(cyclohexanecarbonitrile) (2.53 mg.mL^{-1}) was prepared in de-inhibited dioxane, which was then added to the polymerization mixture. The mixture was transferred to a Schlenk tube and subjected to 5 freeze pump thaw cycles before being submerged in an oil bath pre-heated to 80 °C. After stirring for 18 hours, the polymerization was quenched by exposure to air

and immediate immersion in liquid N_2. The crude polymerization mixture was then diluted with a small amount of dioxane and precipitated three times into ice cold MeOH followed by centrifugation. The resulting purple gum was dried overnight at room temperature in a vacuum oven.

8.3.3.2 RAFT Polymerization of SP-MMA and PEGMEMA (SP-36-PEGMEMA and SP-15-PEGMEMA)

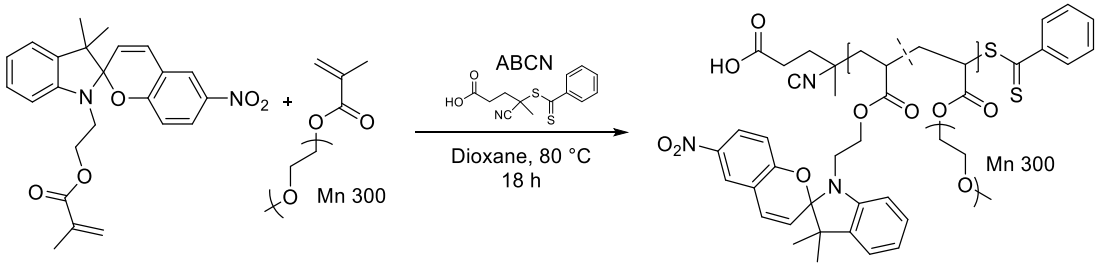

Polyethylene glycol methyl ether methacrylate (PEGMEMA, M_n = 300 g mol^{-1}) and dioxane were purified over a short plug of basic aluminium oxide to remove inhibitors. De-inhibited PEGMEMA (0.748 g, 2.34 mmol, 300 eqv) and dioxane (0.275 mL) were added to a vial containing chain transfer agent, 4-cyano-4-(phenylcarbonothioylthio)-pentanoic acid (0.00217 g, 0.00779 mmol, 1 eqv) and SP-MMA (0.353 g, 0.841 mmol 100 eqv). Separately, a stock solution of 1,1-azobis(cyclohexanecarbonitrile) (3.8 $mg.mL^{-1}$) was prepared in de-inhibited dioxane. 0.1 mL of this solution was then added to the polymerization mixture. The mixture was transferred to a Schlenk tube and subjected to 5 freeze pump thaw cycles before being submerged in an oil bath pre-heated to 80 °C. After stirring for 18 hours, the polymerization was quenched by exposure to air and immediate immersion in liquid N_2. The crude polymerization mixture was then diluted with a small amount of dioxane and precipitated three times into n-hexane: Et_2O, (2:1) followed by centrifugation. The resulting purple gum was dried overnight at room temperature in a vacuum oven affording the polymer **SP-36-PEGMEMA**.

The same procedure was used for the polymer **SP-15-PEGMEMA,** using instead 185 mg of the spiropyran monomer.

8.3.3.3 RAFT Polymerization of PEGMEMA Test Polymer

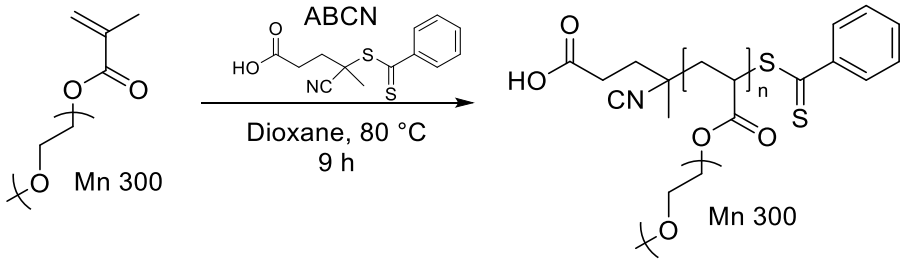

Polyethylene glycol methyl ether methacrylate (PEGMEMA, M_n = 300 g mol^{-1}) and dioxane were purified over a short plug of basic aluminium oxide to remove inhibitors. De-inhibited PEGMEMA (0.748 g, 2.34 mmol, 300 eqv) and dioxane (0.275 mL) were added to a vial containing chain transfer agent, 4-cyano-4-(phenylcarbonothioylthio)-pentanoic acid (0.00217 g, 0.00779 mmol, 1 eqv). Separately, a stock solution of 1,1-azobis(cyclohexanecarbonitrile) (3.8 mg.mL^{-1}) was prepared in de-inhibited dioxane. 0.1 mL of this solution was then added to the polymerization mixture. The mixture was transferred to a Schlenk tube and subjected to 5 freeze pump thaw cycles before being submerged in an oil bath pre-heated to 80 °C. After stirring for 9 hours, the polymerization was quenched by exposure to air and immediate immersion in liquid N_2. The crude polymerization mixture was then diluted with a small amount of dioxane and precipitated three times into n-hexane: Et_2O, (2:1) followed by centrifugation. The resulting pink gum was dried overnight at room temperature in a vacuum oven.

8.3.4 General Spiropyran SCNP procedure

8.3.4.1 SP-20-MMA $CuCl_2$ Crosslinking

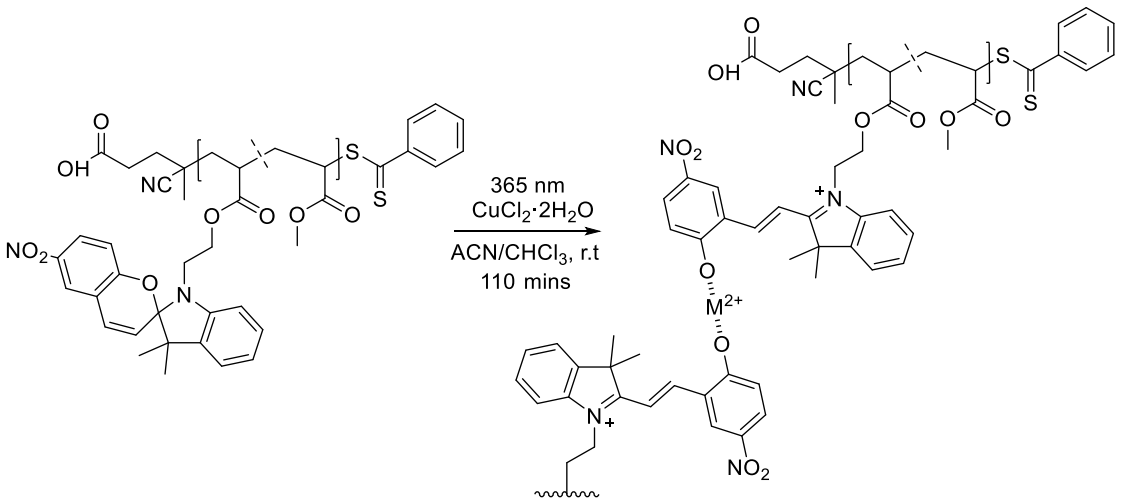

2 mg of polymer was placed in a photo vial, to which was added a mixture of $CHCl_3$: ACN 1:4 (2 mL). Separately, copper chloride dihydrate (0.0014 g, 0.008 mmol, 4 eqv) was dissolved in 0.6 mL of ACN. The copper solution was then added dropwise over a period of 110 mins to the polymer solution via a syringe pump. Irradiation with a 365 nm LED was completed with pulse irradiations of 1 minute, followed by 10 mins of darkness over the same period, totalling 10*1 min irradiations with 365 nm light. After the final irradiation, the solution was allowed to stir in the dark for 90 minutes. The solution was then diluted with DCM (1 mL) before being washed with water (4*2 mL). The organic layer was then concentrated under reduced pressure, affording the SCNP as a light orange solid.

8.3.4.1.1 White Light Decomplexation

The SCNP was dissolved in THF (2 mL) and placed in a photo vial. The solution was then irradiated with white light for 20 minutes, before being analysed directly via SEC.

8.3.4.2 SP-36-PEGMEMA Metal Tetrafluoroborate $(BF_4)_2$ Crosslinking

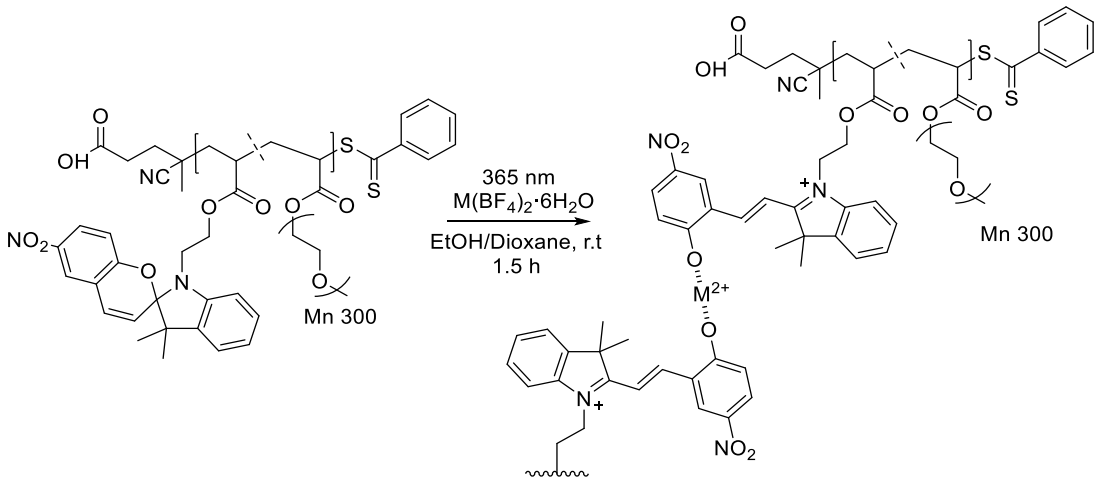

2 mg of polymer was placed under inert N_2 atmosphere in a photo vial. To this was added first 0.2 mL of dry dioxane, followed by 3.8 mL of dry and degassed EtOH. Separately, the appropriate tetrafluoroborate salt (0.00866 mmol 4 eqv to every spiropyran unit) was dissolved in dry and degassed EtOH (0.4 mL) in a photo vial under N_2 atmosphere. The tetrafluoroborate solution was then added dropwise over a period of 90 mins to the polymer solution. Irradiation with a 365nm LED was completed with pulse irradiations of 1 minute, followed by 15 mins of darkness over the same period, totalling 6*1 min irradiations with 365 nm light. After the final

irradiation, the solution was allowed to stir in the dark for 90 minutes. Following this, an aliquot was taken, diluted with THF, and analysed via SEC. The remaining solution was then utilised directly without purification for decomplexation experiments.

8.3.4.3 Zinc SP-36-PEGMEMA EDTA Decomplexation

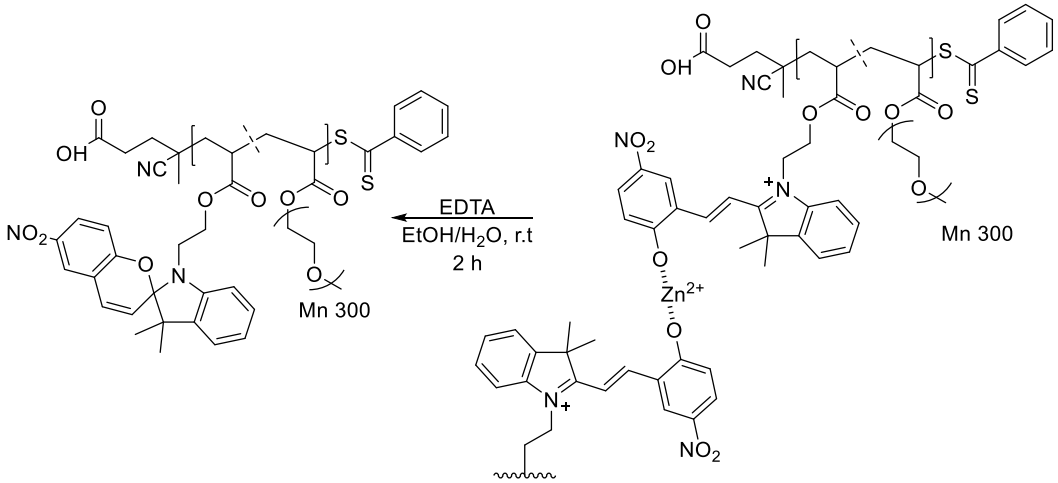

EDTA (3 mg) dissolved in water (1 mL) and basified to a pH of 8 using sodium bicarbonate (1 M) was added directly to the SCNP solution and allowed to stir for 1 hour at room temperature. An aliquot of this solution was then taken, diluted with THF and analysed via SEC.

8.3.4.4 Zinc SP-36-PEGMEMA TAM Decomplexation

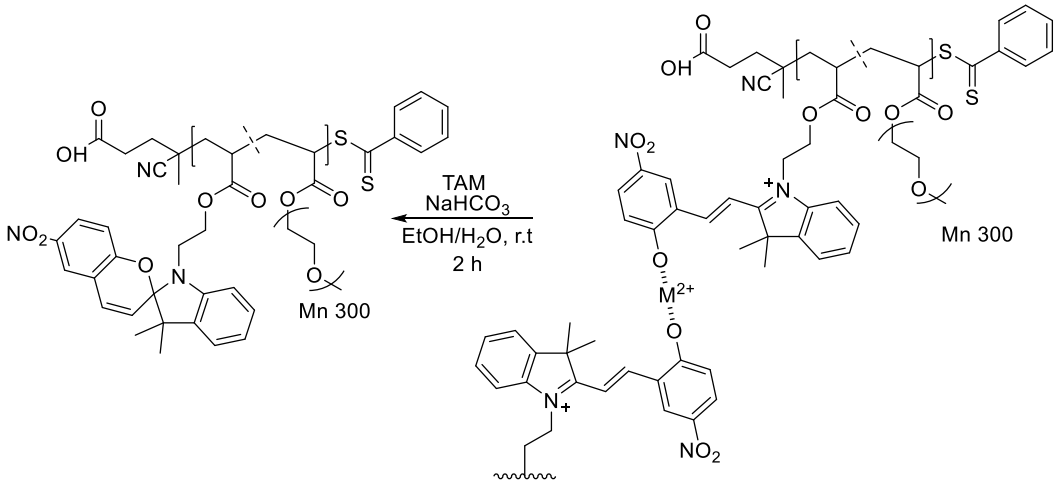

Thioacetamide (0.019 g, 0.252 mmol, 3 eqv to $Zn(BF_4)_2$) was dissolved in water (1 mL) and added directly to the SCNP solution. The combined solutions were then

basified to a pH of 8 using sodium bicarbonate (1 M), heated to 60 °C and stirred for 2 hours. An aliquot of the reaction mixture was then taken, diluted with THF and analysed via SEC.

8.3.4.5 Cobalt SP-36-PEGMEMA Ammonia Decomplexation

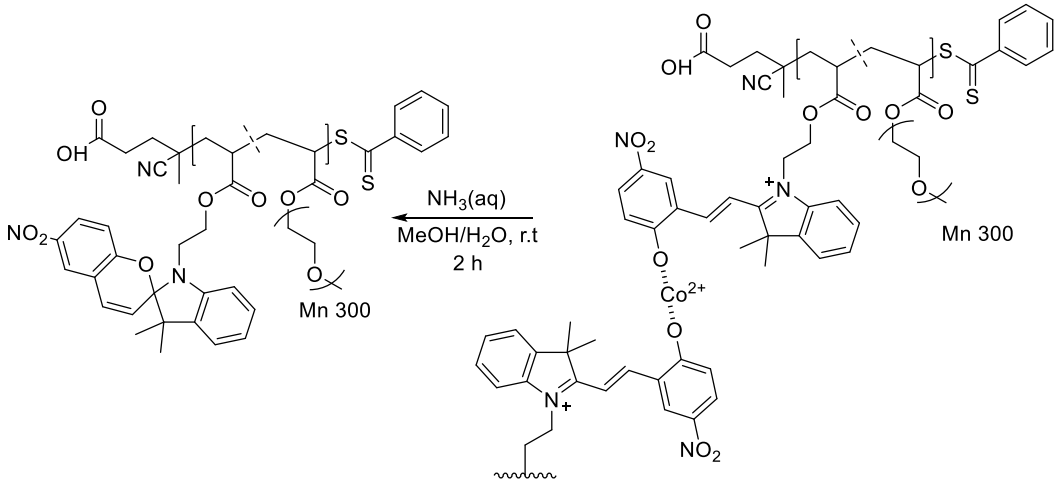

Aqueous ammonia (0.02 mL, 25% in water) was added to 1 mL of water. The diluted ammonia solution was then directly added to the SCNP solution and allowed to stir at room temperature for 2 hours. Aliquots were taken every hour, diluted with THF and analysed via SEC.

8.4 Photoresponsivity

8.4.1 AzoCl$_4$-Au-SCNP NMR switching experiments.

AzoCl$_4$-Au-SCNP-13 was dissolved in $CDCl_3$, added to an NMR tube and placed into a photoreactor. The tube was subsequently irradiated with a red LED (10 W, $\lambda_{1,\,max}$ = 620 nm) for 60 minutes, and the sample analysed via ^{1}H NMR spectroscopy. The same

tube was subsequently irradiated with a blue LED ($\lambda_{1,\ max}$ = 415 nm) for 30 minutes, followed by ^{1}H NMR spectroscopy analysis.

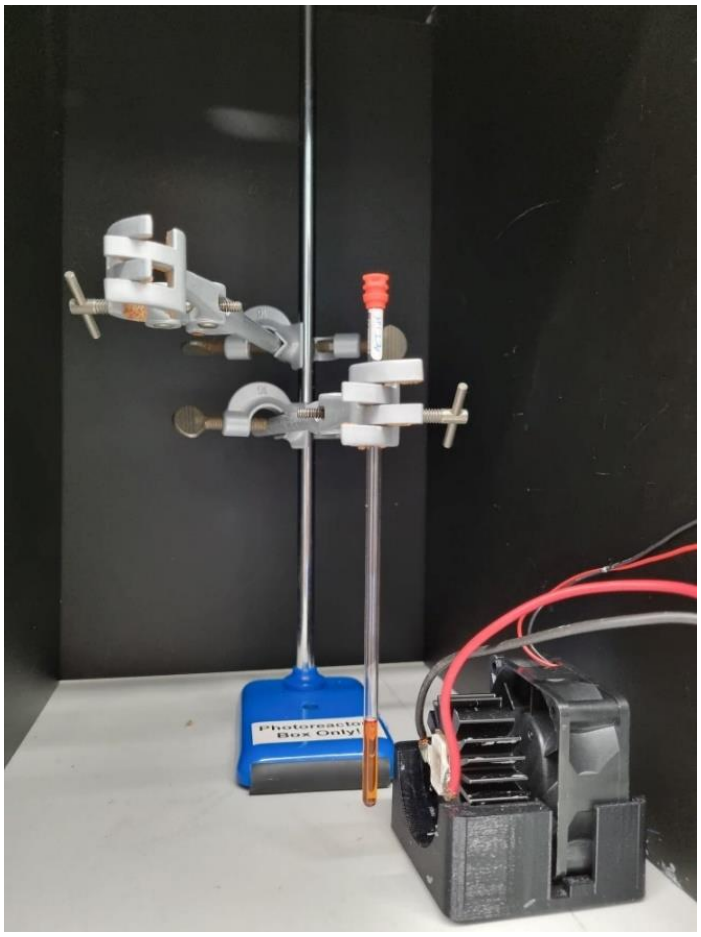

Figure 64 LED Setup for ^{1}H NMR switching and thermal relaxation experiments.

8.4.2 AzoCl$_4$-Au-SCNP SEC switching experiments.

The SCNPs, either **AzoCl$_4$-Au-SCNP-13** or **AzoCl$_4$-Au-SCNP-23** were dissolved in THF, (1 mg.mL^{-1}) placed into an SEC vial and analysed via THF-SEC. After the first injection, the SEC vial was removed and the SCNP sample was poured into a quartz cuvette containing a stir bar. The cuvette was subsequently placed into a photoreactor and irradiated with a red LED (λ_1, max = 620 nm) for 40 minutes, after which it was transferred to an SEC vial and re-analysed. After injection into the SEC, the sample

was again transferred to a quartz cuvette, placed into a photoreactor and irradiated with a blue LED (λ_1, max = 415 nm) for 20 minutes, followed by SEC analysis.

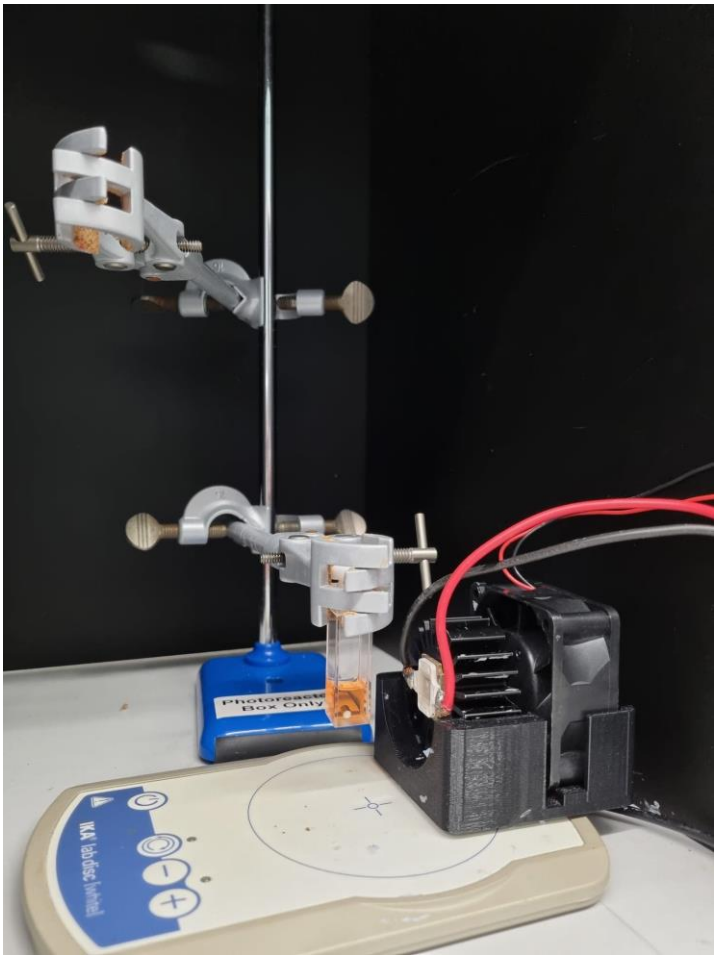

Figure 65 LED Setup for SEC switching and fatigue experiments.

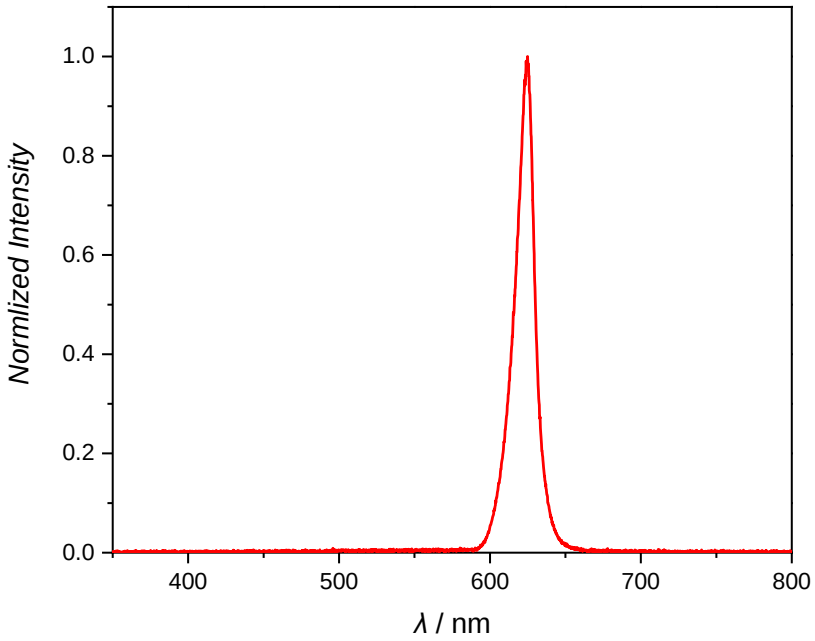

Figure 66 Emission spectrum of the red LED (10 W, λmax = 620 nm) used to switch azobenzene species from the *trans* → *cis* isomer.

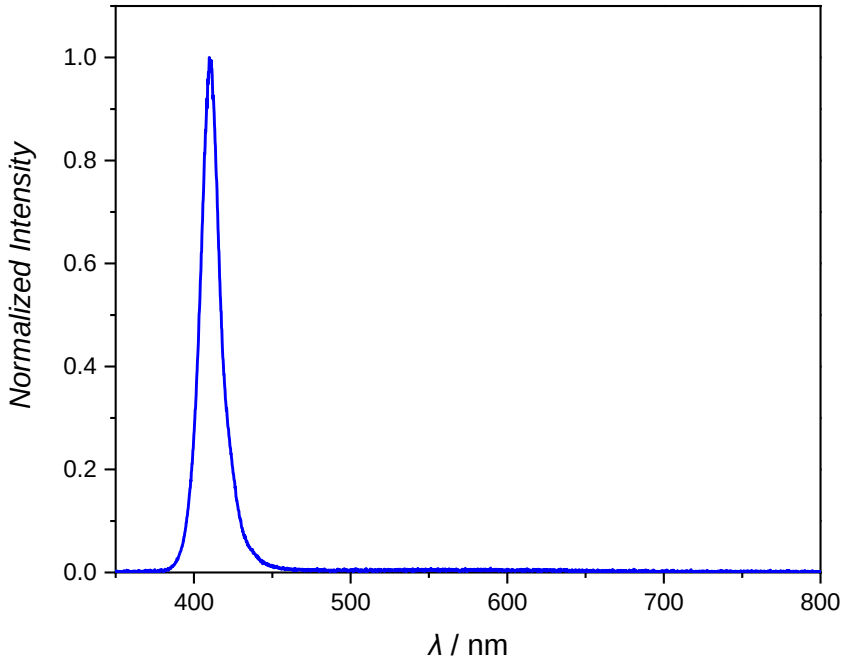

Figure 67 Emission spectrum of the Blue LED (10 W, λmax = 415 nm) used to switch azobenzene species from the *cis* → *trans* isomer.

8.5 Catalysis

8.5.1 Intramolecular Hydroaminations

8.5.1.1 AzoCl$_4$-Au-SCNP-13 Substituted Intramolecular Substrate Catalysis

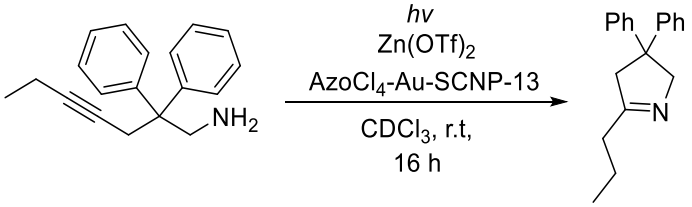

Four stock solutions in anhydrous $CDCl_3$ of $Zn(OTf)_2$ (0.61 mg.mL^{-1}), the intramolecular substrate (131.4 mg.mL^{-1}), **AzoCl$_4$-Au-SCNP-13** (12.9 mg.mL^{-1}) and anisole (10.8 mg.mL^{-1}) were placed into a glove box under the exclusion of oxygen. 0.1 mL of each stock solution and 0.1 mL of anhydrous $CDCl_3$ were added to a gas-tight NMR tube. The NMR tube was subsequently inverted four times, removed from the glovebox, placed in an ice/brine bath and taken out right before insertion into the NMR holder. ^{1}H NMR measurements were recorded at 28 °C every hour for 16 hours. The conversion of the substrate was determined by comparing integrals of the linear starting material, cyclised product and anisole acting as an internal reference.

$$Conversion\ \% = \left(\frac{I_{Product}}{I_{Product} + I_{Starting\ Material}}\right) \times 100$$

8.5.1.2 Ar$_3$PAuCl and Linear Intramolecular Substrate Catalysis

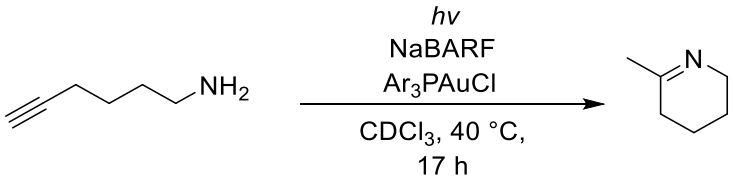

A stock solution of the intramolecular substrate (0.5 mmol.mL^{-1}) and anisole (0.25 mmol.mL^{-1}) were made up in $CDCl_3$. Separately, Ar_3PAuCl and NaBARF were suspended in $CDCl_3$ (0.4 mL) and stirred for 30 minutes to activate the catalyst. 0.1 mL of the catalyst solution was then combined with 0.1 mL aliquots of both the stock solutions in a photo vial. An additional 0.2 mL of $CDCl_3$ was also added. The combined solutions were then briefly mixed before being transferred to an NMR tube and immediately inserted into an NMR holder. ^{1}H NMR measurements were then taken at t = 0, 1, 2, 3, 7, 9, 13, 17 hours. The conversion of the substrate was determined

by comparing integrals of starting material, product and anisole acting as an internal reference.

8.5.2 Inter-molecular Catalysis General Procedure

Stock solutions of the amine (0.5 mmol/mL^{-1}), alkyne (0.5 mmol/mL^{-1}) and anisole (0.25 mmol/mL^{-1}) were made up in $CDCl_3$ (0.25 mmol/mL^{-1}). Separately, Ar_3PAuCl and NaBARF were suspended in $CDCl_3$ (0.4 mL) and stirred for 30 minutes to activate the catalyst. 0.1 mL of the catalyst solution was then combined with 0.1 mL aliquots of all the stock solutions in a photo vial. An additional 0.1 mL of $CDCl_3$ was also added. The combined solutions were then briefly mixed before being transferred to an NMR tube and immediately inserted into an NMR holder. ^1H NMR measurements were then taken at t = 0, 1, 2, 3, 7, 9, 13, 17 hours. The conversion of the substrate was determined by comparing integrals of starting material, product and anisole acting as an internal reference.

9 References

[1] R. Breslow, *Acc. Chem. Res.* **1995**, *28*, 146–153.
[2] A. Stoddart, *Nat. Synth.* **2022**, *1*, 335–335.
[3] P. Vijayaraghavan, S. R. F. Raj, S. G. P. Vincent, in *Agro-Ind. Wastes Feedstock Enzyme Prod.* (Eds.: G.S. Dhillon, S. Kaur), Academic Press, San Diego, **2016**, pp. 95–110.
[4] K. P. Lillerud, U. Olsbye, M. Tilset, *Top. Catal.* **2010**, *53*, 859–868.
[5] In *Homog. Catal.*, **2011**, pp. 51–89.
[6] J. Rubio-Cervilla, E. González, J. A. Pomposo, *Nanomaterials* **2017**, *7*, 341.
[7] H. Rothfuss, N. D. Knöfel, P. W. Roesky, C. Barner-Kowollik, *J. Am. Chem. Soc.* **2018**, *140*, 5875–5881.
[8] P. G. Frank, B. T. Tuten, A. Prasher, D. Chao, E. B. Berda, *Macromol. Rapid Commun.* **2014**, *35*, 249–253.
[9] H. Frisch, F. R. Bloesser, C. Barner-Kowollik, *Angew. Chem. Int. Ed.* **2019**, *58*, 3604–3609.
[10] W. B. Jensen, *J. Chem. Educ.* **2008**, *85*, 624.
[11] C. Stephens, *Br. Dent. J.* **2023**, *234*, 607–610.
[12] L. H. Baekeland, *J. Ind. Eng. Chem.* **1909**, *1*, 149–161.
[13] H. Frey, T. Johann, *Polym. Chem.* **2020**, *11*, 8–14.
[14] In *Princ. Polym.*, **2004**, pp. 1–38.
[15] M. P. Stevens, *Polymer Chemistry: An Introduction*, Oxford University Press, **1999**.
[16] W. H. Carothers, *Chem. Rev.* **1931**, *8*, 353–426.
[17] B. E. Obi, in *Polym. Foams Struct.-Prop.-Perform.* (Ed.: B.E. Obi), William Andrew Publishing, Oxford, **2018**, pp. 17–40.
[18] T. A. Saleh, in *Polym. Hybrid Mater. Nanocomposites* (Ed.: T.A. Saleh), William Andrew Publishing, **2021**, pp. 59–103.
[19] M. U. Kahveci, Y. Yagci, A. Avgeropoulos, C. Tsitsilianis, in *Polym. Sci. Compr. Ref.* (Eds.: K. Matyjaszewski, M. Möller), Elsevier, Amsterdam, **2012**, pp. 455–509.
[20] M. Pitsikalis, in *Ref. Module Chem. Mol. Sci. Chem. Eng.*, Elsevier, **2013**.
[21] D. Braun, *Int. J. Polym. Sci.* **2010**, *2009*, 893234.
[22] M. C. Tanzi, S. Farè, G. Candiani, in *Found. Biomater. Eng.* (Eds.: M.C. Tanzi, S. Farè, G. Candiani), Academic Press, **2019**, pp. 3–103.
[23] J. P. van Hook, A. V. Tobolsky, *J. Polym. Sci.* **1958**, *33*, 429–445.
[24] J. Xia, K. Matyjaszewski, *Macromolecules* **1997**, *30*, 7692–7696.
[25] D. K. Balta, N. Arsu, Y. Yagci, A. K. Sundaresan, S. Jockusch, N. J. Turro, *Macromolecules* **2011**, *44*, 2531–2535.
[26] M. Barsbay, O. Güven, *Radiat. Technol. Synth. Nanoparticles Nanostructured Syst.* **2020**, *169*, 107816.
[27] V. Selvaraj, P. Sakthivel, V. Rajendran, *Ultrason. Sonochem.* **2015**, *22*, 265–271.
[28] G. Moad, in *Polym. Sci. Compr. Ref.* (Eds.: K. Matyjaszewski, M. Möller), Elsevier, Amsterdam, **2012**, pp. 59–118.
[29] G. T. Russell, *Aust. J. Chem.* **2002**, *55*, 399–414.
[30] C. Barner-Kowollik, P. Vana, T. P. Davis, in *Handb. Radic. Polym.*, **2002**, pp. 187–261.

[31] S. Zhu, A. E. Hamielec, *Macromolecules* **1989**, *22*, 3093–3098.
[32] Y. Nakamura, T. Ogihara, S. Hatano, M. Abe, S. Yamago, *Chem. – Eur. J.* **2017**, *23*, 1299–1305.
[33] N. M. Ahmad, F. Heatley, P. A. Lovell, *Macromolecules* **1998**, *31*, 2822–2827.
[34] A. Rudin, P. Choi, in *Elem. Polym. Sci. Eng. Third Ed.* (Eds.: A. Rudin, P. Choi), Academic Press, Boston, **2013**, pp. 341–389.
[35] E. Andrzejewska, in *Three-Dimens. Microfabr. Using Two-Photon Polym.* (Ed.: T. Baldacchini), William Andrew Publishing, Oxford, **2016**, pp. 62–81.
[36] C. Barner-Kowollik, G. T. Russell, *Prog. Polym. Sci.* **2009**, *34*, 1211–1259.
[37] J. W. Gooch, in *Encycl. Dict. Polym.* (Ed.: J.W. Gooch), Springer New York, New York, NY, **2011**, pp. 55–56.
[38] J. Yeow, R. Chapman, A. J. Gormley, C. Boyer, *Chem. Soc. Rev.* **2018**, *47*, 4357–4387.
[39] S. Dworakowska, F. Lorandi, A. Gorczyński, K. Matyjaszewski, *Adv. Sci.* **2022**, *9*, 2106076.
[40] P. Nesvadba, in *Encycl. Radic. Chem. Biol. Mater.*, **2012**.
[41] R. Whitfield, N. P. Truong, A. Anastasaki, *Angew. Chem. Int. Ed.* **2021**, *60*, 19383–19388.
[42] N. A. Lynd, A. J. Meuler, M. A. Hillmyer, *Prog. Polym. Sci.* **2008**, *33*, 875–893.
[43] N. A. Lynd, B. D. Hamilton, M. A. Hillmyer, *J. Polym. Sci. Part B Polym. Phys.* **2007**, *45*, 3386–3393.
[44] E. Chatzigiannakis, J. Vermant, *Soft Matter* **2021**, *17*, 4790–4803.
[45] R. J. Sifri, O. Padilla-Vélez, G. W. Coates, B. P. Fors, *J. Am. Chem. Soc.* **2020**, *142*, 1443–1448.
[46] S. Beck, R. Narain, in *Polym. Sci. Nanotechnol.* (Ed.: R. Narain), Elsevier, **2020**, pp. 21–85.
[47] J. Smid, *J. Polym. Sci. Part Polym. Chem.* **2002**, *40*, 2101–2107.
[48] R. B. Grubbs, R. H. Grubbs, *Macromolecules* **2017**, *50*, 6979–6997.
[49] M. Szwarc, M. Levy, R. Milkovich, *J. Am. Chem. Soc.* **1956**, *78*, 2656–2657.
[50] H. Feng, X. Lu, W. Wang, N.-G. Kang, J. W. Mays, *Polymers* **2017**, *9*, DOI 10.3390/polym9100494.
[51] T. Gleede, E. Rieger, L. Liu, C. Bakkali-Hassani, M. Wagner, S. Carlotti, D. Taton, D. Andrienko, F. R. Wurm, *Macromolecules* **2018**, *51*, 5713–5719.
[52] N. Corrigan, K. Jung, G. Moad, C. J. Hawker, K. Matyjaszewski, C. Boyer, *Prog. Polym. Sci.* **2020**, *111*, 101311.
[53] W. A. Braunecker, K. Matyjaszewski, *50 Years Living Polym.* **2007**, *32*, 93–146.
[54] A. D. Jenkins, R. G. Jones, G. Moad, **2009**, *82*, 483–491.
[55] M. Palà, S. E. Woods, F. L. Hatton, G. Lligadas, *Macromol. Chem. Phys.* **2022**, *223*, 2200005.
[56] D. H. Solomon, *J. Polym. Sci. Part Polym. Chem.* **2005**, *43*, 5748–5764.
[57] J.-S. Wang, K. Matyjaszewski, *J. Am. Chem. Soc.* **1995**, *117*, 5614–5615.
[58] M. Kato, M. Kamigaito, M. Sawamoto, T. Higashimura, *Macromolecules* **1995**, *28*, 1721–1723.
[59] J. Chiefari, Y. K. (Bill) Chong, F. Ercole, J. Krstina, J. Jeffery, T. P. T. Le, R. T. A. Mayadunne, G. F. Meijs, C. L. Moad, G. Moad, E. Rizzardo, S. H. Thang, *Macromolecules* **1998**, *31*, 5559–5562.
[60] V. Hasirci, P. Y. Huri, T. E. Tanir, G. Eke, N. Hasirci, in *Compr. Biomater. II* (Ed.: P. Ducheyne), Elsevier, Oxford, **2017**, pp. 478–506.

[61] J. Nicolas, Y. Guillaneuf, C. Lefay, D. Bertin, D. Gigmes, B. Charleux, *Top. Issue Polym. Chem.* **2013**, *38*, 63–235.
[62] D. Leifert, A. Studer, *Angew. Chem. Int. Ed.* **2020**, *59*, 74–108.
[63] H. Fischer, *Macromolecules* **1997**, *30*, 5666–5672.
[64] A. R. FORRESTER, R. H. THOMSON, *Nature* **1964**, *203*, 74–75.
[65] A. Nilsen, R. Braslau, *J. Polym. Sci. Part Polym. Chem.* **2006**, *44*, 697–717.
[66] H. R. Lamontagne, B. H. Lessard, *ACS Appl. Polym. Mater.* **2020**, *2*, 5327–5344.
[67] R. B. Grubbs, *Polym. Rev.* **2011**, *51*, 104–137.
[68] N. R. Cameron, O. Lagrille, P. A. Lovell, B. Thongnuanchan, *ACS Macro Lett.* **2012**, *1*, 1262–1265.
[69] J. Marchand, L. Autissier, Y. Guillaneuf, J.-L. Couturier, D. Gigmes, D. Bertin, *Aust. J. Chem.* **2010**, *63*, 1237–1244.
[70] C. M. R. Abreu, P. V. Mendonça, A. C. Serra, B. B. Noble, T. Guliashvili, J. Nicolas, M. L. Coote, J. F. J. Coelho, *Macromolecules* **2016**, *49*, 490–498.
[71] E. Guégain, Y. Guillaneuf, J. Nicolas, *Macromol. Rapid Commun.* **2015**, *36*, 1227–1247.
[72] C. Dire, J. Belleney, J. Nicolas, D. Bertin, S. Magnet, B. Charleux, *J. Polym. Sci. Part Polym. Chem.* **2008**, *46*, 6333–6345.
[73] C. Detrembleur, C. Jérôme, J. De Winter, P. Gerbaux, J.-L. Clément, Y. Guillaneuf, D. Gigmes, *Polym. Chem.* **2014**, *5*, 335–340.
[74] O. E. Ansong, S. Jansen, Y. Wei, G. Pomrink, H. Lu, A. Patel, S. Li, *Polym. Int.* **2009**, *58*, 54–65.
[75] X. G. Qiao, Z. Zhou, X. C. Pang, M. Lansalot, E. Bourgeat-Lami, *Polymer* **2019**, *172*, 330–338.
[76] J. Nicolas, C. Dire, L. Mueller, J. Belleney, B. Charleux, S. R. A. Marque, D. Bertin, S. Magnet, L. Couvreur, *Macromolecules* **2006**, *39*, 8274–8282.
[77] A. J. Peltekoff, V. E. Hiller, G. P. Lopinski, O. A. Melville, B. H. Lessard, *ACS Appl. Polym. Mater.* **2019**, *1*, 3210–3221.
[78] A. J. Peltekoff, I. Therrien, B. H. Lessard, *Can. J. Chem. Eng.* **2019**, *97*, 5–16.
[79] O. Garcia-Valdez, T. Brescacin, J. Arredondo, J. Bouchard, P. G. Jessop, P. Champagne, M. F. Cunningham, *Polym. Chem.* **2017**, *8*, 4124–4131.
[80] R. L. Shum, S. R. Liu, A. Caschera, D. A. Foucher, *ACS Appl. Bio Mater.* **2020**, *3*, 4302–4315.
[81] A. Goto, T. Fukuda, *Prog. Polym. Sci.* **2004**, *29*, 329–385.
[82] E. Rizzardo, J. Chiefari, R. T. A. Mayadunne, G. Moad, S. H. Thang, in *Control. Radic. Polym.*, American Chemical Society, **2000**, pp. 278–296.
[83] D. J. Keddie, *Chem. Soc. Rev.* **2014**, *43*, 496–505.
[84] M. Semsarilar, V. Abetz, *Macromol. Chem. Phys.* **2021**, *222*, 2000311.
[85] S. Perrier, *Macromolecules* **2017**, *50*, 7433–7447.
[86] D. J. Keddie, G. Moad, E. Rizzardo, S. H. Thang, *Macromolecules* **2012**, *45*, 5321–5342.
[87] G. Opiyo, J. Jin, *Eur. Polym. J.* **2021**, *159*, 110713.
[88] H. D. Roth, *Angew. Chem. Int. Ed. Engl.* **1989**, *28*, 1193–1207.
[89] D. Tamburini, J. Dyer, M. Vandenbeusch, M. Borla, D. Angelici, M. Aceto, C. Oliva, F. Facchetti, S. Aicardi, P. Davit, M. Gulmini, *Herit. Sci.* **2021**, *9*, 106.
[90] S. Arumugam, S. V. Orski, N. E. Mbua, C. McNitt, G.-J. Boons, J. Locklin, V. V. Popik, **2013**, *85*, 1499–1513.
[91] S. Aubert, M. Bezagu, A. C. Spivey, S. Arseniyadis, *Nat. Rev. Chem.* **2019**, *3*, 706–722.
[92] A. Albini, *Photochem. Photobiol. Sci.* **2016**, *15*, 319–324.

[93] J. W. Draper, *Lond. Edinb. Dublin Philos. Mag. J. Sci.* **1841**, *19*, 195–210.
[94] H. Trommsdorff, *Ann. Pharm.* **1834**, *11*, 190–207.
[95] *Q. J. Chem. Soc. Lond.* **1860**, *12*, 297–392.
[96] W. H. Perkin, *J. Chem. Soc. Trans.* **1881**, *39*, 409–452.
[97] B. J. Feder, *Appl. Opt.* **1981**, *20*, A148–A148.
[98] W.-K. Jo, R. J. Tayade, *Ind. Eng. Chem. Res.* **2014**, *53*, 2073–2084.
[99] B. K. Murkerji, N. R. Dhar, *J. Phys. Chem.* **1931**, *35*, 1790–1794.
[100] M. Planck, *Ann. Phys.* **1901**, *309*, 553–563.
[101] H. G. Pfeiffer, H. A. Liebhafsky, *J. Chem. Educ.* **1951**, *28*, 123.
[102] J. Franck, E. G. Dymond, *Trans. Faraday Soc.* **1926**, *21*, 536–542.
[103] I. R. McNab, in *Encycl. Spectrosc. Spectrom. Third Ed.* (Eds.: J.C. Lindon, G.E. Tranter, D.W. Koppenaal), Academic Press, Oxford, **2017**, pp. 978–987.
[104] M. Hesse, H. Meier, Bernd. Zeeh, *Spectroscopic Methods in Organic Chemistry*, Thieme, Stuttgart ;, **2008**.
[105] V. P. Gupta, in *Princ. Appl. Quantum Chem.* (Ed.: V.P. Gupta), Academic Press, Boston, **2016**, pp. 291–337.
[106] D. J. Nesbitt, R. W. Field, *J. Phys. Chem.* **1996**, *100*, 12735–12756.
[107] Kamm, Philipp, Understanding of Lambda-Orthogonal Photo-Induced Reaction Systems, Queensland University of Technology, **2022**.
[108] J. R. Lakowicz, Ed. , in *Princ. Fluoresc. Spectrosc.*, Springer US, Boston, MA, **2006**, pp. 27–61.
[109] M. Y. Berezin, S. Achilefu, *Chem. Rev.* **2010**, *110*, 2641–2684.
[110] H. Lefebvre-Brion, R. W. Field, in *Spectra Dyn. Diatomic Mol.* (Eds.: H. Lefebvre-Brion, R.W. Field), Academic Press, San Diego, **2004**, pp. 621–739.
[111] T. Morofuji, S. Nagai, Y. Chitose, M. Abe, N. Kano, *Org. Lett.* **2021**, *23*, 6257–6261.
[112] E. G. Leggesse, W.-R. Tong, S. Nachimuthu, T.-Y. Chen, J.-C. Jiang, *J. Photochem. Photobiol. Chem.* **2017**, *347*, 78–85.
[113] E. F. Zwicker, L. I. Grossweiner, N. C. Yang, *J. Am. Chem. Soc.* **1963**, *85*, 2671–2672.
[114] B. P. Kafle, in *Chem. Anal. Mater. Charact. Spectrophotometry* (Ed.: B.P. Kafle), Elsevier, **2020**, pp. 269–296.
[115] J. Volarić, W. Szymanski, N. A. Simeth, B. L. Feringa, *Chem. Soc. Rev.* **2021**, *50*, 12377–12449.
[116] M. Olesińska-Mönch, C. Deo, *Chem. Commun.* **2023**, *59*, 660–669.
[117] S. Crespi, N. A. Simeth, M. Di Donato, S. Doria, C. N. Stindt, M. F. Hilbers, F. L. Kiss, R. Toyoda, S. Wesseling, W. J. Buma, B. L. Feringa, W. Szymański, *Angew. Chem. Int. Ed.* **2021**, *60*, 25290–25295.
[118] S. Axelrod, E. Shakhnovich, R. Gómez-Bombarelli, *ACS Cent. Sci.* **2023**, *9*, 166–176.
[119] F. Nickel, M. Bernien, K. Kraffert, D. Krüger, L. M. Arruda, L. Kipgen, W. Kuch, *Adv. Funct. Mater.* **2017**, *27*, 1702280.
[120] D. J. van Dijken, P. Kovaříček, S. P. Ihrig, S. Hecht, *J. Am. Chem. Soc.* **2015**, *137*, 14982–14991.
[121] J. Sheng, W. Danowski, S. Crespi, A. Guinart, X. Chen, C. Stähler, B. L. Feringa, *Chem. Sci.* **2023**, *14*, 4328–4336.
[122] J. Boelke, S. Hecht, *Adv. Opt. Mater.* **2019**, *7*, 1900404.
[123] M. Jeong, J. Park, Y. Seo, K. Lee, S. Pramanik, S. Ahn, S. Kwon, *Chem. – Eur. J.* **2022**, *28*, e202103972.
[124] S. Wiedbrauk, H. Dube, *Tetrahedron Lett.* **2015**, *56*, 4266–4274.
[125] F. A. Jerca, V. V. Jerca, R. Hoogenboom, *Nat. Rev. Chem.* **2022**, *6*, 51–69.

[126] T. Ueki, Y. Nakamura, T. P. Lodge, M. Watanabe, *Macromolecules* **2012**, *45*, 7566–7573.
[127] S. Yang, J. D. Harris, A. Lambai, L. L. Jeliazkov, G. Mohanty, H. Zeng, A. Priimagi, I. Aprahamian, *J. Am. Chem. Soc.* **2021**, *143*, 16348–16353.
[128] H.-B. Cheng, S. Zhang, E. Bai, X. Cao, J. Wang, J. Qi, J. Liu, J. Zhao, L. Zhang, J. Yoon, *Adv. Mater.* **2022**, *34*, 2108289.
[129] A. S. Kozlenko, I. V. Ozhogin, A. D. Pugachev, M. B. Lukyanova, I. M. El-Sewify, B. S. Lukyanov, *Top. Curr. Chem.* **2023**, *381*, 8.
[130] E. Mitscherlich, *Ann. Pharm.* **1834**, *12*, 305–311.
[131] A. Noble, *Justus Liebigs Ann. Chem.* **1856**, *98*, 253–256.
[132] G. S. HARTLEY, *Nature* **1937**, *140*, 281–281.
[133] Pietro. Bortolus, Sandra. Monti, *J. Phys. Chem.* **1979**, *83*, 648–652.
[134] C.-W. Chang, Y.-C. Lu, T.-T. Wang, E. W.-G. Diau, *J. Am. Chem. Soc.* **2004**, *126*, 10109–10118.
[135] A. A. Beharry, G. A. Woolley, *Chem. Soc. Rev.* **2011**, *40*, 4422–4437.
[136] H. M. D. Bandara, S. C. Burdette, *Chem. Soc. Rev.* **2012**, *41*, 1809–1825.
[137] E. Wagner-Wysiecka, N. Łukasik, J. F. Biernat, E. Luboch, *J. Incl. Phenom. Macrocycl. Chem.* **2018**, *90*, 189–257.
[138] Q. Yu, H. Chen, in *Switch. Responsive Surf. Mater. Biomed. Appl.* (Ed.: Z. Zhang), Woodhead Publishing, Oxford, **2015**, pp. 167–188.
[139] I. C. D. Merritt, D. Jacquemin, M. Vacher, *Phys. Chem. Chem. Phys.* **2021**, *23*, 19155–19165.
[140] N. Siampiringue, G. Guyot, S. Monti, P. Bortolus, *J. Photochem.* **1987**, *37*, 185–188.
[141] S. Malkin, E. Fischer, *J. Phys. Chem.* **1962**, *66*, 2482–2486.
[142] E. Merino, *Chem. Soc. Rev.* **2011**, *40*, 3835–3853.
[143] S. Mehrparvar, Z. N. Scheller, C. Wölper, G. Haberhauer, *J. Am. Chem. Soc.* **2021**, *143*, 19856–19864.
[144] M. Baroncini, J. Groppi, S. Corra, S. Silvi, A. Credi, *Adv. Opt. Mater.* **2019**, *7*, 1900392.
[145] A. Kerckhoffs, K. E. Christensen, M. J. Langton, *Chem. Sci.* **2022**, *13*, 11551–11559.
[146] J. S. Zhu, J. M. Larach, R. J. Tombari, P. W. Gingrich, S. R. Bode, J. R. Tuck, H. T. Warren, J.-H. Son, W. C. Duim, J. C. Fettinger, M. J. Haddadin, D. J. Tantillo, M. J. Kurth, D. E. Olson, *Org. Lett.* **2019**, *21*, 8765–8770.
[147] S. Sun, S. Liang, W.-C. Xu, G. Xu, S. Wu, *Polym. Chem.* **2019**, *10*, 4389–4401.
[148] M. Dong, A. Babalhavaeji, S. Samanta, A. A. Beharry, G. A. Woolley, *Acc. Chem. Res.* **2015**, *48*, 2662–2670.
[149] W.-C. Xu, S. Sun, S. Wu, *Angew. Chem. Int. Ed.* **2019**, *58*, 9712–9740.
[150] D. B. Konrad, G. Savasci, L. Allmendinger, D. Trauner, C. Ochsenfeld, A. M. Ali, *J. Am. Chem. Soc.* **2020**, *142*, 6538–6547.
[151] D. B. Konrad, J. A. Frank, D. Trauner, *Chem. – Eur. J.* **2016**, *22*, 4364–4368.
[152] A. A. Beharry, O. Sadovski, G. A. Woolley, *J. Am. Chem. Soc.* **2011**, *133*, 19684–19687.
[153] J. Volarić, J. Buter, A. M. Schulte, K.-O. van den Berg, E. Santamaría-Aranda, W. Szymanski, B. L. Feringa, *J. Org. Chem.* **2022**, *87*, 14319–14333.
[154] Y. Zhou, L. Wang, H. Zhang, *Polym. Chem.* **2022**, *13*, 3713–3725.
[155] W. Fan, X. Tong, G. Li, Y. Zhao, *Polym. Chem.* **2017**, *8*, 3523–3529.
[156] H. Dong, G. Liu, H. Zhang, *Eur. Polym. J.* **2020**, *135*, 109863.

[157] D. T. Valley, M. Onstott, S. Malyk, A. V. Benderskii, *Langmuir* **2013**, *29*, 11623–11631.
[158] M. Kondo, M. Sugimoto, M. Yamada, Y. Naka, J. Mamiya, M. Kinoshita, A. Shishido, Y. Yu, T. Ikeda, *J. Mater. Chem.* **2010**, *20*, 117–122.
[159] S. Pearson, D. Vitucci, Y. Y. Khine, A. Dag, H. Lu, M. Save, L. Billon, M. H. Stenzel, *Eur. Polym. J.* **2015**, *69*, 616–627.
[160] C. Park, J. Heo, J. Lee, T. Kim, S. Y. Kim, *Polymers* **2020**, *12*, DOI 10.3390/polym12020284.
[161] M. Dowds, D. Bank, J. Strueben, D. P. Soto, F. D. Sönnichsen, F. Renth, F. Temps, A. Staubitz, *J. Mater. Chem. C* **2020**, *8*, 1835–1845.
[162] M. Moniruzzaman, C. J. Sabey, G. F. Fernando, *Polymer* **2007**, *48*, 255–263.
[163] L. Kortekaas, W. R. Browne, *Chem. Soc. Rev.* **2019**, *48*, 3406–3424.
[164] R. Rosario, D. Gust, M. Hayes, J. Springer, A. A. Garcia, *Langmuir* **2003**, *19*, 8801–8806.
[165] R. Rosario, D. Gust, M. Hayes, F. Jahnke, J. Springer, A. A. Garcia, *Langmuir* **2002**, *18*, 8062–8069.
[166] W. Tian, J. Tian, *Dyes Pigments* **2014**, *105*, 66–74.
[167] K. Sakai, Y. Imaizumi, T. Oguchi, H. Sakai, M. Abe, *Langmuir* **2010**, *26*, 9283–9288.
[168] J. D. Steen, D. R. Duijnstee, A. S. Sardjan, J. Martinelli, L. Kortekaas, D. Jacquemin, W. R. Browne, *J. Phys. Chem. A* **2021**, *125*, 3355–3361.
[169] M. Li, Q. Zhang, Y.-N. Zhou, S. Zhu, *Prog. Polym. Sci.* **2018**, *79*, 26–39.
[170] L. Kortekaas, J. Chen, D. Jacquemin, W. R. Browne, *J. Phys. Chem. B* **2018**, *122*, 6423–6430.
[171] M. Wang, G. Liu, H. Gao, C. Su, J. Gao, *Colloids Surf. Physicochem. Eng. Asp.* **2023**, *659*, 130808.
[172] R. Kießwetter, N. Pustet, F. Brandl, A. Mannschreck, *Tetrahedron Asymmetry* **1999**, *10*, 4677–4687.
[173] K. K. Kalninsh, *J. Struct. Chem.* **1998**, *39*, 642–650.
[174] A. A. Khodonov, N. E. Belikov, A. Yu. Lukin, A. V. Laptev, V. A. Barachevsky, S. D. Varfolomeev, O. V. Demina, *Colorants* **2023**, *2*, 264–404.
[175] G. Baillet, G. Giusti, R. Guglielmetti, *J. Photochem. Photobiol. Chem.* **1993**, *70*, 157–161.
[176] M. Sakuragi, K. Aoki, T. Tamaki, K. Ichimura, *Bull. Chem. Soc. Jpn.* **1990**, *63*, 74–79.
[177] K. Arai, Y. Shitara, T. Ohyama, *J. Mater. Chem.* **1996**, *6*, 11–14.
[178] E. I. Balmond, B. K. Tautges, A. L. Faulkner, V. W. Or, B. M. Hodur, J. T. Shaw, A. Y. Louie, *J. Org. Chem.* **2016**, *81*, 8744–8758.
[179] Y. Duan, H. Zhao, C. Xiong, L. Mao, D. Wang, Y. Zheng, *Chin. J. Chem.* **2021**, *39*, 985–998.
[180] V. K. Seiler, K. Robeyns, N. Tumanov, D. Cinčić, J. Wouters, B. Champagne, T. Leyssens, *CrystEngComm* **2019**, *21*, 4925–4933.
[181] Z. Yang, F. Wang, H. Liu, *J. Polym. Res.* **2019**, *26*, 89.
[182] K. M. Trevino, B. K. Tautges, R. Kapre, F. C. Franco Jr, V. W. Or, E. I. Balmond, J. T. Shaw, J. Garcia, A. Y. Louie, *ACS Omega* **2021**, *6*, 10776–10789.
[183] F. Arjmand, Z. Mohamadnia, *Polym. Chem.* **2022**, *13*, 937–945.
[184] R. Klajn, *Chem. Soc. Rev.* **2014**, *43*, 148–184.
[185] A. Perry, C. J. Kousseff, *Beilstein J. Org. Chem.* **2017**, *13*, 1542–1550.
[186] C. Housecroft, A. Sharpe, *Inorganic Chemistry*, Pearson Education, Limited, Harlow, UNITED KINGDOM, **2018**.

[187] Z. Liu, L. Jiang, Z. Liang, Y. Gao, *Tetrahedron* **2006**, *62*, 3214–3220.
[188] J. Filley, M. A. Ibrahim, M. R. Nimlos, A. S. Watt, D. M. Blake, *J. Photochem. Photobiol. Chem.* **1998**, *117*, 193–198.
[189] Y. Wang, Z. Xu, X. Dai, H. Li, S. Yu, W. Meng, *J. Fluoresc.* **2019**, *29*, 569–575.
[190] A. Radu, R. Byrne, N. Alhashimy, M. Fusaro, S. Scarmagnani, D. Diamond, *J. Photochem. Photobiol. Chem.* **2009**, *206*, 109–115.
[191] T. J. Feuerstein, R. Müller, C. Barner-Kowollik, P. W. Roesky, *Inorg. Chem.* **2019**, *58*, 15479–15486.
[192] S. Heng, X. Zhang, J. Pei, A. Adwal, P. Reineck, B. C. Gibson, M. R. Hutchinson, A. D. Abell, *Chem. – Eur. J.* **2019**, *25*, 854–862.
[193] A. V. Chernyshev, V. V. Tkachev, I. A. Rostovtseva, V. A. Lazarenko, A. A. Guda, G. V. Shilov, A. N. Utenyshev, E. V. Solov'eva, E. B. Gaeva, N. A. Voloshin, S. M. Aldoshin, A. V. Metelitsa, *Polyhedron* **2023**, *239*, 116409.
[194] M. Natali, C. Aakeröy, J. Desper, S. Giordani, *Dalton Trans.* **2010**, *39*, 8269–8277.
[195] Y.-L. Lin, Y.-H. Tseng, J.-H. Ho, Y.-F. Chen, J.-T. Chen, *Chem. – Eur. J.* **2021**, *27*, 14981–14988.
[196] Z. Chu, C. Yu, C. Li, *Adv. Funct. Mater.* **2023**, *n/a*, 2307332.
[197] M. Sommer, H. Komber, *Macromol. Rapid Commun.* **2013**, *34*, 57–62.
[198] X. Wang, J. Hu, G. Liu, J. Tian, H. Wang, M. Gong, S. Liu, *J. Am. Chem. Soc.* **2015**, *137*, 15262–15275.
[199] Y. Zhang, M. Cao, B. Yuan, T. Guo, W. Zhang, *Polym. Chem.* **2017**, *8*, 7325–7332.
[200] B. Liu, J. R. Brown, C. Zeng, H. Rajput, R. K. McDonough, P. Westerhoff, T. E. Long, *Polymer* **2023**, *272*, 125827.
[201] C. Gäbert, D. Hicke, J. Bahnemann, L. Mayrhofer, M. Hartlieb, S. Reinicke, *Macromol. Rapid Commun.* **2023**, *44*, 2300108.
[202] L. Zhang, Y. Deng, Y. Tang, C. Xie, Z. Wu, *Mater. Chem. Front.* **2021**, *5*, 3119–3124.
[203] C. P. McCoy, L. Donnelly, D. S. Jones, S. P. Gorman, *Tetrahedron Lett.* **2007**, *48*, 657–661.
[204] H. Eckhardt, A. Bose, V. A. Krongauz, *Polymer* **1987**, *28*, 1959–1964.
[205] N. S. Bell, M. Piech, *Langmuir* **2006**, *22*, 1420–1427.
[206] S. Yagi, S. Nakamura, D. Watanabe, H. Nakazumi, *Dyes Pigments* **2009**, *80*, 98–105.
[207] N. Ye, Y. Pei, Q. Han, L. Y. Jin, *Soft Matter* **2023**, *19*, 1540–1548.
[208] E. S. Epstein, L. Martinetti, R. H. Kollarigowda, O. Carey-De La Torre, J. S. Moore, R. H. Ewoldt, P. V. Braun, *J. Am. Chem. Soc.* **2019**, *141*, 3597–3604.
[209] H. Staudinger, *Berichte Dtsch. Chem. Ges. B Ser.* **1920**, *53*, 1073–1085.
[210] M. Wegner, *SOX Transcr. Factors* **2010**, *42*, 381–390.
[211] M. Raynal, P. Ballester, A. Vidal-Ferran, P. W. N. M. van Leeuwen, *Chem. Soc. Rev.* **2014**, *43*, 1734–1787.
[212] C. M. Goodman, S. Choi, S. Shandler, W. F. DeGrado, *Nat. Chem. Biol.* **2007**, *3*, 252–262.
[213] R. M. Crooks, M. Zhao, L. Sun, V. Chechik, L. K. Yeung, *Acc. Chem. Res.* **2001**, *34*, 181–190.
[214] W. Kuhn, G. Balmer, *J. Polym. Sci.* **1962**, *57*, 311–319.
[215] Von. W. Kuhn, H. Majer, *Makromol. Chem.* **1956**, *18*, 239–253.
[216] J. E. Martin, B. E. Eichinger, *Macromolecules* **1983**, *16*, 1345–1350.
[217] J. E. Martin, B. E. Eichinger, *Macromolecules* **1983**, *16*, 1350–1358.

[218] G. Allen, J. Burgess, S. F. Edwards, D. J. Walsh, *Proc. R. Soc. Lond. Math. Phys. Sci.* **1997**, *334*, 453–463.
[219] M. Antonietti, H. Sillescu, *Macromolecules* **1986**, *19*, 798–803.
[220] M. Antonietti, H. Sillescu, M. Schmidt, H. Schuch, *Macromolecules* **1988**, *21*, 736–742.
[221] Y. Valasatava, A. Rosato, N. Furnham, J. M. Thornton, C. Andreini, *J. Inorg. Biochem.* **2018**, *179*, 40–53.
[222] A. Sanchez-Sanchez, A. Arbe, J. Colmenero, J. A. Pomposo, *ACS Macro Lett.* **2014**, *3*, 439–443.
[223] S. Mavila, I. Rozenberg, N. G. Lemcoff, *Chem. Sci.* **2014**, *5*, 4196–4203.
[224] J. A. Pomposo, A. J. Moreno, A. Arbe, J. Colmenero, *ACS Omega* **2018**, *3*, 8648–8654.
[225] J. T. Offenloch, J. Willenbacher, P. Tzvetkova, C. Heiler, H. Mutlu, C. Barner-Kowollik, *Chem. Commun.* **2017**, *53*, 775–778.
[226] S. Thanneeru, J. K. Nganga, A. S. Amin, B. Liu, L. Jin, A. M. Angeles-Boza, J. He, *ChemCatChem* **2017**, *9*, 1157–1162.
[227] G. Li, F. Tao, L. Wang, Y. Li, R. Bai, *Polym. Ion. Liq.* **2014**, *55*, 3696–3702.
[228] S. Mounicou, J. Szpunar, R. Lobinski, *Chem. Soc. Rev.* **2009**, *38*, 1119–1138.
[229] O. Altintas, C. Barner-Kowollik, *Macromol. Rapid Commun.* **2016**, *37*, 29–46.
[230] B. T. Tuten, D. Chao, C. K. Lyon, E. B. Berda, *Polym. Chem.* **2012**, *3*, 3068–3071.
[231] L. Oria, R. Aguado, J. A. Pomposo, J. Colmenero, *Adv. Mater.* **2010**, *22*, 3038–3041.
[232] C. S. Mahon, C. J. McGurk, S. M. D. Watson, M. A. Fascione, C. Sakonsinsiri, W. B. Turnbull, D. A. Fulton, *Angew. Chem. Int. Ed.* **2017**, *56*, 12913–12918.
[233] E. Harth, B. V. Horn, V. Y. Lee, D. S. Germack, C. P. Gonzales, R. D. Miller, C. J. Hawker, *J. Am. Chem. Soc.* **2002**, *124*, 8653–8660.
[234] A. Sanchez-Sanchez, I. Asenjo-Sanz, L. Buruaga, J. A. Pomposo, *Macromol. Rapid Commun.* **2012**, *33*, 1262–1267.
[235] A. E. Cherian, F. C. Sun, S. S. Sheiko, G. W. Coates, *J. Am. Chem. Soc.* **2007**, *129*, 11350–11351.
[236] H. Frisch, J. P. Menzel, F. R. Bloesser, D. E. Marschner, K. Mundsinger, C. Barner-Kowollik, *J. Am. Chem. Soc.* **2018**, *140*, 9551–9557.
[237] J. He, L. Tremblay, S. Lacelle, Y. Zhao, *Soft Matter* **2011**, *7*, 2380–2386.
[238] A. R. de Luzuriaga, N. Ormategui, H. J. Grande, I. Odriozola, J. A. Pomposo, I. Loinaz, *Macromol. Rapid Commun.* **2008**, *29*, 1156–1160.
[239] O. Altintas, E. Lejeune, P. Gerstel, C. Barner-Kowollik, *Polym. Chem.* **2012**, *3*, 640–651.
[240] O. Altintas, P. Gerstel, N. Dingenouts, C. Barner-Kowollik, *Chem. Commun.* **2010**, *46*, 6291–6293.
[241] C. Heiler, J. T. Offenloch, E. Blasco, C. Barner-Kowollik, *ACS Macro Lett.* **2017**, *6*, 56–61.
[242] O. Altintas, J. Willenbacher, K. N. R. Wuest, K. K. Oehlenschlaeger, P. Krolla-Sidenstein, H. Gliemann, C. Barner-Kowollik, *Macromolecules* **2013**, *46*, 8092–8101.
[243] I. Perez-Baena, I. Loinaz, D. Padro, I. García, H. J. Grande, I. Odriozola, *J. Mater. Chem.* **2010**, *20*, 6916–6922.
[244] A. Sanchez-Sanchez, D. A. Fulton, J. A. Pomposo, *Chem. Commun.* **2014**, *50*, 1871–1874.

[245] N. D. Knöfel, H. Rothfuss, J. Willenbacher, C. Barner-Kowollik, P. W. Roesky, *Angew. Chem. Int. Ed.* **2017**, *56*, 4950–4954.
[246] J. L. Bohlen, B. Kulendran, H. Rothfuss, C. Barner-Kowollik, P. W. Roesky, *Polym. Chem.* **2021**, *12*, 4016–4021.
[247] E. H. H. Wong, S. J. Lam, E. Nam, G. G. Qiao, *ACS Macro Lett.* **2014**, *3*, 524–528.
[248] O. Galant, H. B. Donmez, C. Barner-Kowollik, C. E. Diesendruck, *Angew. Chem. Int. Ed.* **2021**, *60*, 2042–2046.
[249] F. R. Bloesser, S. L. Walden, I. M. Irshadeen, L. C. Chambers, C. Barner-Kowollik, *Chem. Commun.* **2021**, *57*, 5203–5206.
[250] R. Evans, *Prog. Nucl. Magn. Reson. Spectrosc.* **2020**, *117*, 33–69.
[251] F. Genc, G. Temel, B. A. Temel, *Polymer* **2020**, *201*, 122659.
[252] E. B. Berda, E. J. Foster, E. W. Meijer, *Macromolecules* **2010**, *43*, 1430–1437.
[253] J. Wen, L. Yuan, Y. Yang, L. Liu, H. Zhao, *ACS Macro Lett.* **2013**, *2*, 100–106.
[254] R. Upadhya, N. S. Murthy, C. L. Hoop, S. Kosuri, V. Nanda, J. Kohn, J. Baum, A. J. Gormley, *Macromolecules* **2019**, *52*, 8295–8304.
[255] J. Engelke, B. T. Tuten, R. Schweins, H. Komber, L. Barner, L. Plüschke, C. Barner-Kowollik, A. Lederer, *Polym. Chem.* **2020**, *11*, 6559–6578.
[256] A. Sanchez-Sanchez, S. Akbari, A. Etxeberria, A. Arbe, U. Gasser, A. J. Moreno, J. Colmenero, J. A. Pomposo, *ACS Macro Lett.* **2013**, *2*, 491–495.
[257] A. Sanchez-Sanchez, S. Akbari, A. J. Moreno, F. L. Verso, A. Arbe, J. Colmenero, J. A. Pomposo, *Macromol. Rapid Commun.* **2013**, *34*, 1681–1686.
[258] E. Verde-Sesto, A. Arbe, A. J. Moreno, D. Cangialosi, A. Alegría, J. Colmenero, J. A. Pomposo, *Mater. Horiz.* **2020**, *7*, 2292–2313.
[259] S. Basasoro, M. Gonzalez-Burgos, A. J. Moreno, F. L. Verso, A. Arbe, J. Colmenero, J. A. Pomposo, *Macromol. Rapid Commun.* **2016**, *37*, 1060–1065.
[260] R. A. Patel, S. Colmenares, M. A. Webb, *ACS Polym. Au* **2023**, DOI 10.1021/acspolymersau.3c00007.
[261] H. Rothfuss, N. D. Knöfel, P. Tzvetkova, N. C. Michenfelder, S. Baraban, A.-N. Unterreiner, P. W. Roesky, C. Barner-Kowollik, *Chem. – Eur. J.* **2018**, *24*, 17475–17486.
[262] S. Thanneeru, S. S. Duay, L. Jin, Y. Fu, A. M. Angeles-Boza, J. He, *ACS Macro Lett.* **2017**, *6*, 652–656.
[263] Y. Li, J. Wen, M. Qin, Y. Cao, H. Ma, W. Wang, *ACS Biomater. Sci. Eng.* **2017**, *3*, 979–989.
[264] J. Jeong, Y.-J. Lee, B. Kim, B. Kim, K.-S. Jung, H. Paik, *Polym. Chem.* **2015**, *6*, 3392–3397.
[265] M. A. Reith, S. Kardas, C. Mertens, M. Fossépré, M. Surin, J. Steinkoenig, F. E. Du Prez, *Polym. Chem.* **2021**, *12*, 4924–4933.
[266] N. D. Knöfel, H. Rothfuss, P. Tzvetkova, B. Kulendran, C. Barner-Kowollik, P. W. Roesky, *Chem. Sci.* **2020**, *11*, 10331–10336.
[267] A. Sanchez-Sanchez, A. Arbe, J. Kohlbrecher, J. Colmenero, J. A. Pomposo, *Macromol. Rapid Commun.* **2015**, *36*, 1592–1597.
[268] Z. Hu, H. Pu, *Eur. Polym. J.* **2021**, *143*, 110194.
[269] S. Gillhuber, J. O. Holloway, H. Frisch, F. Feist, F. Weigend, C. Barner-Kowollik, P. W. Roesky, *Chem. Commun.* **2023**, *59*, 4672–4675.
[270] W. Wang, J. Wang, S. Li, C. Li, R. Tan, D. Yin, *Green Chem.* **2020**, DOI 10.1039/D0GC00949K.
[271] Á. Molnár, A. Papp, *Coord. Chem. Rev.* **2017**, *349*, 1–65.

[272] M. Q. Lombardo Arianna; Chiarucci, Michel; Trombini, Claudio, *Synlett* **2010**, *2010*, 1746–1765.
[273] M. Lombardo, M. Chiarucci, C. Trombini, *Green Chem.* **2009**, *11*, 574–579.
[274] R. Amengual, E. Genin, V. Michelet, M. Savignac, J.-P. Genêt, *Adv. Synth. Catal.* **2002**, *344*, 393–398.
[275] Y. S. Wagh, D. N. Sawant, K. P. Dhake, B. M. Bhanage, *Catal. Sci. Technol.* **2012**, *2*, 835–840.
[276] R. Lambert, A.-L. Wirotius, D. Taton, *ACS Macro Lett.* **2017**, *6*, 489–494.
[277] S. Garmendia, A. P. Dove, D. Taton, R. K. O'Reilly, *Polym. Chem.* **2018**, *9*, 5286–5294.
[278] R. H. Crabtree, *Chem. Rev.* **2015**, *115*, 127–150.
[279] Y. Azuma, T. Terashima, M. Sawamoto, *ACS Macro Lett.* **2017**, *6*, 830–835.
[280] J. Chen, K. Li, S. E. Bonson, S. C. Zimmerman, *J. Am. Chem. Soc.* **2020**, *142*, 13966–13973.
[281] C. A. Tooley, S. Pazicni, E. B. Berda, *Polym. Chem.* **2015**, *6*, 7646–7651.
[282] J. Willenbacher, O. Altintas, V. Trouillet, N. Knöfel, M. J. Monteiro, P. W. Roesky, C. Barner-Kowollik, *Polym. Chem.* **2015**, *6*, 4358–4365.
[283] T. Terashima, T. Mes, T. F. A. De Greef, M. A. J. Gillissen, P. Besenius, A. R. A. Palmans, E. W. Meijer, *J. Am. Chem. Soc.* **2011**, *133*, 4742–4745.
[284] Y. Bai, X. Feng, H. Xing, Y. Xu, B. K. Kim, N. Baig, T. Zhou, A. A. Gewirth, Y. Lu, E. Oldfield, S. C. Zimmerman, *J. Am. Chem. Soc.* **2016**, *138*, 11077–11080.
[285] R. Dorel, A. M. Echavarren, *Chem. Rev.* **2015**, *115*, 9028–9072.
[286] K. Mundsinger, A. Izuagbe, B. Tuten, P. Roesky, C. Barner-Kowollik, *Angew. Chem. Int. Ed.* **2023**, *n/a*, e202311734.
[287] Gü. Wulff, J. Liu, *Acc. Chem. Res.* **2012**, *45*, 239–247.
[288] G. Wulff, B.-O. Chong, U. Kolb, *Angew. Chem. Int. Ed.* **2006**, *45*, 2955–2958.
[289] I. Perez-Baena, F. Barroso-Bujans, U. Gasser, A. Arbe, A. J. Moreno, J. Colmenero, J. A. Pomposo, *ACS Macro Lett.* **2013**, *2*, 775–779.
[290] A. Sathyan, S. Croke, A. M. Pérez-López, B. F. M. de Waal, A. Unciti-Broceta, A. R. A. Palmans, *Mol. Syst. Des. Eng.* **2022**, *7*, 1736–1748.
[291] E. S. Garcia, T. M. Xiong, A. Lifschitz, S. C. Zimmerman, *Polym. Chem.* **2021**, *12*, 6755–6760.
[292] H. Frisch, B. T. Tuten, C. Barner-Kowollik, *Isr. J. Chem.* **2020**, *60*, 86–99.
[293] K. Mundsinger, B. T. Tuten, L. Wang, K. Neubauer, C. Kropf, M. L. O'Mara, C. Barner-Kowollik, *Angew. Chem. Int. Ed.* **2023**, *62*, e202302995.
[294] J. J. Piane, L. E. Chamberlain, S. Huss, L. T. Alameda, A. C. Hoover, E. Elacqua, *ACS Catal.* **2020**, *10*, 13251–13256.
[295] J. J. Piane, S. Huss, L. T. Alameda, S. J. Koehler, L. E. Chamberlain, M. J. Schubach, A. C. Hoover, E. Elacqua, *J. Polym. Sci.* **2021**, *59*, 2867–2877.
[296] L. C. Chambers, C. Barner-Kowollik, L. Barner, L. Michalek, H. Frisch, *ACS Macro Lett.* **2022**, *11*, 532–536.
[297] P. H. Maag, F. Feist, V. X. Truong, H. Frisch, P. W. Roesky, C. Barner-Kowollik, *Angew. Chem. Int. Ed.* **2023**, *62*, e202309259.
[298] D. Kodura, H. A. Houck, F. R. Bloesser, A. S. Goldmann, F. E. Du Prez, H. Frisch, C. Barner-Kowollik, *Chem. Sci.* **2021**, *12*, 1302–1310.
[299] R. Gu, J. Lamas, S. K. Rastogi, X. Li, W. Brittain, S. Zauscher, *Colloids Surf. B Biointerfaces* **2015**, *135*, 126–132.
[300] V. Wang, J. Kim, J. Kim, S. W. Lee, K. T. Kim, *Polym. Chem.* **2021**, *12*, 5027–5036.
[301] W. Wen, A. Chen, *Polym. Chem.* **2021**, *12*, 2447–2456.

[302] H. Yu, *J. Mater. Chem. C* **2014**, *2*, 3047–3054.
[303] J.-F. Gohy, Y. Zhao, *Chem. Soc. Rev.* **2013**, *42*, 7117–7129.
[304] L. Greb, H. Mutlu, C. Barner-Kowollik, J.-M. Lehn, *J. Am. Chem. Soc.* **2016**, *138*, 1142–1145.
[305] I. Guzman, M. Gruebele, *J. Phys. Chem. B* **2014**, *118*, 8459–8470.
[306] D. M. Mitrea, R. W. Kriwacki, *FEBS Lett.* **2013**, *587*, 1081–1088.
[307] A. M. Hanlon, C. K. Lyon, E. B. Berda, *Macromolecules* **2016**, *49*, 2–14.
[308] C. K. Lyon, A. Prasher, A. M. Hanlon, B. T. Tuten, C. A. Tooley, P. G. Frank, E. B. Berda, *Polym. Chem.* **2015**, *6*, 181–197.
[309] Lutz Jean-François, Ouchi Makoto, Liu David R., Sawamoto Mitsuo, *Science* **2013**, *341*, 1238149.
[310] M. J. Austin, A. M. Rosales, *Biomater. Sci.* **2019**, *7*, 490–505.
[311] B. T. Tuten, D. Chao, C. K. Lyon, E. B. Berda, *Polym. Chem.* **2012**, *3*, 3068–3071.
[312] T. S. Fischer, D. Schulze-Sünninghausen, B. Luy, O. Altintas, C. Barner-Kowollik, *Angew. Chem. Int. Ed.* **2016**, *55*, 11276–11280.
[313] D. E. Whitaker, C. S. Mahon, D. A. Fulton, *Angew. Chem. Int. Ed.* **2013**, *52*, 956–959.
[314] G. Yilmaz, V. Uzunova, R. Napier, C. R. Becer, *Biomacromolecules* **2018**, *19*, 3040–3047.
[315] N. Hosono, A. M. Kushner, J. Chung, A. R. A. Palmans, Z. Guan, E. W. Meijer, *J. Am. Chem. Soc.* **2015**, *137*, 6880–6888.
[316] J. P. Cole, J. J. Lessard, K. J. Rodriguez, A. M. Hanlon, E. K. Reville, J. P. Mancinelli, E. B. Berda, *Polym. Chem.* **2017**, *8*, 5829–5835.
[317] Y. Gao, R. Guo, Y. Feng, L. Zhang, C. Wang, J. Song, T. Jiao, J. Zhou, Q. Peng, *ACS Omega* **2018**, *3*, 11663–11672.
[318] L. D. Thai, T. R. Guimaraes, L. C. Chambers, J. A. Kammerer, D. Golberg, H. Mutlu, C. Barner-Kowollik, *J. Am. Chem. Soc.* **2023**, *145*, 14748–14755.
[319] J. ter Schiphorst, M. van den Broek, T. de Koning, J. N. Murphy, A. P. H. J. Schenning, A. C. C. Esteves, *J. Mater. Chem. A* **2016**, *4*, 8676–8681.
[320] K. Shimizu, R. Métivier, S. Kobatake, *J. Photochem. Photobiol. Chem.* **2020**, *390*, 112341.
[321] X. Hou, S. Guan, T. Qu, X. Wu, D. Wang, A. Chen, Z. Yang, *ACS Macro Lett.* **2018**, *7*, 1475–1479.
[322] S. Guan, Z. Deng, T. Huang, W. Wen, Y. Zhao, A. Chen, *ACS Macro Lett.* **2019**, *8*, 460–465.
[323] J. Shin, J. Sung, M. Kang, X. Xie, B. Lee, K. M. Lee, T. J. White, C. Leal, N. R. Sottos, P. V. Braun, D. G. Cahill, *Proc. Natl. Acad. Sci.* **2019**, *116*, 5973.
[324] Y. Zhou, M. Chen, Q. Ban, Z. Zhang, S. Shuang, K. Koynov, H.-J. Butt, J. Kong, S. Wu, *ACS Macro Lett.* **2019**, *8*, 968–972.
[325] A. S. Kuenstler, K. D. Clark, J. Read de Alaniz, R. C. Hayward, *ACS Macro Lett.* **2020**, *9*, 902–909.
[326] B. Yang, Y. Zhao, Y. Wei, C. Fu, L. Tao, *Polym Chem* **2015**, *6*, 8233–8239.
[327] Y. Chu-Farseeva, N. Mustafa, A. Poulsen, E. C. Tan, J. J. Y. Yen, W. J. Chng, B. W. Dymock, *Eur. J. Med. Chem.* **2018**, *158*, 593–619.
[328] Z. Ge, Z. Yang, J. Liang, D. Dong, M. Zhu, *ChemBioChem* **2019**, *20*, 2916–2920.
[329] Q. Cheng, Y. Zhang, T. Luan, Z. Wang, R. Tang, P. Xing, A. Hao, *ChemPlusChem* **2019**, *84*, 328–332.
[330] X. T. Xia Patrick H., *Synlett* **2015**, *26*, 1737–1743.

[331] M. H. Furigay, M. M. Boucher, N. A. Mizgier, C. S. Brindle, *J. Vis. Exp. JoVE* **2018**, 57639.
[332] N. Azizi, S. Dezfooli, M. M. Hashemi, *Comptes Rendus Chim.* **2013**, *16*, 1098–1102.
[333] A. Dömling, I. Ugi, *Angew. Chem. Int. Ed.* **2000**, *39*, 3168–3210.
[334] S. Marcaccini, T. Torroba, *Nat. Protoc.* **2007**, *2*, 632–639.
[335] C. E. A. de Melo, C. R. Nicoleti, L. G. Nandi, F. S. S. Schneider, R. da S. Oliboni, G. F. Caramori, V. G. Machado, *J. Mol. Liq.* **2020**, *301*, 112330.
[336] A. Kerckhoffs, Z. Bo, S. E. Penty, F. Duarte, M. J. Langton, *Org. Biomol. Chem.* **2021**, *19*, 9058–9067.
[337] R. Madhavachary, T. Zarganes-Tzitzikas, P. Patil, K. Kurpiewska, J. Kalinowska-Tłuścik, A. Dömling, *ACS Comb. Sci.* **2018**, *20*, 192–196.
[338] J.-C. AU - Bradley, K. AU - Baig Mirza, T. AU - Osborne, A. AU - Wiliams, K. AU - Owens, *J. Vis. Exp.* **2008**, e942.
[339] C. C. Epley, M. D. Love, A. J. Morris, *Inorg. Chem.* **2017**, *56*, 13777–13784.
[340] M. J. Harper, E. J. Emmett, J. F. Bower, C. A. Russell, *J. Am. Chem. Soc.* **2017**, *139*, 12386–12389.
[341] S. Feng, Q. Wang, Y. Gao, Y. Huang, F.-L. Qing, *J. Appl. Polym. Sci.* **2009**, *114*, 2071–2078.
[342] A. P. P. Kröger, J.-W. D. Paats, R. J. E. A. Boonen, N. M. Hamelmann, J. M. J. Paulusse, *Polym. Chem.* **2020**, *11*, 6056–6065.
[343] Q. Liu, X. Luo, S. Wei, Y. Wang, J. Zhu, Y. Liu, F. Quan, M. Zhang, C. Xia, *Tetrahedron Lett.* **2019**, *60*, 1715–1719.
[344] M. D. Thum, D. C. Ratchford, R. Casalini, J. H. Wynne, J. G. Lundin, *ACS Appl. Nano Mater.* **2021**, *4*, 297–304.
[345] D. Dattler, G. Fuks, J. Heiser, E. Moulin, A. Perrot, X. Yao, N. Giuseppone, *Chem. Rev.* **2020**, *120*, 310–433.
[346] K. E. Lee, J. U. Lee, D. G. Seong, M.-K. Um, W. Lee, *J. Phys. Chem. C* **2016**, *120*, 23172–23179.
[347] C. J. Barrett, J. Mamiya, K. G. Yager, T. Ikeda, *Soft Matter* **2007**, *3*, 1249–1261.
[348] E. Merino, M. Ribagorda, *Beilstein J. Org. Chem.* **2012**, *8*, 1071–1090.
[349] T. E. Müller, K. C. Hultzsch, M. Yus, F. Foubelo, M. Tada, *Chem. Rev.* **2008**, *108*, 3795–3892.
[350] H.-J. Jiang, K. Liu, J. Yu, L. Zhang, L.-Z. Gong, *Angew. Chem. Int. Ed.* **2017**, *56*, 11931–11935.
[351] J. Kaneti, A. J. Kirby, A. H. Koedjikov, I. G. Pojarlieff, *Org. Biomol. Chem.* **2004**, *2*, 1098–1103.
[352] B. Zelenay, P. Munton, X. Tian, S. Díez-González, *Eur. J. Org. Chem.* **2019**, *2019*, 4725–4730.
[353] S. Kramer, K. Dooleweerdt, A. T. Lindhardt, M. Rottländer, T. Skrydstrup, *Org. Lett.* **2009**, *11*, 4208–4211.
[354] H. Duan, S. Sengupta, J. L. Petersen, N. G. Akhmedov, X. Shi, *J. Am. Chem. Soc.* **2009**, *131*, 12100–12102.
[355] T. Scherpf, C. Schwarz, L. T. Scharf, J.-A. Zur, A. Helbig, V. H. Gessner, *Angew. Chem. Int. Ed.* **2018**, *57*, 12859–12864.
[356] C. H. Leung, M. Baron, A. Biffis, *Catalysts* **2020**, *10*, DOI 10.3390/catal10101210.
[357] I. Asenjo-Sanz, T. Claros, E. González, J. Pinacho-Olaciregui, E. Verde-Sesto, J. A. Pomposo, *Mater. Lett.* **2021**, *304*, 130622.

[358] M. A. Sanders, S. S. Chittari, N. Sherman, J. R. Foley, A. S. Knight, *J. Am. Chem. Soc.* **2023**, *145*, 9686–9692.
[359] E. C. Constable, C. E. Housecroft, *Molecules* **2019**, *24*, DOI 10.3390/molecules24213951.
[360] N. D. Knöfel, H. Rothfuss, C. Barner-Kowollik, P. W. Roesky, *Polym. Chem.* **2019**, *10*, 86–93.
[361] I. Mohamed Irshadeen, V. X. Truong, H. Frisch, C. Barner-Kowollik, *Chem. Commun.* **2022**, *58*, 12975–12978.
[362] *ADVANCED INORGANIC CHEMISTRY, 6TH ED*, Wiley India Pvt. Limited, **2007**.
[363] C. Gouda, D. Barik, C. Maitra, K.-C. Liang, F.-C. Ho, V. Srinivasadesikan, S. Chandran, S.-P. Wu, M.-C. Lin, H.-C. Lin, *J. Mater. Chem. C* **2021**, *9*, 2321–2333.
[364] A. A. Vasilev, S. Baluschev, S. Ilieva, D. Cheshmedzhieva, *Photochem* **2023**, *3*, 301–312.
[365] J. Chen, W. Zhong, Y. Tang, Z. Wu, Y. Li, P. Yi, J. Jiang, *Macromolecules* **2015**, *48*, 3500–3508.
[366] J. Piard, *J. Chem. Educ.* **2014**, *91*, 2105–2111.
[367] A. Radu, S. Scarmagnani, R. Byrne, C. Slater, K. Tong Lau, D. Diamond, *J. Phys. Appl. Phys.* **2007**, *40*, 7238.
[368] J. Whelan, J. T. C. Wojtyk, E. Buncel, *Chem. Mater.* **2008**, *20*, 3797–3799.
[369] H. Malik, T. Halbritter, A. Heckel, T. G. Gopakumar, *J. Phys. Chem. Lett.* **2021**, *12*, 5463–5468.
[370] C. Kaiser, T. Halbritter, A. Heckel, J. Wachtveitl, *ChemistrySelect* **2017**, *2*, 4111–4123.
[371] M. Natali, S. Giordani, *Org. Biomol. Chem.* **2012**, *10*, 1162–1171.
[372] K. H. Fries, J. D. Driskell, S. Samanta, J. Locklin, *Anal. Chem.* **2010**, *82*, 3306–3314.
[373] S. Chen, H. Liu, H. Cui, J. Hu, H. Cai, *Des. Monomers Polym.* **2015**, *18*, 574–582.
[374] K. H. Fries, J. D. Driskell, G. R. Sheppard, J. Locklin, *Langmuir* **2011**, *27*, 12253–12260.
[375] H. Cui, H. Liu, S. Chen, R. Wang, *Dyes Pigments* **2015**, *115*, 50–57.
[376] J. Chen, S. K. Spear, J. G. Huddleston, R. D. Rogers, *Green Chem.* **2005**, *7*, 64–82.
[377] V. Malatesta, C. Neri, M. L. Wis, L. Montanari, R. Millini, *J. Am. Chem. Soc.* **1997**, *119*, 3451–3455.
[378] A. Perry, *Org. Biomol. Chem.* **2019**, *17*, 4825–4834.
[379] A. Perry, D. Miles, *Tetrahedron Lett.* **2016**, *57*, 5788–5793.
[380] W. Wang, G. B. Hammond, B. Xu, *J. Am. Chem. Soc.* **2012**, *134*, 5697–5705.
[381] A. J. Young, M. Sauer, G. M. D. M. Rubio, A. Sato, A. Foelske, C. J. Serpell, J. M. Chin, M. R. Reithofer, *Nanoscale* **2019**, *11*, 8327–8333.
[382] T. T. Dang, F. Boeck, L. Hintermann, *J. Org. Chem.* **2011**, *76*, 9353–9361.
[383] S. Basasoro, M. Gonzalez-Burgos, A. J. Moreno, F. L. Verso, A. Arbe, J. Colmenero, J. A. Pomposo, *Macromol. Rapid Commun.* **2016**, *37*, 1060–1065.
[384] C. Zhao, J. Lu, X. X. Zhu, *ACS Appl. Polym. Mater.* **2020**, *2*, 256–262.
[385] Q. Zhang, P. Schattling, P. Theato, R. Hoogenboom, *Eur. Polym. J.* **2015**, *62*, 435–441.
[386] S. Wiktorowicz, H. Tenhu, V. Aseyev, *Macromolecules* **2013**, *46*, 6209–6216.
[387] T. Ueki, Y. Nakamura, A. Yamaguchi, K. Niitsuma, T. P. Lodge, M. Watanabe, *Macromolecules* **2011**, *44*, 6908–6914.

[388] M. Rumyantsev, S. Rumyantsev, *Polymer* **2018**, *136*, 101–108.
[389] M. Liu, W. Wenzel, H. Frisch, *Polym. Chem.* **2020**, *11*, 6616–6623.
[390] I. F. Reis, F. B. Miguez, C. A. A. Vargas, T. G. Menzonatto, I. M. S. Silva, T. Verano-Braga, J. F. Lopes, T. A. S. Brandão, F. B. De Sousa, *ACS Appl. Mater. Interfaces* **2020**, *12*, 28607–28615.
[391] B. Champagne, A. Plaquet, J.-L. Pozzo, V. Rodriguez, F. Castet, *J. Am. Chem. Soc.* **2012**, *134*, 8101–8103.
[392] S. Isayama, T. Mukaiyama, *Chem. Lett.* **1989**, *18*, 1071–1074.
[393] S. W. M. Crossley, C. Obradors, R. M. Martinez, R. A. Shenvi, *Chem. Rev.* **2016**, *116*, 8912–9000.
[394] W. M. Haynes, W. M. Haynes, D. R. Lide, T. J. Bruno, *CRC Handbook of Chemistry and Physics : A Ready-Reference Book of Chemical and Physical Data.*, CRC Press, Boca Raton, Florida ;, **2017**.
[395] N. Kühl, D. Graf, J. Bock, M. A. M. Behnam, M.-M. Leuthold, C. D. Klein, *J. Med. Chem.* **2020**, *63*, 8179–8197.
[396] K. Bujak, K. Nocoń, A. Jankowski, A. Wolińska-Grabczyk, E. Schab-Balcerzak, H. Janeczek, J. Konieczkowska, *Eur. Polym. J.* **2019**, *118*, 186–194.
[397] M. R. Banghart, A. Mourot, D. L. Fortin, J. Z. Yao, R. H. Kramer, D. Trauner, *Angew. Chem. Int. Ed.* **2009**, *48*, 9097–9101.
[398] K. Dąbrowa, P. Niedbała, J. Jurczak, *Chem. Commun.* **2014**, *50*, 15748–15751.
[399] M. Rémond, P. Colinet, E. Jeanneau, T. Le Bahers, C. Andraud, Y. Bretonnière, *Dyes Pigments* **2021**, *193*, 109485.
[400] B. N. Bhawal, J. C. Reisenbauer, C. Ehinger, B. Morandi, *J. Am. Chem. Soc.* **2020**, *142*, 10914–10920.
[401] J. P. Hooker, F. Feist, L. Delafresnaye, L. Barner, C. Barner-Kowollik, *Adv. Funct. Mater.* **2020**, *30*, 1905399.
[402] L. He, G. Wang, Q. Tang, X. Fu, C. Gong, *J. Mater. Chem. C* **2014**, *2*, 8162–8169.
[403] C. Zhang, N. Jiao, *Angew. Chem. Int. Ed.* **2010**, *49*, 6174–6177.

10 Appendix

10.1 Small Molecule NMR Spectra

10.1.1 Sequence Defined Main Chain Amine

10.1.1.1 Boc Protected Phenylenediamine

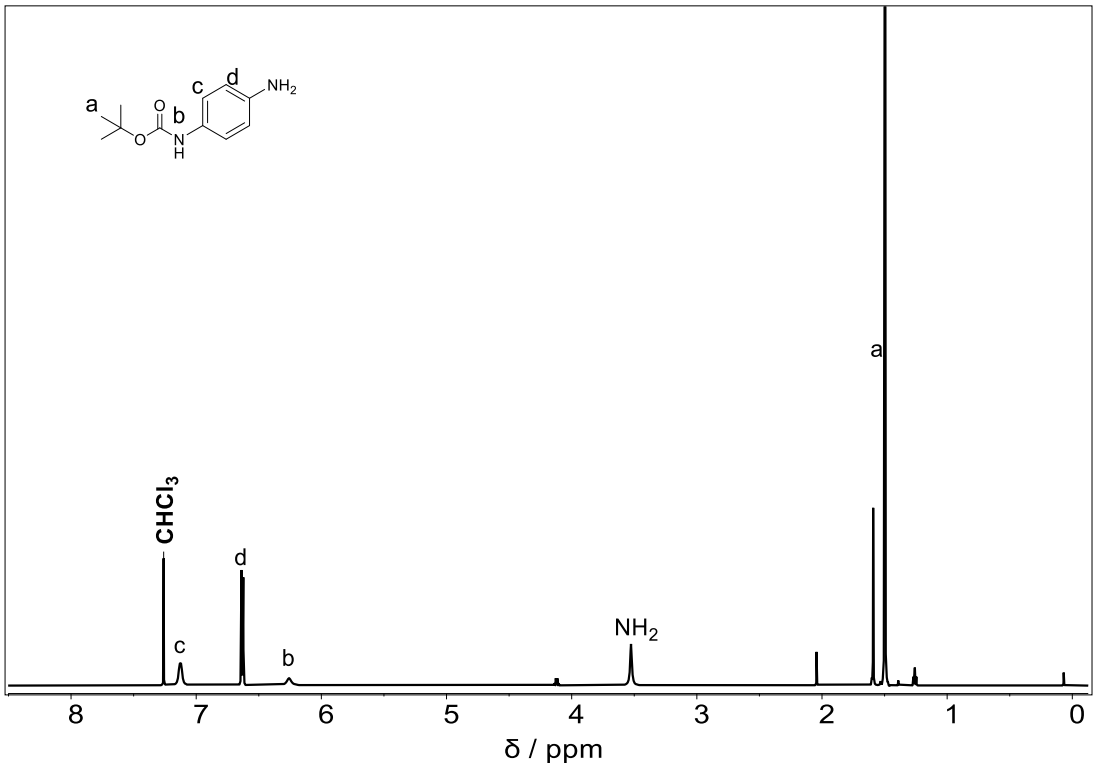

Figure 68. ^{1}H NMR spectrum of Boc protected phenylenediamine in $CDCl_3$.

10.1.1.2 Boc Protected Nitrosobenzene

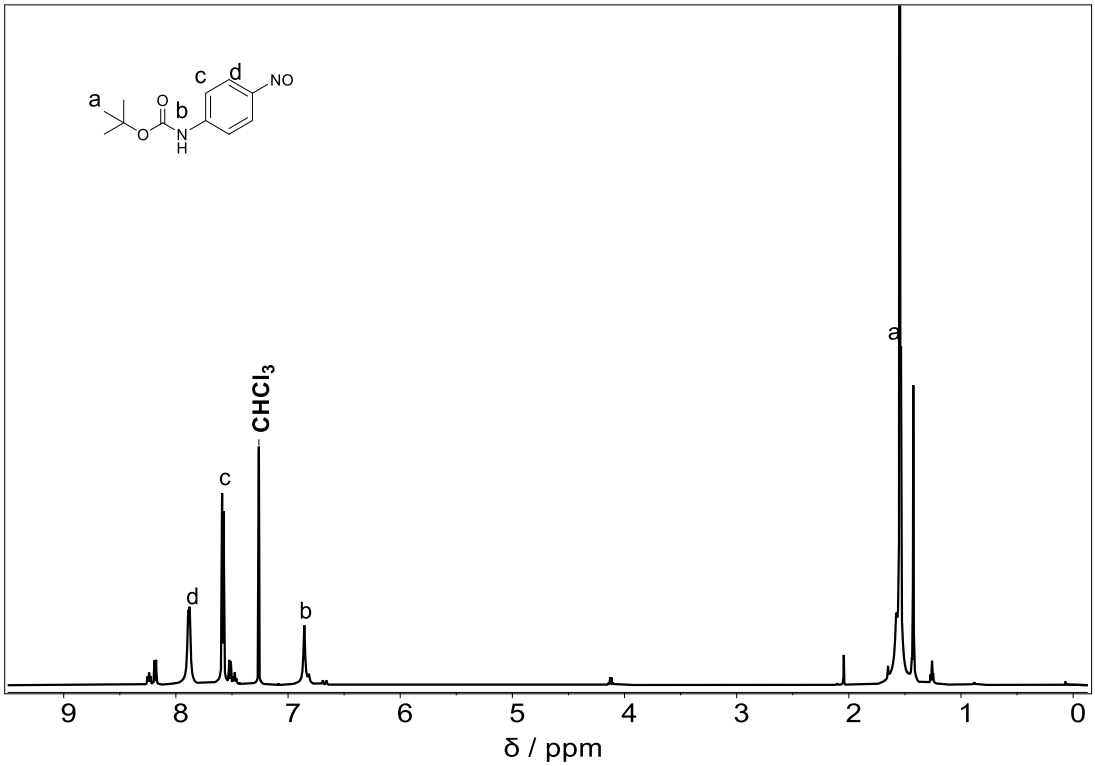

Figure 69. ^{1}H NMR spectrum of the Boc protected nitroso in $CDCl_3$.

10.1.1.3 Boc Protected Azobenzene

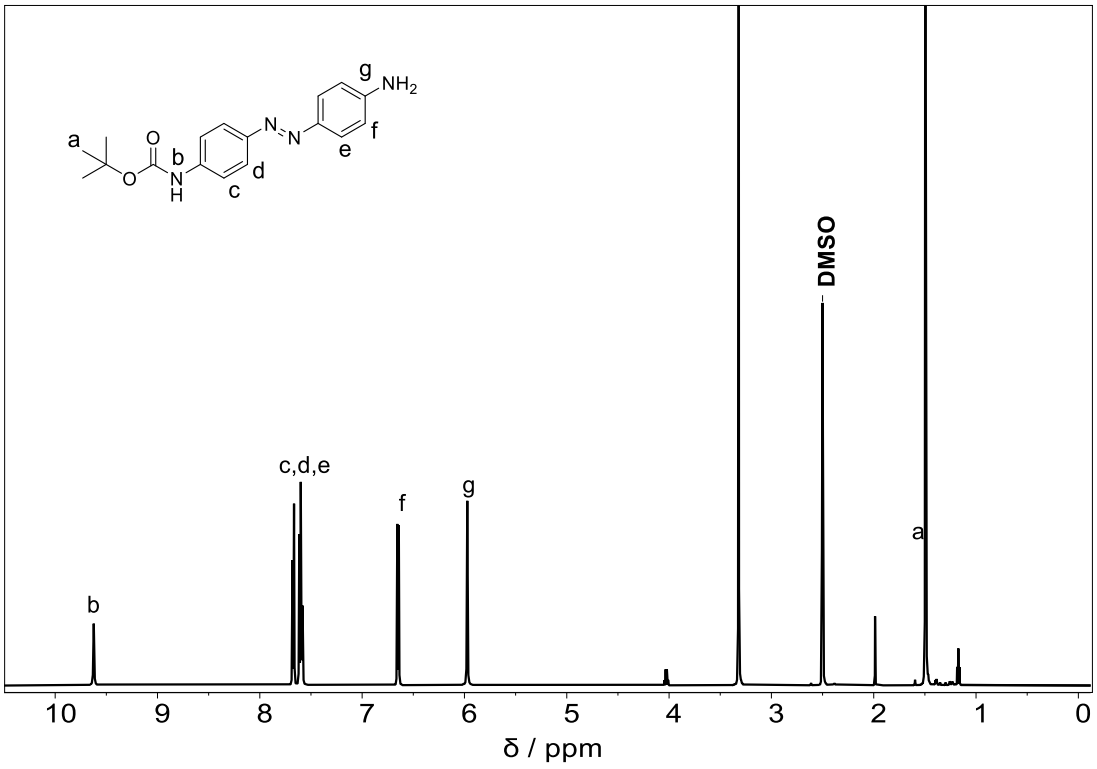

Figure 70. ^{1}H NMR spectrum of the Boc protected azobenzene in DMSO.

10.1.1.4 Boc Protected Imine Azobenzene

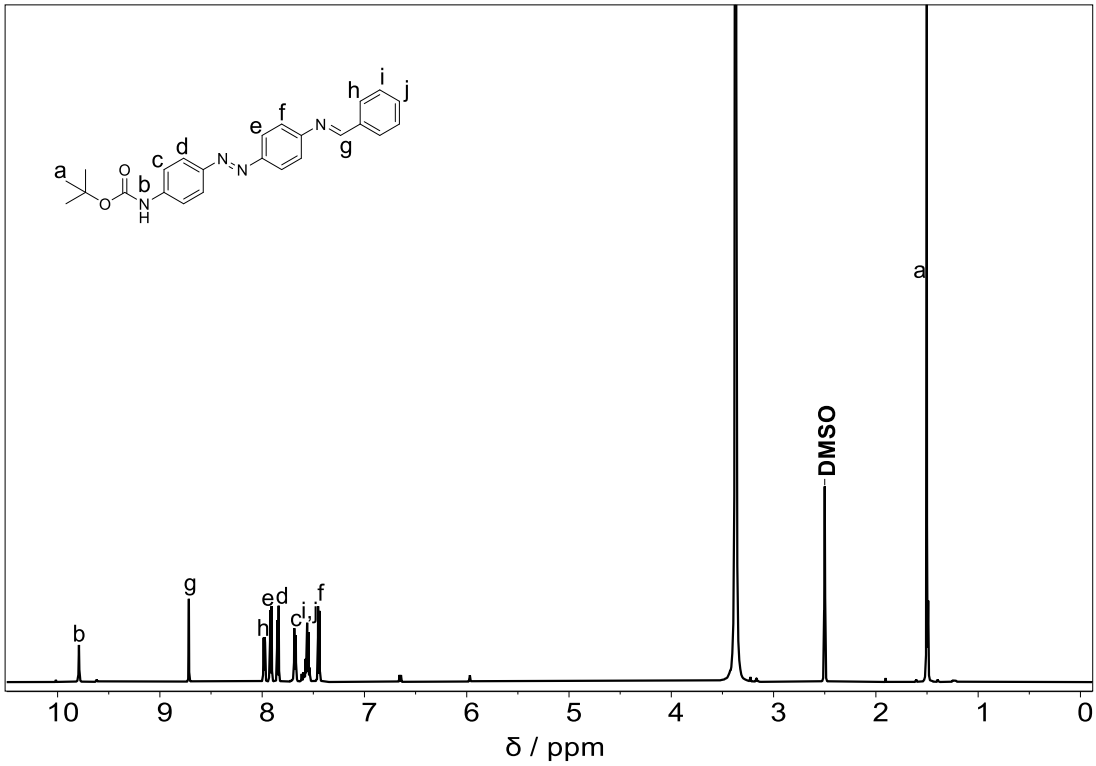

Figure 71. ^{1}H NMR spectrum of the Boc imine azobenzene in DMSO.

10.1.1.5 Fmoc Protected Diamine

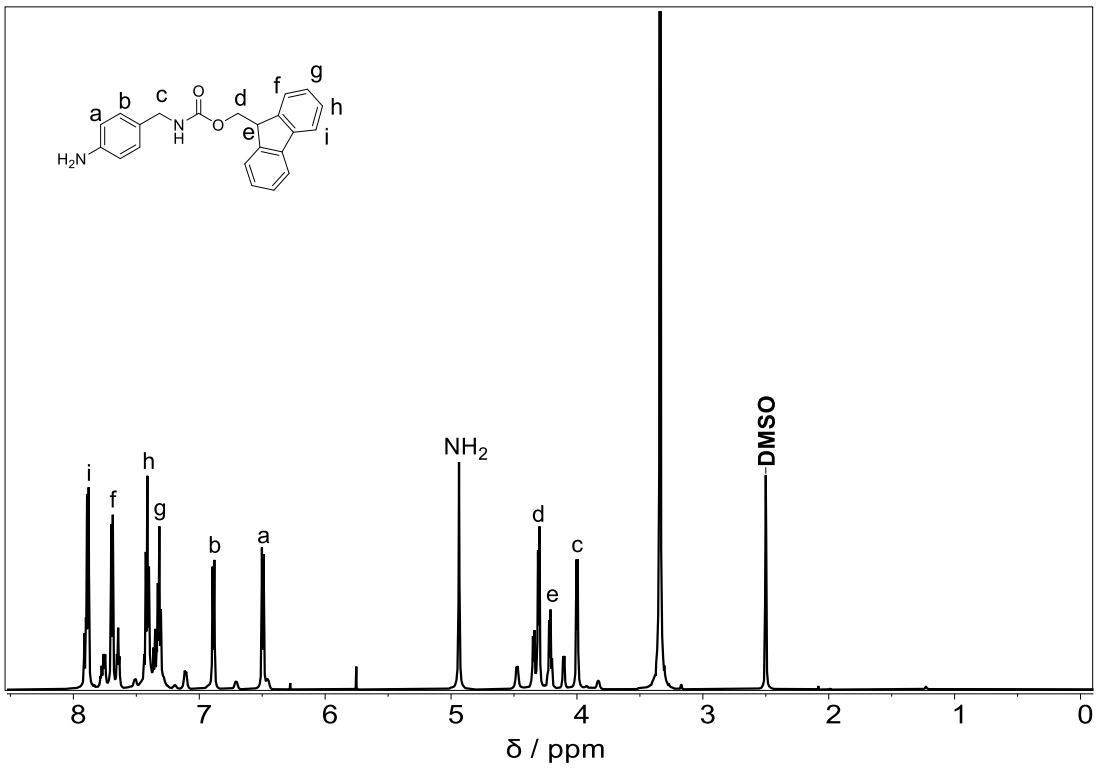

Figure 72. ^{1}H NMR spectrum of the Fmoc protected diamine in DMSO.

10.1.1.6 Fmoc/Boc Protected Azobenzene

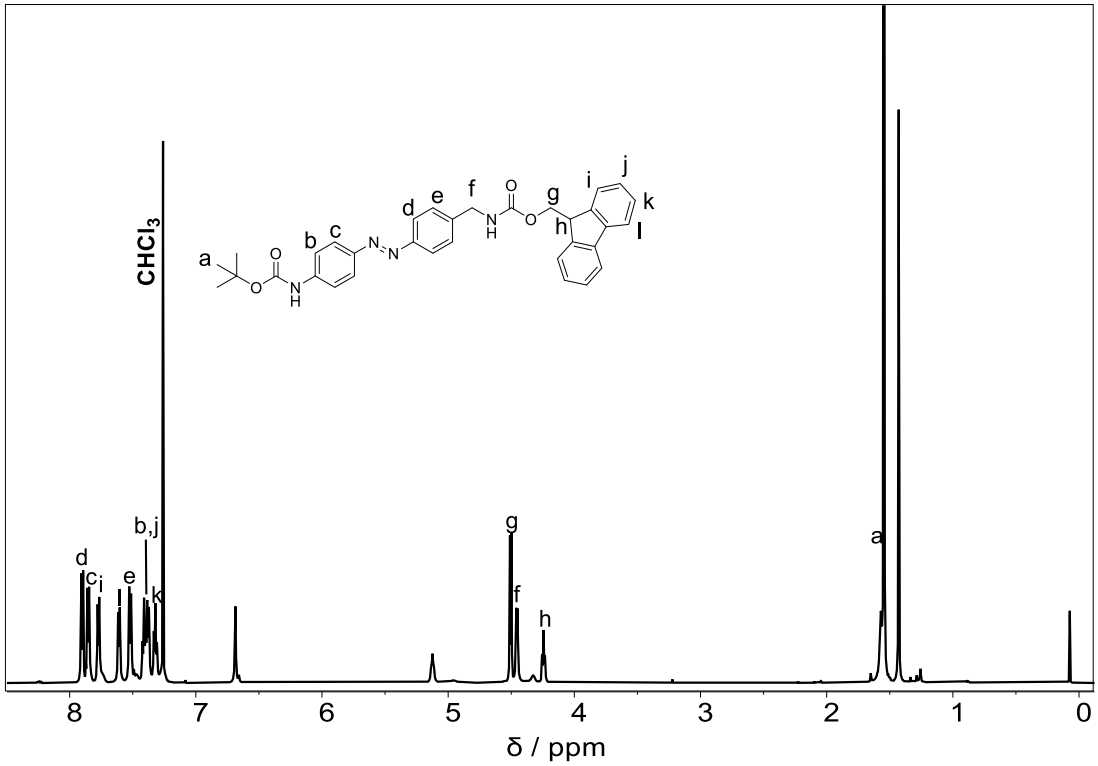

Figure 73. ^{1}H NMR spectrum of the Fmoc/Boc protected azobenzene in $CDCl_3$.

10.1.2 Sequence Defined Main Chain Acid

10.1.2.1 Nitroso Acetanilide

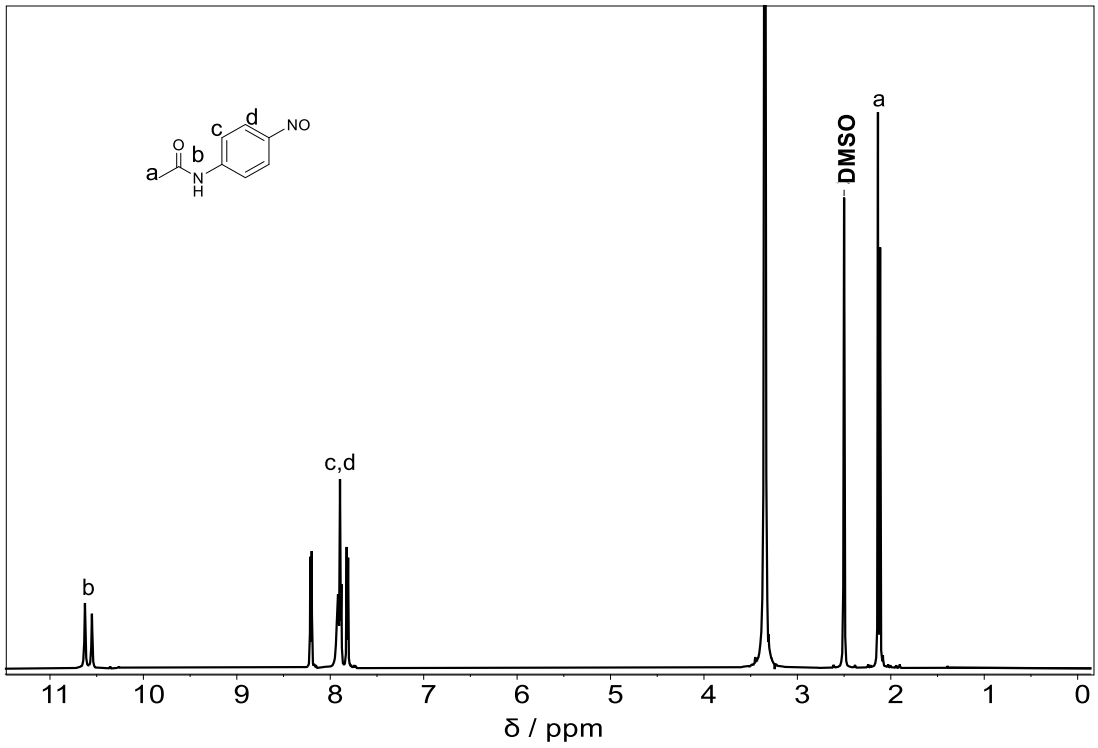

Figure 74. [1]H NMR spectrum of nitroso acetanilide in DMSO.

10.1.2.2 Acetanilide Azobenzene

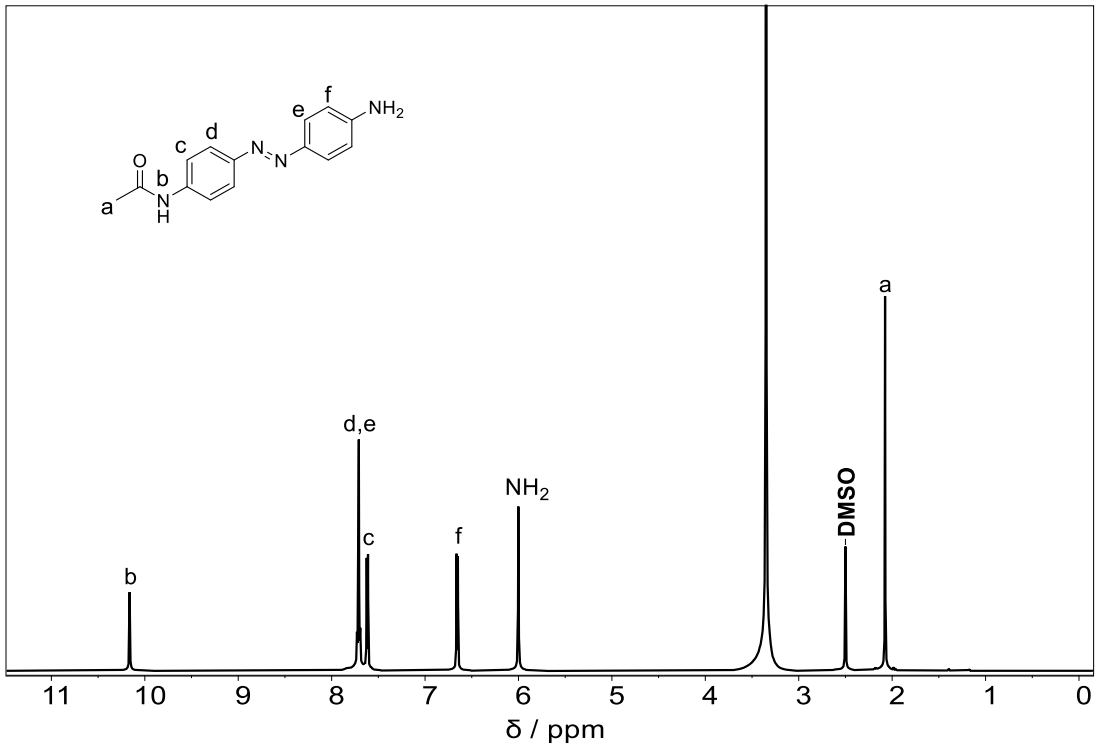

Figure 75. [1]H NMR spectrum of the Acetanilde azobenzene in DMSO.

10.1.2.3 Diamino Azobenzene

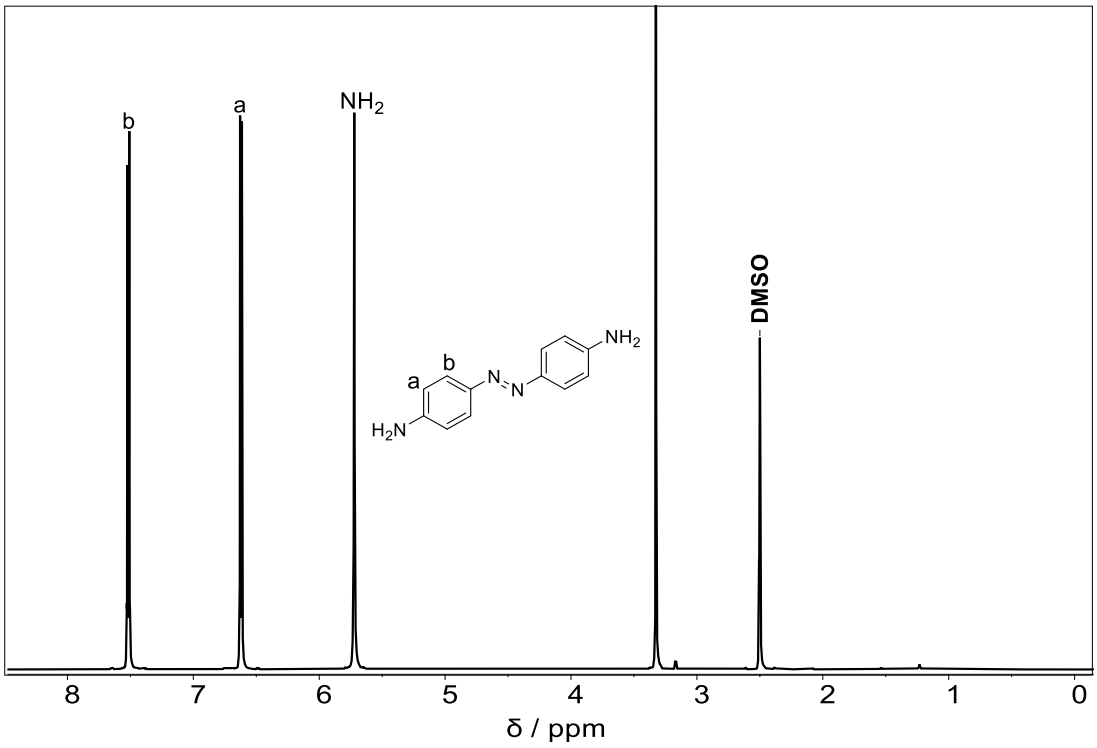

Figure 76. [1]H NMR spectrum of diamino azobenzene in DMSO.

10.1.2.4 Amino/Carboxy Azobenzene

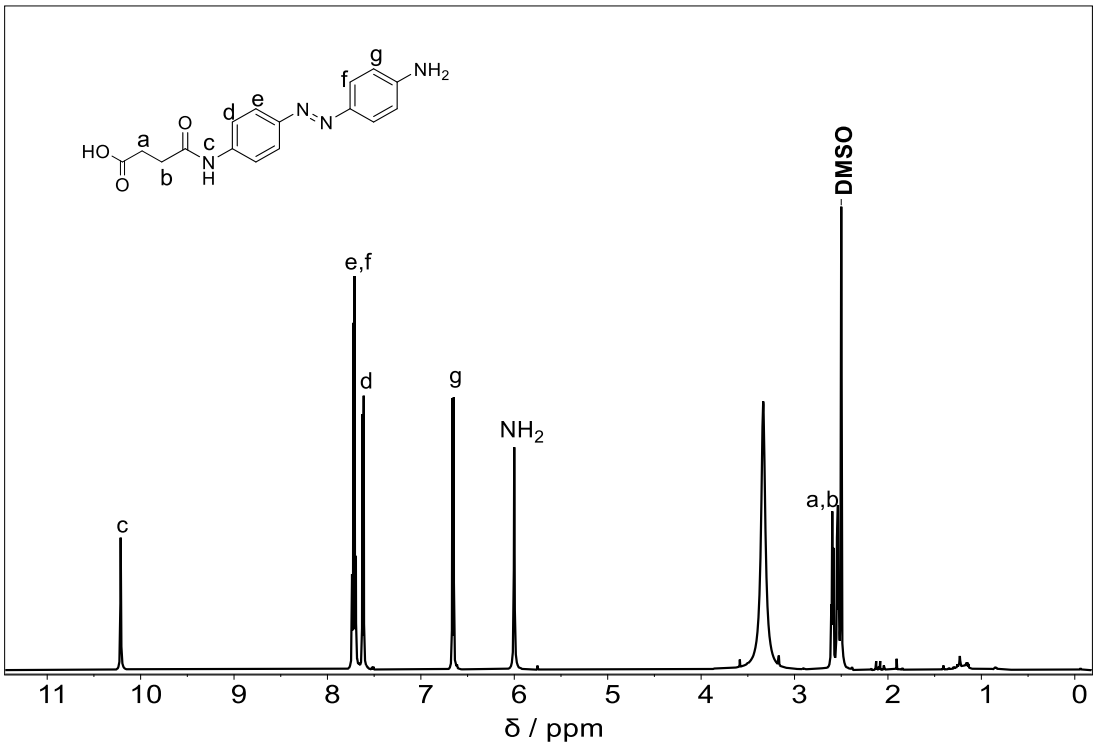

Figure 77. [1]H NMR spectrum of the Amino/Carboxy azobenzene in DMSO.

10.1.3 Sequence Defined Main Chain Aldehyde

10.1.3.1 Acetal Protected Benzaldehyde

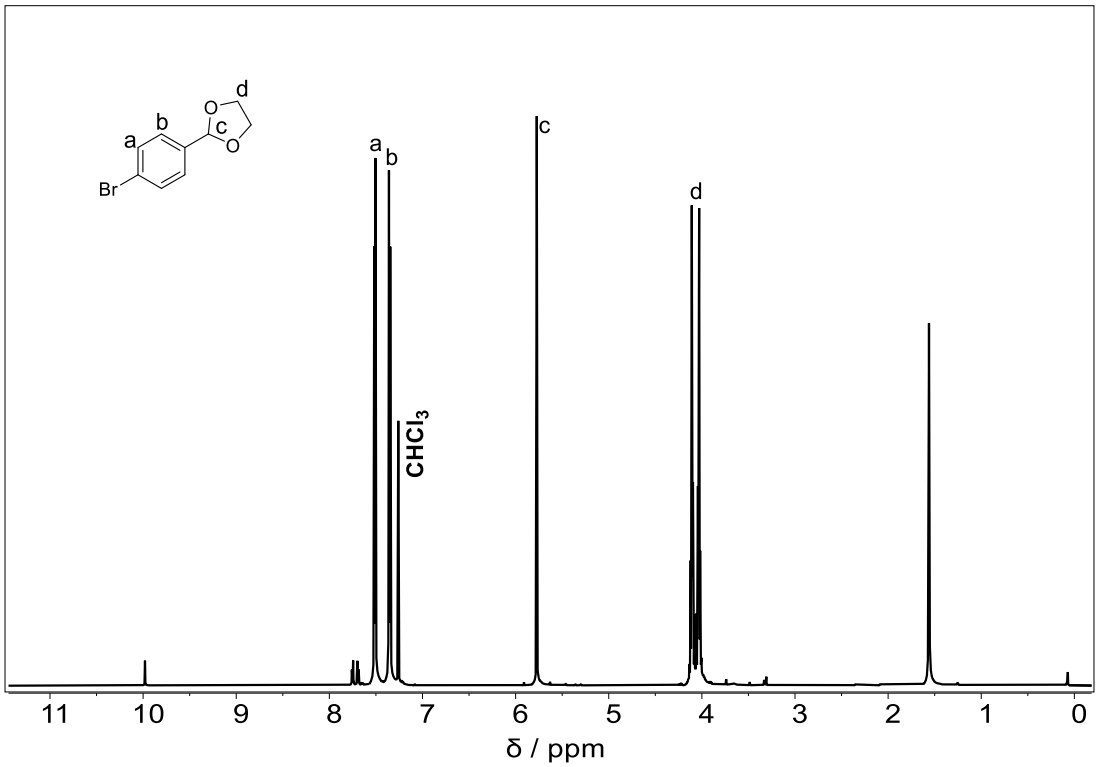

Figure 78. ^{1}H NMR spectrum of Acetal protected benzaldehyde in $CDCl_3$.

10.1.3.2 Acetal Protected Phosphine

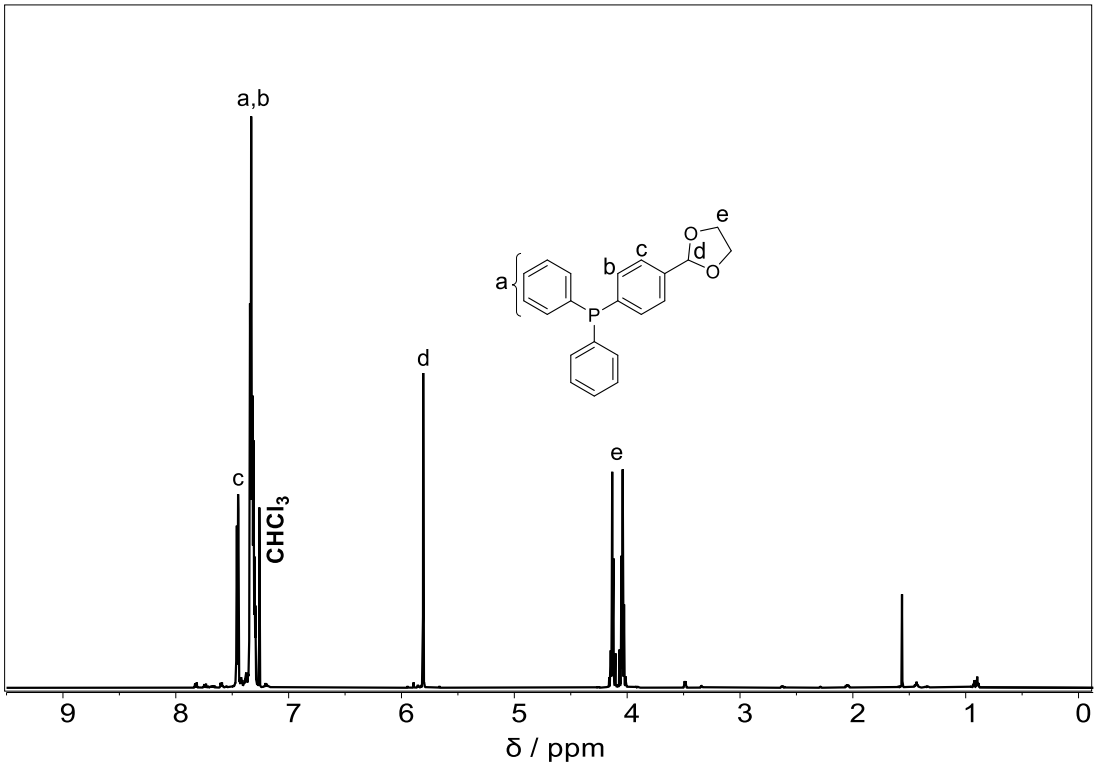

Figure 79. ^{1}H NMR spectrum of Acetal protected phosphine in $CDCl_3$.

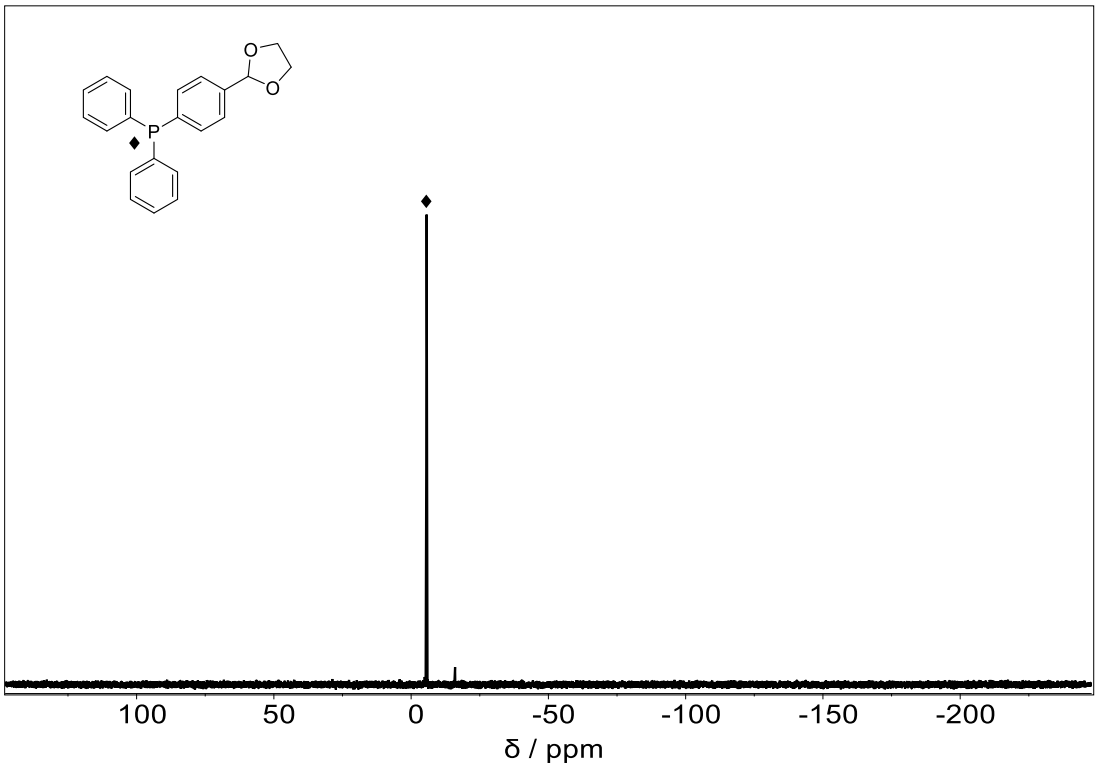

Figure 80. ^{31}P NMR spectrum of acetal protected phosphine in $CDCl_3$.

10.1.3.3 Phosphine Aldehyde

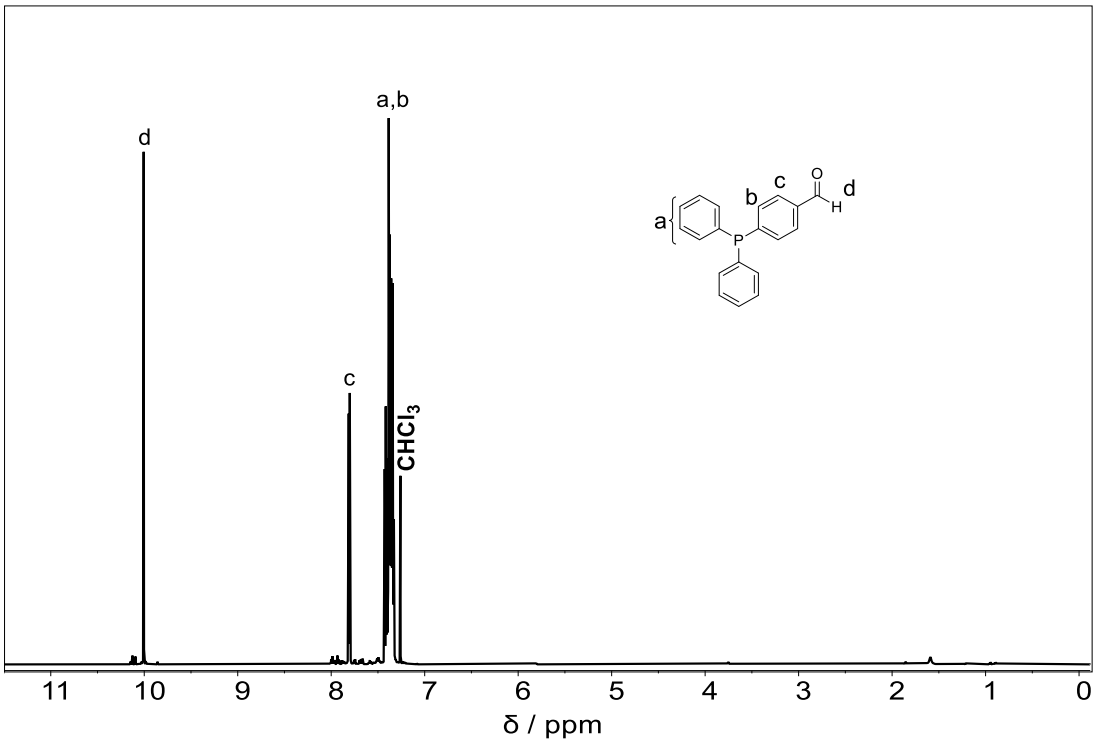

Figure 81. ^{1}H NMR spectrum of the phosphine aldehyde in $CDCl_3$.

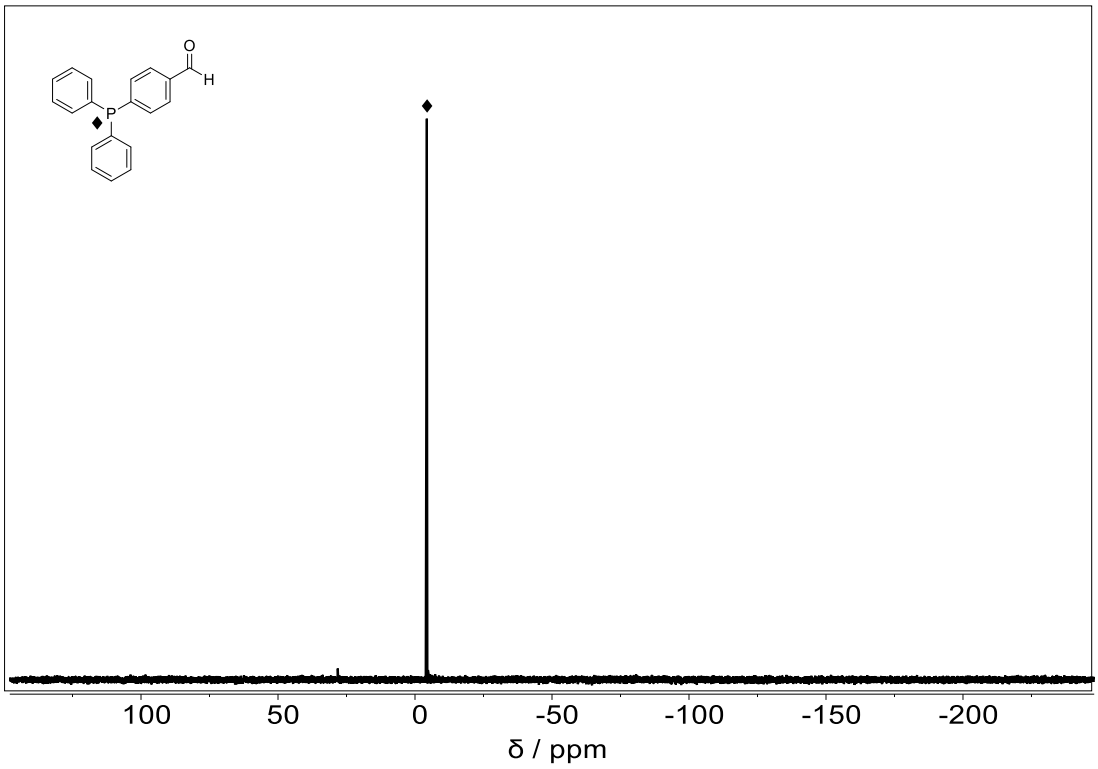

Figure 82. ^{31}P NMR spectrum of the phosphine aldehyde in $CDCl_3$.

10.1.4Polydisperse Main Chain Acid

10.1.4.1 Di-butanoic Acid Azobenzene

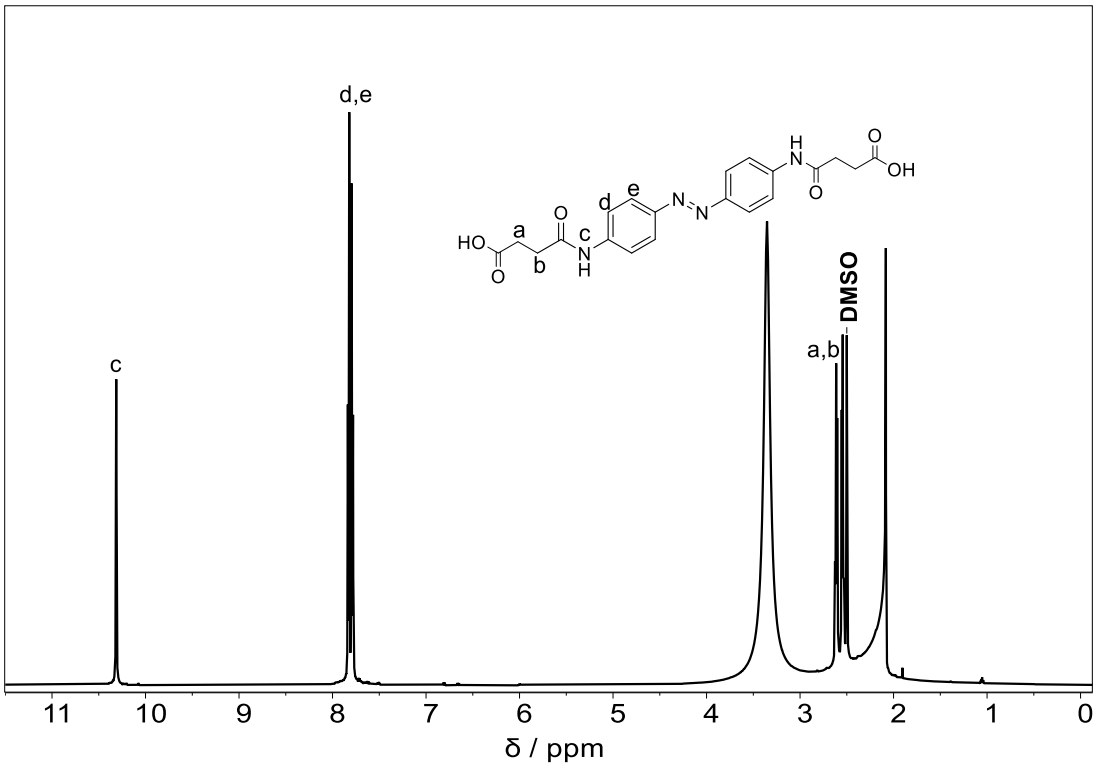

Figure 83. [1]H NMR spectrum of di-butanoic acid azobenzene in DMSO.

10.1.5 Polydisperse Main Chain Amine

10.1.5.1 Undecenoyl Chloride

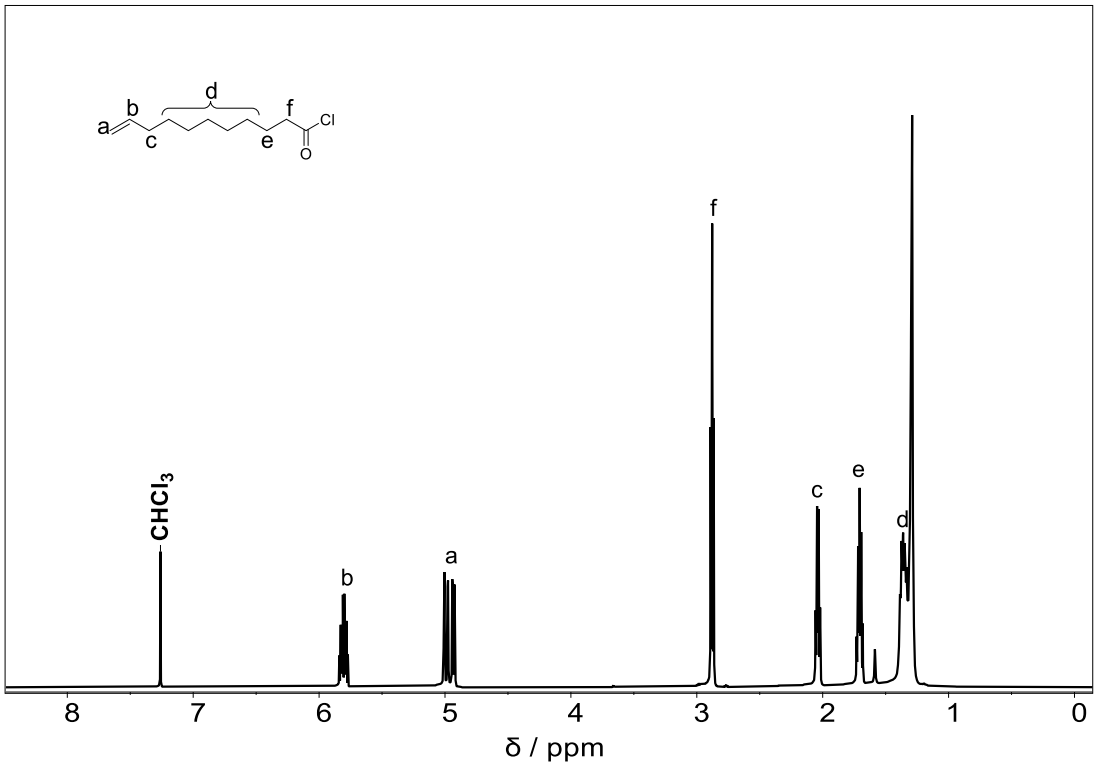

Figure 84. ^{1}H NMR spectrum of undecanoyl chloride in $CDCl_3$.

10.1.5.2 Undecene Amide

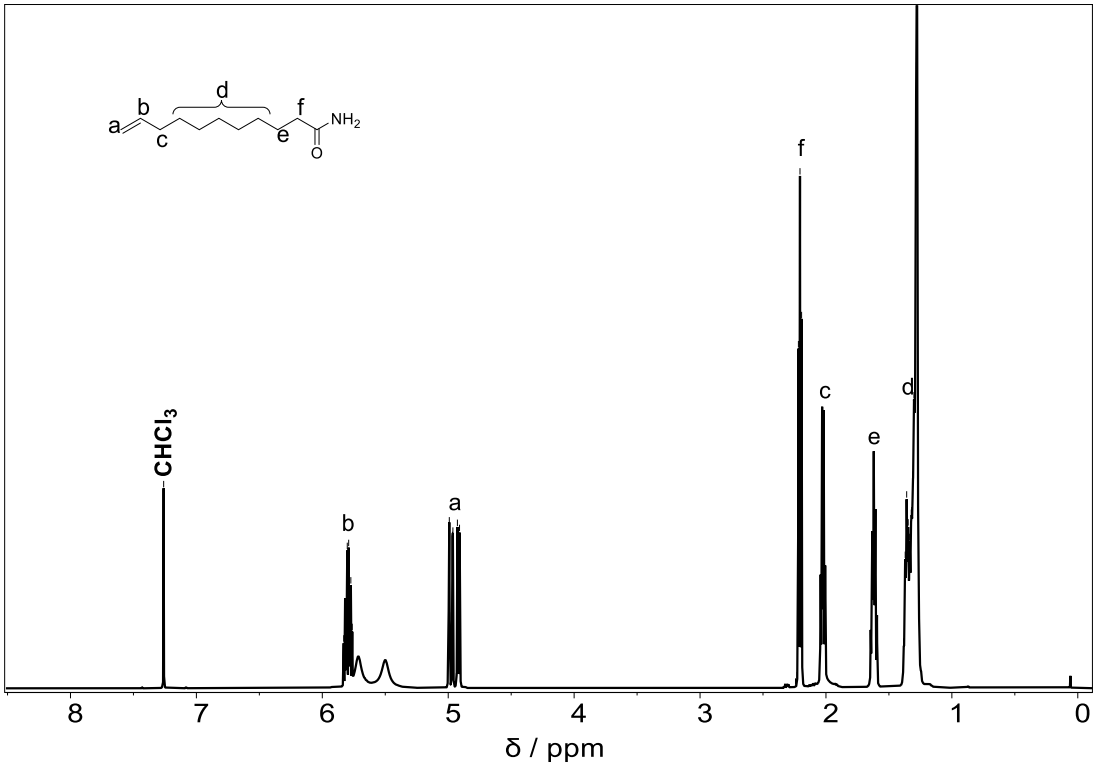

Figure 85. ^{1}H NMR spectrum of Undecene Amide in $CDCl_3$

10.1.5.3 Undecene Amine

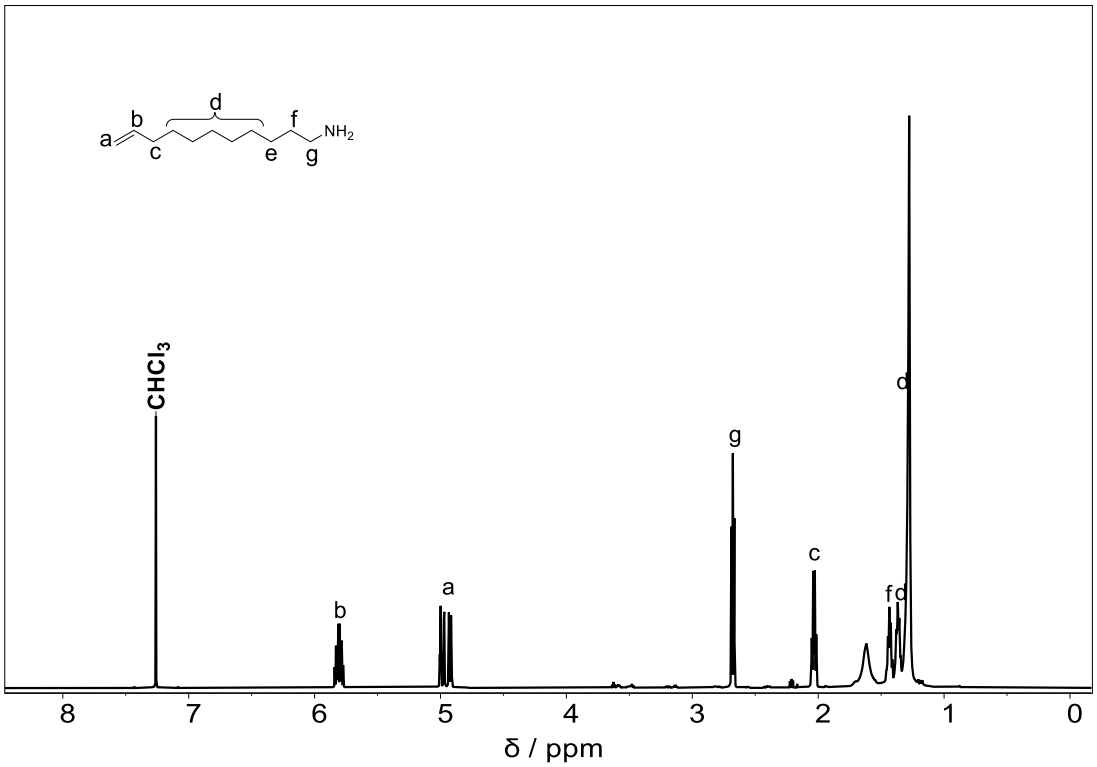

Figure 86. ^{1}H NMR spectrum of Undecene Amine in $CDCl_3$

10.1.5.4 Ugi Reaction

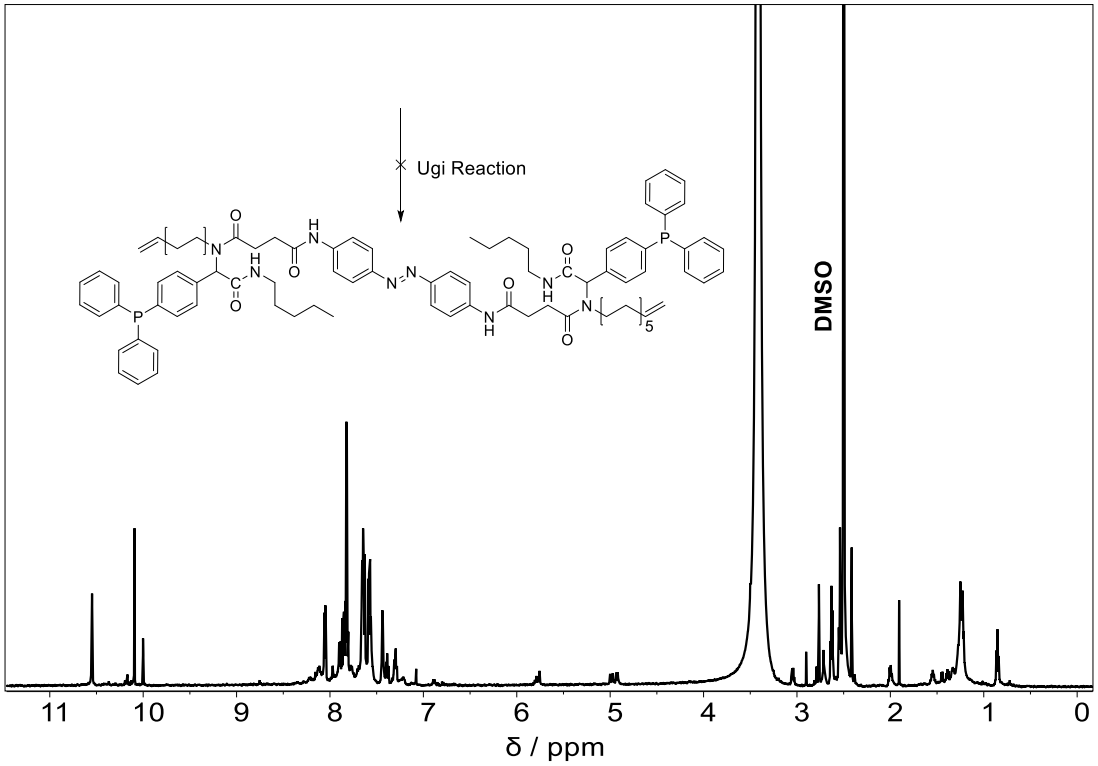

Figure 87. ^{1}H NMR spectrum of the attempted Ugi reaction in DMSO.

10.1.6 Catalytic SCNP via Azobenzene Crosslinks: Monomers

10.1.6.1 Vinyl Benzyl Acetate

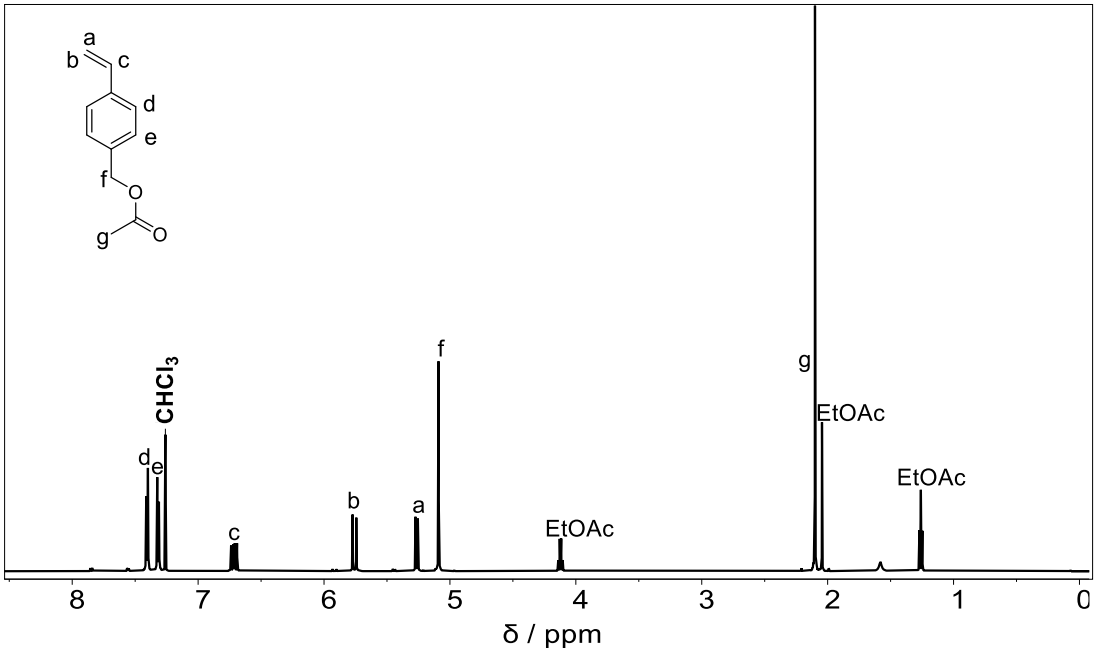

Figure 88. ^{1}H NMR spectrum of vinyl benzyl acetate in $CDCl_3$.

10.1.6.2 Vinyl Benzyl Alcohol

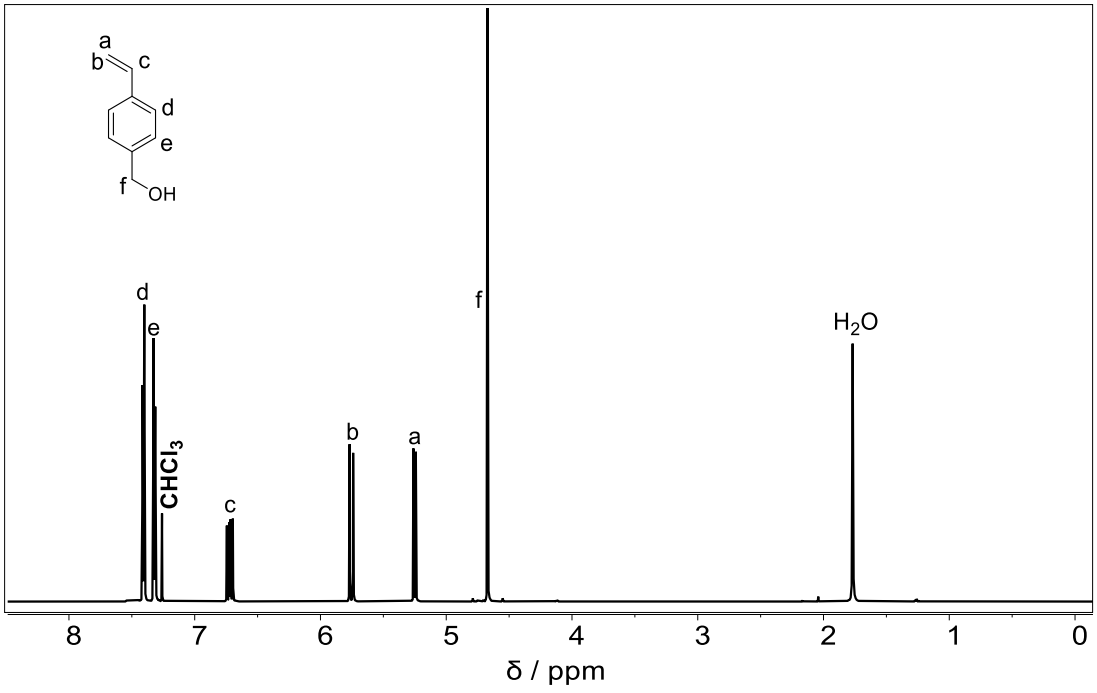

Figure 89. ^{1}H NMR spectrum of vinyl benzyl alcohol in $CDCl_3$.

10.1.6.3 Nitroxide Initiator

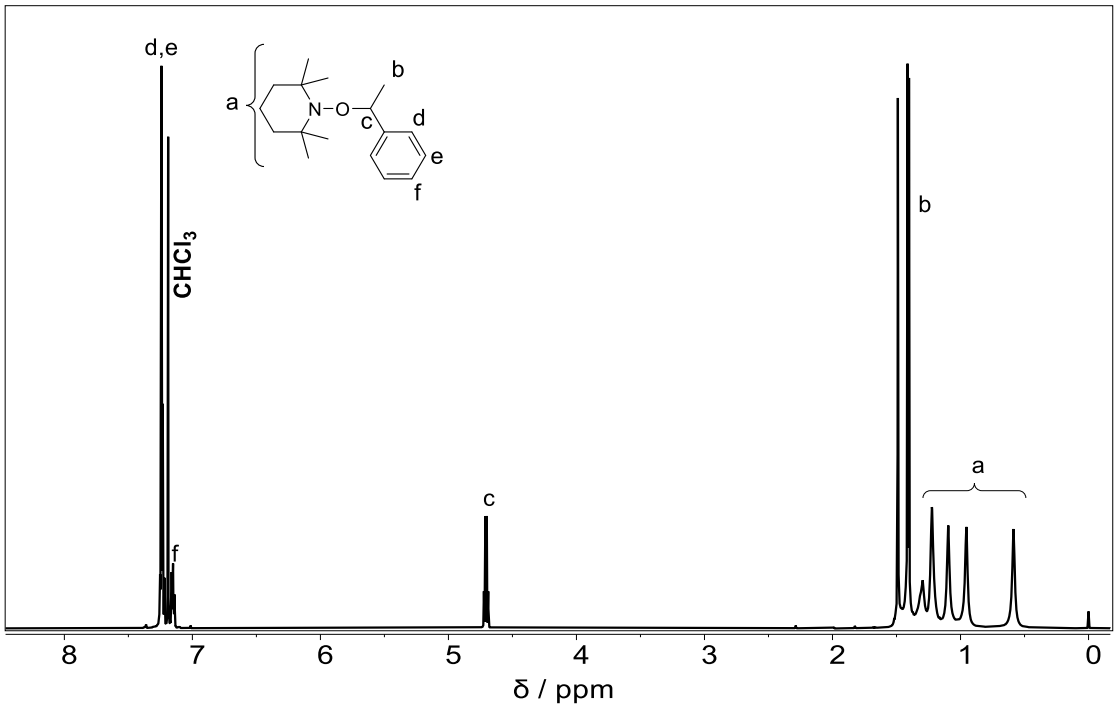

Figure 90. ^{1}H NMR spectrum of the nitroxide initiator in $CDCl_3$.

10.1.6.4 Small Molecule Phosphine Gold Catalyst

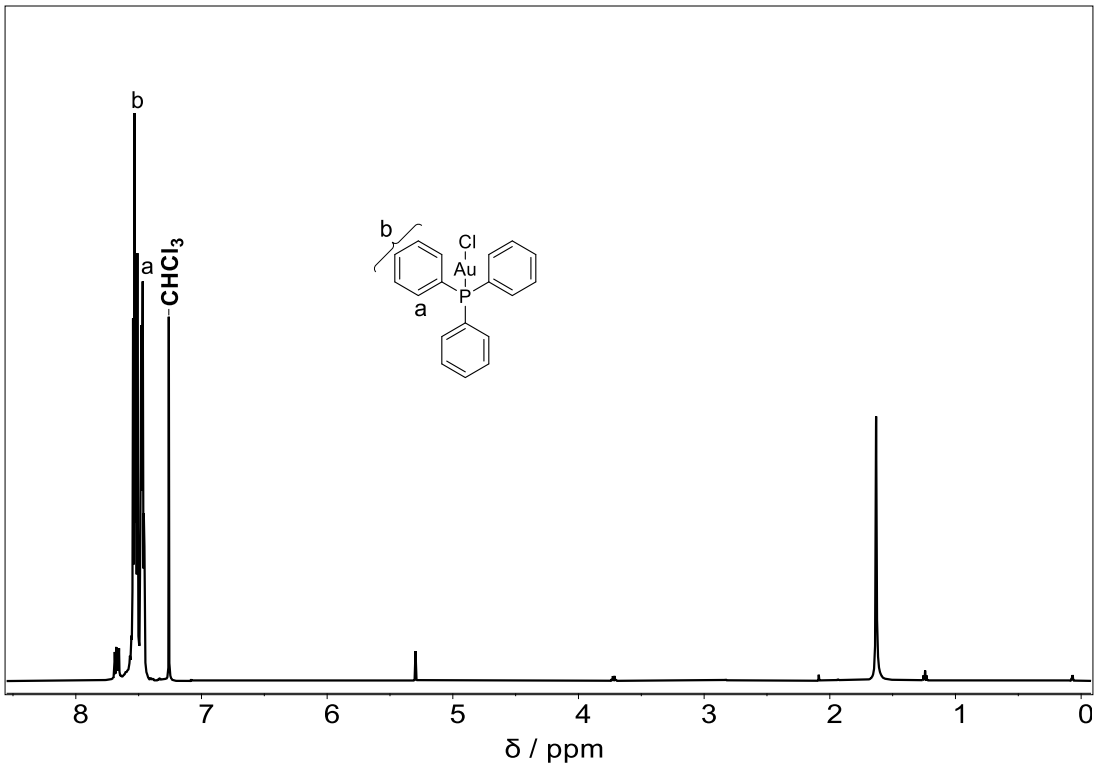

Figure 91. ^{1}H NMR spectrum of the gold phosphine catalyst in $CDCl_3$.

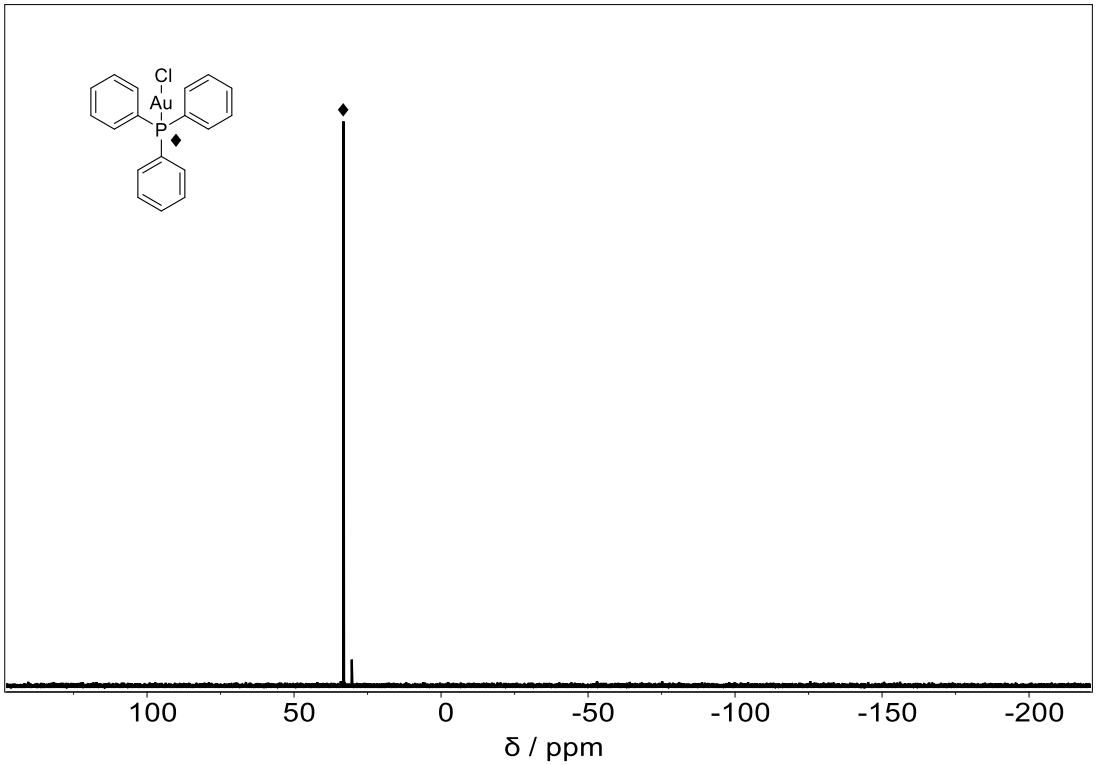

Figure 92. ^{31}P NMR spectrum of the gold phosphine catalyst in $CDCl_3$.

10.1.6.5 Gold Complexed Phosphine Monomer

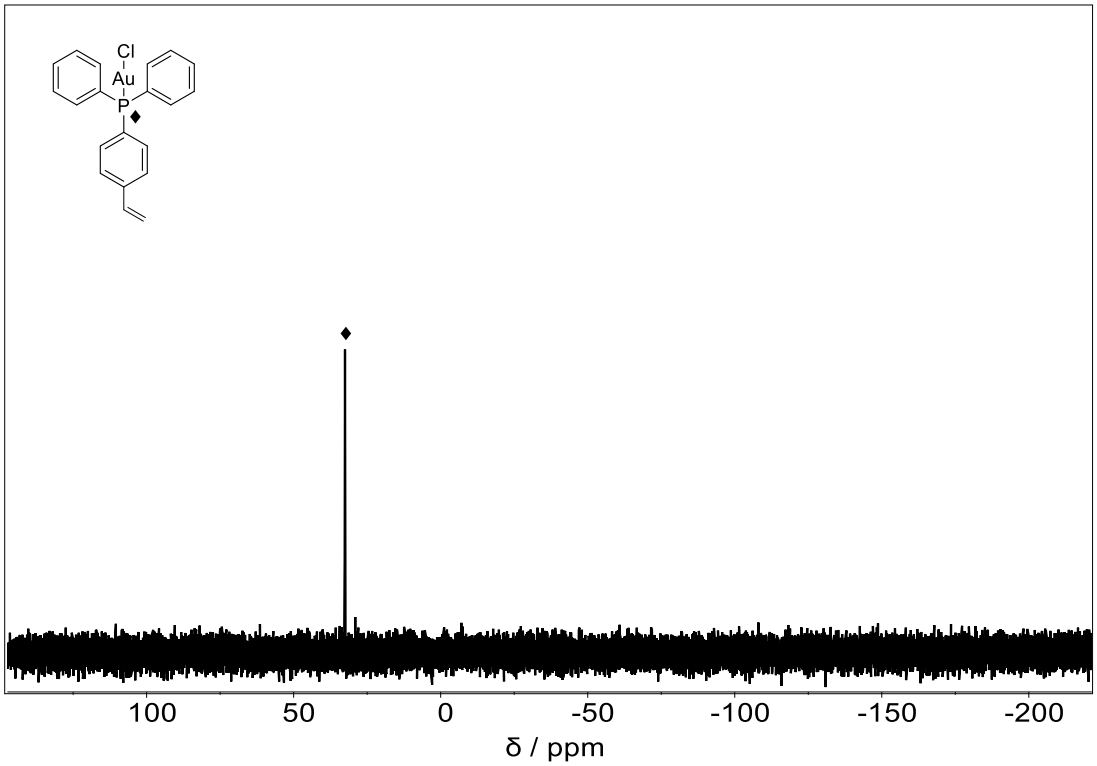

Figure 93. ^{31}P NMR spectrum of the gold phosphine styrene monomer in $CDCl_3$.

10.1.7 Catalytic SCNP via Azobenzene Crosslinks: Substrates

10.1.7.1 Substituted Intramolecular Substrate Nitrile

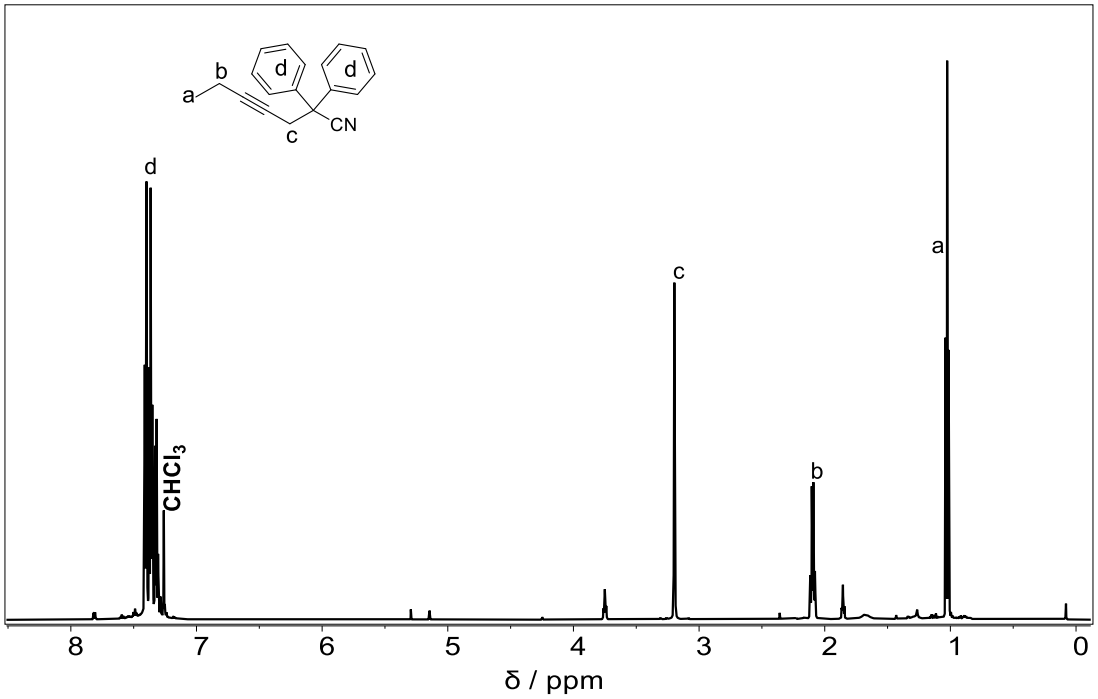

Figure 94. ^{1}H NMR spectrum of the substituted nitrile intermediate in $CDCl_3$.

10.1.7.2 Substituted Intramolecular Substrate Amine

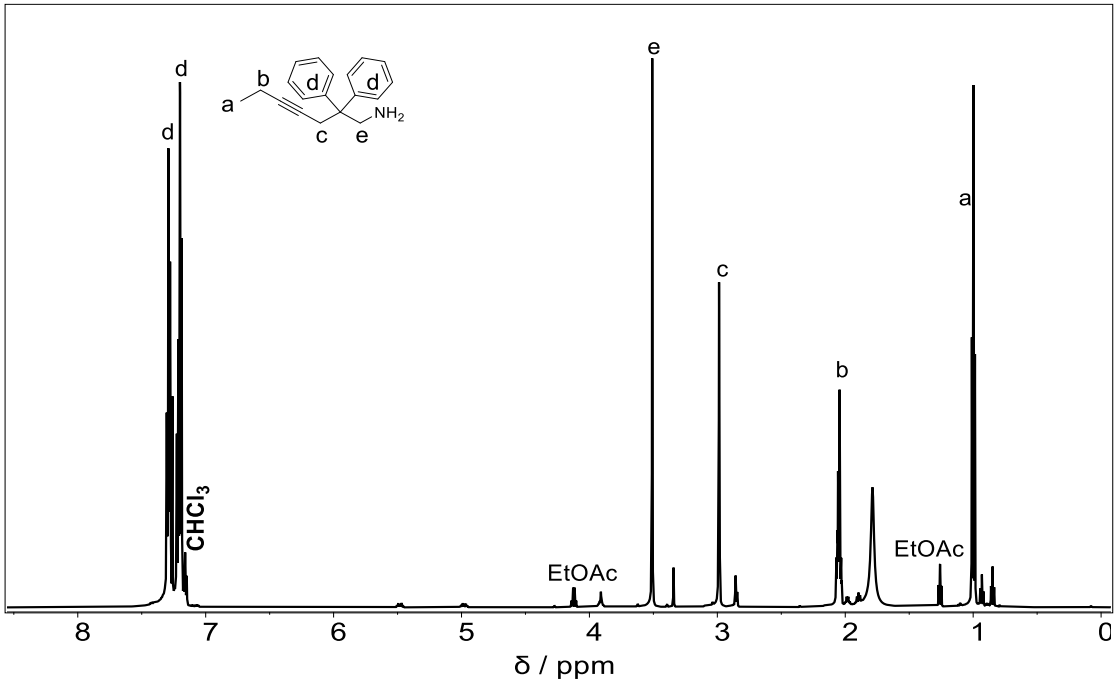

Figure 95. ^{1}H NMR spectrum of the substituted amine substrate in $CDCl_3$.

10.1.7.3 Linear Intramolecular Substrate Phthalimide

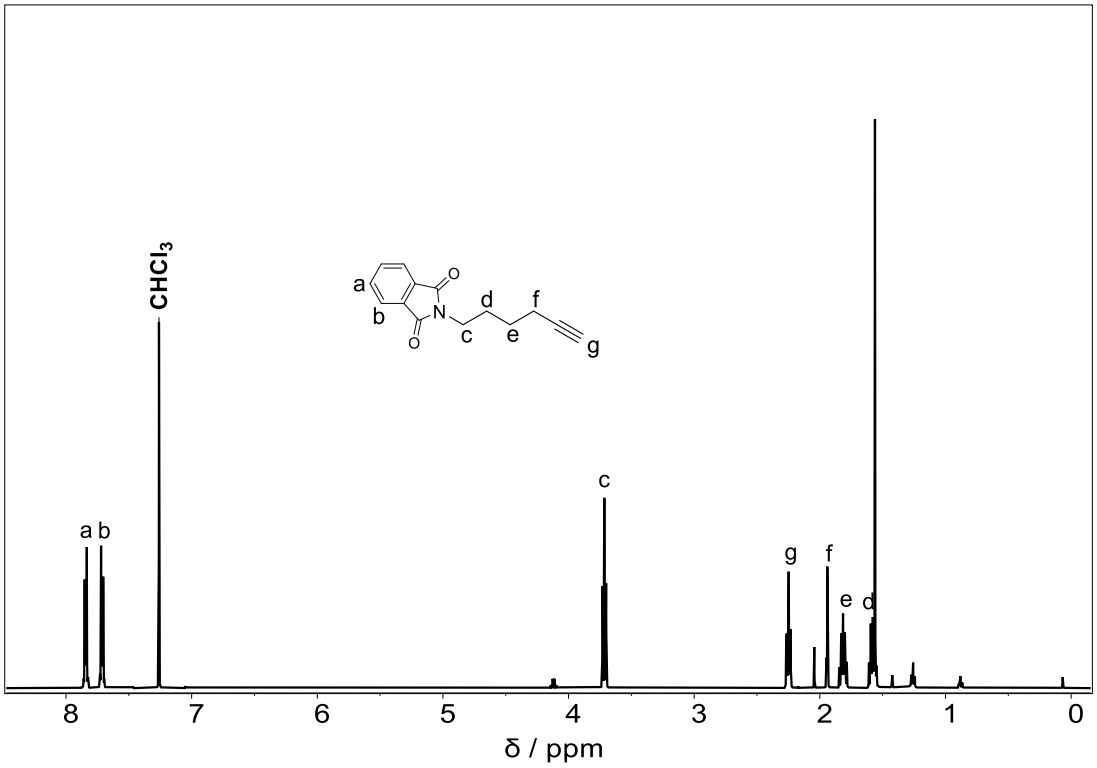

Figure 96. ^{1}H NMR spectrum of the linear phthalimide intermediate in $CDCl_3$.

10.1.7.4 Linear Intramolecular Substrate Amine

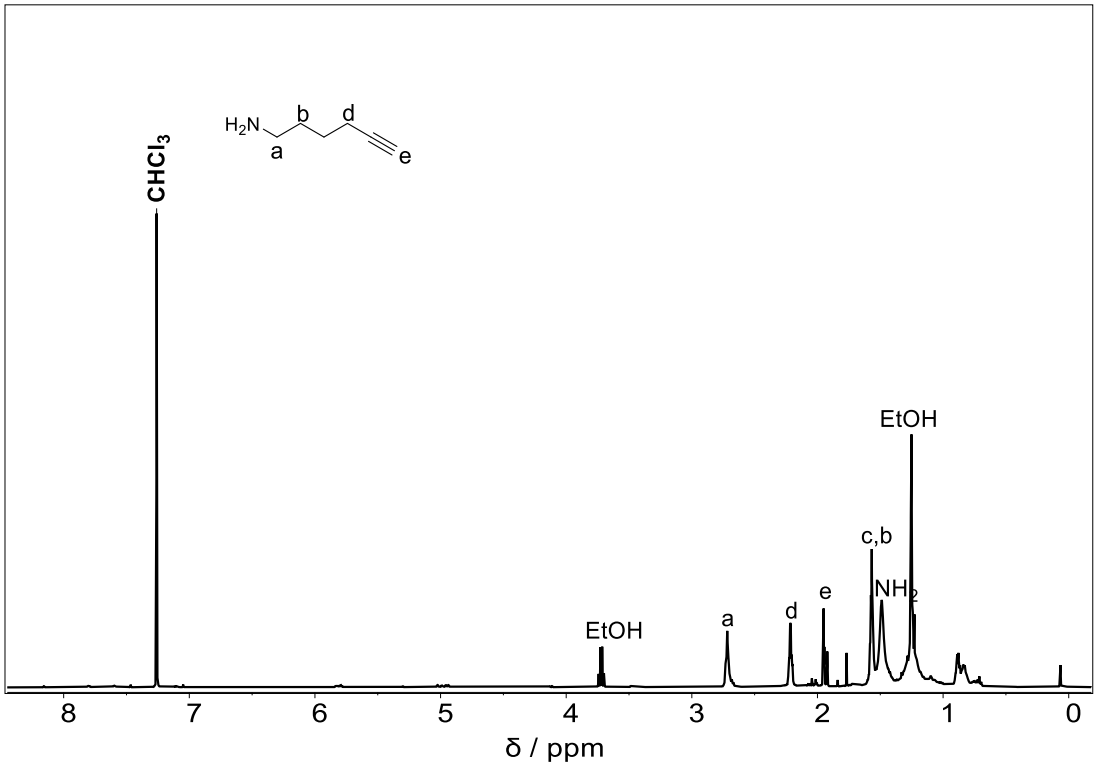

Figure 97. ^{1}H NMR spectrum of the linear amine intermediate in $CDCl_3$.

10.1.8 Catalytic SCNP via Azobenzene Crosslinks: PFP Azobenzene

10.1.8.1 Di-acid Azobenzene

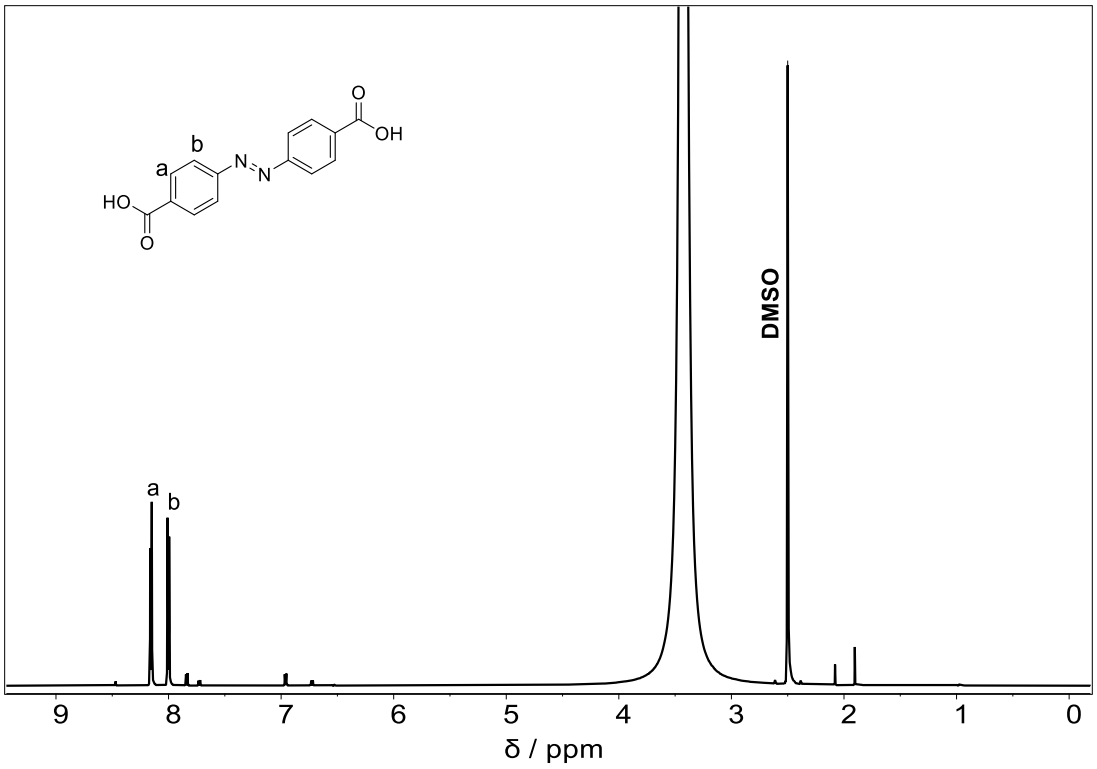

Figure 98. ^{1}H NMR spectrum of the di-acid azobenzene in DMSO.

10.1.8.2 Di-acid Chloride Azobenzene

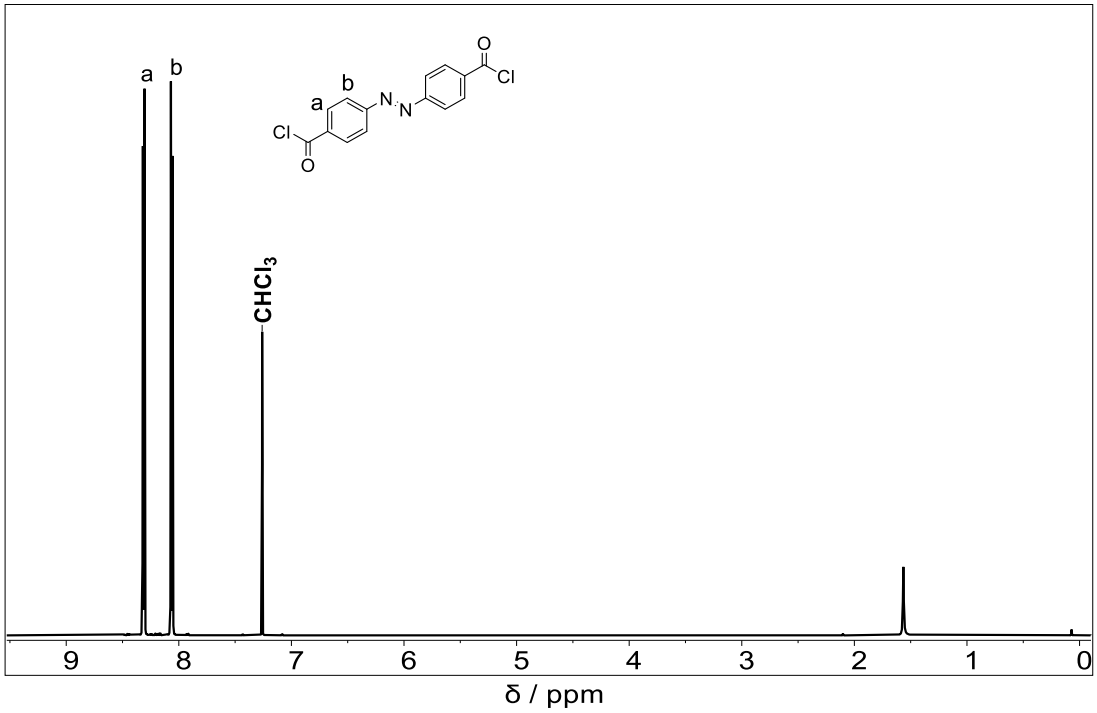

Figure 99. ^{1}H NMR spectrum of the di-acid chloride azobenzene in $CDCl_3$.

10.1.8.3 PFP-ester Azobenzene

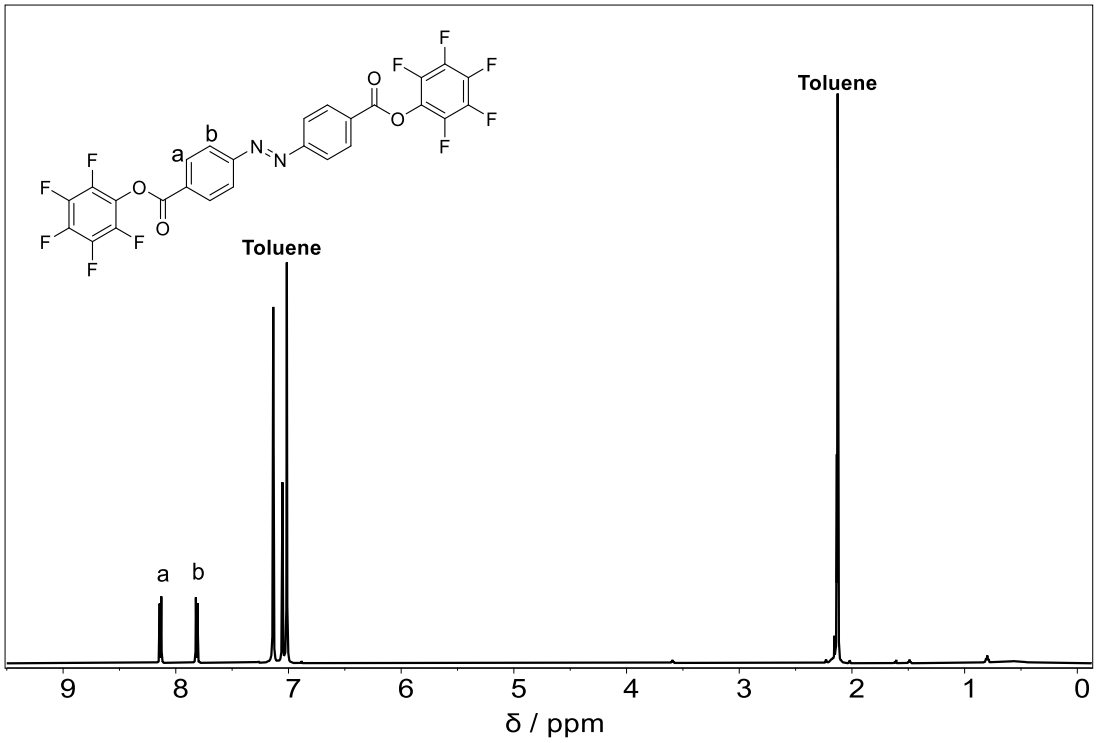

Figure 100. ^{1}H NMR spectrum of the PFP-ester azobenzene in tol-$_{d8}$.

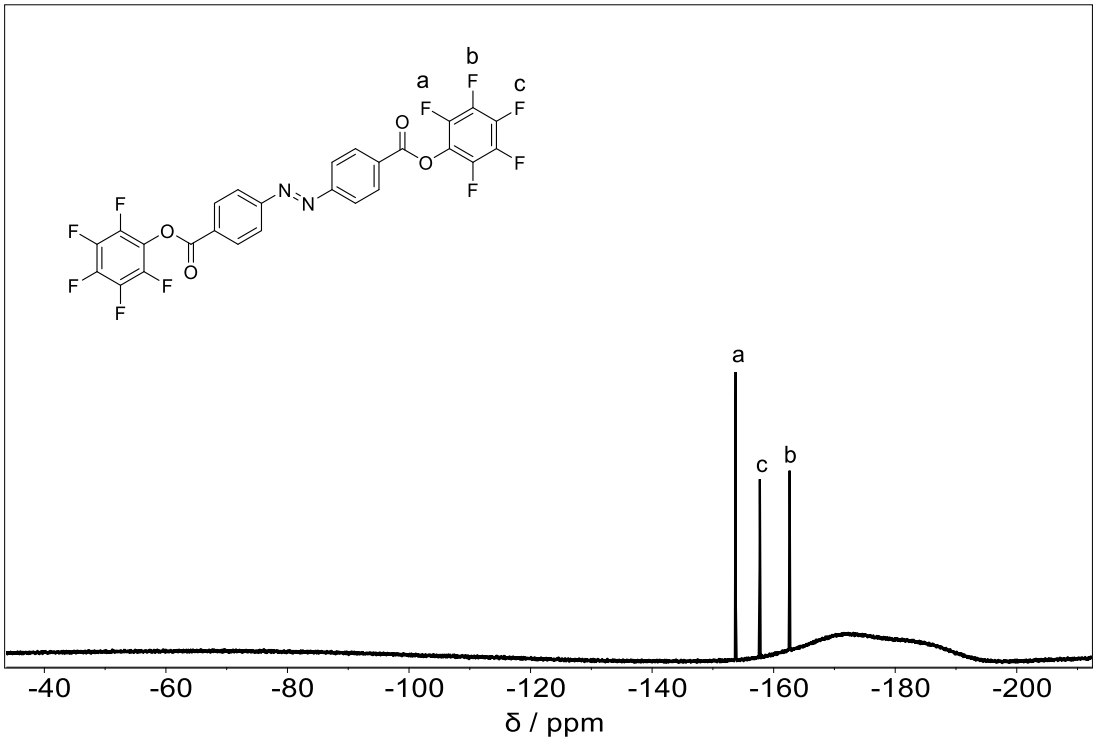

Figure 101. ^{19}F NMR spectrum of the PFP-ester azobenzene in tol-$_{d8}$.

10.1.9 Catalytic SCNP via Azobenzene Crosslinks: Chlorinated Azobenzenes

10.1.9.1 NCS Azobenzene Chlorination

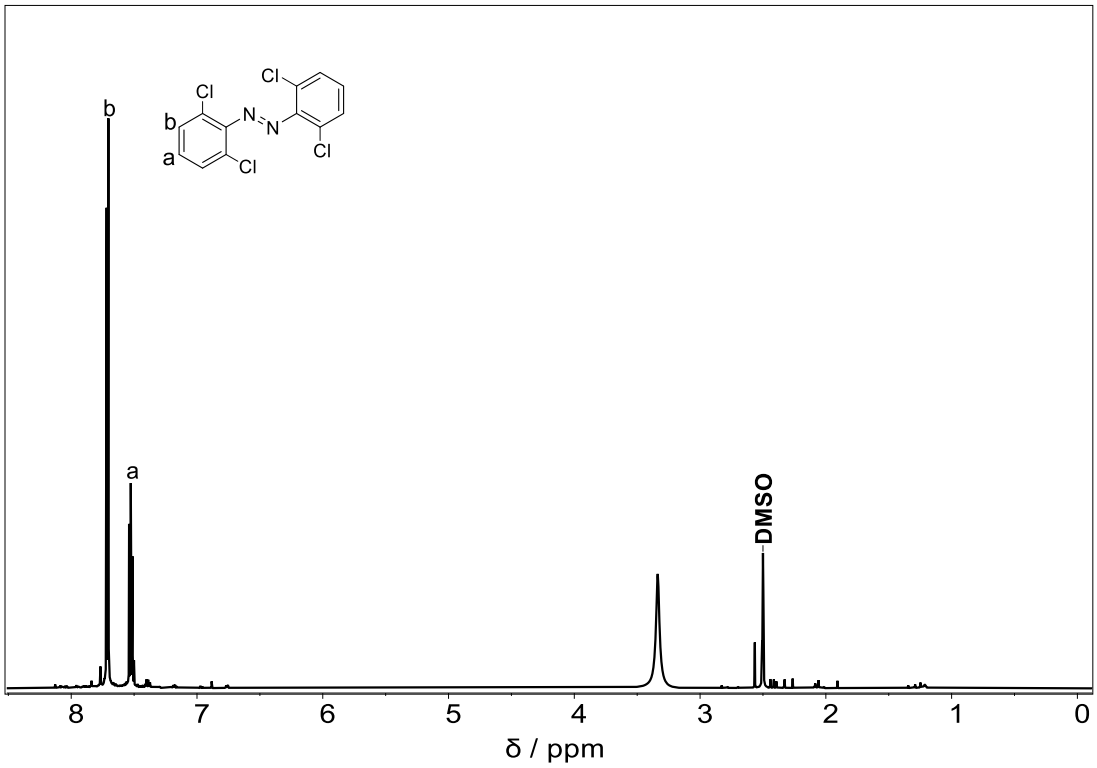

Figure 102. ^{1}H NMR spectrum of the tetra-chlorinated azobenzene in DMSO.

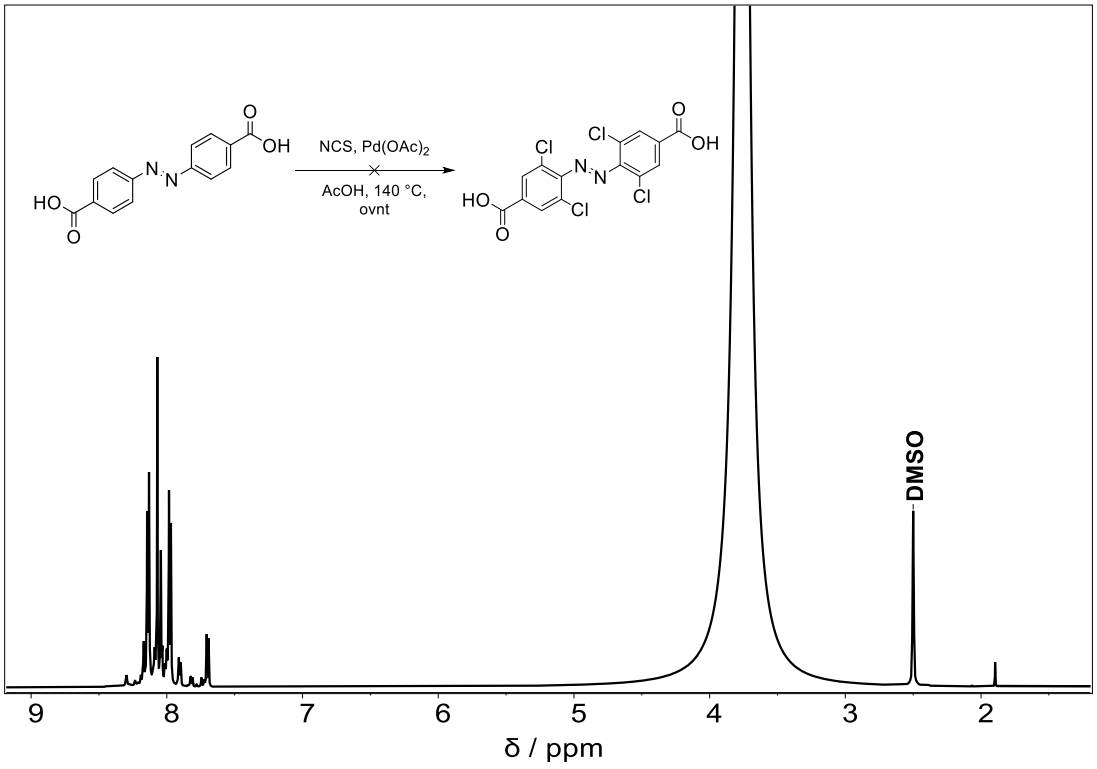

Figure 103. [1]H NMR spectrum of the attempted tetra-chlorination of the di-acid azobenzene in DMSO.

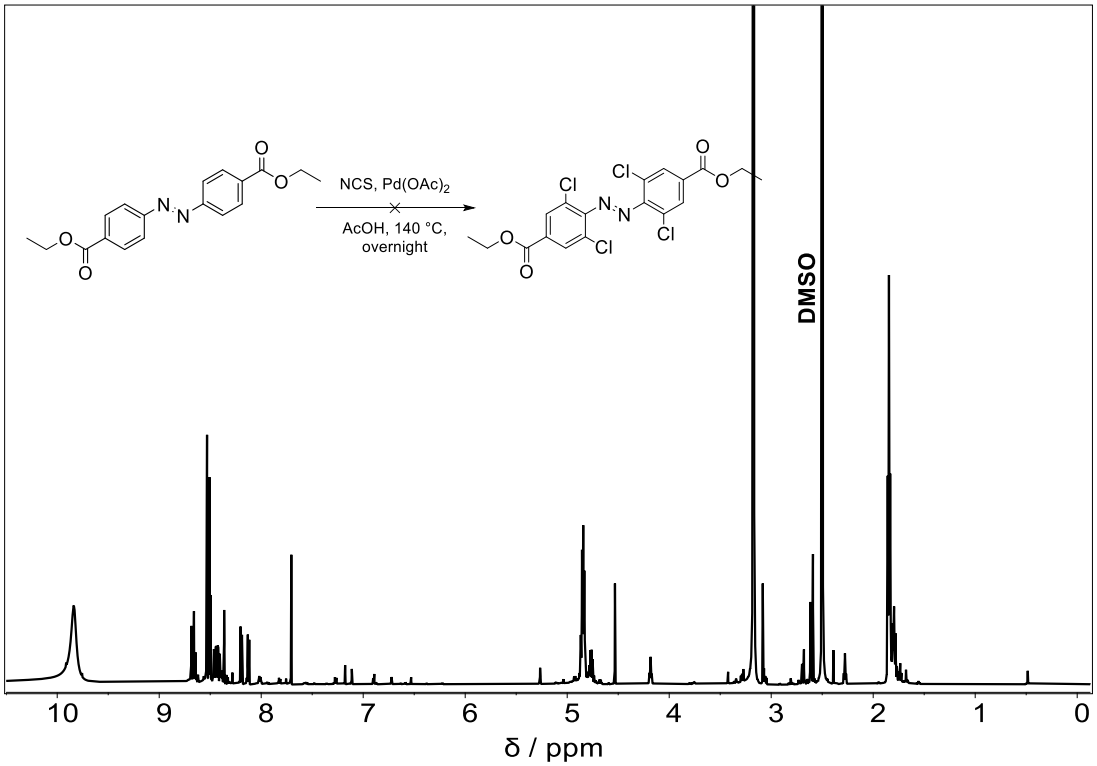

Figure 104. [1]H NMR spectrum of the attempted tetra-chlorination of the di-ester azobenzene in DMSO.

10.1.9.2 Di-ester Azobenzene

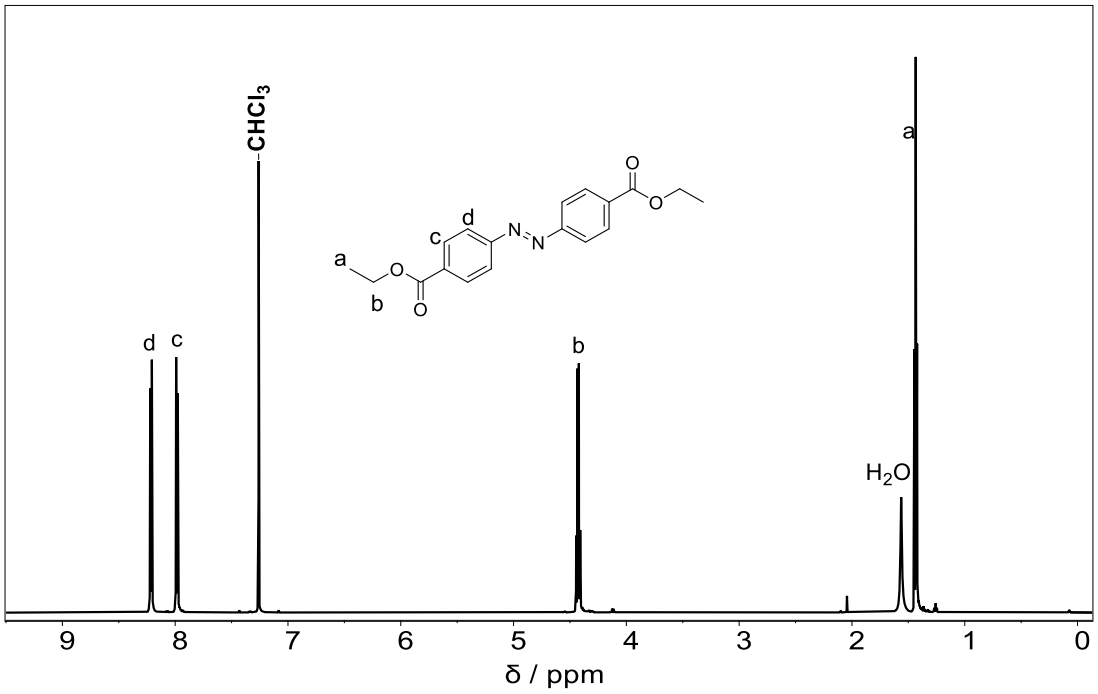

Figure 105. ^{1}H NMR spectrum of di-ester azobenzene of the di-acid azobenzene in $CDCl_3$.

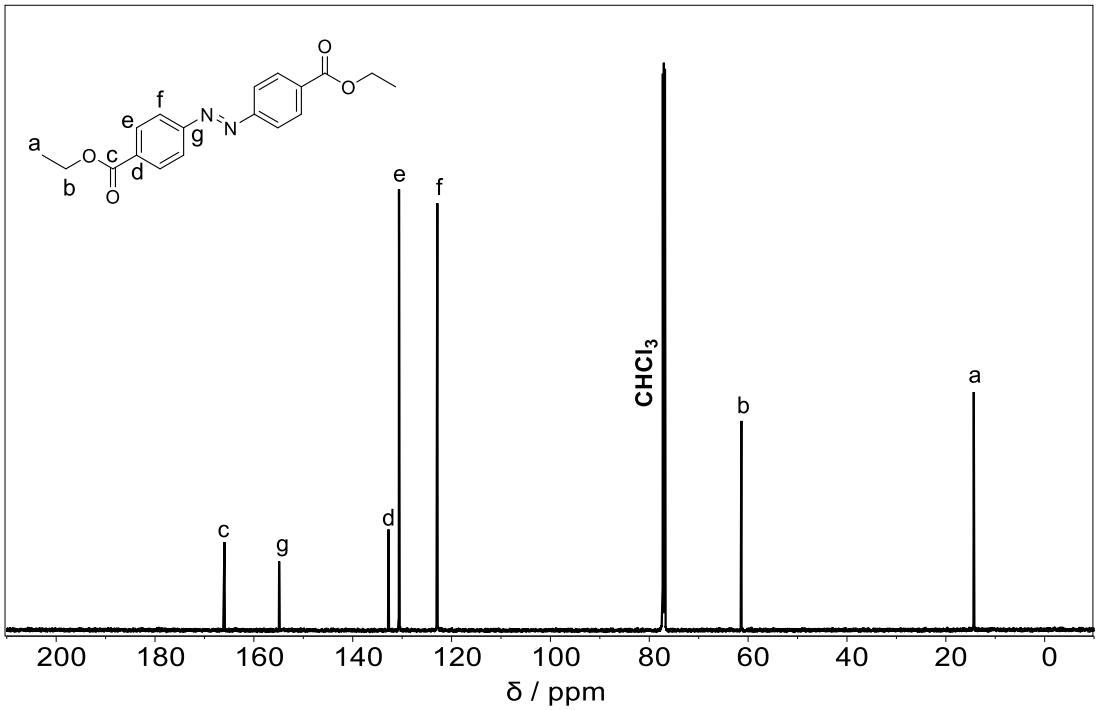

Figure 106. ^{13}C NMR spectrum of di-ester azobenzene of the di-ester azobenzene in $CDCl_3$.

10.1.9.3 Tetra Chlorinated Di-ester Azobenzene

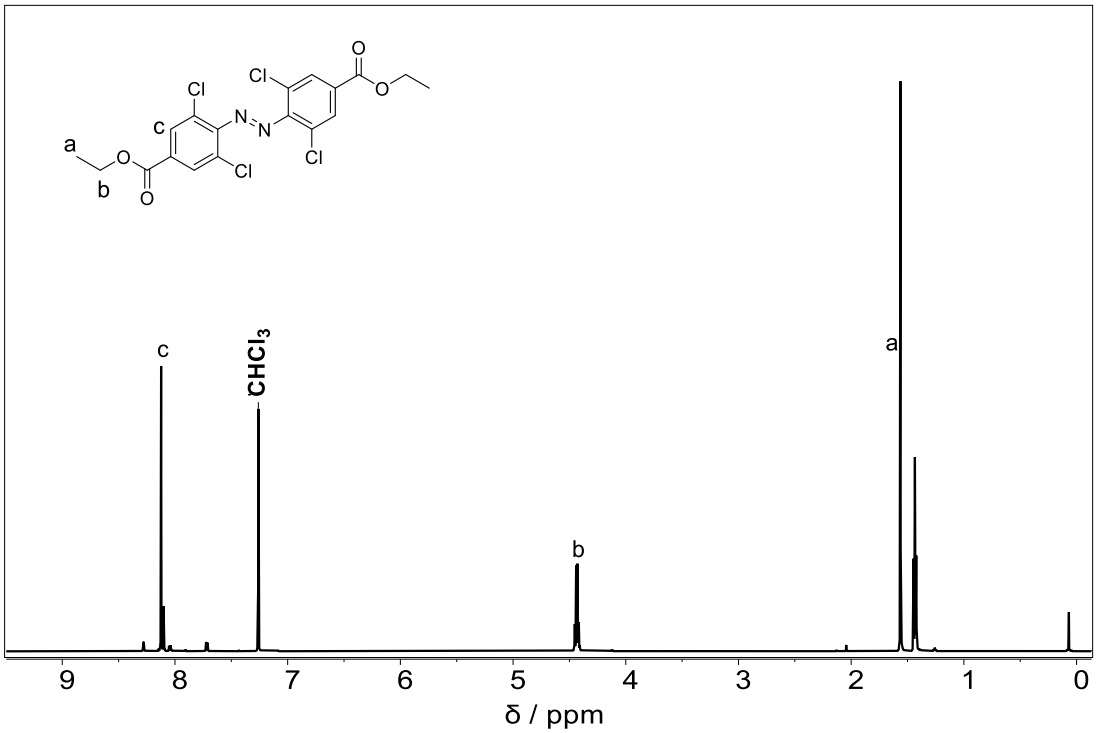

Figure 107. ^{1}H NMR spectrum of tetra-chlorinated di-ester azobenzene in $CDCl_3$.

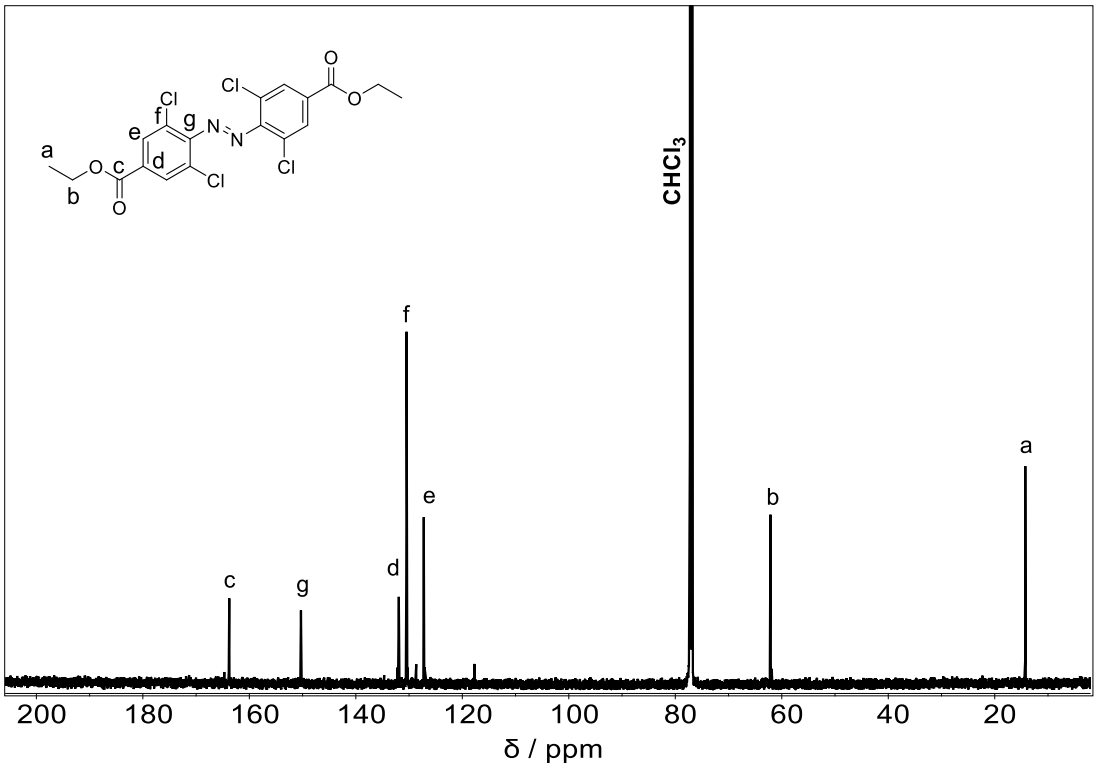

Figure 108. ^{13}C NMR spectrum of tetra-chlorinated di-ester azobenzene in $CDCl_3$.

10.1.9.4 Tetra Chlorinated Di-acid Chloride Azobenzene

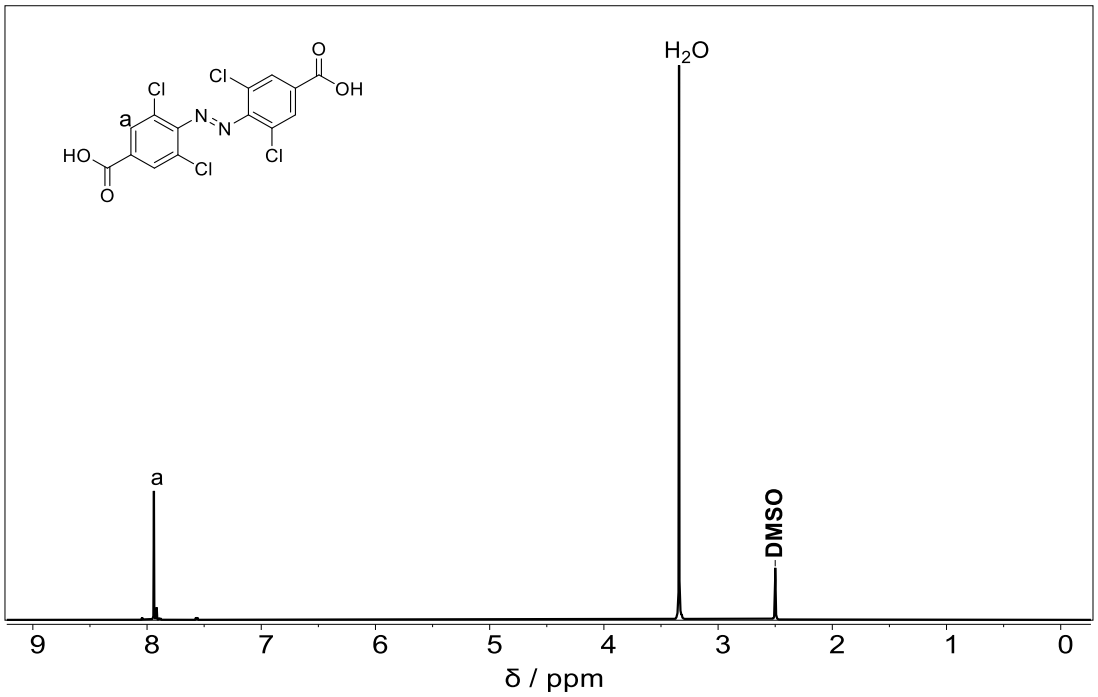

Figure 109. ^{1}H NMR spectrum of tetra-chlorinated di-acid azobenzene in DMSO.

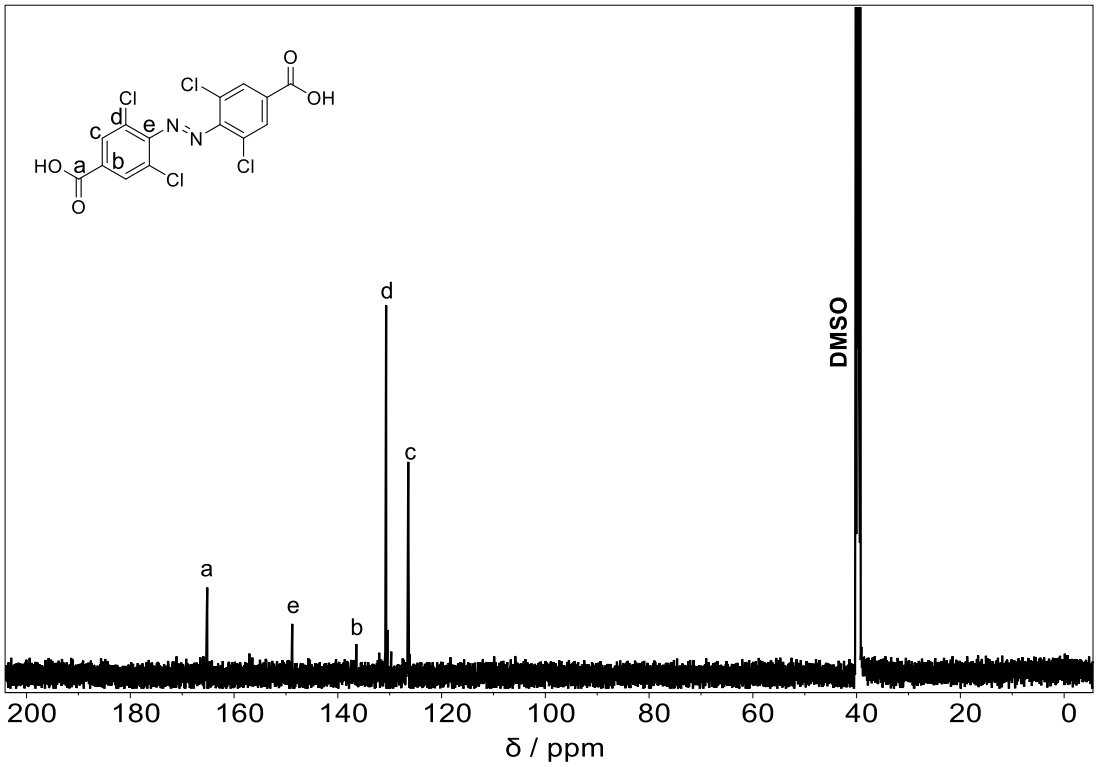

Figure 110. ^{13}C NMR spectrum of tetra-chlorinated di-acid azobenzene in DMSO.

10.1.9.5 Tetra Chlorinated Di-acid Chloride Azobenzene

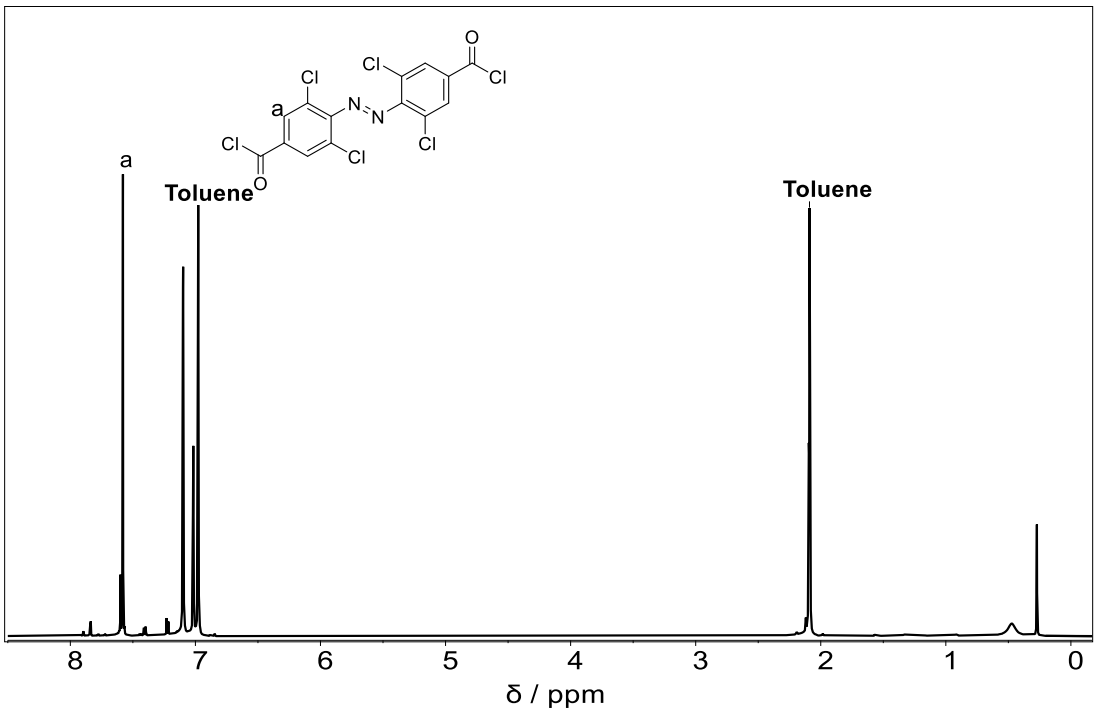

Figure 111. ^{1}H NMR spectrum of tetra-chlorinated di-acid chloride azobenzene in tol_{d8}.

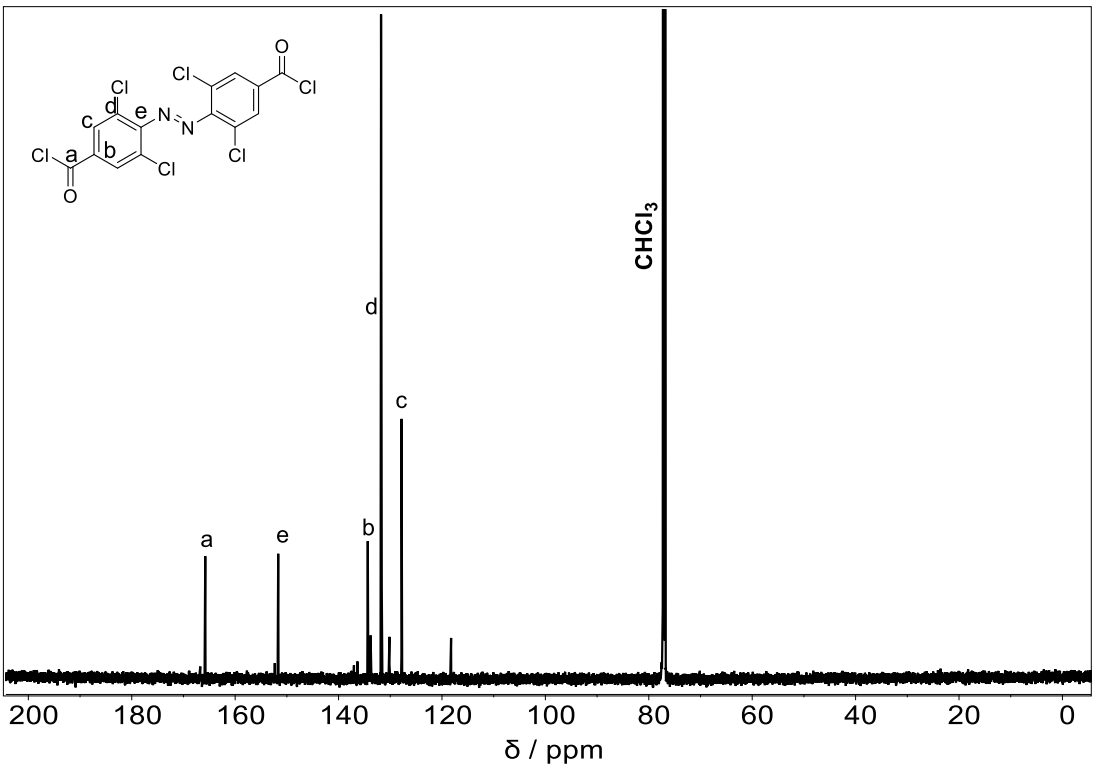

Figure 112. ^{13}C NMR spectrum of tetra-chlorinated di-acid chloride azobenzene in $CDCl_3$.

10.1.9.6 Tetra Chlorinated PFP-ester Azobenzene

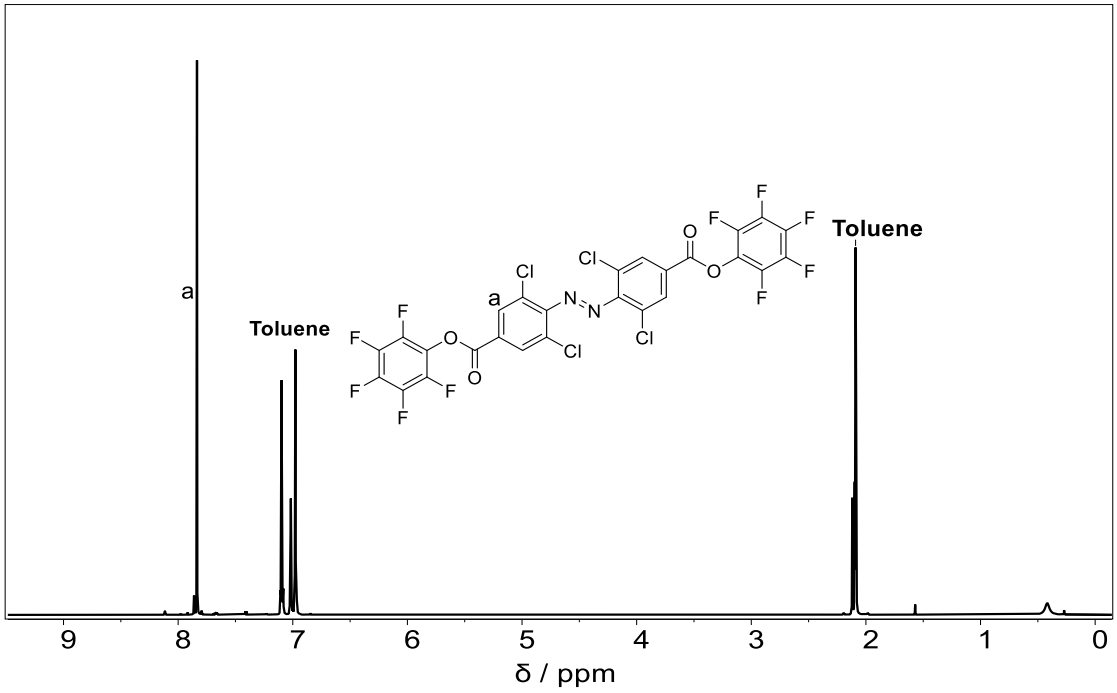

Figure 113. ^{1}H NMR spectrum of tetra-chlorinated PFP-ester azobenzene in tol_{d8}.

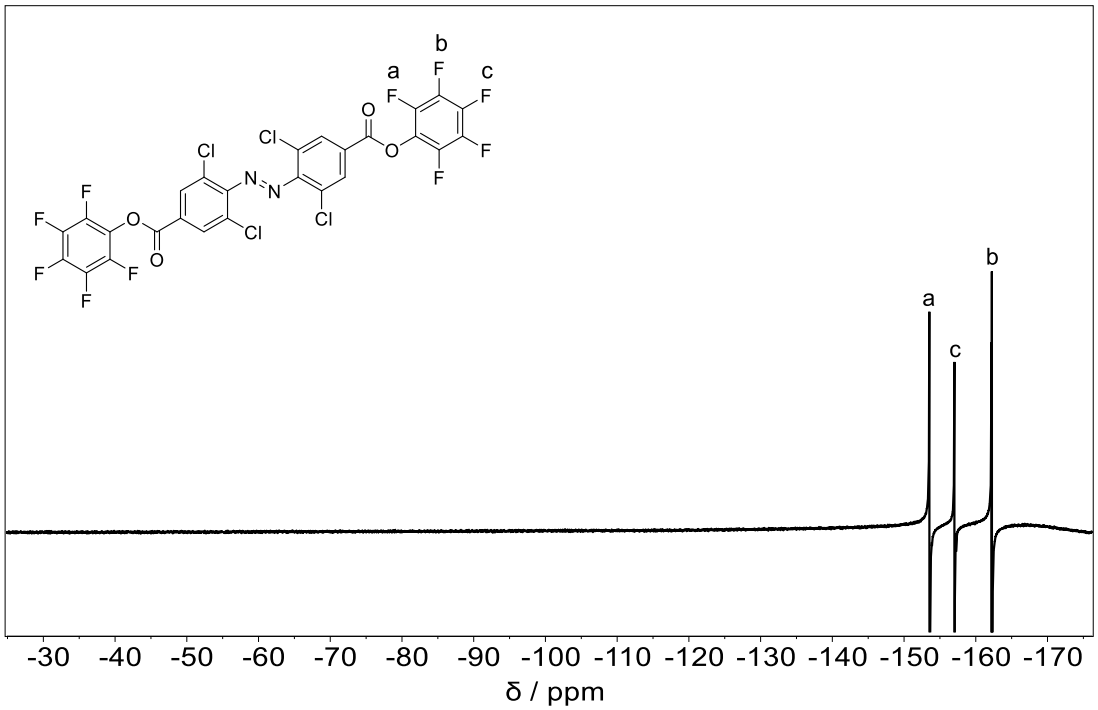

Figure 114. ^{19}F NMR spectrum of tetra-chlorinated PFP-ester azobenzene in tol_{d8}.

10.1.10 Light-Driven Folding via Metal-Complexation

10.1.10.1 Oxazole Indolenine

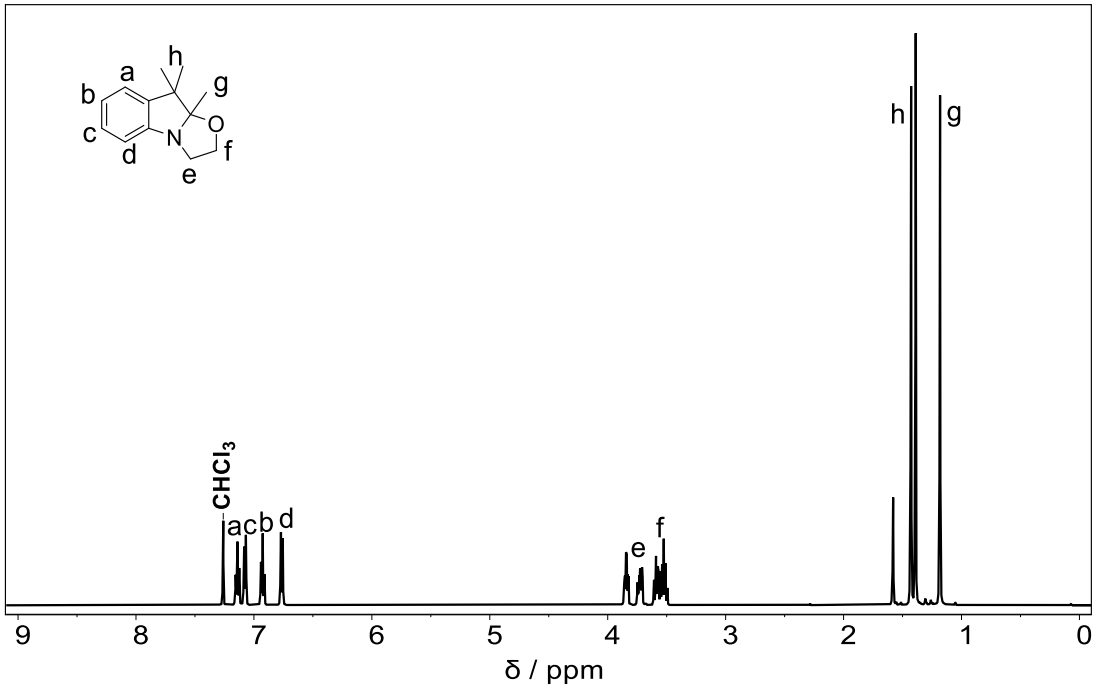

Figure 115. [1]H NMR spectrum of oxazole indolenine in $CDCl_3$.

10.1.10.2 Hydroxyethyl Spiropyran

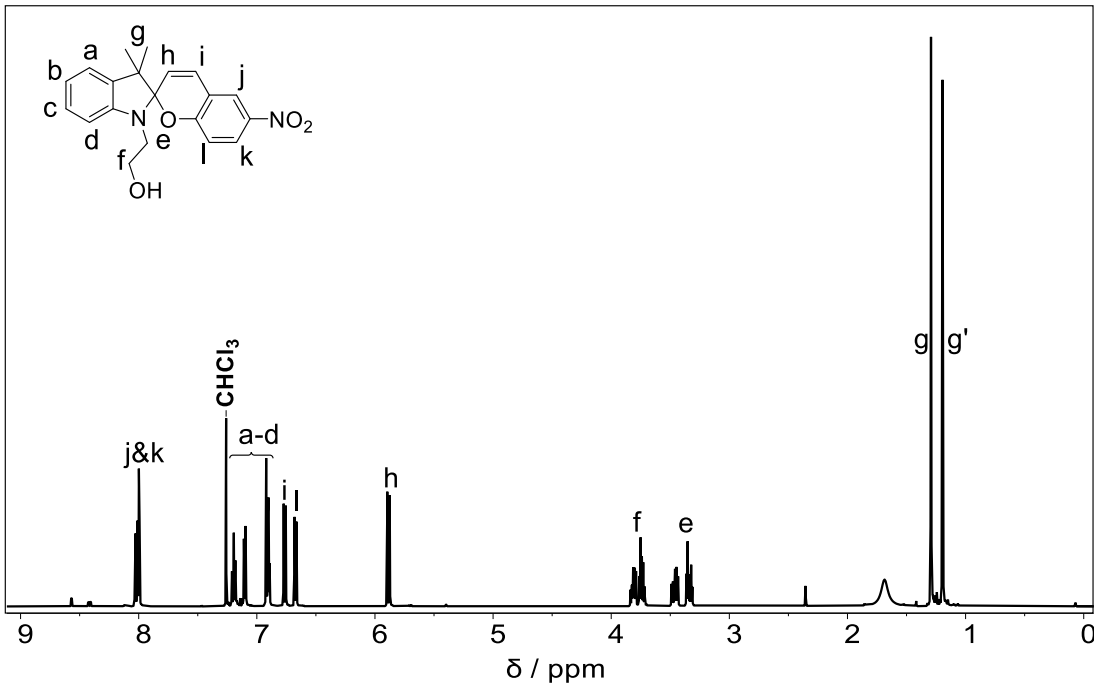

Figure 116. [1]H NMR spectrum of hydroxyethyl spiropyran in $CDCl_3$.

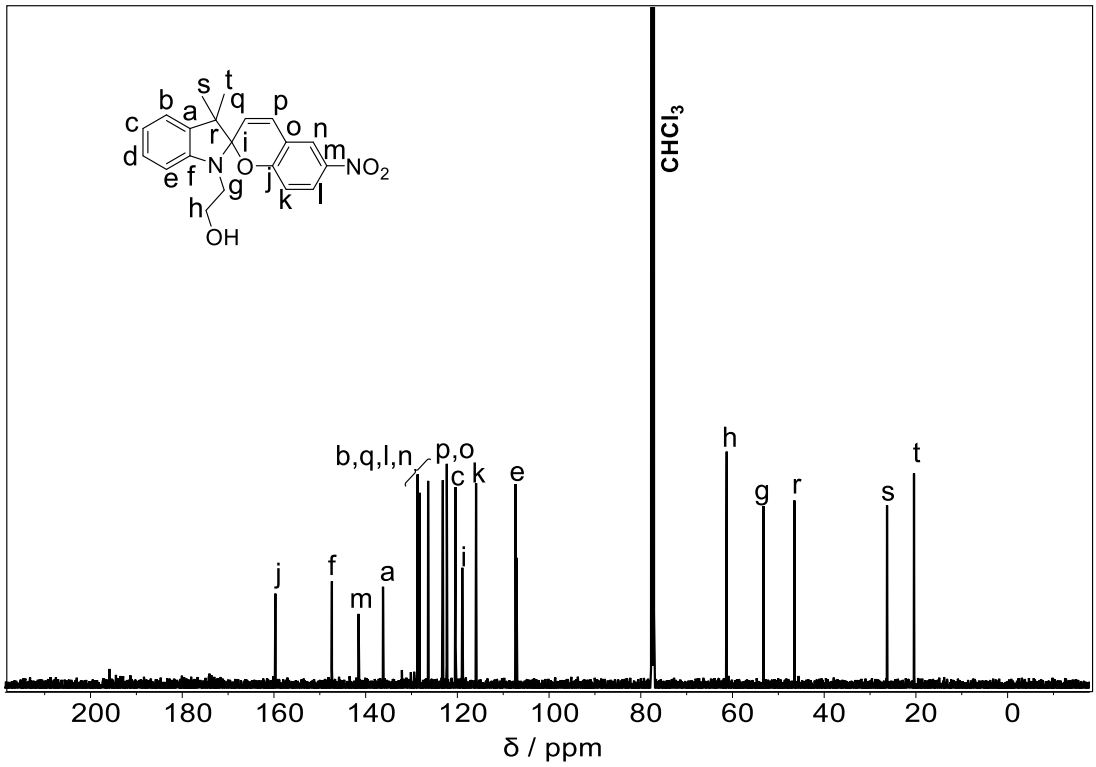

Figure 117. ^{13}C NMR spectrum of hydroxyethyl spiropyran in $CDCl_3$.

10.1.10.3 Spiropyran Methyl Methacrylate

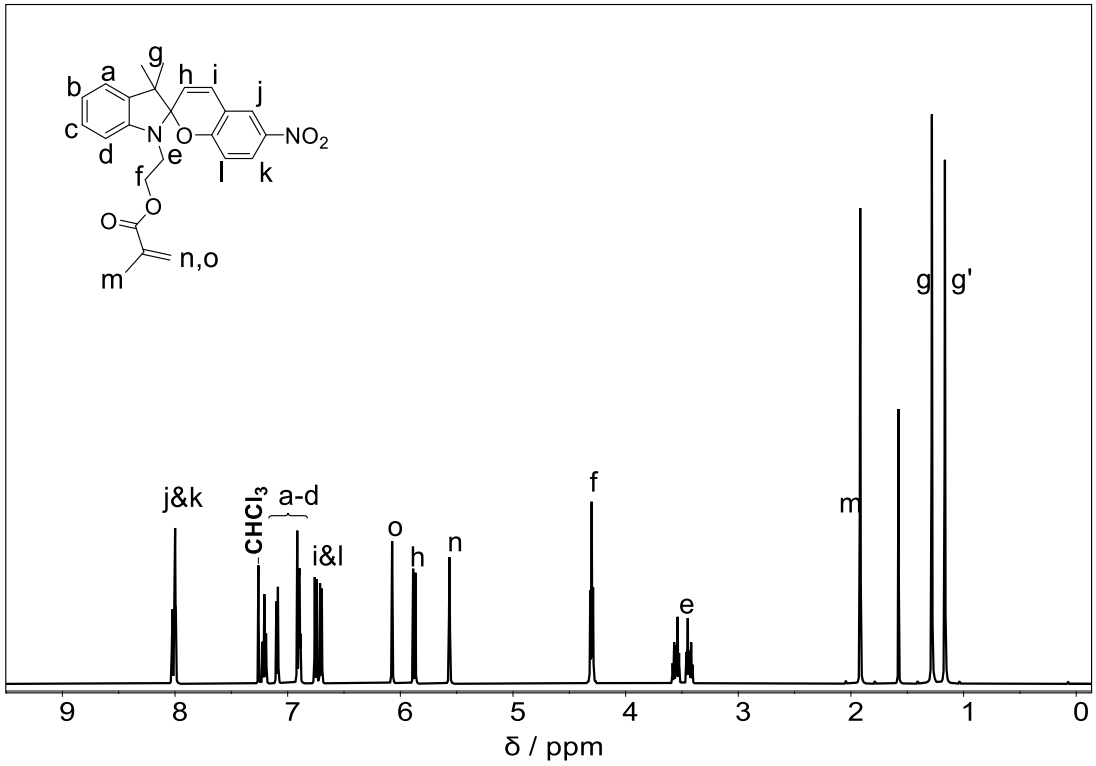

Figure 118. ^{1}H NMR spectrum of spiropyran methyl methacrylate in $CDCl_3$.

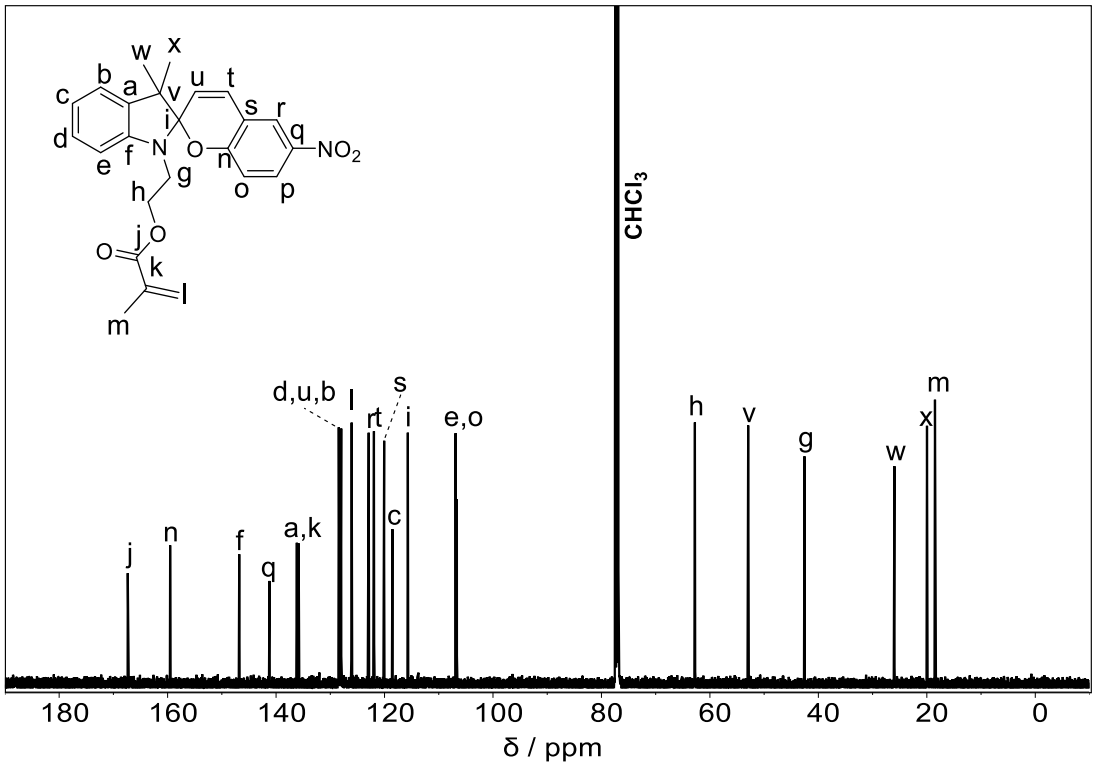

Figure 119. ^{13}C NMR spectrum of spiropyran methyl methacrylate in $CDCl_3$.

10.2 Styrene Polymers

10.2.1 Benzyl Chloride Polymer

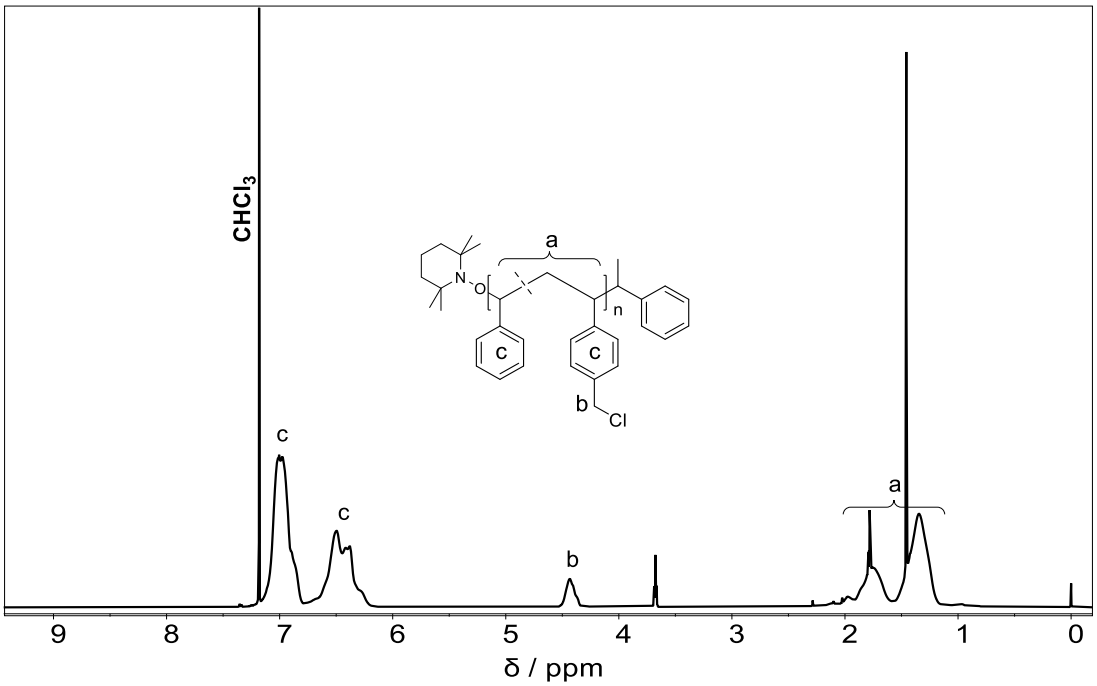

Figure 120. ^{1}H NMR spectrum of the linear benzyl chloride polymer in $CDCl_3$.

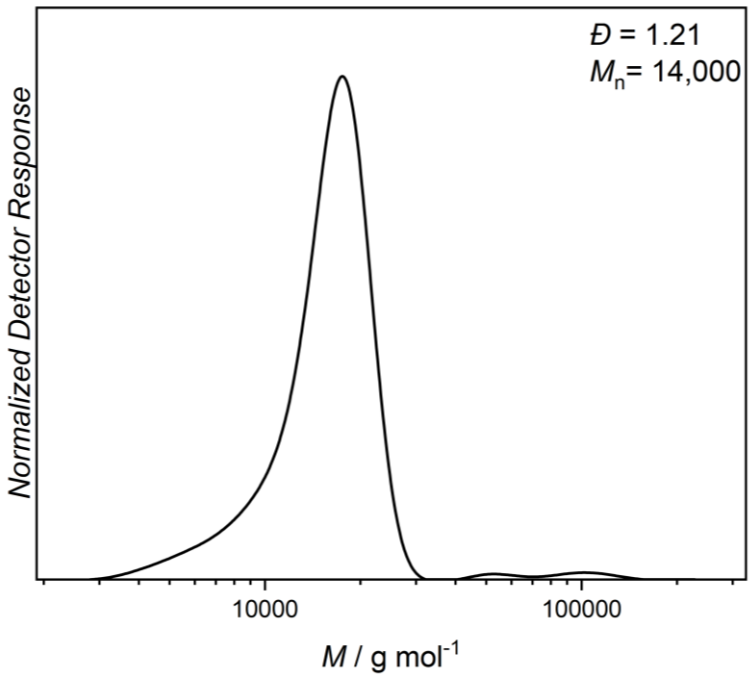

Figure 121. SEC elugram of the linear benzyl chloride polymer measured in THF (polystyrene calibration standards).

10.2.2 Benzyl Chloride, Gold-Complexed Phosphine Polymer

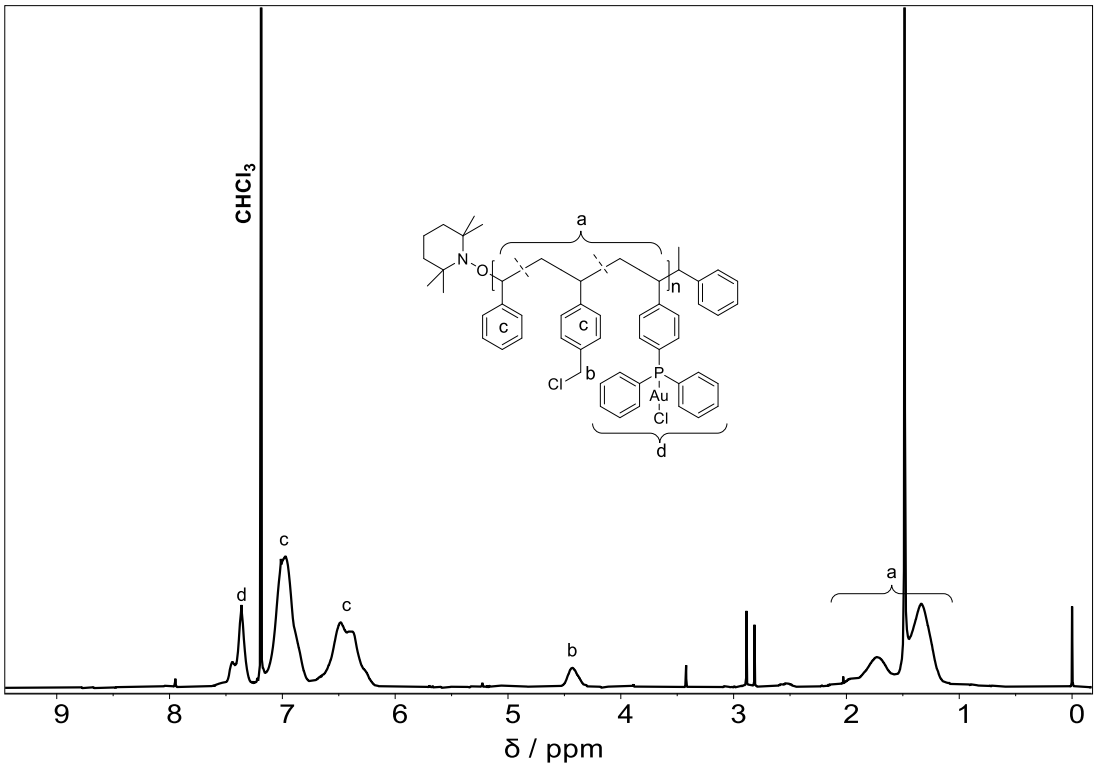

Figure 122. ^{1}H NMR spectrum of the linear benzyl chloride, gold-phosphine in polymer in $CDCl_3$.

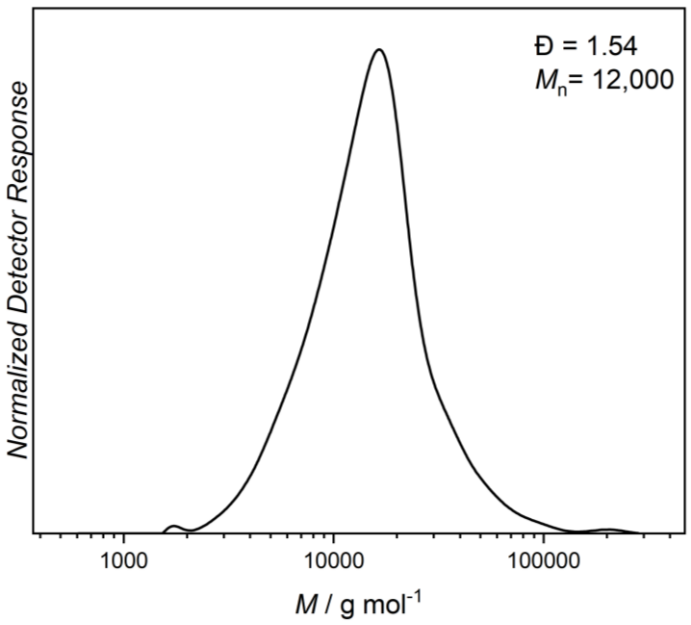

Figure 123. SEC elugram of the linear benzyl chloride, gold-phosphine polymer measured in THF (polystyrene calibration standards).

10.2.3 P-13

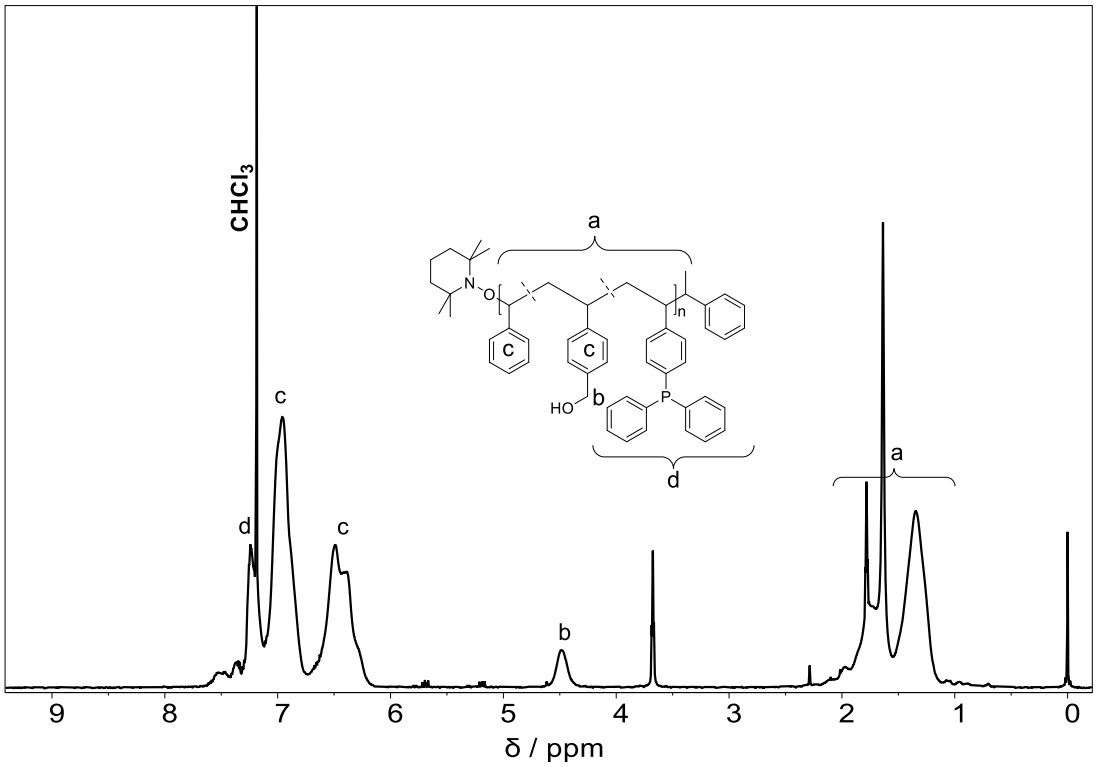

Figure 124. ^{1}H NMR spectrum of **P-13** in $CDCl_3$.

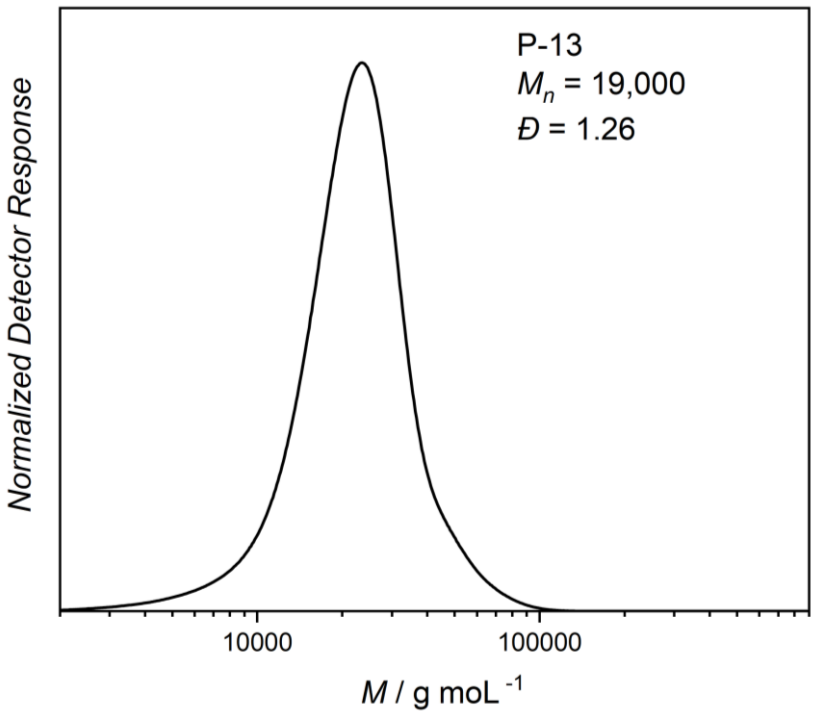

Figure 125. SEC elugram of **P-13** measured in THF (polystyrene calibration standards).

10.2.4 Au-P-13

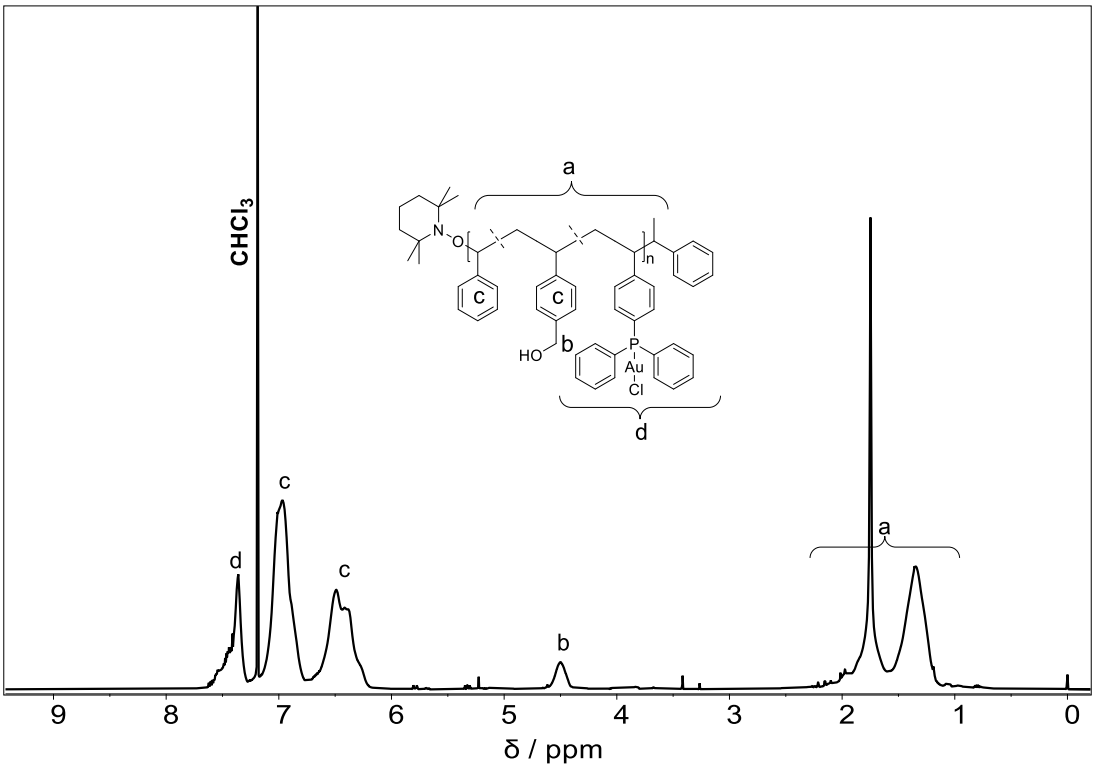

Figure 126. ^{1}H NMR spectrum of **Au-P-13** in $CDCl_3$.

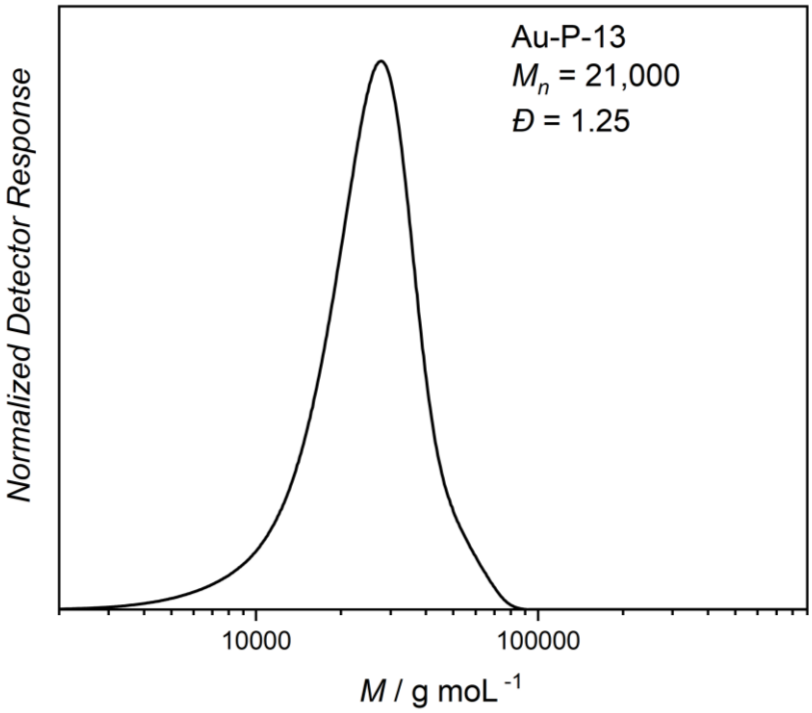

Figure 127. SEC elugram of **Au-P-13** measured in THF (polystyrene calibration standards).

10.2.5 P-23

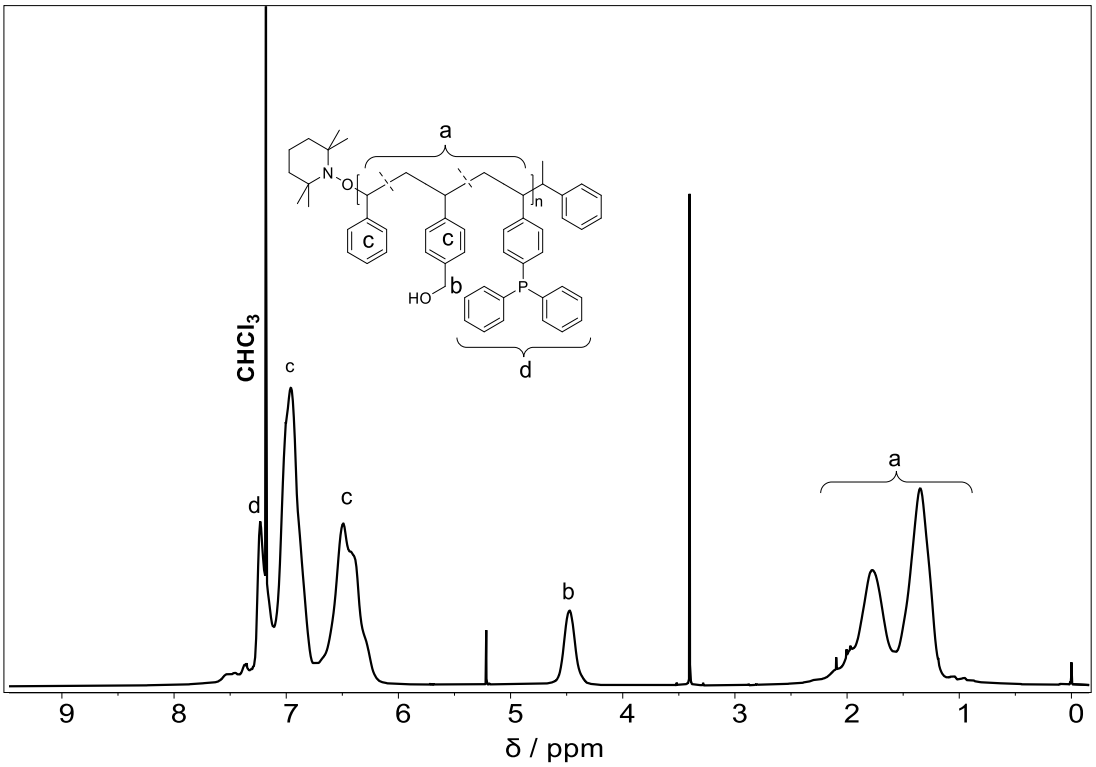

Figure 128. ^{1}H NMR spectrum of **P-23** in $CDCl_3$.

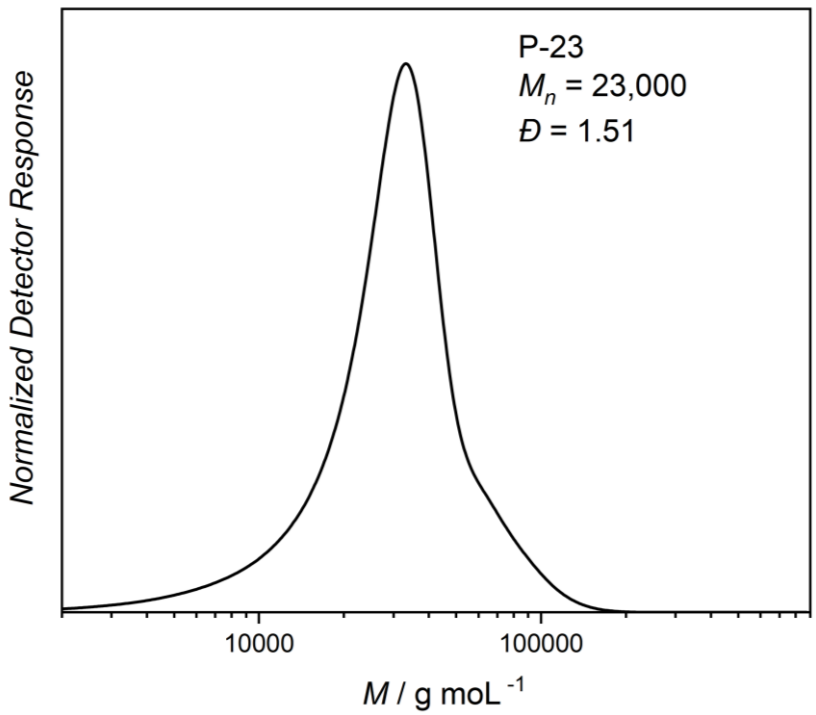

Figure 129. SEC elugram of **P-23** measured in THF (polystyrene calibration standards).

10.2.6 Au-P-23

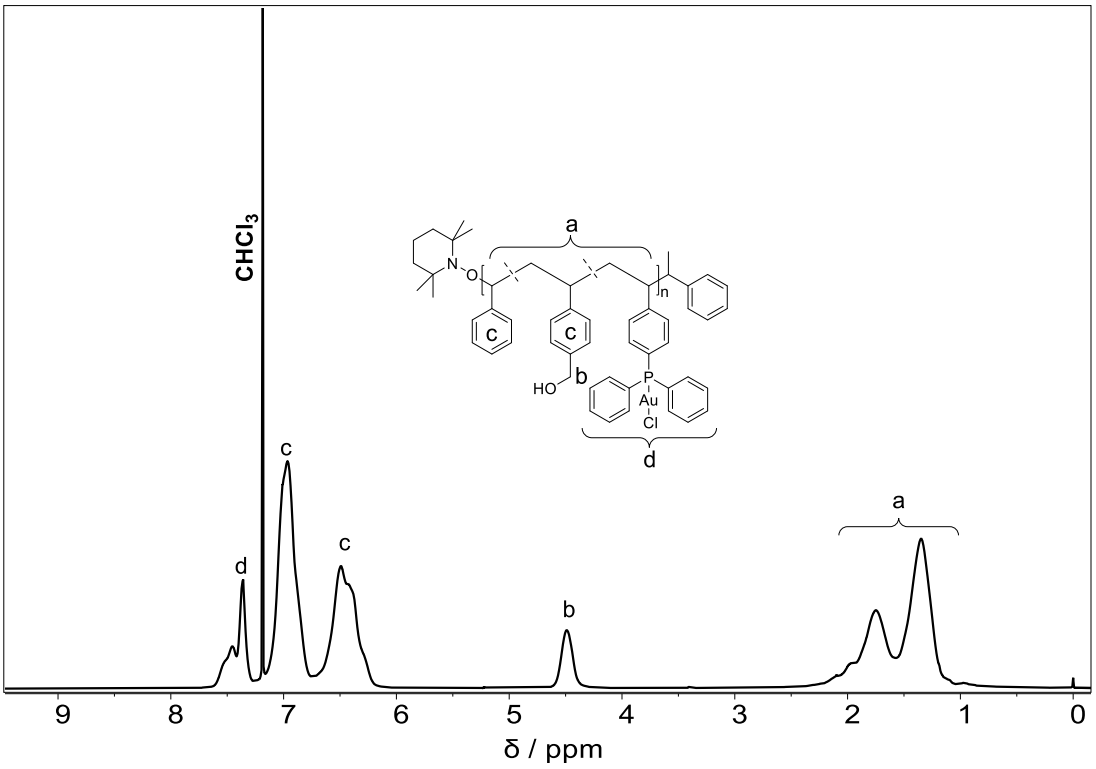

Figure 130. ^{1}H NMR spectrum of **Au-P-23** in $CDCl_3$.

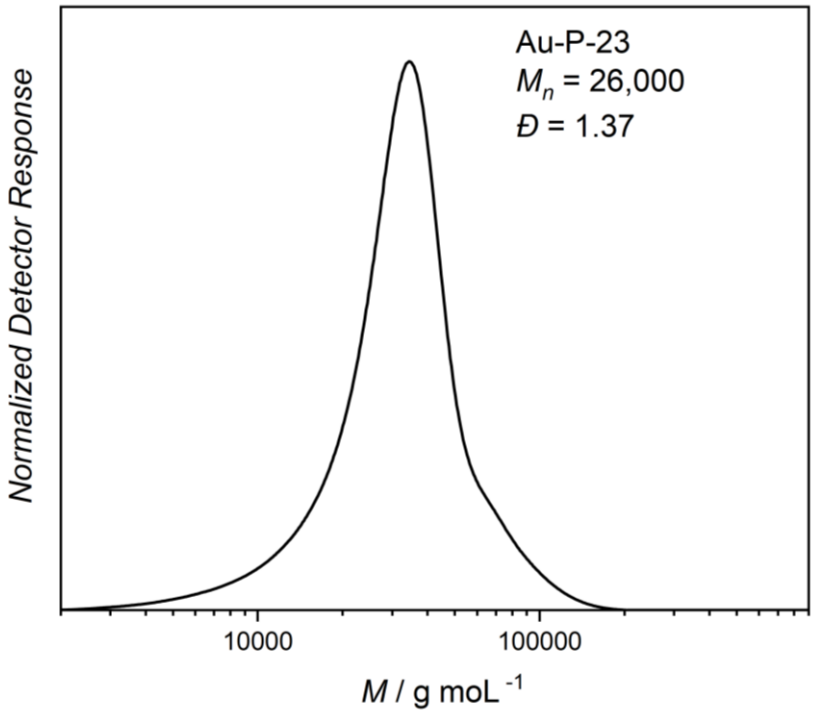

Figure 131. SEC elugram of **Au-P-23** measured in THF (polystyrene calibration standards).

10.3 Methyl Methacrylate Polymers

10.3.1 SP-36-PEGMEMA

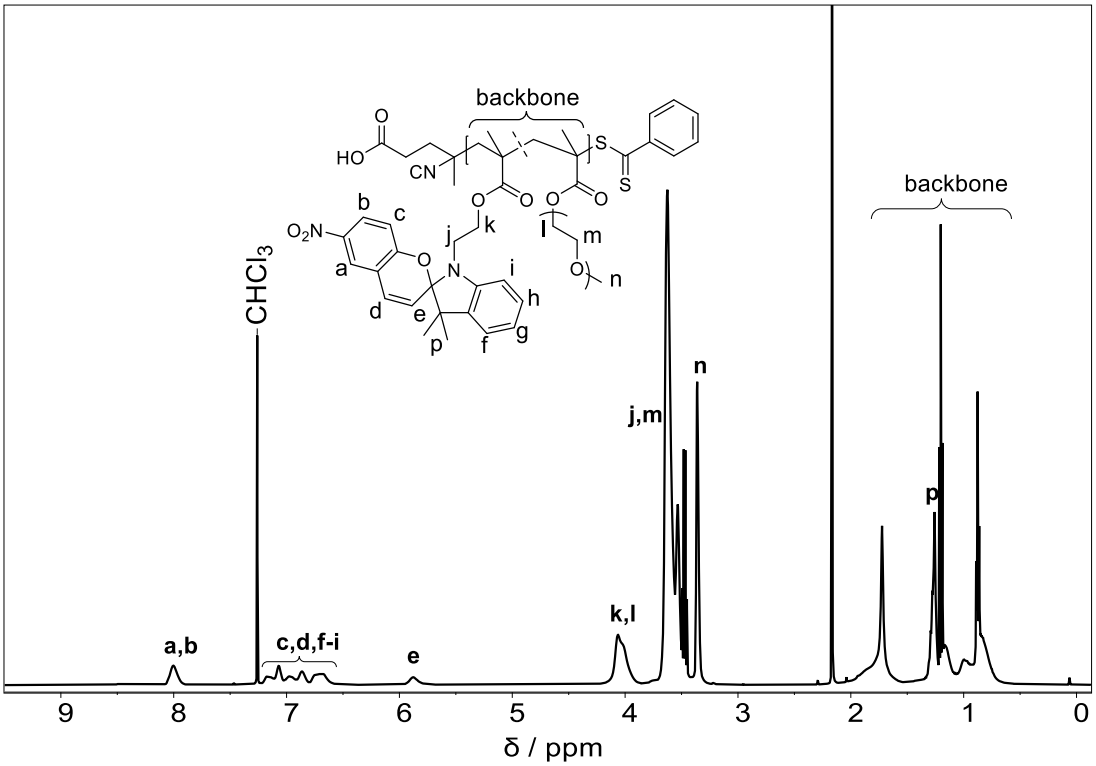

Figure 132. ^{1}H NMR spectrum of **SP-36-PEGMEMA** in $CDCl_3$.

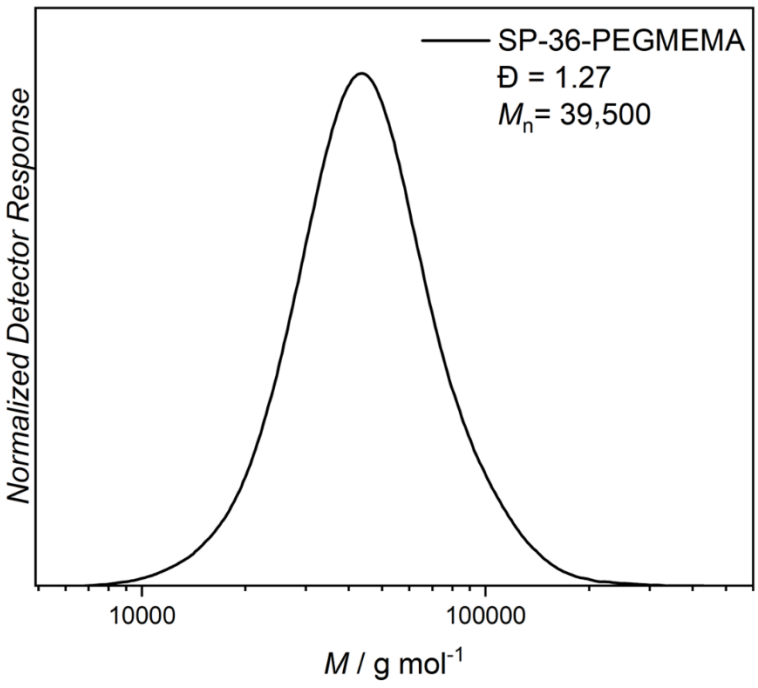

Figure 133. SEC elugram of **SP-36-PEGMEMA** measured in THF (polystyrene calibration standards).

10.3.2 SP-15-PEGEMEMA

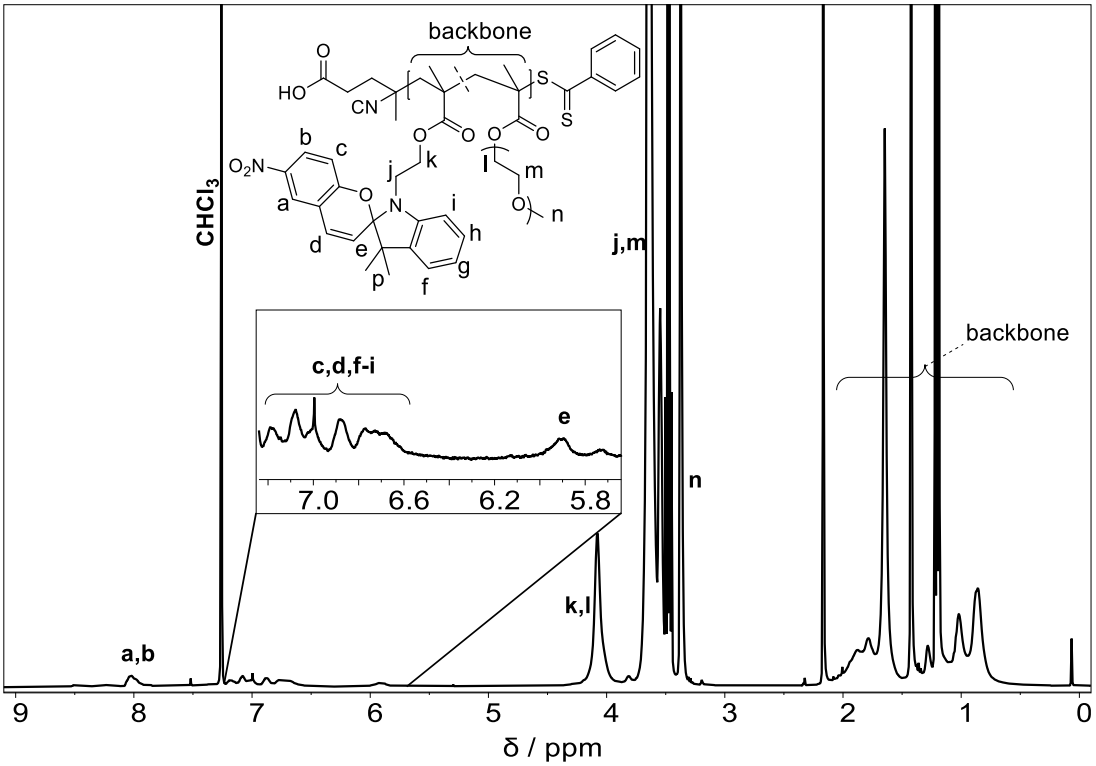

Figure 134. ^{1}H NMR spectrum of **SP-15-PEGMEMA** in $CDCl_3$.

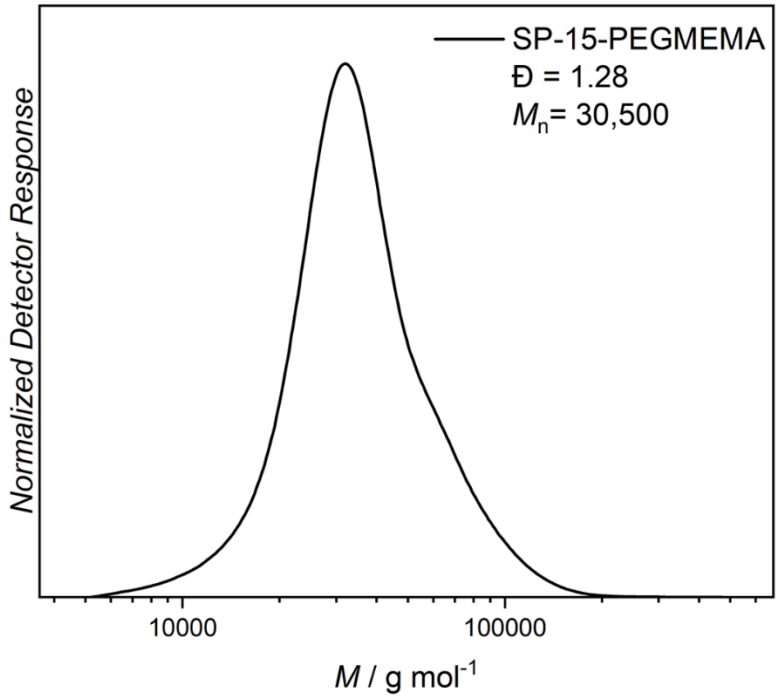

Figure 135. SEC elugram of **SP-15-PEGMEMA** measured in THF (polystyrene calibration standards).

10.3.3 SP-20-MMA

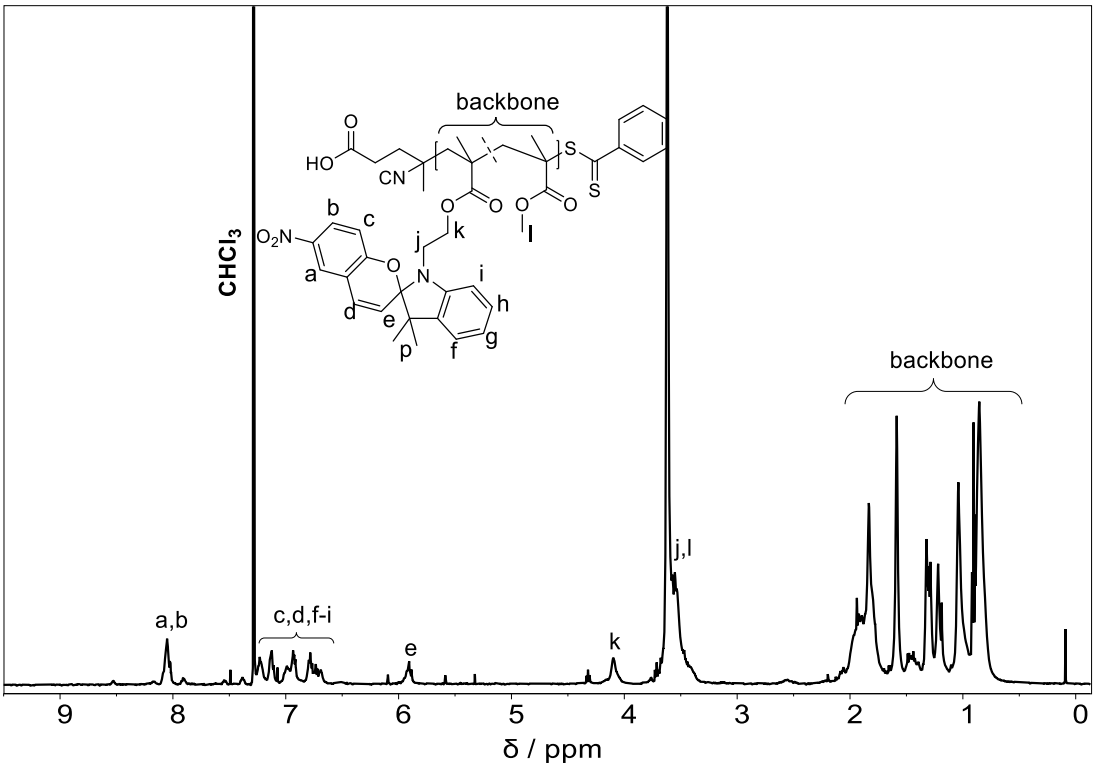

Figure 136. ^{1}H NMR spectrum of **SP-20-MMA** in $CDCl_3$.

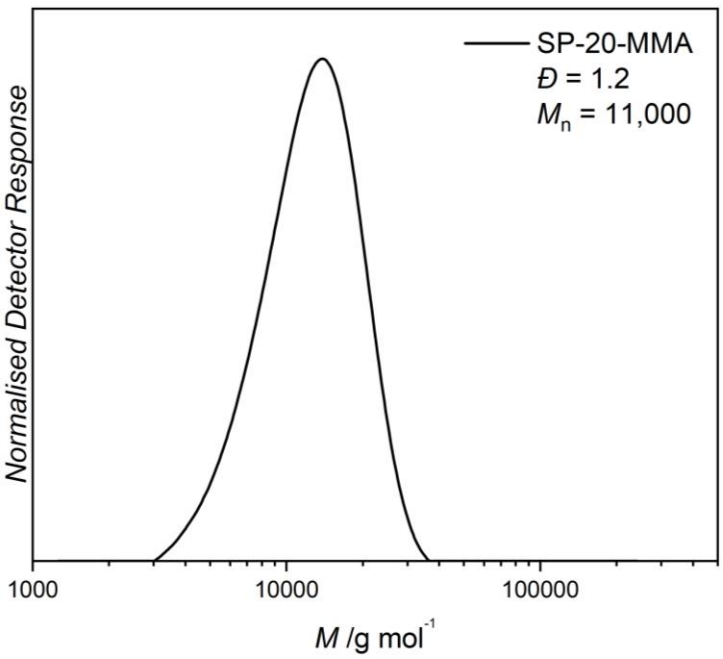

Figure 137. SEC elugram of **SP-20-MMA** measured in THF (polystyrene calibration standards).

10.3.4Test PEGMEMA Polymer

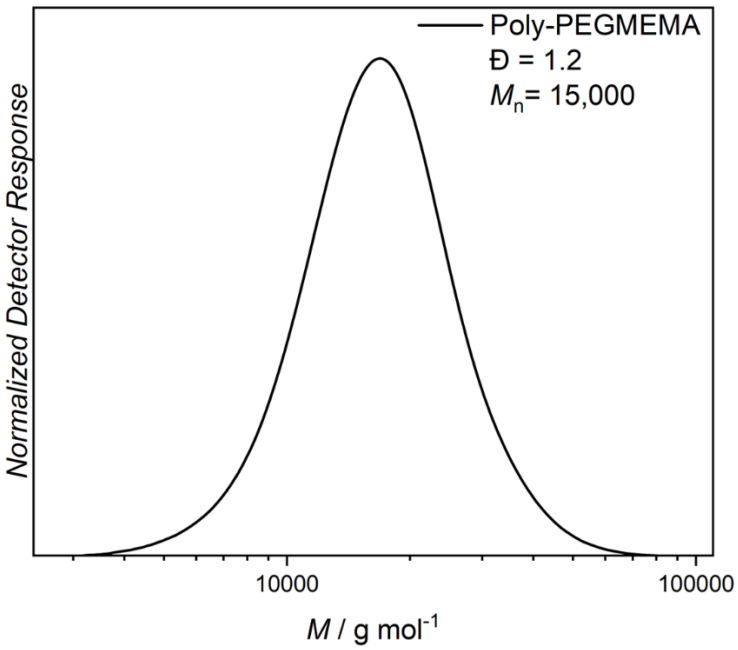

Figure 138. SEC elugram of the test PEGMEMA polymer measured in THF (polystyrene calibration standards).

10.4 SCNPs

10.4.1 Di-acid Azobenzene Test Crosslinking

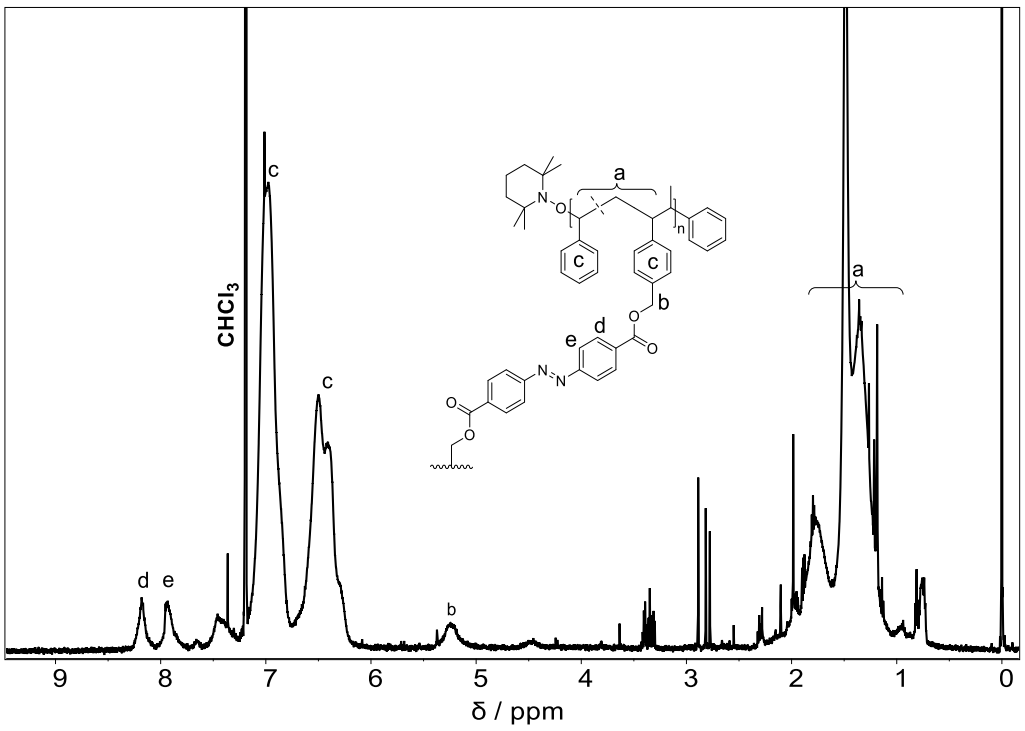

Figure 139. ^{1}H NMR spectrum of the SCNP generated via the crosslinking of the linear benzyl chloride polymer with di-acid azobenzene in $CDCl_3$

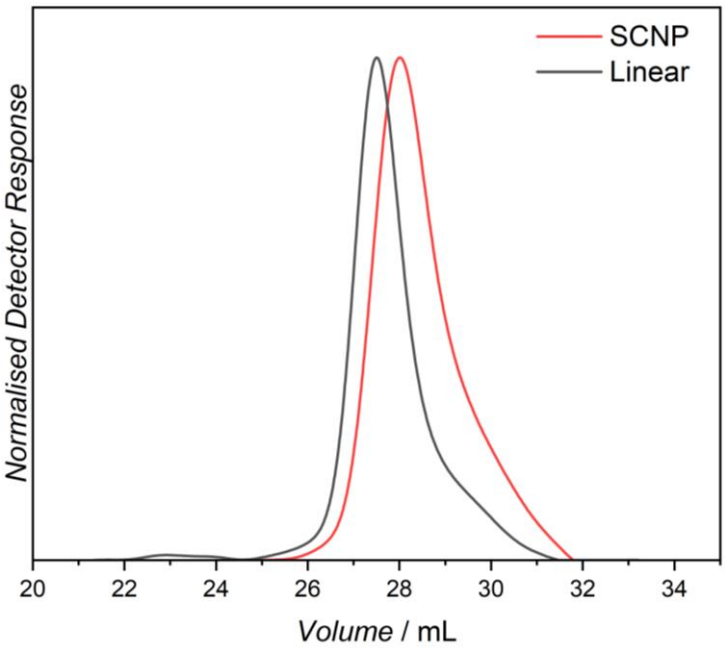

Figure 140. SEC elugram of the SCNP and benzyl chloride linear polymer measured in THF (polystyrene calibration standards).

10.4.2 Di-acid Azobenzene Crosslinking

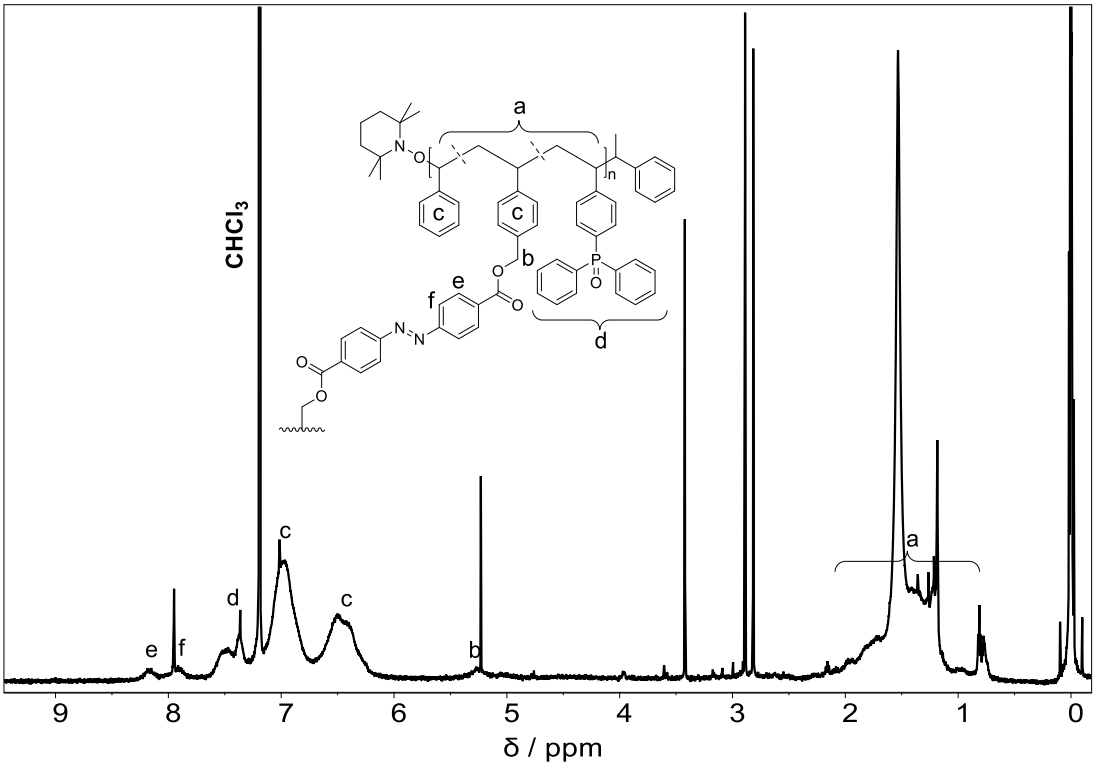

Figure 141. ^{1}H NMR spectrum of the SCNP generated via the crosslinking of the benzyl chloride, gold-phosphine polymer with di-acid azobenzene in $CDCl_3$.

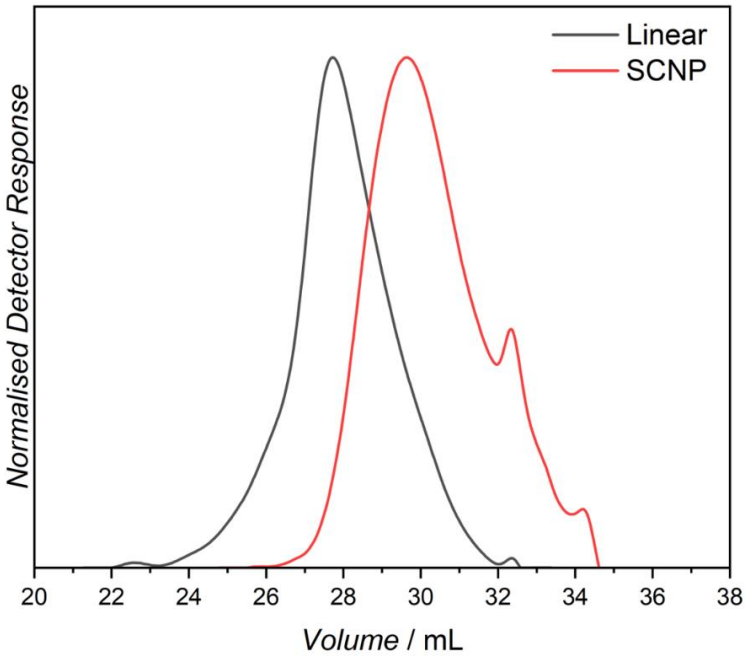

Figure 142. SEC elugram of the SCNP and the linear benzyl chloride, gold-phosphine polymer measured in THF (polystyrene calibration standards).

10.4.3 PFP-Azo Crosslinking

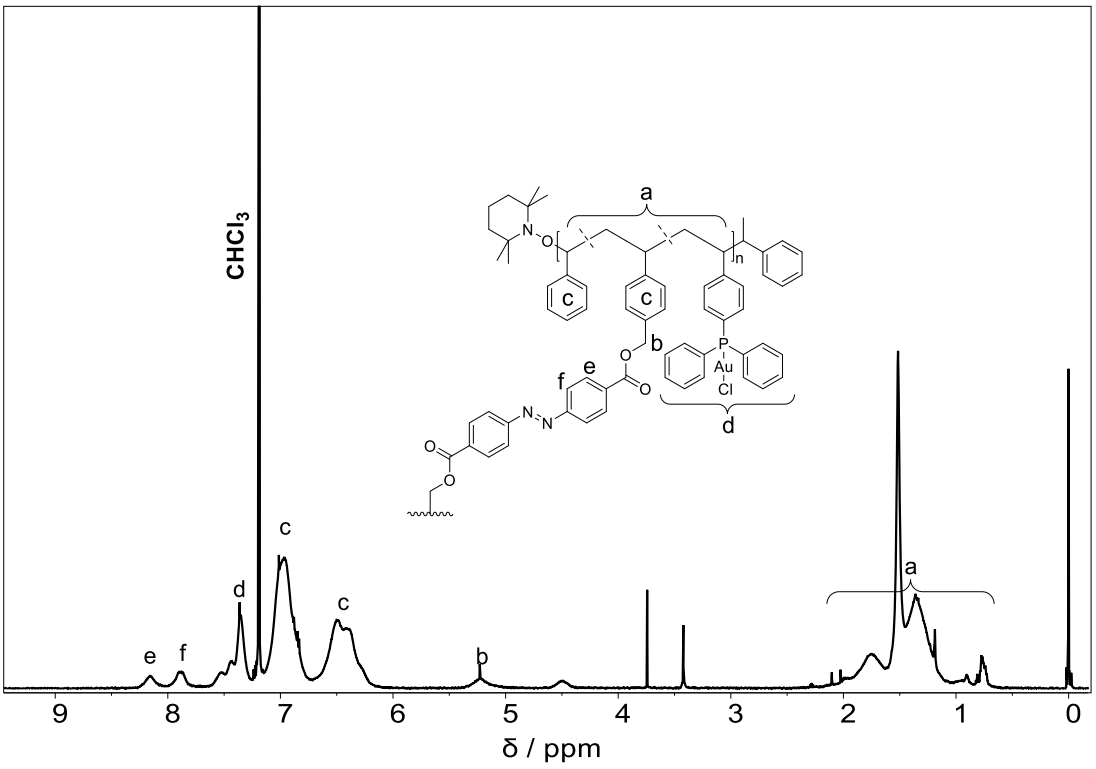

Figure 143. ^{1}H NMR spectrum of the SCNP generated via the crosslinking of the **Au-P-13** polymer with PFP-azobenzene in $CDCl_3$.

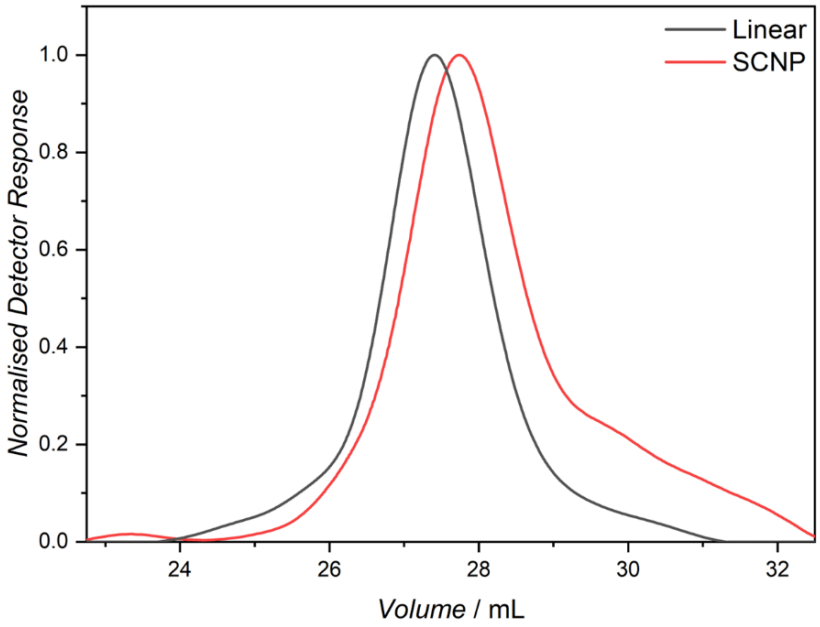

Figure 144. SEC elugram of the SCNP and the linear **Au-P-13** polymer measured in THF (polystyrene calibration standards).

10.4.4 *o*-AzoCl$_4$-PFP Crosslinking (AzoCl$_4$-Au-SCNP-23)

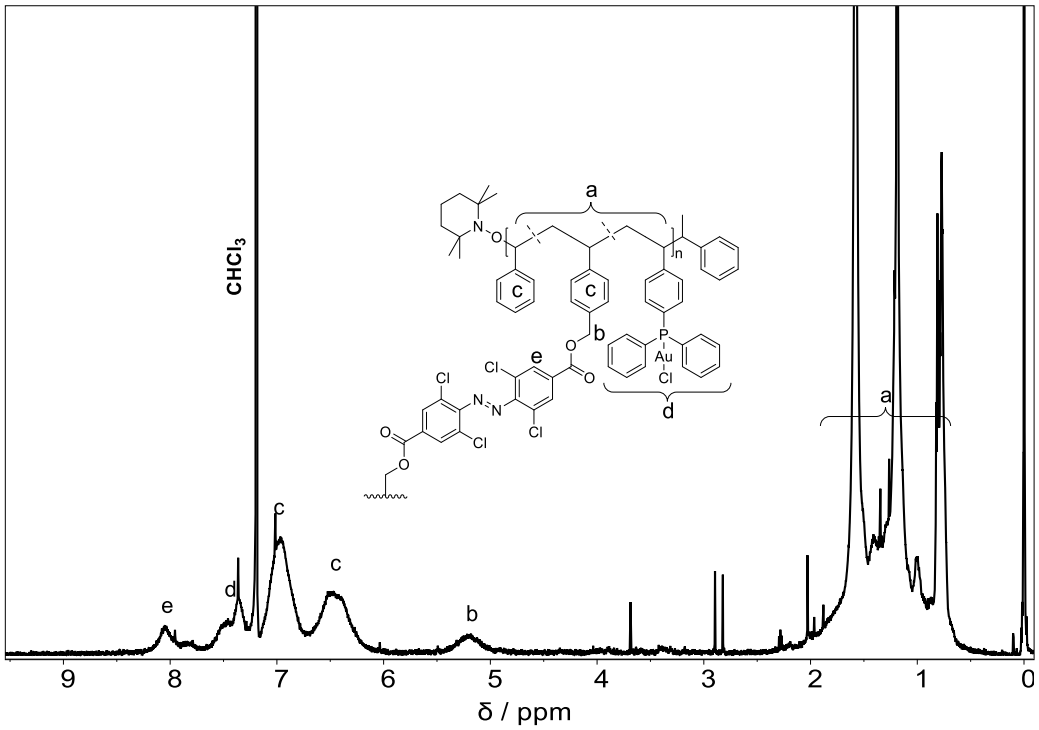

Figure 145. ^{1}H NMR spectrum of the SCNP generated via the crosslinking of the **Au-P-23** polymer with the ***o*-AzoCl$_4$-PFP** crosslinker in $CDCl_3$.

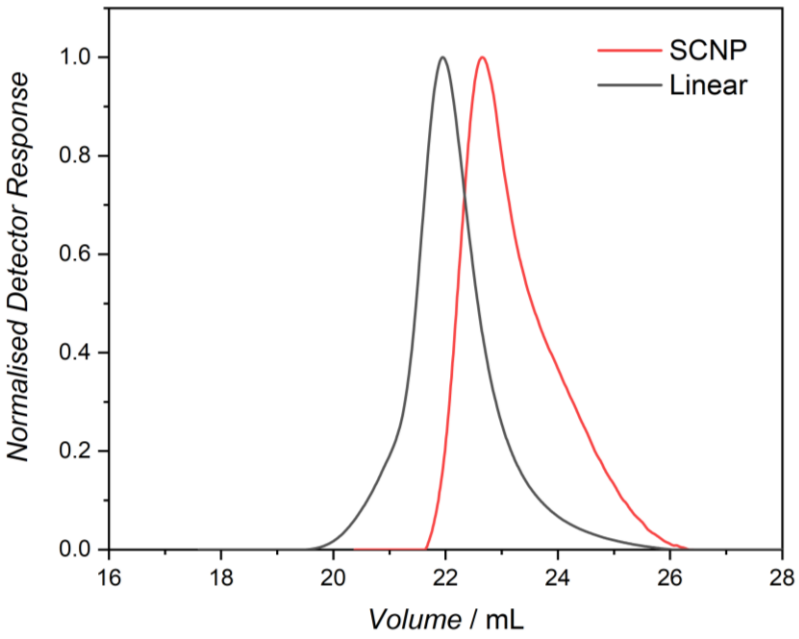

Figure 146. SEC elugram of the SCNP and the linear **Au-P-23** polymer measured in THF (polystyrene calibration standards).

10.4.5 **AzoCl$_4$-Au-SCNP-13 RI and Uv-Vis Trace Overlay**

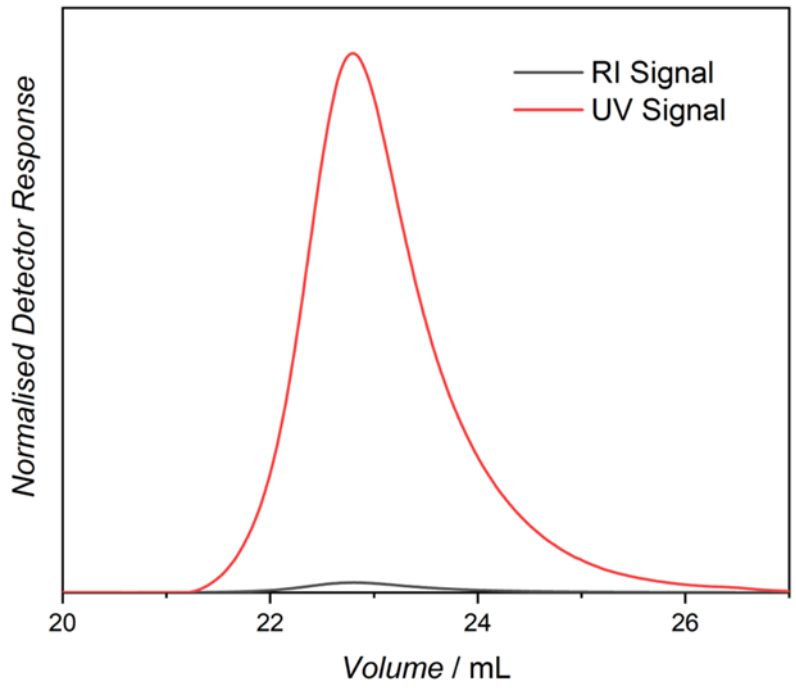

Figure 147. Non-normalized UV signal of **AzoCl$_4$-Au-SCNP-13** overlayed with the non-normalized RI signal, indicating incorporation of azobenzene crosslinks into the SCNP**.**

10.4.6 SP-20-MMA Copper Complexation

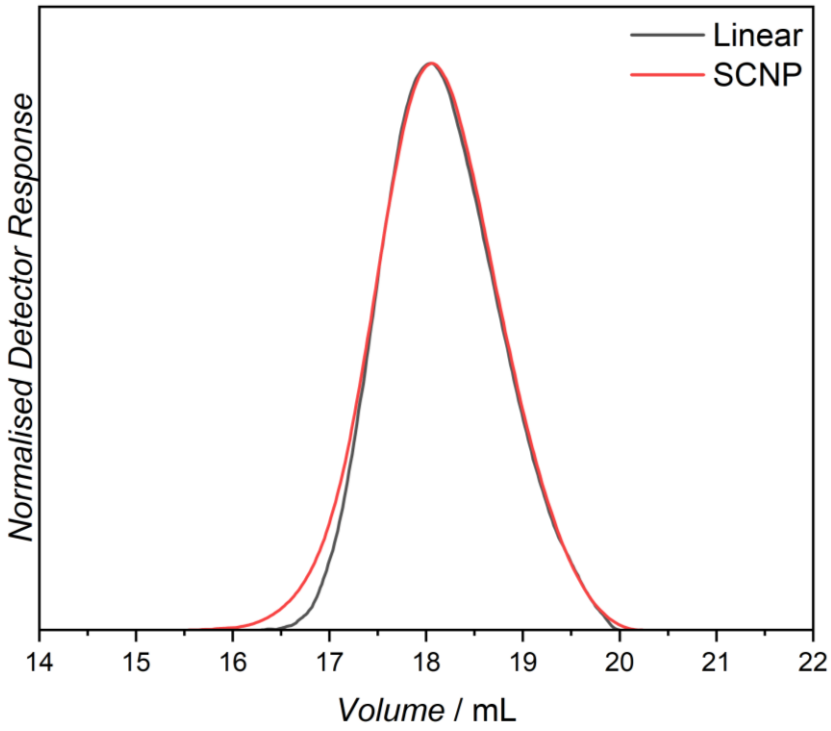

Figure 148. Attempted Crosslinking of **SP-20-MMA** with 1 eqv of $CuCl_2 \cdot 2H_2O$.

10.4.7 Cobalt Complexation, SP-15-PEGMEMA

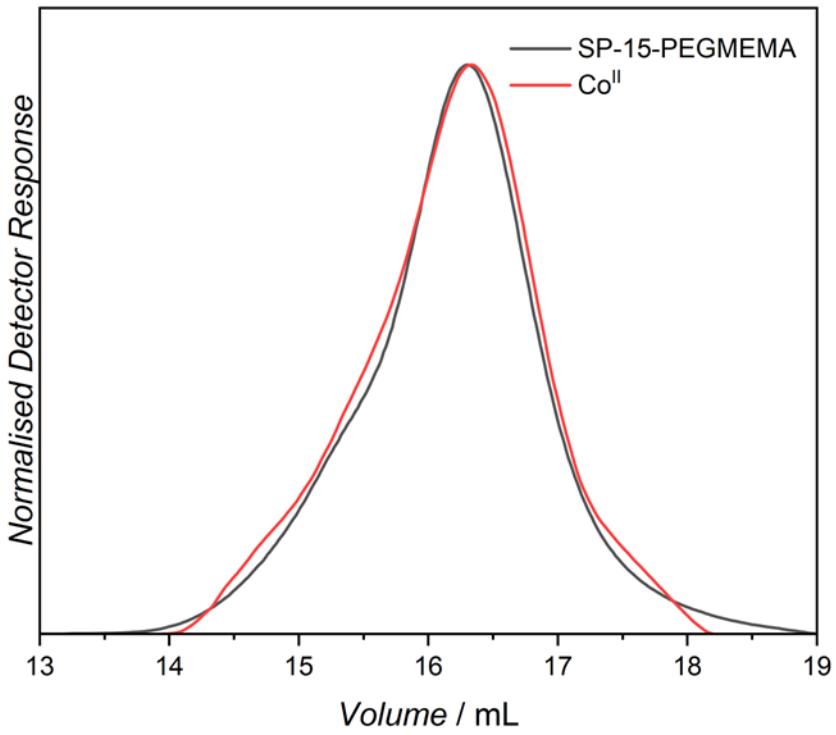

Figure 149. Attempted Crosslinking of **SP-15-PEGMEMA** with 4 eqv of $Co(BF_4)_2$.

10.4.8 Iron Complexation, SP-15-PEGMEMA

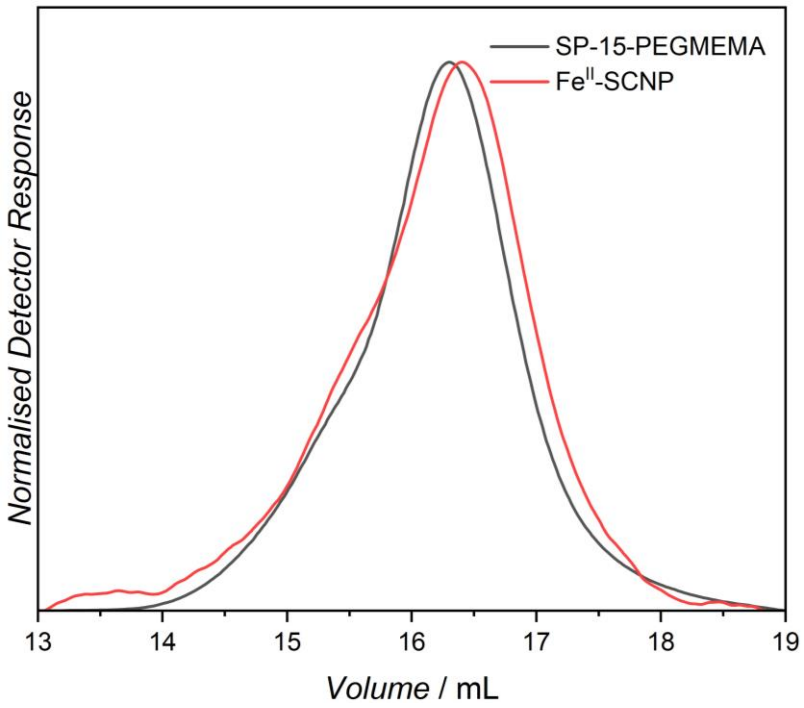

Figure 150. Attempted Crosslinking of **SP-15-PEGMEMA** with 4 eqv of $Fe(BF_4)_2$.

10.5 Catalysis

10.5.1 Substituted Substrate Catalysis

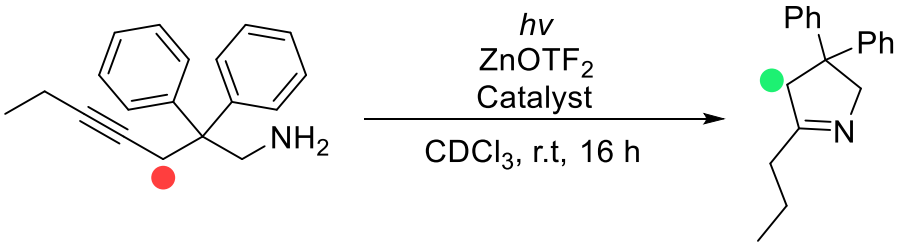

Anisole is used as an internal standard for all catalytic run, in subsequent spectra the anisole resonance (δ = 3.8 ppm) is highlighted in blue.

10.5.1.1 Catalyst: AzoCl$_4$-Au-SCNP-13 & 620 nm Irradiation

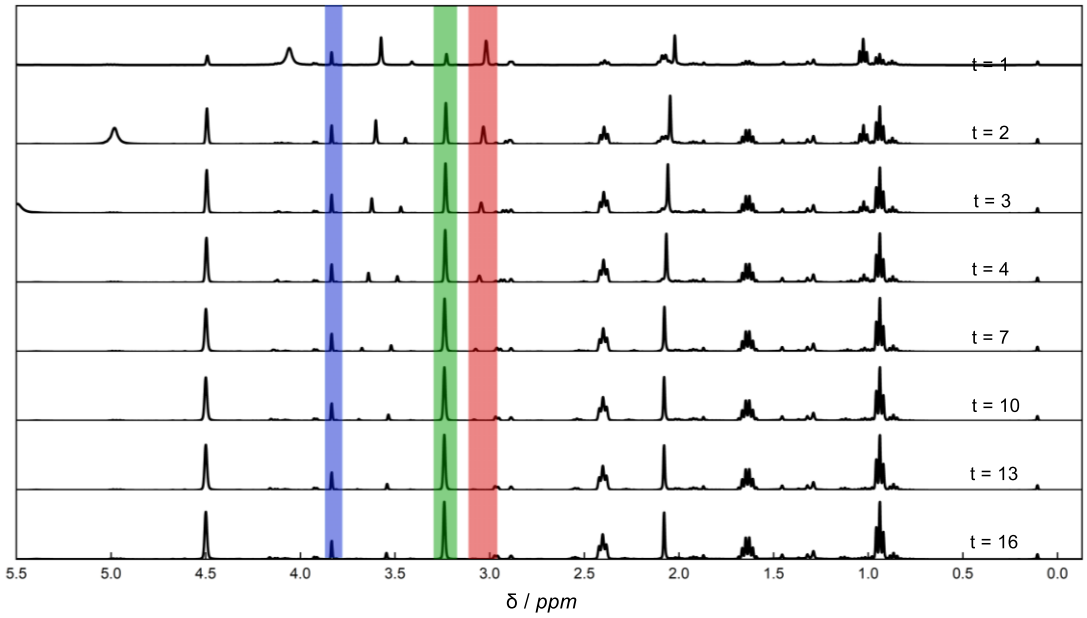

10.5.1.2 Catalyst: AzoCl$_4$-Au-SCNP-13 & 415 nm Irradiation

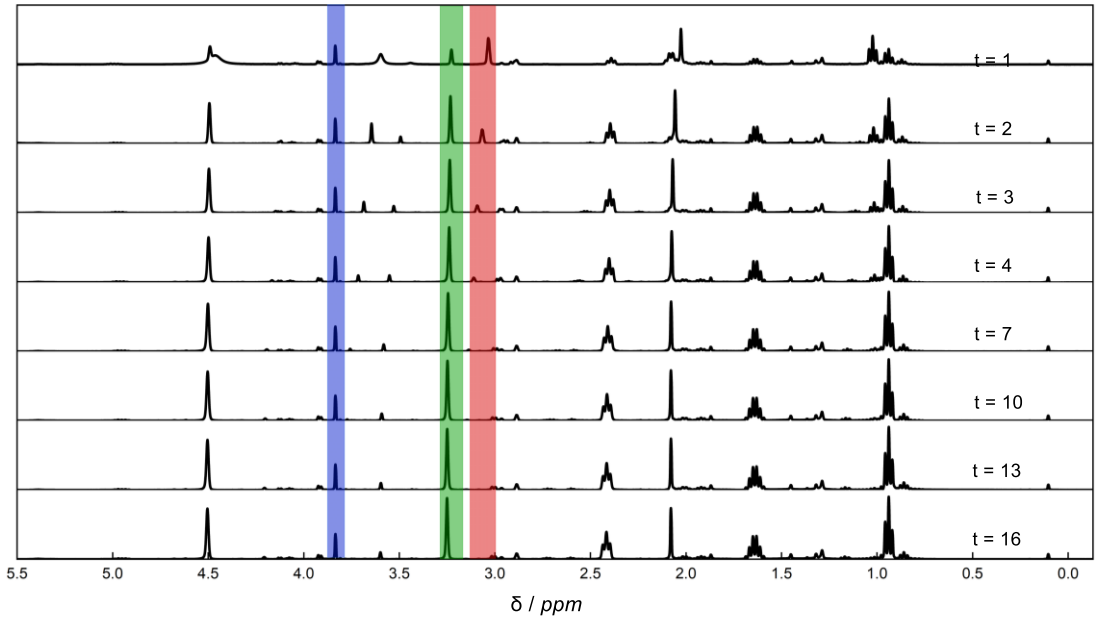

10.5.1.3 Catalyst: Au-P-13

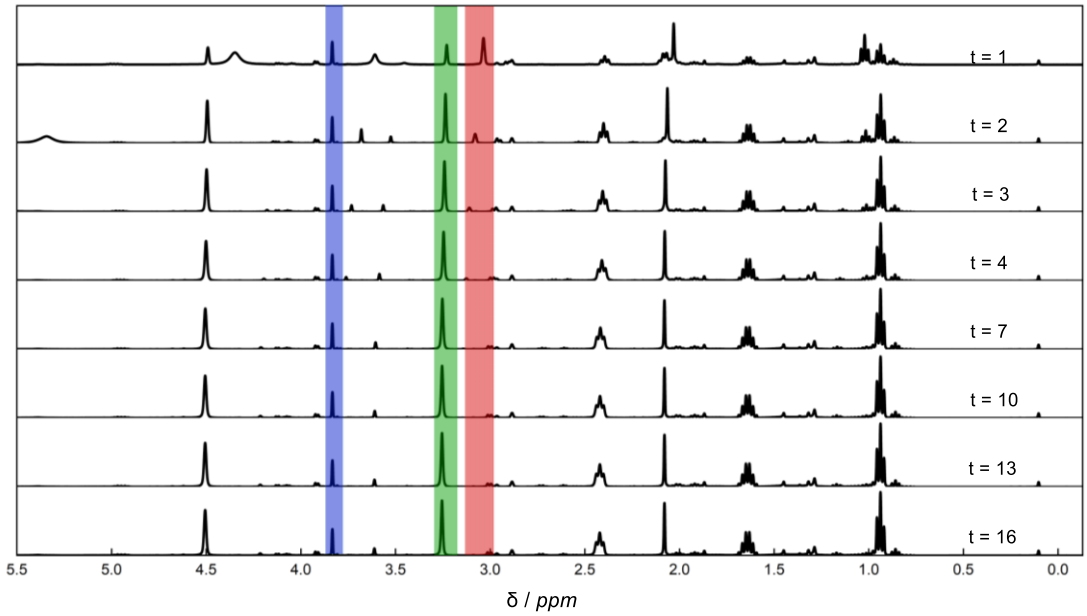

10.5.1.4 Catalyst: Ar_3PAuCl

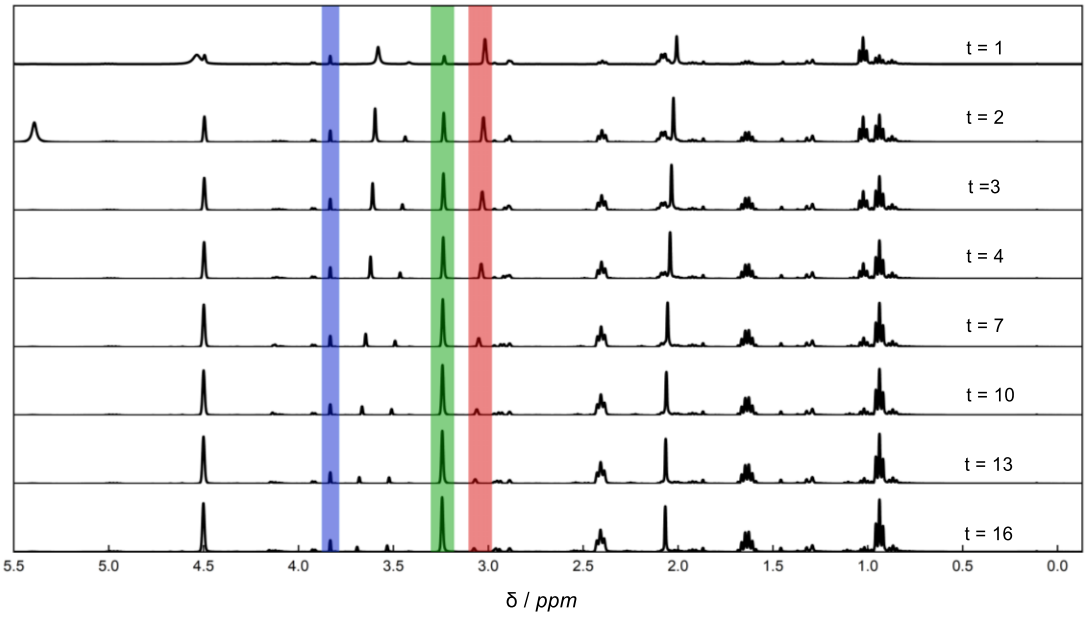

10.5.1.5 Catalyst: AzoCl4-Au-SCNP-13 & 415 nm Repeat

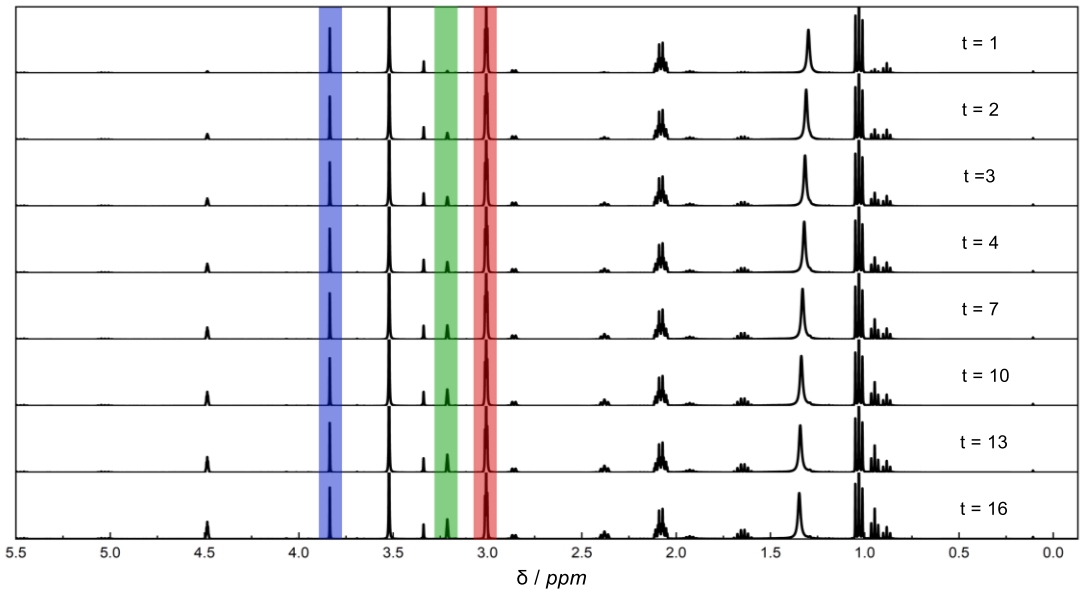

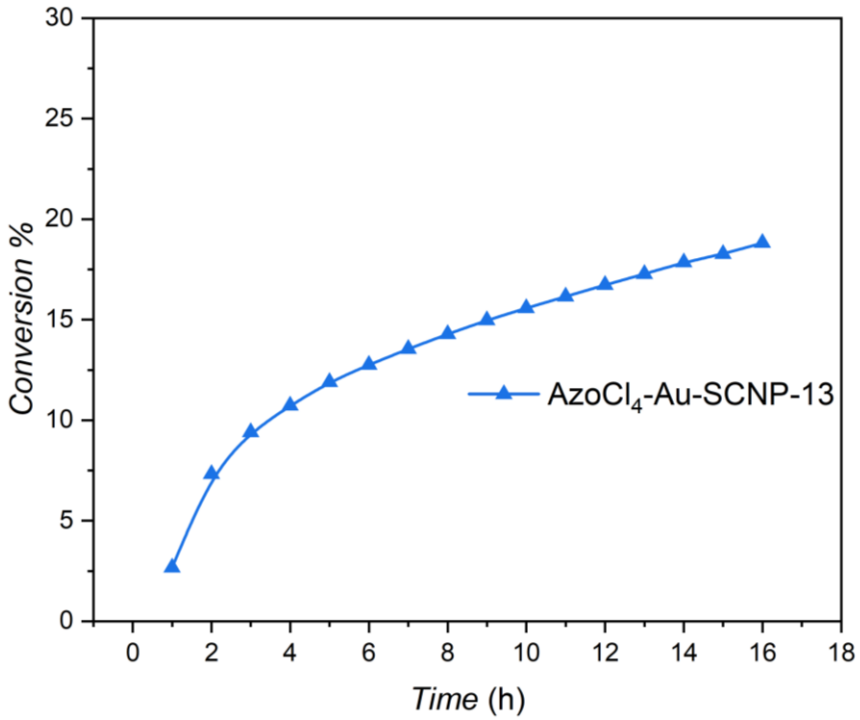

10.5.2 ArP_3AuCl Intramolecular Hydroamination

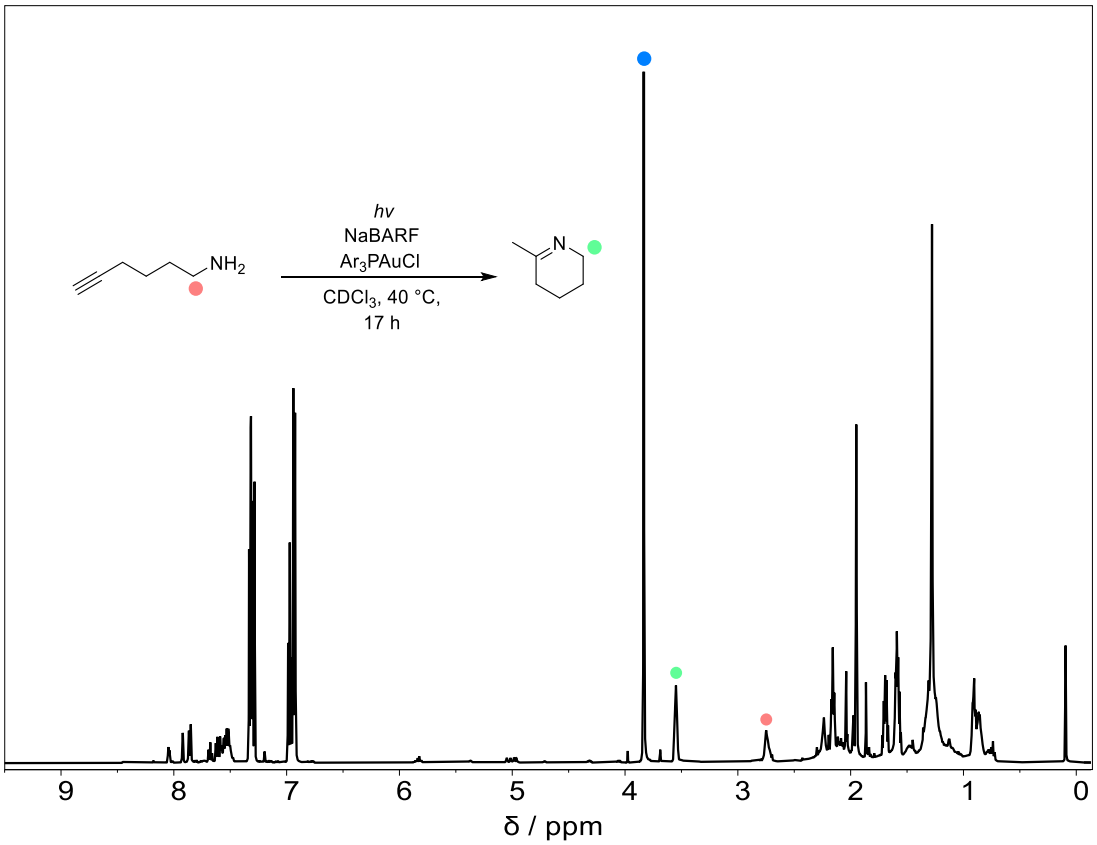

10.5.3 Intermolecular Catalysis

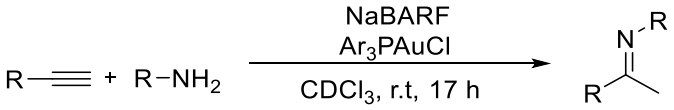

Anisole is used as an internal standard for all catalytic runs, in subsequent spectra the anisole resonance (δ = 3.8 ppm) is highlighted in blue.

10.5.3.1 Aniline and Phenyl Acetylene

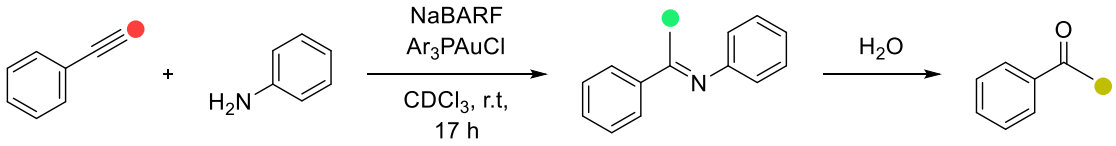

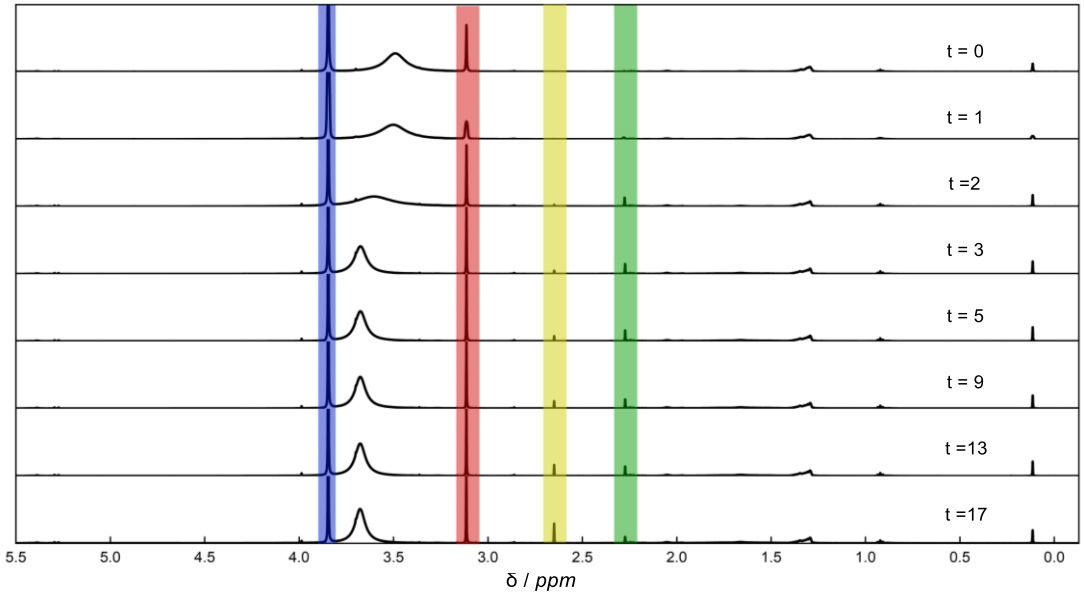

10.5.3.2 Aniline and Methyl Propiolate

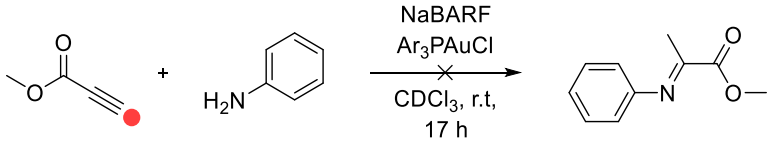

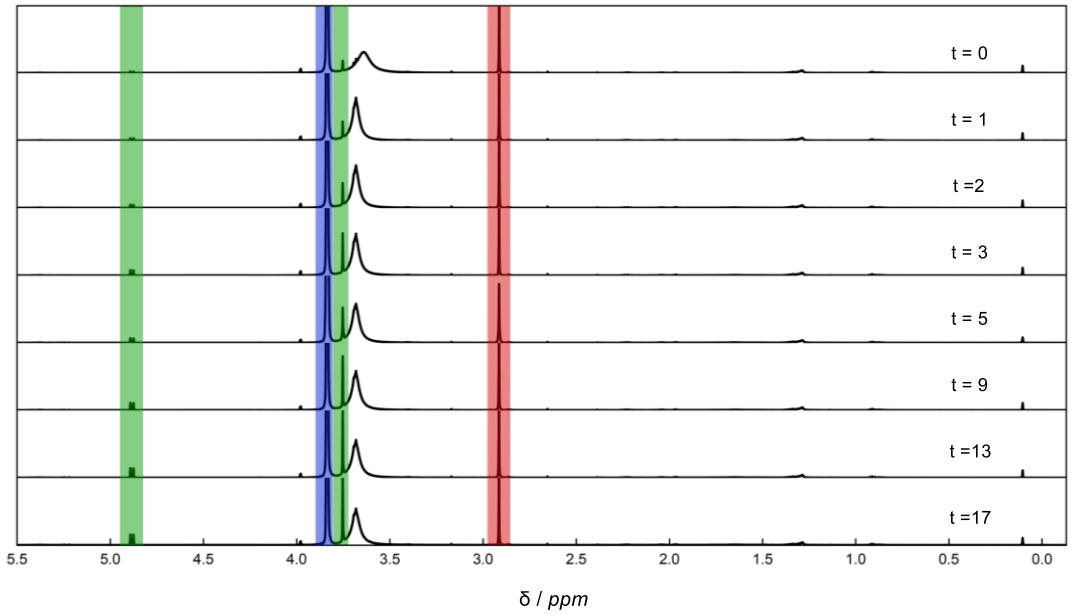

10.5.3.3 Hexylamine and Phenyl Acetylene

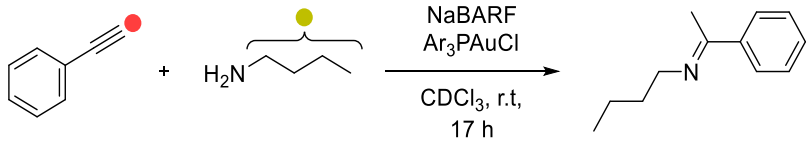

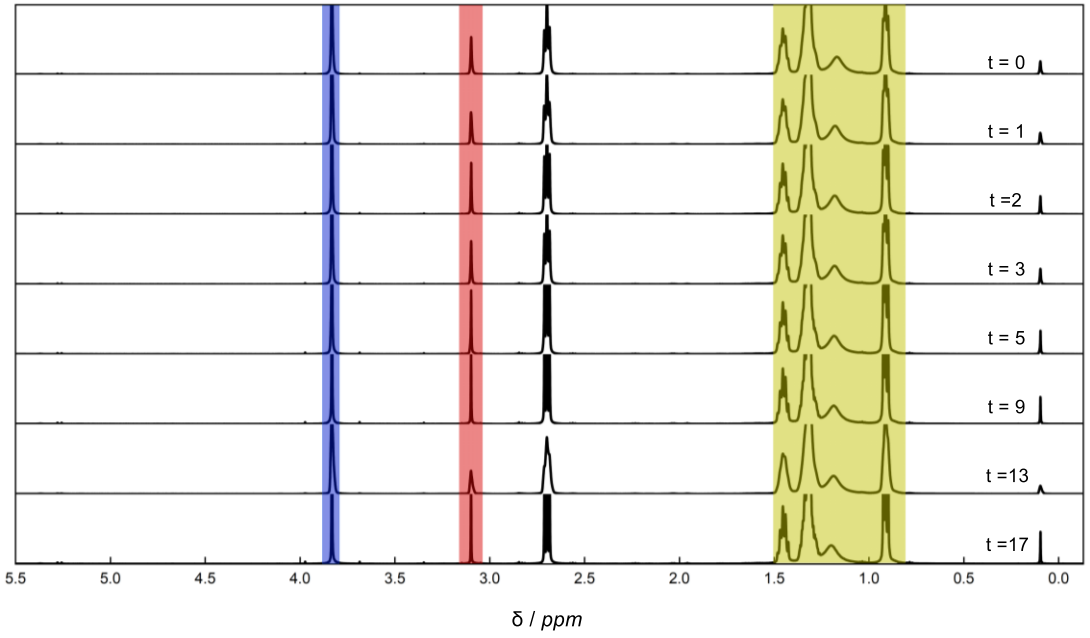

10.6 Photoresponsivity

10.6.1 AzoCl$_4$-Au-SCNP-13 Triplicates

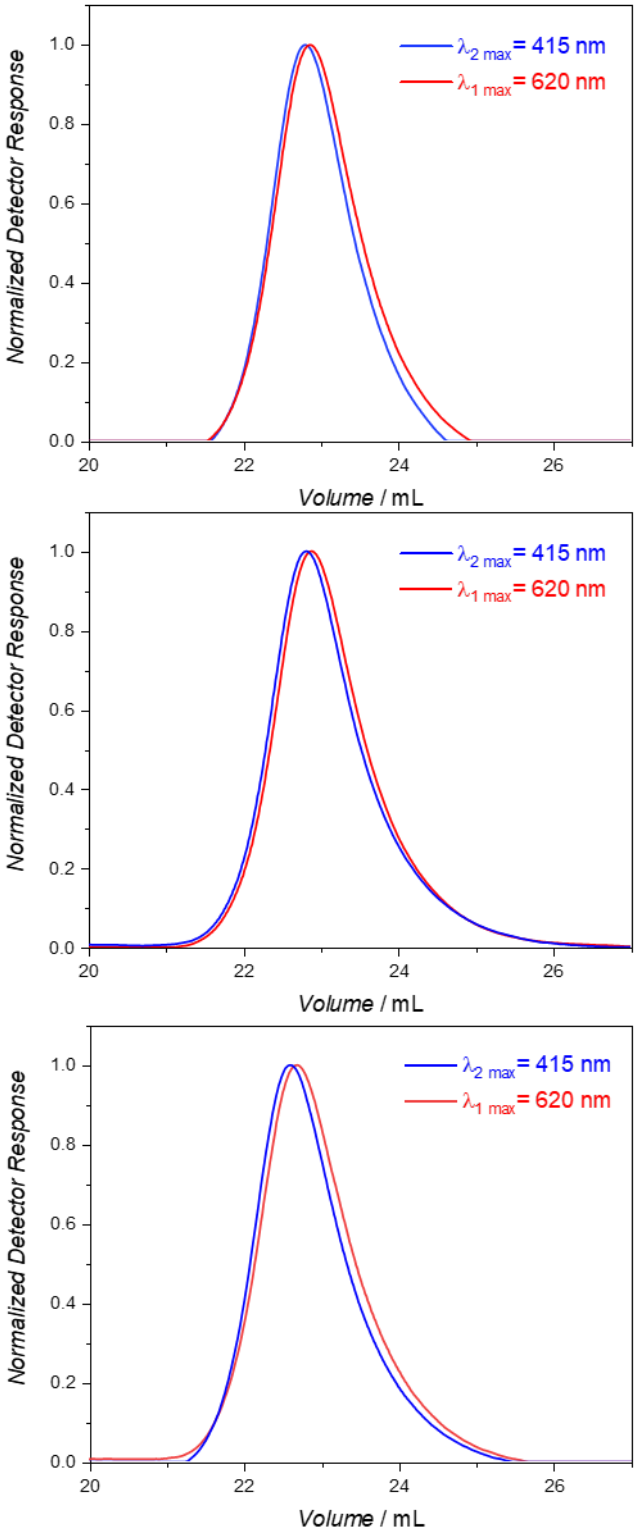

Figure 151. Repeat experiments monitored by SEC displaying the reversible compaction of **Azo-Au-SCNP-13** recorded in THF after 620 nm (red) and 415 nm light (blue) irradiation.

	M_p / g mol^{-1}	
	620 nm	**415 nm**
1st Cycle	19000	19800
2nd Cycle	18800	19500
3rd Cycle	21200	22300

Table 2. M_p values of the repeated switching of **Azo-Au-SCNP-13** with different colours of light, monitored by SEC.

10.6.2 Tetra-chlorinated Di-acid Azobenzene UV-Vis Switching

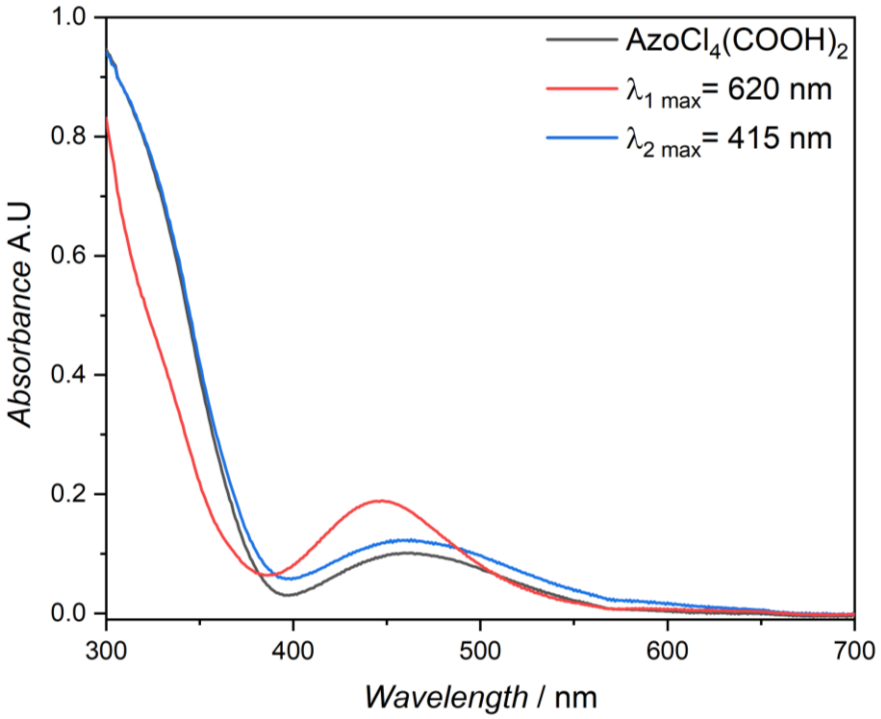

Figure 152. UV-Vis spectra of the tetra-chlorinated di-acid azobenzene prior to any irradiation (black), after 620 nm (red) and 415 nm irradiation (blue).

10.6.3 AzoCl$_4$-SCNP-23 ^{1}H NMR Switching

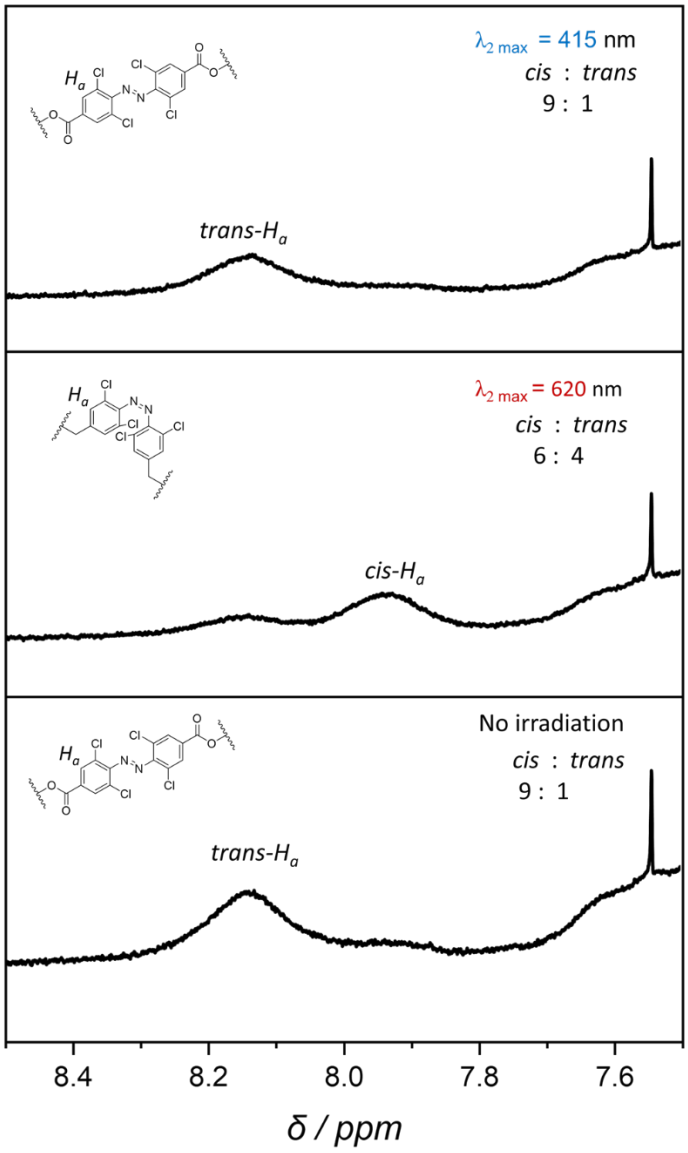

Figure 153. ^{1}H NMR spectra tracing the photodynamic switching of **Azo-Au-SCNP-23** compacted via ***o*-AzoCl$_4$ crosslinks** $\lambda_{1,\,max}$ = 620 nm, $\lambda_{2,\,max}$ = 415 nm irradiation.

10.6.4 $AzoCl_4$-SCNP-23 SEC Switching

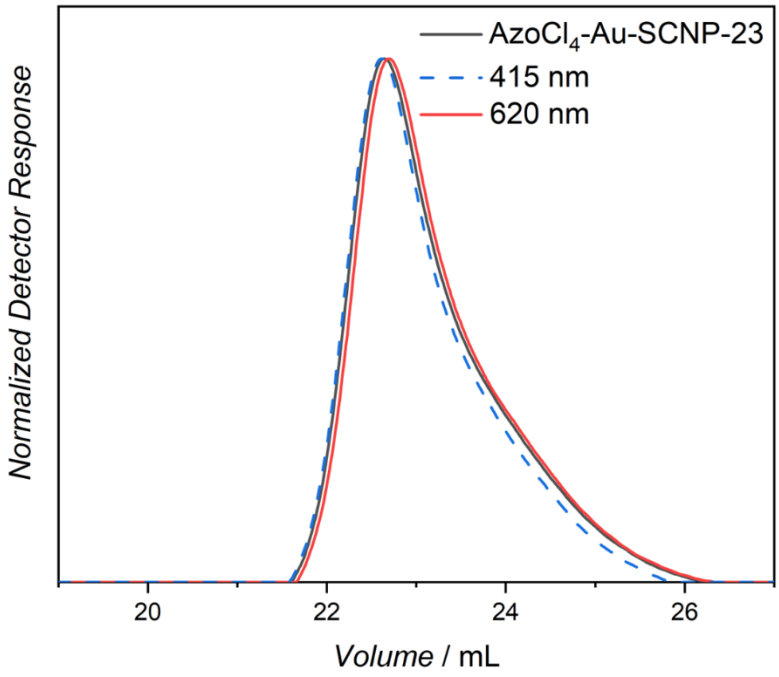

Figure 154. Elugrams displaying the compaction of **$AzoCl_4$-Au-SCNP-23** recorded in THF with no light irradiation (black), 620 nm (red) and 415 nm light (blue) irradiation.

10.6.5 Attempted SEC switching of Azo-SCNP-13

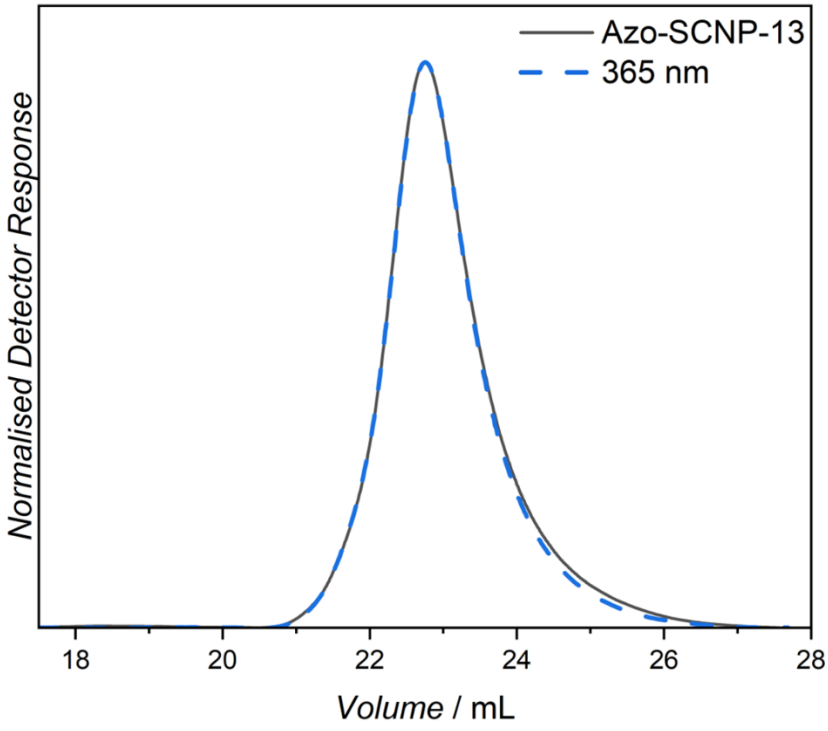

Figure 155. Elugrams displaying the attempted compaction of **Azo-SCNP-13** recorded in THF with no light irradiation (black), 365 nm (blue).

10.7 Primary DOSY Data

10.7.1 Au-P-13

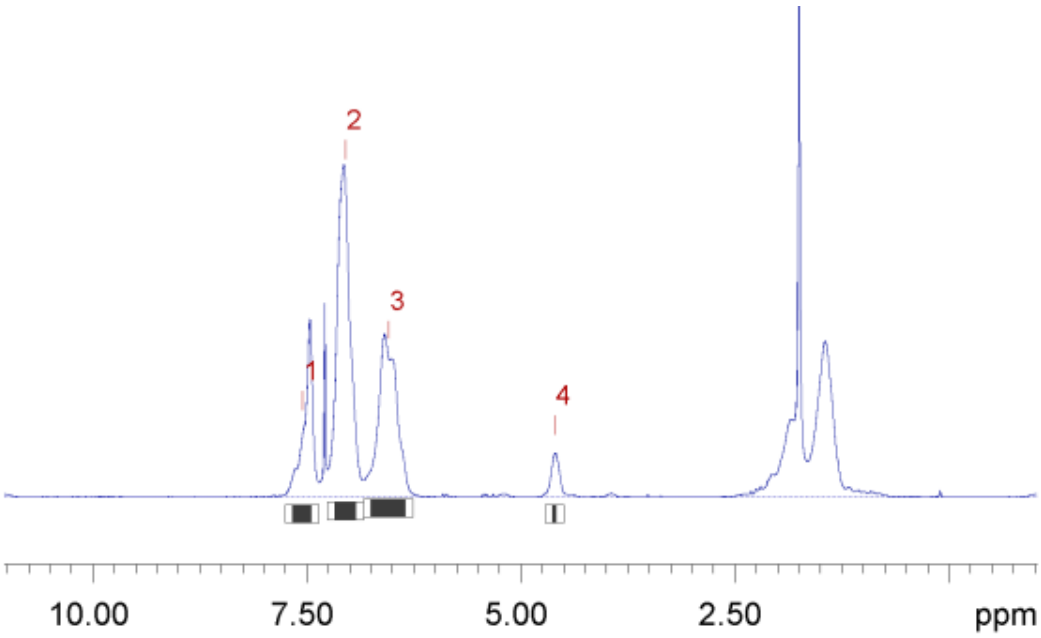

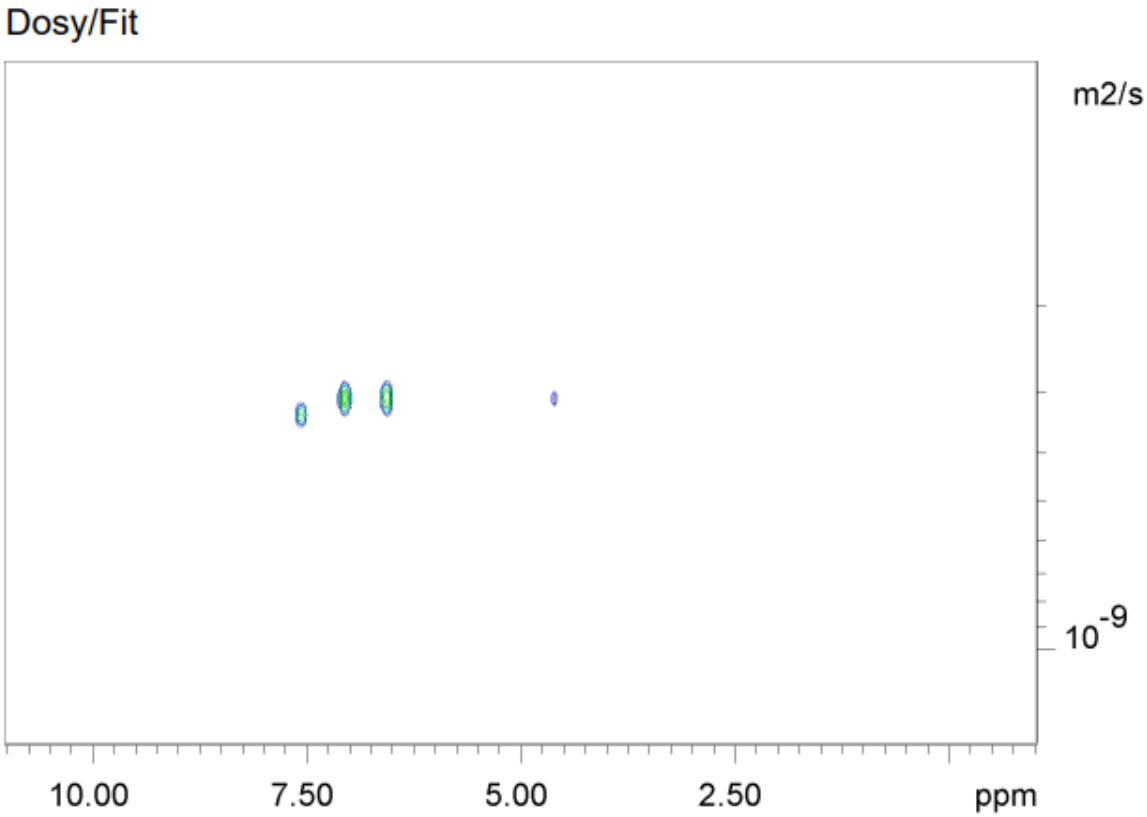

Fitted function:	f (x) = Io * exp (-D * x^2 * gamma^2 * littleDelta^2 (bigDelta-littleDelta/3)* 10^4
used gamma:	26752 rad/(s*Gauss)
used little delta:	0.0024000 s
used big delta:	0.099900 s
used gradient strength:	variable
Random error estimation of data:	RMS per spectrum (or trace/plane)
Systematic error estimation of data:	worst case per peak scenario
Fit parameter Error estimation method:	from fit using arbitrary y uncertainties
Confidence level:	95%
Used peaks:	peaks from C:/Data/Chemists/Aidanl/3_AEI_154/4/pdata/1/peaklist1D.xml
Used integrals:	area integral
Used Gradient strength:	all values (including replicates) used

Peak name	F2 [ppm]	Io	error	D [m2/s]	error	fitInfo
1	7.551	3.98e+10	3.189e+08	3.33e-10	6.304e-12	Done
2	7.044	1.17e+11	1.128e+09	3.11e-10	7.170e-12	Done
3	6.545	7.96e+10	8.143e+08	3.10e-10	7.547e-12	Done
4	4.602	9.21e+09	9.894e+07	3.11e-10	7.951e-12	Done

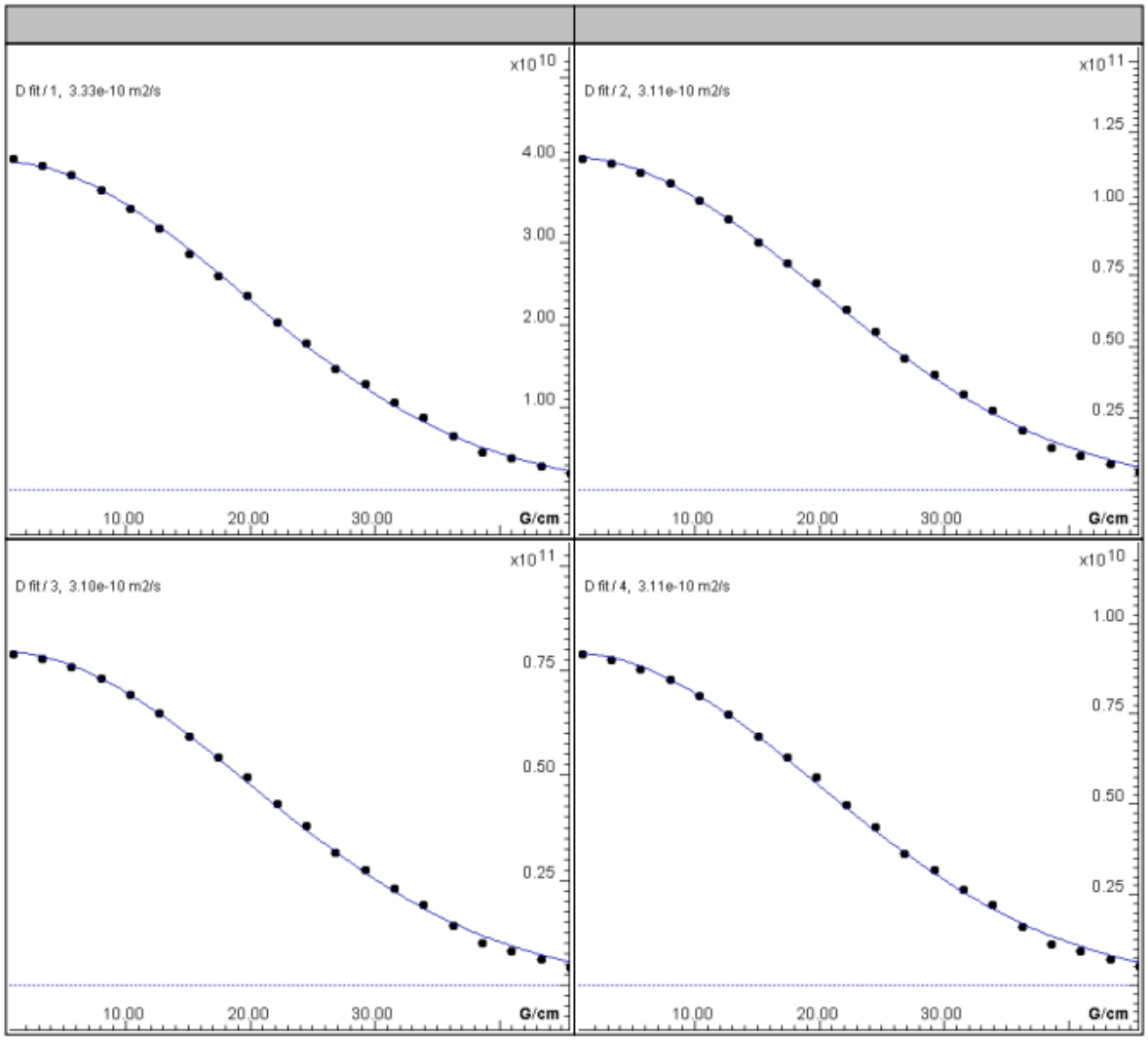
D fit / 1, 3.33e-10 m2/s
x10^10
4.00
3.00
2.00
1.00
10.00
20.00
30.00
G/cm
D fit / 2, 3.11e-10 m2/s
x10^11
1.25
1.00
0.75
0.50
0.25
10.00
20.00
30.00
G/cm
D fit / 3, 3.10e-10 m2/s
x10^11
0.75
0.50
0.25
10.00
20.00
30.00
G/cm
D fit / 4, 3.11e-10 m2/s
x10^10
1.00
0.75
0.50
0.25
10.00
20.00
30.00
G/cm

10.7.2 AzoCl$_4$-Au-SCNP-13

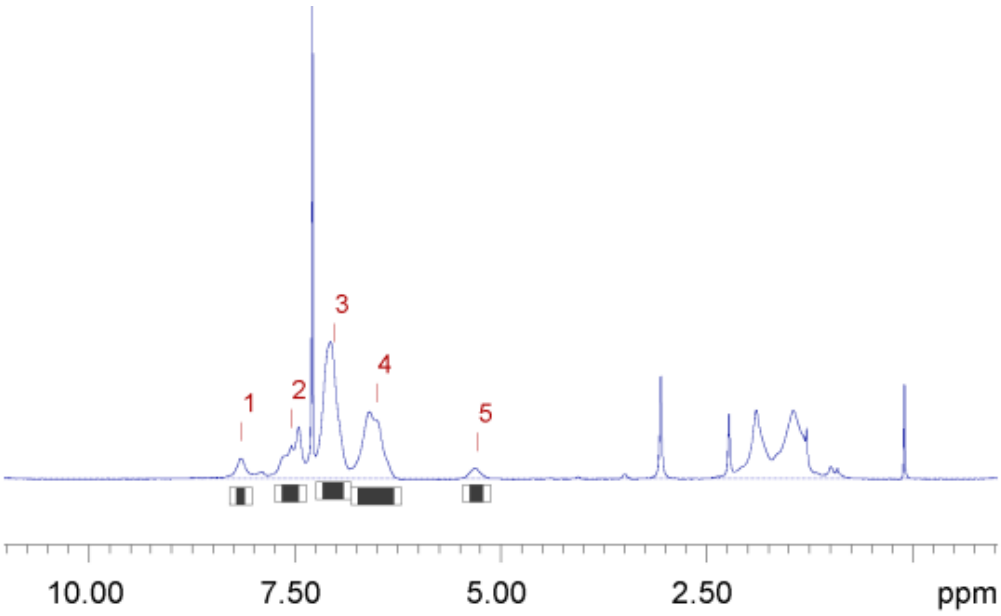

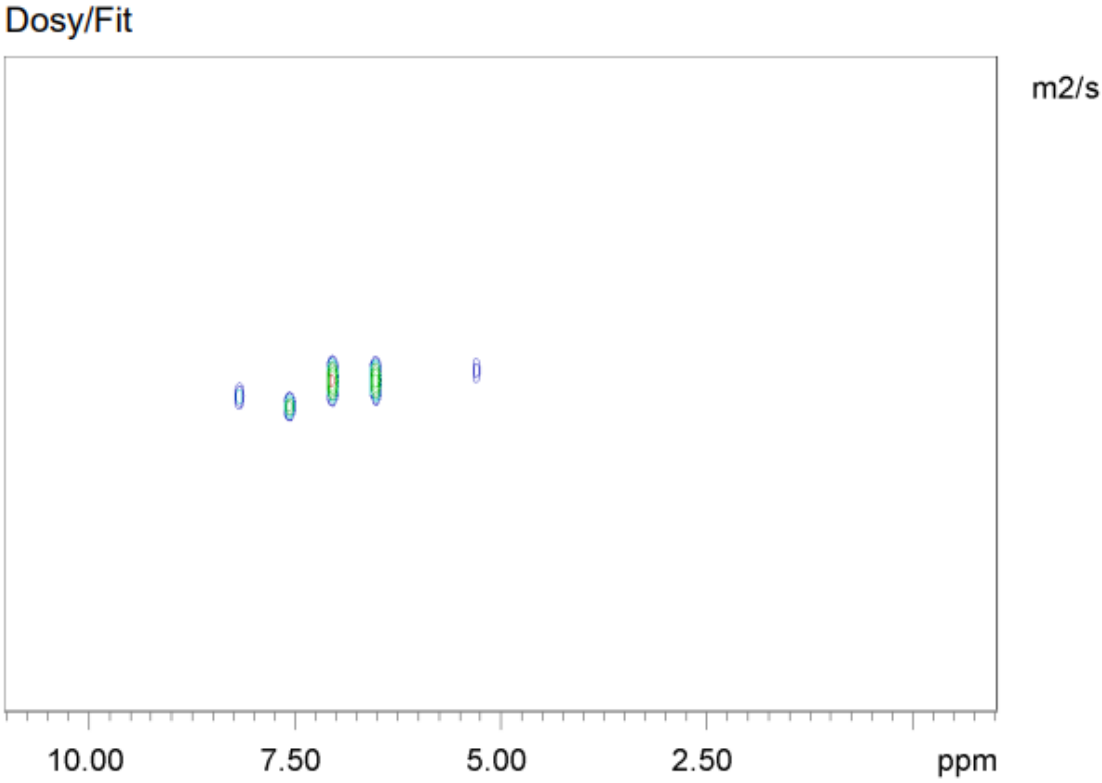

Fitted function:	f (x) = Io * exp (-D * x^2 * gamma^2 * littleDelta^2 (bigDelta-littleDelta/3)* 10^4
used gamma:	26752 rad/(s*Gauss)
used little delta:	0.0019200 s
used big delta:	0.099900 s
used gradient strength:	variable
Random error estimation of data:	RMS per spectrum (or trace/plane)
Systematic error estimation of data:	worst case per peak scenario
Fit parameter Error estimation method:	from fit using arbitrary y uncertainties
Confidence level:	95%
Used peaks:	peaks from C:/Data/Chemists/AidanI/3_AEI_046/4/pdata/1/peaklist1D.xml
Used integrals:	area integral
Used Gradient strength:	all values (including replicates) used

Peak name	F2 [ppm]	Io	error	D [m2/s]	error	fitInfo
1	8.152	6.19e+09	8.522e+07	5.01e-10	1.649e-11	Done
2	7.551	2.13e+10	2.263e+08	5.14e-10	1.305e-11	Done
3	7.032	6.28e+10	9.792e+08	4.80e-10	1.798e-11	Done
4	6.510	4.10e+10	6.739e+08	4.79e-10	1.891e-11	Done
5	5.288	3.76e+09	6.615e+07	4.69e-10	1.984e-11	Done

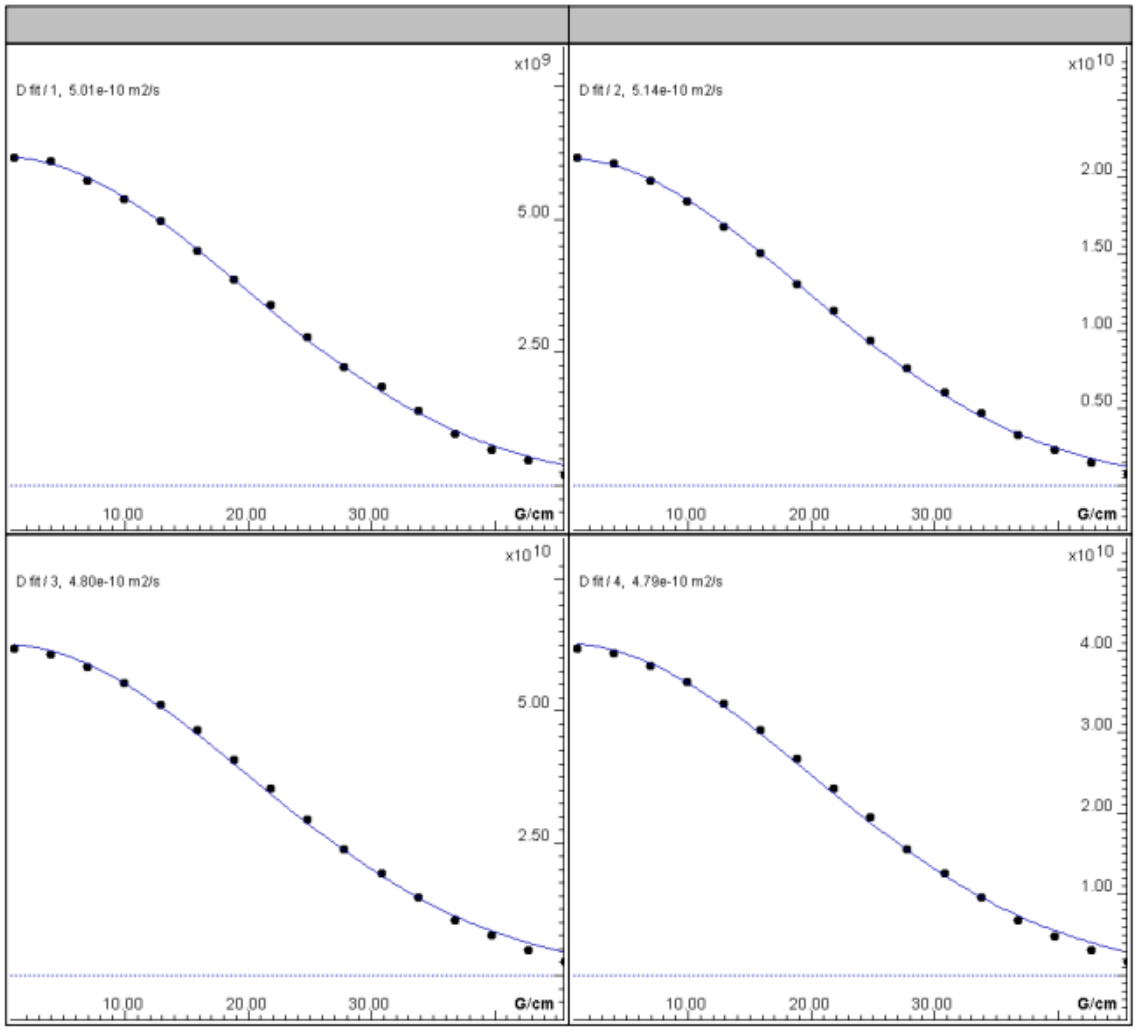

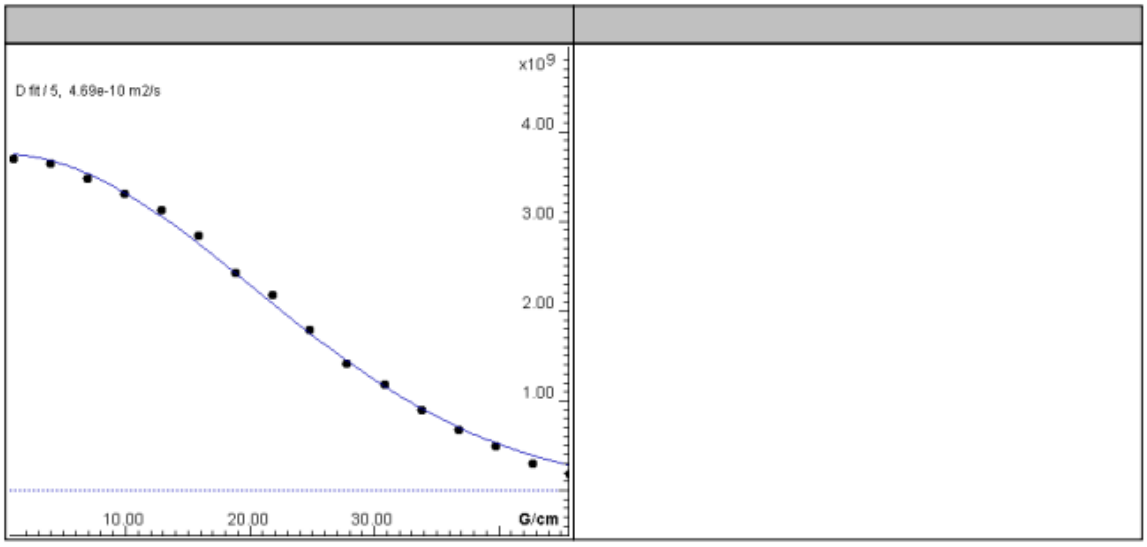
D fit / 5, 4.69e-10 m2/s
x10^9
4.00
3.00
2.00
1.00
10.00
20.00
30.00
G/cm

10.7.3 Au-P-23

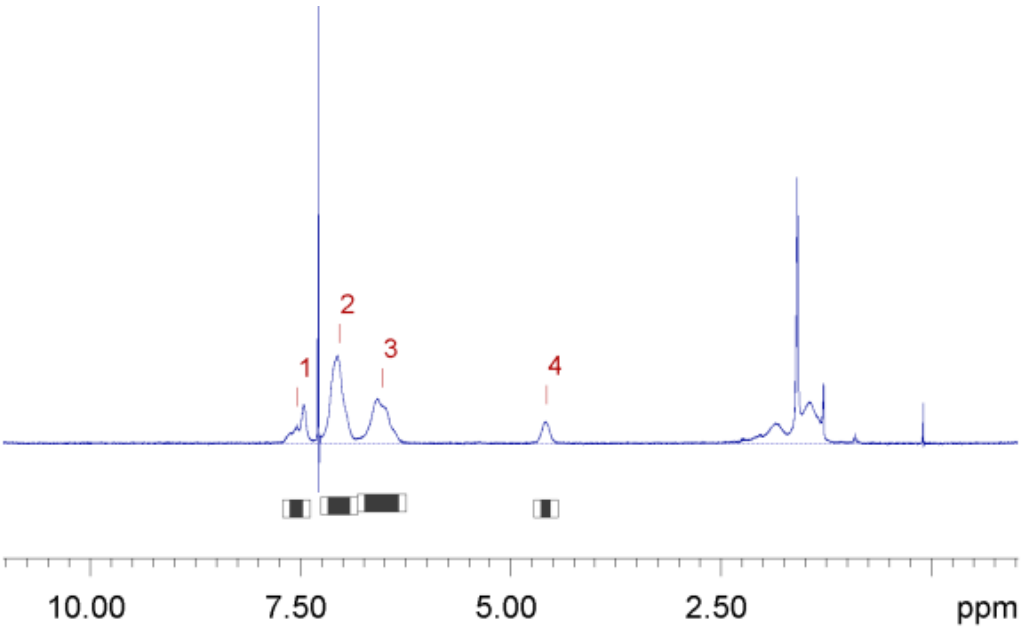
1
2
3
4
10.00
7.50
5.00
2.50
ppm

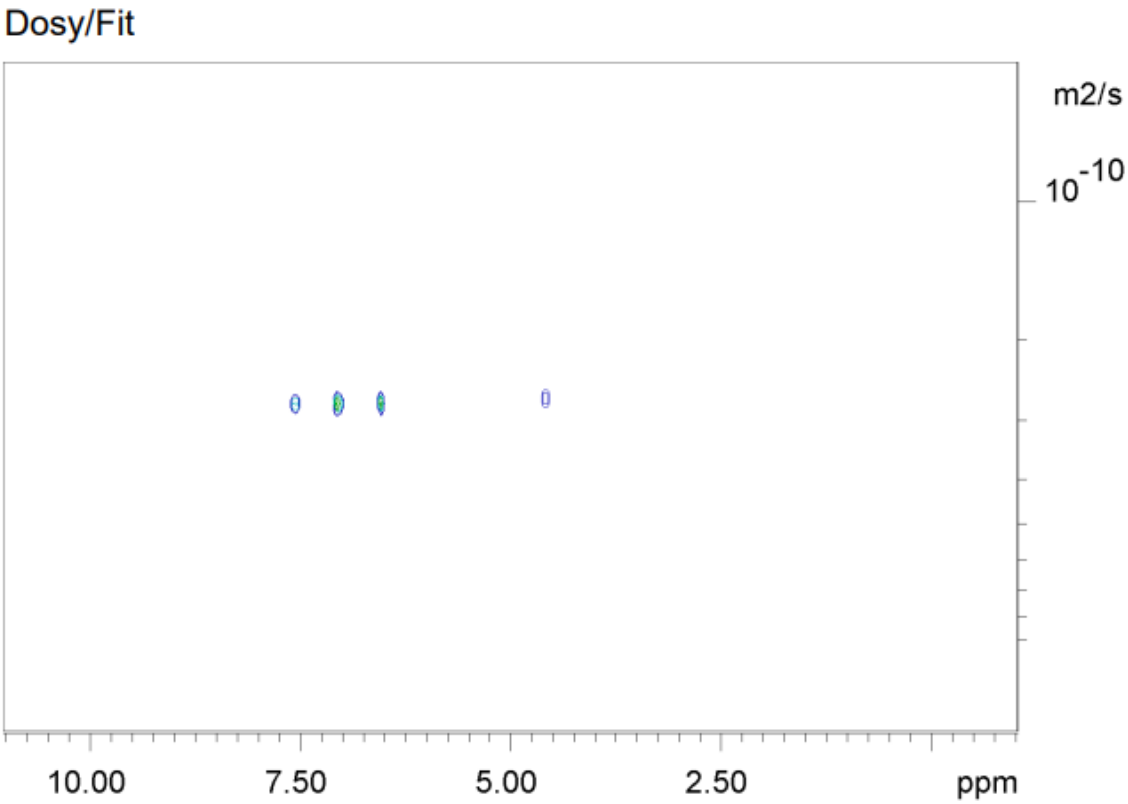
Dosy/Fit
m2/s
10-10
10.00
7.50
5.00
2.50
ppm

Fitted function:	f (x) = Io * exp (-D * x^2 * gamma^2 * littleDelta^2 (bigDelta-littleDelta/3)* 10^4
used gamma:	26752 rad/(s*Gauss)
used little delta:	0.0025000 s
used big delta:	0.099900 s
used gradient strength:	variable
Random error estimation of data:	RMS per spectrum (or trace/plane)
Systematic error estimation of data:	worst case per peak scenario
Fit parameter Error estimation method:	from fit using arbitrary y uncertainties
Confidence level:	95%
Used peaks:	peaks from C:/Data/Chemists/Aidanl/3_AEI_091_DOSY/4/pdata/1/peaklist1D.xml
Used integrals:	area integral
Used Gradient strength:	all values (including replicates) used

Peak name	F2 [ppm]	Io	error	D [m2/s]	error	fitInfo
1	7.539	1.38e+10	1.092e+08	2.77e-10	5.288e-12	Done
2	7.036	4.75e+10	3.277e+08	2.74e-10	4.549e-12	Done
3	6.530	3.30e+10	2.570e+08	2.77e-10	5.174e-12	Done
4	4.575	7.36e+09	7.051e+07	2.72e-10	6.268e-12	Done

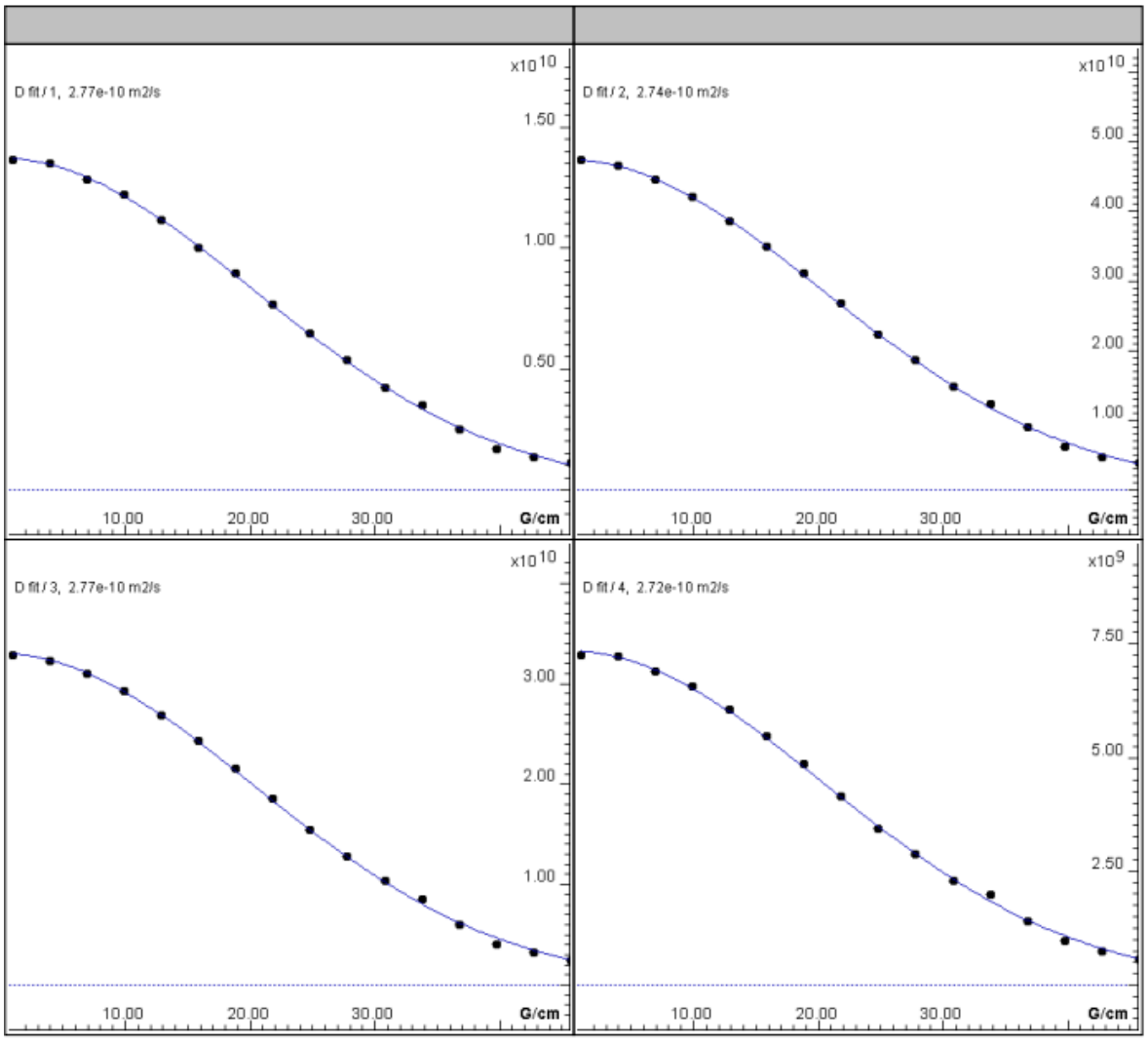

10.7.4 AzoCl$_4$-Au-SCNP-23

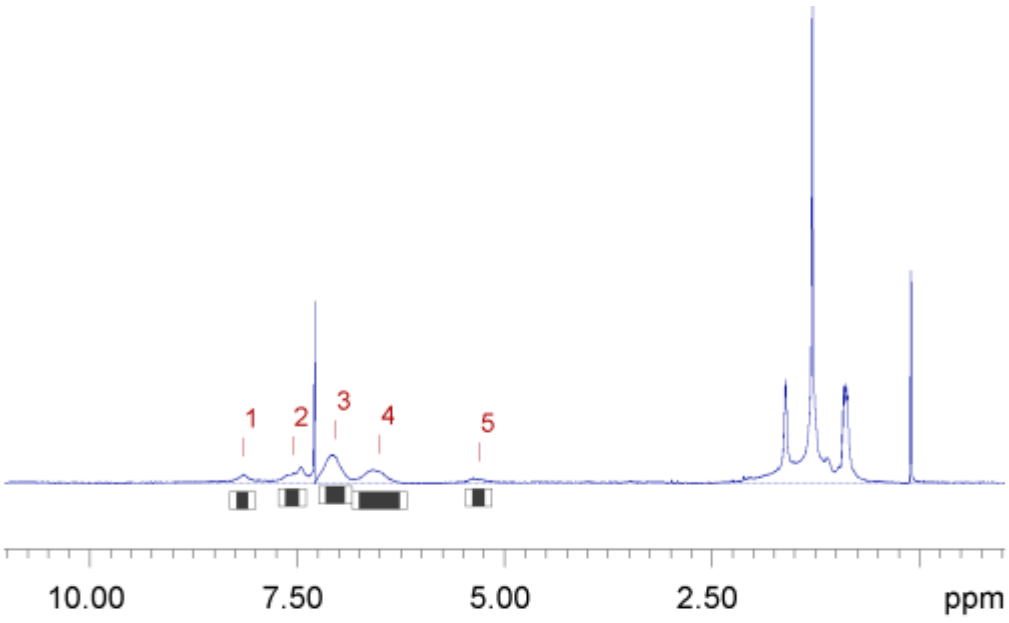

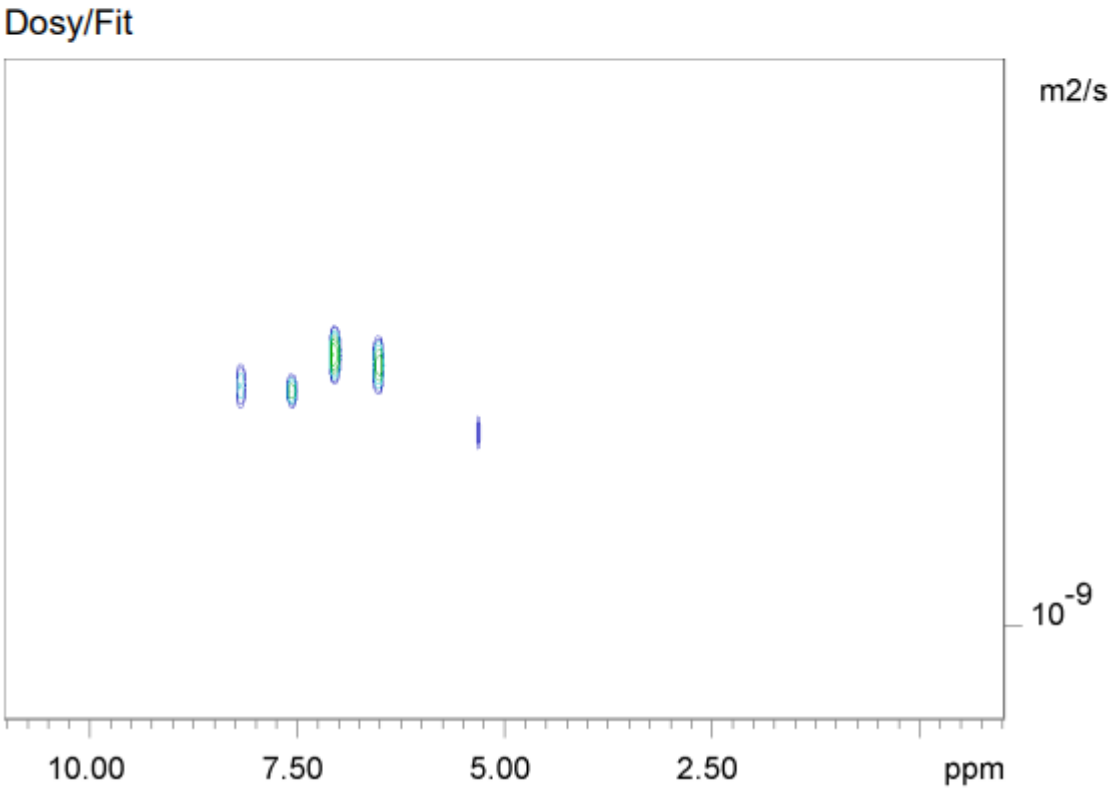

Fitted function:	f (x) = Io * exp (-D * x^2 * gamma^2 * littleDelta^2 (bigDelta-littleDelta/3)* 10^4
used gamma:	26752 rad/(s*Gauss)
used little delta:	0.0020000 s
used big delta:	0.085000 s
used gradient strength:	variable
Random error estimation of data:	RMS per spectrum (or trace/plane)
Systematic error estimation of data:	worst case per peak scenario
Fit parameter Error estimation method:	from fit using arbitrary y uncertainties
Confidence level:	95%
Used peaks:	peaks from C:/Data/Chemists/Aidanl/3_AEI_124_DOSY/4/pdata/1/peaklist1D.xml
Used integrals:	area integral
Used Gradient strength:	all values (including replicates) used

Peak name	F2 [ppm]	Io	error	D [m2/s]	error	fitInfo
1	8.156	2.40e+09	5.674e+07	4.89e-10	2.795e-11	Done
2	7.551	5.18e+09	7.554e+07	4.93e-10	1.736e-11	Done
3	7.036	1.20e+10	2.570e+08	4.47e-10	2.342e-11	Done
4	6.503	6.99e+09	1.634e+08	4.61e-10	2.625e-11	Done
5	5.303	1.34e+09	3.347e+07	5.59e-10	3.321e-11	Done

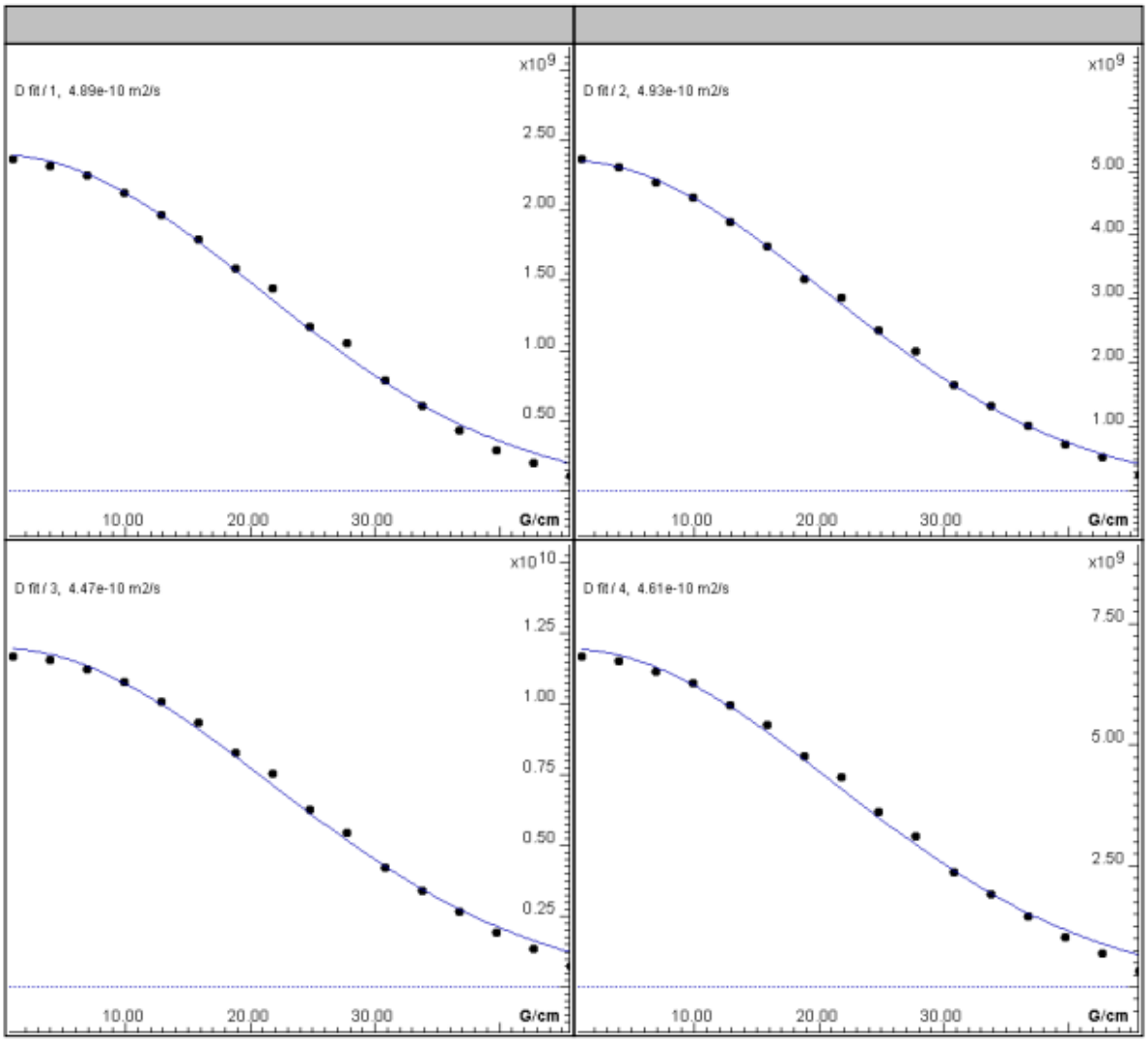

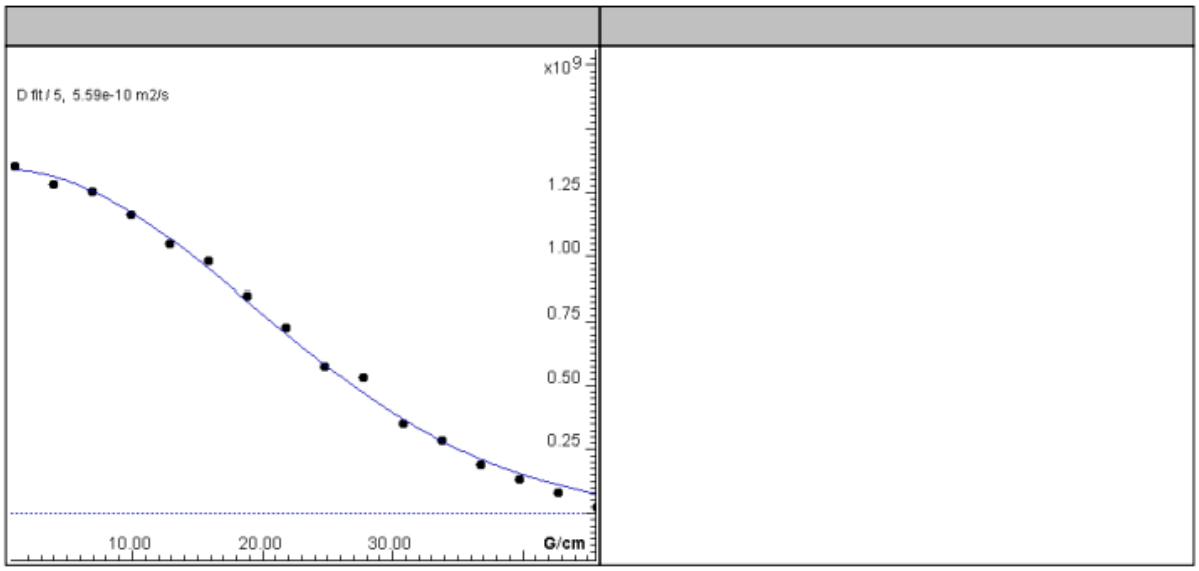
D fit / 5, 5.59e-10 m2/s
x10^9
1.25
1.00
0.75
0.50
0.25
10.00
20.00
30.00
G/cm